SALT EFFECTS ON MICELLIZATION, MICELLAR GROWTH, AND PHASE BEHAVIOR OF AQUEOUS SOLUTIONS OF NONIONIC SURFACTANTS

by

Maria Teresa Reyes Carale

B.S., Chemical Engineering
University of the Philippines, 1984

Submitted to the Department of Chemical Engineering
in Partial Fulfillment of the Requirements
for the Degree of

DOCTOR OF PHILOSOPHY
in Chemical Engineering
at the

MASSACHUSETTS INSTITUTE OF TECHNOLOGY

June 1993

Signature of Author _____
Department of Chemical Engineering
May 5, 1993

Certified by _____
Daniel Blankschtein
Associate Professor of Chemical Engineering
Thesis Supervisor

Accepted by _____
Robert E. Cohen
Professor of Chemical Engineering
Departmental Committee on Graduate Studies

SALT EFFECTS ON MICELLIZATION, MICELLAR GROWTH, AND PHASE BEHAVIOR OF AQUEOUS SOLUTIONS OF NONIONIC SURFACTANTS

by

Maria Teresa Reyes Carale

Submitted to the Department of Chemical Engineering
on May 5, 1993, in partial fulfillment of the
requirements for the degree of
Doctor of Philosophy in Chemical Engineering

Abstract

The addition of salts to aqueous solutions of nonionic surfactants can give rise to very significant changes in both equilibrium and rheological micellar solution properties. This thesis focuses on elucidating and quantifying the effects of salts on intramicellar and intermicellar interactions, micellization, micellar growth, and phase behavior of aqueous solutions of nonionic surfactants. Specifically, the effects of adding LiCl, NaCl, KCl, KBr, and KI to aqueous solutions containing the alkyl poly(ethylene oxide), C_iE_j, nonionic surfactants, $C_{10}E_6$, $C_{12}E_6$, and $C_{12}E_8$, have been investigated through a combined theoretical and experimental study.

The theoretical studies include:
(1) The development of a molecular-thermodynamic formulation to characterize and model salt effects on both intramicellar and intermicellar interactions, and the utilization of this formulation to predict (*i*) the onset of micelle formation at the critical micelle concentration (CMC), (*ii*) the one-dimensional growth of these micelles into flexible rod-like microstructures which can interpenetrate and form entangled transient nets, and (*iii*) the solution phase behavior, including liquid-liquid phase separation, as a function of salt type and concentration, as well as temperature;

(2) The implementation of a Rotational Isomeric State Monte-Carlo Approach to determine the average conformational characteristics of the short poly(ethylene oxide), PEO, hydrophilic chains which are grafted at one end to the micellar core surface;

(3) The generalization of polymer theories to account for the unique self-assembling nature of micelles, and the implementation of these theories to predict (*i*) the crossover surfactant concentration, X^*, signalling the transition from the dilute

micellar solution regime, where relatively short rod-like micelles are singly dispersed in solution, to the semidilute micellar solution regime, where elongated and flexible rod-like micelles interpenetrate and become fully entangled, and (*ii*) the specific viscosity of dilute micellar solutions containing C_iE_j rod-like micelles;

(4) The development of a statistical-thermodynamic description, as well as the implementation of concepts and methodologies from colloid and interface science, to calculate the interactions between micelles of various shapes (spheres and rods). Specifically, the van der Waals interactions between micellar cores, as well as the interactions resulting from the interpenetration of the PEO chains present in the hydrophilic layers of two approaching micelles, have been calculated.

The experimental studies include:
(1) Surface tension measurements, which provided indirect information about the nature of intramicellar interactions, as well as permitted the experimental determination of the CMC as a function of salt type and concentration;

(2) Light scattering measurements (both intensity and quasielastic light scattering), which were utilized to study the growth (or the suppression of growth) of micelles upon the addition of salts, as well as upon raising the temperature and increasing surfactant concentration;

(3) Viscosity measurements, which were utilized to experimentally determine the crossover surfactant concentration, X^*;

(4) Phase diagram measurements, specifically, the determination of cloud-point curves, which served as sensitive indicators of the variation of the strength of intermicellar interactions with salt type and concentration, as well as temperature.

Using the theoretical tools described above, we have found that the theoretically predicted CMC's agree reasonably well with those determined experimentally for the three surfactants studied ($C_{10}E_6$, $C_{12}E_6$, and $C_{12}E_8$) in the presence of LiCl, NaCl, KCl, and KBr. The predictions for KI are less accurate due to specific interactions of I^- with the PEO hydrophilic chains which are not accounted for in the theory.

The light scattering studies provided evidence for salt-induced (for KCl and KBr), as well as temperature-induced, growth of $C_{12}E_6$ micelles, and confirmed the predicted $C_{12}E_6$ micellar growth based on the theoretical studies of salt and temperature effects on intramicellar interactions. Interestingly, the light scattering results indicate that the addition of KI suppresses temperature-induced micellar growth, as compared to the no salt case, which is consistent with our conjecture that I^- complexes specifically with the PEO hydrophilic chains. This, in turn, effectively transforms the nonionic surfactant into an anionic surfactant, and, therefore, can

suppress micellar growth due to repulsive electrostatic interactions between the "negatively" charged PEO chains.

The predicted growth of $C_{12}E_6$ micelles into flexible, elongated rod-like microstructures upon raising temperature and increasing surfactant concentration, which can result in the entanglement of the micelles to form transient net-like structures, is consistent with the rapid increase of the viscosity of $C_{12}E_6$ aqueous micellar solutions which is observed experimentally in response to increasing temperature and surfactant concentration. The onset of entanglements is also consistent with the experimentally observed dependence of the mean hydrodynamic radius of $C_{12}E_6$ micelles on temperature and surfactant concentration obtained using quasielastic light scattering measurements. The X^* values deduced from viscosity and quasielastic light scattering measurements agree reasonably well with those predicted theoretically.

The measured cloud-point curves indicate that the addition of LiCl, NaCl, KCl, and KBr promotes phase separation of C_iE_j aqueous micellar solutions, while the addition of KI suppresses phase separation. As before, the effect of KI can be rationalized in terms of the specific complexation of I^- with the PEO chains. Interestingly, the strength of the attractive intermicellar interactions at the critical point (the lowest point on the cloud-point curve), as deduced from the experimentally measured cloud-point curves using a mean-field treatment of intermicellar interactions, has a constant value of about 1 kT per surfactant molecule.

Our calculations indicate that the van der Waals interactions between micelles are insufficient to account for the magnitude of the attraction needed to induce phase separation. We conjecture that the needed additional attraction is provided by the interpenetration of the PEO chains present in the hydrophilic layers of two approaching micelles under poor-solvent conditions. The theory developed to describe the interpenetration of PEO chains can qualitatively explain the phase separation of the alkyl poly(ethylene oxide) surfactant solutions considered in this thesis. Specifically, the predicted effects of varying (*i*) the length of the PEO chains, (*ii*) the type and concentration of added salt, and (*iii*) the temperature on the surfactant solution phase separation are consistent with the experimentally observed effects.

Thesis Supervisor: Dr. Daniel Blankschtein
Associate Professor of Chemical Engineering

ACKNOWLEDGEMENTS

I thank Professor Blankschtein, my thesis advisor, for unfailing support and superb guidance throughout my stay at MIT. He never ceased to be generous with his time. His availability was so very helpful, specially during the last few months, when this thesis was being written. I also appreciate his concern for his students' professional well-being, even after graduating from MIT.

I thank Professors Benedek, Deen and Hatton, the members of my thesis committee.

I thank Yvonne, Claudia, and Sudhakar, all of whom helped me tremendously in research, through stimulating discussions and by assisting me in various aspects of the theoretical modelling work.

I thank Quynh, whose assistance in the experimental aspect of the thesis is invaluable.

I am grateful to Chia-li, a good friend and lab partner, for being very supportive. I thank Nick, Leo, Pak, Mark, Ayal, Crist, Anat, and Nancy, members of our research group, for making life in the lab interesting and enjoyable.

I owe special thanks to the people I live with, who helped me never lose sight of the right perspective in life, when the going was tough, and when it was easy. Thanks to Sue and Karen for being good friends and classmates.

I owe a debt of gratitude to many more people. Space does not permit me to acknowledge them all. No one can do a PhD on her own, and of that I am keenly aware of.

To Mom and Dad...

this work is more theirs than mine.

TABLE OF CONTENTS

LIST OF FIGURES

LIST OF TABLES

CHAPTER 2

CHAPTER 4

CHAPTER 5

CHAPTER 1. INTRODUCTION

I. DEFINITION OF SURFACTANTS

Surfactants are molecules composed of two distinct components chemically bonded to each other: an ionic, a zwitterionic, or a highly polar nonionic moiety (referred to hereafter as the "head"), and a nonpolar moiety (referred to hereafter as the "tail") which typically is a hydrocarbon chain.[1] The difference in the nature of the two components, the head and the tail, results in a wide range of interesting phenomena. Thus, since the head is hydrophilic while the tail is hydrophobic, surfactant molecules normally adsorb at interfaces between two phases having different dielectric properties, for example, aqueous-air and aqueous-organic. During adsorption, the hydrophilic heads orient towards the phase having the higher dielectric constant (aqueous), while the tails orient towards the low-dielectric constant phase (organic)[2]. This positive adsorption at interfaces results in the lowering of both surface and interfacial tensions, which is observed when surfactant molecules are added to solutions.

The Difference between Surfactant Aggregates (Micelles) and Colloids: Physical Forces versus Chemical Forces. Surfactant molecules, when dissolved in aqueous solutions at the appropriate solution conditions (for example, surfactant concentration, temperature, and pressure), form aggregates in which the hydrophobic tails cluster together to form a hydrocarbon interior surrounded by a layer of hydrophilic heads.[3] Such aggregates are called micelles. The free-energy advantage of micellization is a manifestation of the hydrophobic effect[4], derived from the more attractive interactions between water molecules as compared to those between hydrocarbon tails and water molecules[3]. This hydrophobic effect is a balance of entropic and enthalpic contributions which results in a free energy of micellization which is almost independent of temperature[5].

In forming the micellar aggregates, no actual chemical bonding, that is, bonds characterized by the electrons being shared between two or more atoms so that the discrete nature of the atoms is lost[6], occurs. Accordingly, the forces responsible for surfactant monomer aggregation into micelles are physical forces, namely, interaction forces between unbonded molecules[6]. In essence, since physical forces control micellization, the factors that would affect aggregation are the same factors which vary the strength of these physical forces. Among these are the polarity of the heads, the length of the hydrocarbon tails, temperature, pressure, surfactant concentration, and salt type and salt concentration. Hence, it is observed that a rich variety of surfactant aggregates can form depending on the surfactant molecular structure: spherical micelles, rod-like micelles, disc-like micelles, bilayers, and vesicles.[7] Furthermore, by changing solution conditions (temperature, pressure, surfactant concentration, salt type, and salt concentration) one can vary the magnitude of the forces which drive aggregate formation, leading to a change in the balance of forces within a micellar aggregate (intra-aggregate or intramicellar forces), and therefore to a change in the aggregate structure. For example, it is observed that increasing the temperature can induce growth of spherical nonionic micelles into rod-like micelles having higher aggregation numbers[8].

In ordinary colloidal particles, these changes in the particles themselves are not observed, mainly because the atoms in a colloidal particle are held together by chemical bonds (either covalent or metallic). Therefore, in spite of the fact that the interactions are of the same type in the colloidal system and in the micellar solution, the response of the two systems to the environment is essentially different. The dependence of the intramicellar forces on solution conditions, which results in changing the interacting species themselves, adds a new dimension to the study of interactions in micellar systems which is not present in ordinary colloidal dispersions.

II. BRIEF HISTORICAL SKETCH

The 1917 work of Irving Langmuir established that the formation of surfactant

monolayers resulted from the very significant difference in the solubility of the polar heads and the hydrocarbon tails in water, and not from a chemical reaction, or any type of chemical bonding.[9] He was thus the first to recognize and show the physical character of the forces of aggregation of amphiphilic molecules.[10] Based on Langmuir's principle, some important landmarks in surfactant science resulted: the structure of soap, as interpreted by Perrin[11] in 1918, the lipid bilayer structure of biomembranes proposed by Gorter and Grendel[12] in 1925, and the Hartley model of a micelle[3], otherwise known as the alkane-sphere model. This model[3] describes the micelle as a hydrocarbon-like core surrounded by a polar layer of heads, counterions (if the surfactant molecules are ionic), and water.

Theoretical Developments. It is evident that micellization of surfactant molecules has been recognized for decades. Initially, standard thermodynamic treatments were used to characterize micellization. These treatments included: (i) the pseudo-phase model[13], which considers the micelles as another phase and thereby describes micellization as a phase-separation phenomenon, (ii) the monomer-micelle equilibrium model[3], which assumes equilibrium between monomers and monodisperse micelles, (iii) the multiple-equilibrium model[14], where each *n*-mer (micelle composed of *n* monomers) is treated as a distinct species, and where chemical equilibrium exists between the free monomers and each of the n-mers, and (iv) the small-system model which uses small-system thermodynamics[15]. The multiple-equilibrium model is capable of treating the formation of nonspherical micelles and the polydispersity of micellar sizes[16].

The importance of molecular interactions in understanding and characterizing the micellization process was treated in detail by Tanford in 1973[4]. It was then recognized that micellization reflects a balance between the hydrophobic effect, which tends to drive micellization, and the repulsive head interactions, which tend to oppose micellization. Since then, numerous authors have made more extensive studies which identified other interactions involved in micellization, and which went deeper into the understanding of these interactions. In this way, these interactions were integrated into micellization theories, increasing the accuracy of the predictions

of the various theories. Included among the additional considerations made are (i) packing arguments[7b], (ii) interfacial tension at the hydrocarbon core-aqueous solution interface, loss in translational and rotational degrees of freedom of the monomers upon micellization, and hydrocarbon-hydrocarbon interactions[17], (iii) the free-energy change associated with hydrocarbon-chain packing for different micellar shapes (based on the loss in the conformational degrees of freedom of the hydrocarbon chains upon micellization[18]), and (iv) incorporation of curvature effects on the interfacial component of the free energy of micellization, an explicit calculation of the "optimum" equilibrium values of the micellar-core minor radius and the free energy of micellization, for a given micellar shape, a computational procedure to determine whether the micelles exhibit two-dimensional, one-dimensional, or no growth, all introduced recently in the context of a molecular-thermodynamic framework[19]. The molecular-thermodynamic framework builds on a proposed thermodynamic theory of micelle formation and growth (into rod-like micelles) which is able to explain the experimental evidence for micellar size polydispersity.[20]

Intermicellar interactions, recognized to be an important aspect of micellar systems and essential to the description of observed phase-separation phenomena, have been treated in various theories. The most common ones make use of the Flory-Huggins polymer theory, treating the micelles as monodisperse polymers[21]. These theories are limited, however, since they do not incorporate polydispersity, and they completely disregard the dynamic nature of the micelles through their neglect of chemical equilibrium conditions. In addition, these theories fail to predict the experimentally observed surfactant solution behavior. The first theory of micellization which incorporated polydispersity, chemical equilibrium, and intermicellar interactions and which was able to predict in a self-consistent way various micellar solution properties was a phenomenological theory proposed by Blankschtein, et al., in 1986[22]. This theory contains two phenomenological parameters: $\Delta\mu$, embodying the driving force for micellar growth, and, C, a phenomenological interaction parameter. Determination of the values of these parameters from coexistence curve

data, for example, makes possible the prediction of other solution properties such as the weight-average micellar aggregation number, and the osmotic compressibility. A recently developed molecular-thermodynamic framework[19] makes possible the independent determination of the value of $\Delta\mu$ to be used in this theory. The logical offshoot would be the independent determination of the interaction parameter, C, which will be attempted in this thesis.

III. MOTIVATION AND RESEARCH GOALS

The central goal of this thesis is the prediction of micellar characteristics and phase behavior of aqueous salt solutions of alkyl poly(ethylene oxide), C_iE_j, nonionic surfactants. Note that in this thesis, the hydrophilic poly(ethylene oxide) chain (E_j) in C_iE_j surfactants will be referred to as the "head", and the hydrophobic alkyl chain (C_i) will be referred to as the "tail". The predictions made include (i) the onset of micellization, described by the critical micelle concentration (CMC), the surfactant concentration at which micelles first form, (ii) the shape of the micelles, (iii) the micellar size distribution, (iv) the separation of an isotropic micellar solution into two coexisting phases, (v) the crossover surfactant concentration marking the transition of a micellar solution from the dilute to the semidilute regimes, and (vi) the solution viscosity. The theoretical approach involves constructing a free-energy model which incorporates explicitly the molecular architecture of the C_iE_j surfactant molecules, as well as solution conditions, specifically salt type and concentration, as well as temperature. The free energy of the system was modelled as the sum of three additive contributions, the free energy of forming the micellar aggregates, the entropy contribution reflecting the various spatial configurations of the micelles and the solvent molecules, and the contribution from the interactions between micellar aggregates. From the resulting free-energy expression, chemical potentials of the various solution species have been calculated, leading to the prediction of thermodynamic properties of the solution.

The construction of the free-energy model entails an understanding of the

interactions that exist both at the micellar level (intramicellar interactions), as well as between micellar aggregates (intermicellar interactions). In contrast to ionic micellar systems, where Coulombic interactions play the dominant role, the various intramicellar interactions involved in the formation of the C_iE_j nonionic micelles considered in this thesis, as well as the intermicellar interactions between C_iE_j nonionic micelles, are delicately balanced, and therefore must be modelled with great care. In this thesis, for example, a new description of the interactions between PEO head chains in the micelle head layer was formulated. Whereas a previous molecular model of micellization[19] developed by our group made use of steric-type interactions between effective disc-like heads on the micellar core surface, the theoretical description in this thesis accounts explicitly for the chain characteristics of the PEO heads, and calculates the free-energy change associated with transferring (and subsequently grafting at one end) the PEO chains from the bulk solution to the micelle head layer. Furthermore, an understanding and quantification of salt effects on the various intramicellar interactions was developed, which made possible the theoretical prediction of critical micelle concentrations, as well as salt-induced micellar growth. Extensive micellar growth was anticipated to lead to the formation of transient entangled micellar nets which could, in turn, lead to changes in solution properties such as viscosity[23], as well as the partitioning behavior of macromolecules in coexisting micellar solution phases[24]. A computational framework to predict the change in the underlying structure of the micellar solution from the dilute regime (singly-dispersed rod-like micelles) to the semidilute regime (entangled transient net of elongated, rod-like micelles) was thus developed. Finally, a molecular clarification of the mean-field interaction parameter, C, describing the phase behavior of the micellar solution was also accomplished. These entailed detailed calculations of (1) van der Waals interactions between micellar cores of various shapes (spheres and rods), and (2) interactions between micelle head layers, which behave in a way similar to short polymer brushes, and can thereby either stabilize the micelles in an isotropic solution, or become the source of an attractive potential, due to the interpenetration of head chains in poor-solvent conditions leading to liquid-liquid

phase separation. All these calculations were motivated by the desire to predict the phase behavior of C_iE_j micellar solutions in the presence of salts.

In parallel to the theoretical modelling work described above, experiments were conducted to probe the nature of the salt effects on both intramicellar and intermicellar interactions. Surface tension measurements were conducted to gain insight into the competing interactions of the ions and the surfactants at the macroscopic solution-air surface, as well as to determine the value of the critical micelle concentration. Viscosity measurements were conducted to examine the dilute to semidilute transition occurring in C_iE_j micellar solutions which exhibit significant micellar growth. Light scattering measurements were conducted to probe micellar shapes and sizes, as well as to determine the effect of salts and temperature on the micellar size distribution. Finally, phase separation studies were conducted to probe the magnitudes of the various forces contributing to the observed intermicellar interactions, and the effects of salts on these forces. The combination of theoretical analysis and experimental measurements led to a deeper understanding of the phase behavior of isotropic micellar solutions in the presence of salts. This, in turn, may lead to a more efficient utilization of these surfactant salt solutions in the various fields of applications.

Applications. Even though the production of nonionic surfactants, which parallels the demand for them, is still second to that of anionic surfactants, the production, relative to the anionic surfactants, has been increasing from year to year. Nonionic surfactants are thus playing a more dominant role in the surfactant industry[13]. The key properties of surfactants which make them essential in the different applications include emulsification and deemulsification, wetting, foaming, dispersing, defoaming, detergency, and solubilizing.

Industries will benefit from a deeper understanding of salt effects on nonionic micellar systems. In the first place, the major industrial applications of nonionic surfactants are in settings where the solvent is not devoid of electrolytic impurities. Hard-water conditions are typical in these applications. Thus, any understanding of

pure surfactant solution behavior should be extended to surfactants in salt solutions. In the second place, salt type and salt concentration provide additional means of controlling surfactant phase behavior. Thus, a knowledge of how salts affect surfactant phase behavior would provide industries with a way to increase the efficiency and versatility of utilization of these surfactants.

The remainder of this thesis is structured as follows. Chapter II describes the effects of salts on intramicellar interactions, micellization, and micellar growth, and, in particular, on the value of the critical micelle concentration. Chapter III describes the light scattering measurements (both intensity and quasielastic light scattering), which were utilized to study the growth (or the suppression of growth) of micelles upon the addition of salts, as well as raising the temperature and increasing surfactant concentration. Chapter IV considers in detail micellar systems that exhibit extensive one-dimensional growth, exploring the possibility of micellar entanglements, and the resulting changes in solution structure and behavior resulting from these entanglements. Chapter V focuses on intermicellar interactions, the effects of salts on these, and changes in solution phase behavior due to the presence of salts. In particular, the occurrence of phase separation is analyzed, and attempts are made to both rationalize and predict the solution phase separation in the presence of salts. Finally, Chapter VI summarizes the accomplishments of this thesis, and discusses possibilities for future work.

REFERENCES FOR CHAPTER 1

1. Laughlin, R. G. *Advances in Liquid Crystals* **1978**, *3*, 41. It was emphasized that not all molecules composed of a hydrophilic head and a hydrophobic tail (often called amphiphiles) can be called surfactants. The head should be sufficiently hydrophilic in order to exhibit surfactant behavior.

2. Davies, J. T.; and Rideal, E. K. Interfacial Phenomena, 2nd Ed., Academic Press, New York (1963).

3. Hartley, G. S. Aqueous Solutions of Paraffin-Chain Salts, Hermann and Cie, Paris (1936).

4. Tanford, C. The Hydrophobic Effect: Formation of Micelles and Biological Membranes, John Wiley & Sons, Inc., New York (1973).

5. Evans, D. F. *Langmuir* **1988**, *4*, 3.

6. Israelachvili, J. N. Intermolecular and Surface Forces, Academic Press Inc. Ltd., London (1985).

7. (a) Corkill, J. M.; Goodman, J. F. *Advan. Colloid Interface Sci.* **1969**, *2*, 297.
   (b) Israelachvili, J. N.; Mitchell, D. J.; Ninham, B. W. *J. Chem. Soc. Faraday Trans. 2* **1976**, *72*, 1525.

8. Nilsson, P. G.; Wennerstrom, H.; Lindman, B. *Chemica Scripta* **1985**, *25*, 67.

9. Langmuir, I. *J. Am. Chem. Soc.* **1917**, *39*, 1848.

10. The development was described by K. A. Dill, in Surfactants in Solution, (Mittal, K. L. and Lindman, B., eds.), Plenum Press, New York (1984).

11. Perrin, J. *Ann. Phys.* **1918**, *9*, 160.

12. Gorter, E.; Grendel, F. *J. Exp. Med.* **1925**, *41*, 439.

13. Stainsby, G.; Alexander, A. E. *Trans. Faraday Soc.* **1950**, *46*, 587.

14. Corkill, J. M.; Goodman, J. F.; Walker, T.; Wyer, J. *Proc. Roy. Soc. A* **1969**, *312*, 243.

15. Hall, D. G.; Pethica, B. A. Nonionic Surfactants, (ed. M. J. Shick), Arnold, London (1967).

16. Reiss-Husson, F.; Luzzati, V. *J. Phys. Chem.* **1964**, *68*, 3504.

17. Nagarajan, R.; Ruckenstein, E. *J. Coll. Int. Sci.* **1979**, *71*, 580.

18. Gruen, D. W. R.; Lacey, E. H. B., in Surfactants in Solution, Vol. 1, (ed. K. L. Mittal), Plenum Press, New York (1984). Ben-Shaul, A.; Szleifer, I.; Gelbart, W. M. *J. Chem. Phys.* **1985**, *83*, 3597. Dill, K. A.; Flory, P. J. *Proc. Nat'l Acad. Sci.* **1980**, *77*, 3115. Dill, K. A. *Adv. Coll. Int. Sci.* **1986**, *26*, 99.

19. Puvvada, S.; Blankschtein, D. *J. Chem. Phys.* **1990**, *92*, 3710.

20. Missel, P. J.; Mazer, N. A.; Benedek, G. B.; Young, C. Y.; Carey, M. C. *J. Phys. Chem.* **1980**, *84*, 1044.

21. (a) Doren, A.; Goldfarb, J. *J. Colloid and Interface Science* **1970**, *32*, 67.
(b) Weckstrom, K.; Zulauf, M. *J. Chem. Soc., Faraday Trans.1* **1985**, *81*, 2947.
(c) Kjellander, R. *J. Chem. Soc. Faraday Trans. 2* **1982**, *78*, 2025.

22. (a) Blankschtein, D.; Thurston, G. M.; Benedek, G. B. *Phys. Rev. Lett.* **1985**, *54*, 955.
(b) Thurston, G. M.; Blankschtein, D.; Fisch, M. R.; Benedek, G. B. *J. Chem. Phys.* **1986**, *84*, 4558.
(c) Blankschtein, D.; Thurston, G. M.; Benedek, G. B. *J. Chem. Phys.* **1986**, *85*, 7268.

23. Carale, T. R.; Blankschtein, D. *J. Phys. Chem.* **1992**, *96*, 459.

24. Nikas, Y. J.; Liu, C. L.; Srivastava, T.; Abbott, N. L.; Blankschtein, D. *Macromolecules* **1992**, *25*, 4797.

CHAPTER 2. THE EFFECT OF SALTS ON THE FORMATION OF NONIONIC SURFACTANT MICELLES

I. INTRODUCTION

The addition of a third component, such as salts, to a surfactant-water solution may result in a modification of both intramicellar and intermicellar interactions. Consequently, solution properties, such as the critical micelle concentration, the surfactant concentration at which micelles first begin to form, as well as the phase behavior of the system, may be modified significantly when salts are added to surfactant solutions. An understanding of how salts affect the behavior of surfactant solutions may lead to a more effective utilization of these systems in various applications.

The nonionic surfactants chosen for the studies reported in this thesis belong to the alkyl poly(ethylene oxide), C_iE_j, family. These surfactants are useful model systems, because by varying the number of methylene groups, *i*, in the hydrophobic alkyl tail, or the number of ethylene oxide units, *j*, in the hydrophilic head, a systematic study of the effect of salts on these surfactants can be conducted. Specifically, experiments were conducted using the surfactants $C_{12}E_6$, $C_{10}E_6$, and $C_{12}E_8$. The salts were likewise chosen in order to identify the effects of varying both the anion and the cation, by using the salts KCl, KBr, KI, and LiCl, NaCl, KCl, respectively.

Experimental studies of salt effects on the critical micelle concentration of nonionic surfactants, primarily of the alkyl (C_i) or alkylphenoxy (C_iPh) poly(ethylene oxide), E_j, type, have been conducted in the past.[1,2,3,4,5,6,7] These studies showed that most salts lower the critical micelle concentration (CMC), and, in most cases, the effect on the CMC follows the relation

$$\ln cmc = \ln cmc_{nosalt} - k_s m_s \,, \qquad (1)$$

where k_s is a constant numerical coefficient which depends on the type of salt, and m_s is the salt molality. The salt effects were correlated to the Hofmeister series, which is derived from studies on the salting-out of proteins[8]. It was also found that the salt effects were virtually independent of the number of ethylene oxide units in the hydrophilic head[6].

Theoretically, salt effects on the CMC of nonionic surfactants have been investigated in the past in the context of the mass-action model[9] of micellization, as well as the pseudo-phase separation model[10,5] of micellization. In both models, the activity coefficient of the surfactant monomer is expressed as the sum of two contributions, one resulting from the hydrophilic (head) moiety, and the other from the hydrophobic (tail) moiety. The effect of the salts on the activity coefficient of the surfactant tail can then be estimated from solubilities of these alkanes in aqueous salt solutions. More specifically, the empirical solubility relation of the series methane to butane in NaCl solutions[11] was used to estimate the solubility of higher alkanes, and thereby estimate the activity coefficient of a surfactant monomeric tail in NaCl solutions. The contribution from the head was then deduced from the experimentally measured variation of the CMC with salt concentration, and the independently estimated activity coefficient of the tail. The utilization of these two models, the mass-action[9] and pseudo-phase separation[10] models, yielded conflicting results regarding the salt effects attributed to the heads. Specifically, using the mass-action model, the effect of increasing the concentration of NaCl on the activity coefficient of the poly(ethylene oxide), PEO, head was found to be negligible as compared to the effect on the tail[9], while the use of the pseudo-phase separation model showed a very significant "salting-out" contribution of the head[10]. This "salting-out" effect, which corresponds to a decrease in the activity coefficient of the heads, indicates that the transfer of the heads from the bulk solution to the micelle head layer is very much enhanced in the presence of these "salting-out" ions. Therefore, the value of the CMC is lower in the presence of these "salting-out" ions.

In this chapter, a recently developed molecular theory of micellization[12] was implemented and generalized to predict salt effects on micellization of nonionic surfactants belonging to the C_iE_j series. By more systematically accounting for the various molecular contributions to the micellization process, as well as working with free-energy changes rather than with activity coefficients, this theory circumvents the existing controversy between the mass-action and pseudo-phase separation treatments of salt effects on micellization, as well as the limitations of these approaches. In this thesis, the original molecular theory of micellization[12] was generalized in order to account for the salt effects on the various micellization free-energy contributions. The McDevit-Long theory[13], used in earlier works to rationalize salt effects on the activity coefficients of hydrocarbon tails[9], was utilized here in a slightly different context to quantitatively capture the effect of salts on the formation of the micellar hydrocarbon cores. Macroscopic determinations of salt effects on interfacial tensions were used to capture the corresponding effects at the molecular level, that is, on the aqueous solution-micellar core interfacial free energy. A further generalization of the original theory consists of explicitly incorporating the chainlike character of the short PEO heads. Indeed, instead of representing the PEO heads as hard discs residing at the micellar-core surface, as was done in the original theory[12], in this chapter we will model the PEO heads as short polymer chains grafted to the micellar-core surface. Whereas in the original theory, the contribution of the hydrophilic heads to the micellization free energy was in the form of a steric repulsive term, in the theory presented in this chapter, the contribution of the PEO heads is in the form of a free-energy change associated with transferring the polymeric PEO heads from bulk solution (the monomer phase) to the micelle head layer, which was modelled as a solution of grafted polymeric (PEO) chains. The magnitude of the head transfer free energy depends on several factors, including the number of EO units in the head, the shape of the micellar core, and the quality of the solvent, which, in turn, may be affected by the type and concentration of added salt, as well as by changes in the solution temperature.

The theoretical predictions presented in this chapter were done without

utilizing any freely adjustable parameters. These predictions will be compared to results from a systematic experimental CMC study, using the surface-tension method, on the effects of various salts (LiCl, NaCl, KCl, KBr, KI) on the CMC of the nonionic surfactants $C_{12}E_6$, $C_{12}E_8$, and $C_{10}E_6$.

The remainder of this chapter is organized as follows. Section II describes the modifications and generalizations made to the recently developed molecular theory of micellization in order to account for the salt effects on the CMC. Section III describes the surface tension measurements conducted to determine CMC's. Section IV presents the experimental results, and compares these with the results of the theoretical calculations. Finally, Section V presents some concluding remarks.

II. THEORY

The theory presented below is based on a recently developed molecular-thermodynamic theory[12], which was generalized to predict the CMC's of C_iE_j nonionic surfactants in aqueous solutions in the presence of various salts. This theoretical approach blends a molecular theory of micellization[12], which captures the essential physico-chemical forces operating at the micellar level, with a thermodynamic framework for micellar solutions[14], which captures the salient features of the solution at the macroscopic level.

The molecular-thermodynamic theory of micellization has been successfully utilized in the past to predict micellar properties of aqueous solutions of single[12] as well as mixed[15] nonionic surfactants, belonging to the alkyl poly(ethylene oxide) and glucoside families, as a function of surfactant molecular architecture, surfactant concentration, temperature, and urea concentration[16] (an additive that changes the solvent quality). The predicted properties, such as the CMC, micelle shape, micelle size distribution and its characteristics, coexistence curves (including the critical surfactant concentration for phase separation), and other thermodynamic properties such as the osmotic compressibility, compare favorably with available experimental data. The thermodynamic framework has also been successfully utilized to describe

the phase behavior of aqueous solutions of zwitterionic surfactants, in the presence of added electrolytes[17] and urea[18] over a wide range of surfactant concentrations and temperatures. More recently, the theoretical framework has been utilized for the theoretical predictions of the crossover surfactant concentrations (marking the transition from the dilute micellar solution regime to the semidilute micellar solution regime)[19], as well as surface tensions[20], of aqueous solutions of C_iE_j surfactants. These predictions were found to compare favorably with available experimental data.

The following discussions will describe the molecular theory of micellization, emphasizing each of the contributions to the free energy of micellization, and the salt effects on these contributions. A discussion of the method for estimating the CMC from the free energy of micellization, in the context of the molecular theory of micellization, will then follow.

A. Molecular Theory of Micellization

Micellization involves the aggregation of monomers such that the hydrocarbon tails cluster together, with the heads oriented towards the aqueous solution forming a "polar" shell. This aggregation behavior limits the contact between the tails and the aqueous solution.

There is no direct method to calculate the free-energy change involved in micellization. Thus, models are typically devised to simulate micelle formation. The molecular theory of micellization[12], which generalizes and improves on previous work[21,22], is based on the well-known thermodynamic principle that the free energy is a state function, and thus, an overall reversible reaction, like the micellization process, can be replaced by a series of simpler, well-characterized, reversible reactions connecting the initial state with the final state. Thus, the chosen initial state for the formation of an n-mer is n monomers free in solution, while the final state is an n-mer in the same solution.

As stated earlier, we have generalized the molecular theory of micellization[12] to incorporate the effects of salts on the free energy of micellization, $g_{mic}(n,l_c,S)$.

Note that $g_{mic}(n,l_c,S)$ is the free-energy change per surfactant molecule associated with forming a micelle at a fixed position in bulk solvent, having aggregation number, n, core-minor radius, l_c, and shape, S, from n monomers dispersed in solution. In the context of this theory, a conceptual thought process was introduced whereby the micellization of C_iE_j surfactant molecules can be broken down into a series of steps, each reflecting an important physico-chemical factor involved in micellization. Specifically, the following steps are involved: (1) breaking the surfactant head-tail bond, (2) transferring the tail from the aqueous salt solution (*s*) to bulk hydrocarbon (*hc*), characterized by a free-energy contribution, $g_{s/hc}$, (3) forming the aqueous-micellar hydrocarbon core interface, characterized by a free-energy contribution, g_σ, (4) packing the hydrocarbon chains within the micellar core with one end of each chain attached to the interface, characterized by a free-energy contribution, g_{pack}, (5) the reformation of the head-tail bond (where the free energy of forming the bond is assumed to be equal in magnitude and opposite in sign to that of breaking it), and (6) the transfer of the heads from the bulk salt solution (*s*) to the micelle head layer (*hl*), characterized by a free-energy contribution, $g_{s/hl}$. Note that since the heads are nonionic, it was assumed that the electrostatic free-energy contribution, g_{elec}, is vanishingly small, that is, we assumed that $g_{elec}=0$ for these surfactants. Thus, the free energy of micellization can be expressed as follows

$$g_{mic} = g_{s/hc} + g_\sigma + g_{pack} + g_{s/hl} \cdot \qquad (2)$$

The four free-energy contributions to g_{mic} shown in Eq (2) will be briefly discussed below, with the goal of identifying and predicting the mode by which the presence of salts in the solution would affect each of these contributions.

a. The Transfer of the Hydrocarbon Tails from the Salt Solution to Bulk Hydrocarbon. The hydrophobic driving force for micellization can be viewed operationally as the free-energy change involved in the transfer of the hydrocarbon tails, the hydrophobic part of the surfactant, from the aqueous salt solution (*s*) to

bulk hydrocarbon (*hc*). This transfer free-energy contribution, $g_{s/hc}$, can be estimated from solubility data of hydrocarbons in the aqueous salt solution. Specifically,

$$g_{s/hc} = kT \ln s_s \,, \tag{3}$$

where s_s is the solubility of the hydrocarbon in the salt solution. However, there is very little available solubility data of hydrocarbons in salt solutions, primarily because of their very low solubility in salt solutions as compared to that (which is already low) in pure water. In general, the low solubility of hydrocarbons in aqueous solutions can be rationalized in terms of the relatively large work contribution required to create a cavity in order to accommodate the nonpolar surfactant tail. This work reflects the strong attractive forces (particularly of the hydrogen-bond type) that exist between water molecules, which have to be weakened in order to create the cavity. The addition of salts to water increases this already large work contribution even more, because the polarizing power of the ions binds water molecules more strongly to each other, thus resulting in stronger solvent-solvent interactions, where the ions are considered part of this "hypersolvent". This low solubility of hydrocarbons in aqueous salt solutions makes solubility measurements difficult; hence the absence of available experimental solubility data. Therefore, the transfer of the surfactant tails from the aqueous salt solution (*s*) to bulk hydrocarbon (*hc*), a reversible thermodynamic process, was decomposed into two transfer processes: (1) the transfer of the tails from the aqueous salt solutions to water (*w*), with a corresponding free-energy change, $g_{s/w}$, and (2) the subsequent transfer of the tails from water (*w*) to bulk hydrocarbon (*hc*), with a corresponding free-energy change, $g_{w/hc}$. Accordingly, $g_{s/hc}$ can be expressed as

$$g_{s/hc} = g_{s/w} + g_{w/hc} \,. \tag{4}$$

The free-energy change corresponding to the second transfer step, $g_{w/hc}$, can be estimated from available solubility data of hydrocarbons in pure water[23]. Specifically,

$$g_{w/hc} = kT \ln s_w \,, \tag{5}$$

where s_w is the solubility of the hydrocarbon tails in pure water. The free-energy change involved in the first step, $g_{s/w}$, was estimated using the McDevit-Long theory[13]. Specifically,

$$\lim_{C_{hc}\to 0, C_s \to 0} \frac{d(g_{s/w})}{dC_s} = \frac{v_c(\bar{V}_s^o - V_s)}{\beta_o} \,, \tag{6}$$

where C_{hc} is the concentration of the hydrocarbon tails in the aqueous salt solution, C_s is the molarity of the salt, v_c is the volume of a hydrocarbon tail, V_s is the molar volume of pure (liquid) salt, $\bar{V}_s^0$ is the partial molar volume of salt at infinite dilution, and β_o is the compressibility of water[24]. Note that Eq.(6) is valid in the limit of low concentrations of the hydrocarbon tails, and, therefore, is particularly appropriate for hydrocarbons in aqueous salt solutions. In deriving Eq.(6), it was assumed that the only role of the solute molecules (the hydrocarbon tails in this case) is to modify the ion-water interactions by occupying volume. Building on this simple concept, it was shown[13] that the excess work done against the ion-solvent forces upon the introduction of the nonpolar solute volume, v_c, into a salt solution having low salt molarity, is proportional to the volume change which occurs upon mixing (liquid) salt and water. Eq.(6) indicates that the contraction in the total solution volume upon mixing salt and water, which results in an increase in internal pressure, makes it more difficult to "insert" the volume of the nonpolar solute. Since it has been found experimentally[13] that the free energy of transfer, $g_{s/w}$, varies linearly with salt concentration over a wide range of salt concentrations, Eq.(6) can be integrated to yield

$$g_{s/w} = \frac{v_c(\bar{V}_s^o - V_s)}{\beta_o} C_s \,. \tag{7}$$

In order to calculate the free energy of transferring a tail from bulk aqueous salt

solution to the micellar hydrocarbon core, we need to define precisely which part of the surfactant molecule constitutes the tail and which part constitutes the head. In our considerations, the last methylene group (CH_2) of a hydrocarbon chain composed of n_c carbon atoms, was considered part of the head, since it is in direct contact with the aqueous salt solution. Therefore, this last methylene group is not explicitly "transferred" from the aqueous salt solution to the micellar hydrocarbon core. The tail will thus be defined as the hydrocarbon chain containing (n_c-2) CH_2 groups and one CH_3 group, a total of (n_c-1) carbon atoms, while the head will include the last CH_2 group, the j ethylene oxide units, and the terminal hydroxy (-OH) group.

The volume of the hydrocarbon tail, v_c, was estimated using the empirical equation introduced by Tanford, v_c = 27.4 + 26.9 (n_c-1), where v_c is in units of $Å^3$/molecule[21]. A compilation of $\bar{V}_s^0$ data has been done[25], and is reported in the third column of Table I. Note that values of V_s cannot be measured (except at temperatures above the melting point of the salt), and therefore were estimated as discussed below in Section IVb1.

b. Formation of a Hydrocarbon Core-Salt Solution Interface. The next step in the micellization thought process is the formation of the hydrocarbon core-aqueous salt solution interface, which represents a free-energy cost to micellization. The resulting interfacial free-energy change per monomer is estimated as follows[12]

$$g_o = \sigma_o\left(1-\frac{(S-1)\delta}{l_c}\right)(a-a_o)\ , \qquad (8)$$

where σ_o is the interfacial tension between bulk hydrocarbon and the salt solution, δ is the Tolman distance[26], a measure of the interfacial thickness, a is the interfacial area per monomer [= Sv_c/l_c, where S is a shape factor (3 for spheres, 2 for cylinders, and 1 for discs or bilayers), and l_c is the micellar core-minor radius], and a_o is the screened interfacial area per monomer which corresponds to the bond between the hydrocarbon tail and the head (typically 21$Å^2$).

The addition of salts to pure water will increase the (organic-aqueous)

interfacial free energy, as reflected by the increase in the (organic-aqueous) interfacial tension as the salt concentration is increased[27]. The low dielectric constant of the hydrocarbon medium drives the ions deeper into the aqueous phase where the ions can surround themselves with polarized water molecules. Therefore, the polarizing power of the ions makes it energetically more favorable for them to be farther away from the interface, resulting in an apparent repulsion (desorption or negative adsorption) between the interface and the ions. This desorption of the ions from the organic-aqueous interface can be correlated to the change in the interfacial tension (as a function of the salt activity, $a_s = \gamma_s m_s$, where γ_s is the activity coefficient of the salt in water, and m_s is the salt molality), as seen in the Gibbs Adsorption Equation[28],

$$\Gamma_s^{(w)} = -kT\frac{d\sigma}{d(\ln a_s)}, \qquad (9)$$

where $\Gamma_s^{(w)}$ denotes the relative salt adsorption onto the interface, which in the case of most salts, except iodides, is negative, giving a positive gradient of the interfacial tension with salt activity, and correspondingly, with salt concentration[28]. In general, the higher the ion surface charge density (the smaller the bare ion radius), the more polarizing it is, and consequently, the greater the desorption from the interface [more negative $\Gamma_s^{(w)}$], and the greater the magnitude of the increase in the interfacial free-energy [$d\sigma/d(ln\ a_s)$]. The salt concentration dependence of the hydrocarbon-water interfacial tension, σ, at 25°C has been determined[27] for dodecane and decane, and is reported for dodecane in the second column of Table II. These values can be used in Eq.(8) to estimate the value of g_σ. It should be noted that there is very little perceivable difference between the salt effects on $\sigma_{dodecane}$ and σ_{decane}[27]. Therefore, it was assumed that the values reported in Table II can be used for both the C_{11} and C_9 tails corresponding to the surfactants examined in this chapter.

Experimentally, it was observed that for the salts examined, the interfacial tension is a linear function of salt concentration up to $m_s \approx 1$ molal[27]. In this chapter, on the other hand, salt concentrations as high as 3 molal were examined. It should

be noted, however, that the surface tensions of aqueous salt solutions increase linearly with salt molality for concentrations of up to 4 molal[24]. Therefore, it was assumed that the linearity in the aqueous salt solution-hydrocarbon interfacial tension observed in the studies reported in Ref. 27 extends to higher salt concentrations (up to 3 molal), similar to the observed linearity in the variation of the aqueous salt solution surface tension with salt concentration[24].

c. Packing of the Hydrocarbon Tails in the Micellar Core. This free-energy contribution arises from the loss of conformational degrees of freedom of the tails upon anchoring one end of each tail at the micellar core-aqueous solution interface[12]. As discussed in Section IIAa, only (n_c-1) carbon atoms were considered part of the tail, and consequently, only (n_c-1) carbon atoms were included in the packing calculations. This step in the micellization process is independent of salt conditions, since it focuses exclusively on the environment within the micellar core. The repulsive contribution, g_{pack}, is calculated by using a single-chain mean-field approximation.[29] The calculation involves the use of the rotational isomeric state approximation to generate a large number of conformations of a single tail inside the micellar core. Typically, the evaluation of g_{pack} needs to be performed numerically. Recently, however, the numerical values of g_{pack} were fitted to a second-order polynomial of the form[30]

$$g_{pack} = A_2(l_c/l_{max})^2 + A_1(l_c/l_{max}) + A_0 \ , \qquad (10)$$

where l_c is the micellar core-minor radius, and $l_{max} = 1.54 + 1.265(n_c\text{-}1)$, in Å, is the fully extended length of the hydrocarbon tail having (n_c-1) carbon atoms. The values of the coefficients A_0, A_1, and A_2 were tabulated for various micellar shapes, and for hydrocarbon tails having 6 to 16 carbon atoms[30].

d. The Interactions between the Hydrophilic PEO Heads. The last contribution which may be affected by the presence of salts is the free-energy change, $g_{s/hl}$, due

to the transfer of the poly(ethylene oxide), PEO, heads from the bulk solution (*s*) to the micelle head layer (*hl*), and the subsequent "grafting" of the PEO head chains at one end onto the micellar-core surface. In the original molecular theory of micellization[12], this contribution was modelled using an ideal-localized monolayer, that is,

$$g_{s/hl} = -kT \ln\left(1 - \frac{a_h}{a}\right), \tag{11}$$

where k is the Boltzmann constant, T is the absolute temperature, a_h is the average cross-sectional area of the head, and a is the previously defined interfacial area per monomer. In essence, the head was modelled as an effective hard disc whose cross-sectional area, a_h, was estimated from chain properties of PEO, and was assumed to be independent of the shape of the micelle, S, and the micellar core-minor radius, l_c. The effective disc model was then utilized to compute $g_{s/hl}$, through the use of a scaling relation, $a_h(j) = a_h(6)(j/6)^y$, where the two parameters, $a_h(6)$ and y were estimated from experimental data[12]. The effective disc model assumed that a_h is independent of S and l_c. It is evident, however, that the effective disc model does not account for the chain-like character of the PEO heads. In order to address these issues, the calculation of $g_{s/hl}$ in this chapter attempts to improve on Eq.(11)[12] by accounting explicitly for the chain-like character of the PEO head chains in calculating this free-energy contribution. Prior to this work, the PEO micelle head layers were modelled as polymer solutions, using one of two simplifying assumptions: (*i*) uniform concentration of polymer segments, and (*ii*) uniform deformation of polymer chains[31]. Flory's mean-field approach was utilized in Ref.31 to model the polymer solution. Other theoretical approaches are available which have been applied to the micellization of block copolymers. Among these are scaling theories (blob models)[32], and the self-consistent field model[33]. Note, however, that scaling theories cannot be used because the heads are short PEO chains, and that "blobs" are physically reasonable only for long polymer chains.

In the micellization process, a monomeric head, in particular a short PEO

chain in our case, is transferred from the bulk aqueous salt solution (*hb*) to the micelle head layer (*hl*) where it is subsequently grafted to the micellar-core surface. The PEO head of a monomeric surfactant molecule in bulk aqueous salt solution is represented as an isolated free PEO chain in an infinitely dilute solution, $\phi_{hb} \to 0$ (recall that the monomer concentration is of the order of the CMC, which is very low). On the other hand, the PEO chains present in the micelle head layer can be modelled as a solution of grafted PEO chains having a head volume fraction, ϕ_{hl}. The free-energy change corresponding to the transfer of a PEO chain from the bulk salt solution (*s*) to the micelle head layer (*hl*), $g_{s/hl}$, is therefore given by

$$g_{s/hl} = g_{hl}(\phi_{hl}) - g_{hb}(\phi_{hb}) \ , \tag{12}$$

where $g_{hl}(\phi_{hl})$ is the free energy of a "grafted" PEO head chain in the micelle head layer, and $g_{hb}(\phi_{hb})$ is the free energy of a singly dispersed PEO chain in the bulk salt solution. Based on the thermodynamic relationship, $g = h + Ts$, where h and s are the enthalpy and entropy per molecule, respectively, Eq.(12) can be rewritten as

$$g_{s/hl} = [h_{hl}(\phi_{hl}) - h_{hb}(\phi_{hb})] - T\,[s_{hl}(\phi_{hl}) - s_{hb}(\phi_{hb})] \ . \tag{13}$$

Note that the entropy of a monomer in the bulk salt solution, and, consequently, the entropy of the PEO head in the bulk salt solution, $s_{hb}(\phi_{hb})$, is not explicitly accounted for in g_{mic}[34]. Instead, in the calculation of g_{mic} it is assumed that the surfactant monomer is transferred into the micelle from a fixed position in the bulk solution. Furthermore, the head is a short PEO chain grafted to the micellar-core surface in the micelle head layer, and, accordingly, has very limited available degrees of freedom, both of the conformational type (since the number of bonds is small), as well as of the translational type (since the chain is grafted). Consequently, it is reasonable to assume that, to leading order, the dominant contribution to the transfer free energy, $g_{s/hl}$, arises from the enthalpy terms in Eq.(13) [minimal entropic contribution, namely, $\Delta h >> T\Delta s$]. Making this approximation, Eq.(13) yields

$$g_{s/hl} \sim [h_{hl}(\phi_{hl}) - h_{hb}(\phi_{hb})] = h_{hb/hl} \ . \qquad (14)$$

The enthalpy change, $h_{hb/hl}$, shown in Eq.(14) originates from the increase in the number of PEO head-head contacts as compared to the number of PEO head-solvent contacts, when a PEO chain is transferred from the bulk salt solution to the micelle head layer. Note that this enthalpy change, $h_{hb/hl}$, is the negative of the enthalpy of dilution per PEO molecule. More specifically,

$$h_{hb/hl} = -\Delta h_{dilution}(\phi_{hl} \rightarrow \phi_{hb}) \ . \qquad (15)$$

Dilution enthalpies for PEO in water have been measured[35]. We fitted the experimental data[35] to the following approximate relation, per EO segment,

$$\Delta h_{dilution} = \nu[\phi_{hb} - \phi_{hl}] \ . \qquad (16)$$

It is noteworthy that the dilution of PEO with water is exothermic[35]. Hence, ν is a positive number, which in our case would represent the enthalpy needed to transfer an EO segment from a dilute aqueous solution, where it is more fully (or completely, in the case of infinitely dilute solutions) surrounded by water molecules, to the micelle head layer where some of the EO-water contacts are replaced by EO-EO contacts. Therefore, using Eqs.(15) and (16) in Eq.(14), the following expression for $g_{s/hl}$ is obtained

$$g_{s/hl} \sim [h_{hl}(\phi_{hl}) - h_{hb}(\phi_{hb})] = -\Delta h_{dilution}(\phi_{hl} \rightarrow \phi_{hb}) = \nu j[\phi_{hl} - \phi_{hb}] \simeq \nu j \phi_{hl} \ , \qquad (17)$$

where j is the number of ethylene oxide (EO) units in the PEO head, and the reasonable assumption that $\phi_{hl} >> \phi_{hb}$ was made.

e. The Head Volume Fraction in the Micelle Head Layer, ϕ_{hl}. The head volume fraction, ϕ_{hl}, which we assume to be constant in the micelle head layer, can be estimated as the ratio of the volume of the PEO head divided by the volume of the micelle head layer per surfactant molecule, v_{hl}. As discussed in Section IIc, the

last methylene group in the alkyl chain is considered part of the micelle head layer. Thus, each PEO head, E_j, having j ethylene oxide units, will have $3j+2$ bonds, the first being a C-C bond, followed by j (C-O,O-C and C-C) bonds, and finally a C-O bond corresponding to the terminal hydroxy group. The volume of the PEO head is given by the product of the number of EO units in the head, $j'=(j+⅔)$, and the volume of an EO unit, V_{EO}, where $V_{EO}=63.5$ (Å^3) is the dry volume of a monomer of polyethylene oxide[36]. Note that we have assumed that the first C-C bond and the last C-O bond have a volume equal to roughly ⅔ that of an EO segment, Therefore,

$$\phi_{hl} \sim \frac{j' V_{EO}}{v_{hl}} . \tag{18}$$

In order to estimate v_{hl}, the thickness of the micelle head layer, l_{hl}, is needed. Subsequently, v_{hl} can be calculated by dividing the total volume of the micelle head layer, which is a function of l_{hl}, by the number of surfactant molecules per micelle. The resulting equations for v_{hl} are

$$v_{hl}^{sph} = \frac{\frac{4}{3}\pi[(l_{hl}+l_c)^3 - l_c^3]}{\frac{4}{3}\pi l_c^3 / v_c} = \frac{v_c[(l_{hl}+l_c)^3 - l_c^3]}{l_c^3} , \tag{19}$$

for spherical micelles, and

$$v_{hl}^{rod} = \frac{\pi L[(l_{hl}+l_c)^2 - l_c^2]}{\pi l_c^2 L / v_c} = \frac{v_c[(l_{hl}+l_c)^2 - l_c^2]}{l_c^2} , \tag{20}$$

for rodlike micelles. Eq.(18) thus becomes

$$\phi_{hl}(l_c) = \frac{(l_c^3 / v_c) V_{EO} j'}{(l_c+l_{hl})^3 - (l_c)^3} , \tag{21}$$

for spherical micelles ($S=3$), and

$$\phi_{hl}(l_c) = \frac{(l_c^2/v_c)V_{EO}\, j'}{(l_c + l_{hl})^2 - (l_c)^2}\ , \qquad (22)$$

for rodlike micelles (S=2). Using these expressions for ϕ_{hl}, Eq.(17) takes the following simple form

$$g_{s/hl}(l_c) \sim \frac{j'jv(l_c^3/v_c)V_{EO}}{(l_c + l_{hl})^3 - (l_c)^3}\ , \qquad (23)$$

for spherical micelles, and

$$g_{s/hl}(l_c) \sim \frac{j'jv(l_c^2/v_c)V_{EO}}{(l_c + l_{hl})^2 - (l_c)^2}\ , \qquad (24)$$

for rodlike micelles. Recall that in Eqs. (21) and (24), $j'=j+\frac{2}{3}$.

The micelle head layer thickness, l_{hl}, was defined as the distance from the micellar-core surface up to which the PEO chain extends into the aqueous environment. In order to estimate this distance, the PEO head chain segment distribution was determined using a method based on the rotational isomeric state (RIS) approximation, combined with a Monte-Carlo approach to generate chain conformations. This method was utilized recently to determine the root-mean-square end-to-end distance of short chains of polyethylene oxide attached to an inert wall[36]. We have extended this method to incorporate curvature effects associated with the shape of the micellar-core surface (cylindrical or spherical). In addition, we have also estimated the effect of the presence of other PEO chains in the micelle head layer on the conformations of a single chain, as well as the effect of the micellar core-minor radius, l_c. In order to account for the effect of the presence of other chains on the conformations of a given PEO head chain, the PEO head is confined within a conical section (see Fig.1a), whose radius, R_r, varies as the distance from the micellar-core surface, r. It is noteworthy that both the value of this "cylinder" radius

at the micellar-core surface, $R_{r=0}$, as well as its variation, R_r, with distance from the core surface, r, depend on the shape of the micellar-core surface. Note that $R_{r=0}$ is the radius corresponding to the area per surfactant molecule at the micellar-core surface, which can be estimated by assuming a constant density in the hydrocarbon core. Specifically, using well-known geometrical arguments[37], one finds that

$$R_{r=0} = \sqrt{\frac{S v_c}{\pi l_c}} , \tag{25}$$

where S is the shape factor introduced earlier ($S=2$ for rods, and $S=3$ for spheres), v_c is the volume of the hydrocarbon tail, and l_c is the micellar core-minor radius. In a similar manner, the area per surfactant molecule can be calculated as one moves away from the micellar-core surface by a distance r. The resulting radius, R_r, for rodlike micelles is given by

$$R_r = R_{r=0} \left(\frac{l_c + r}{l_c} \right)^{\frac{1}{2}} , \tag{26}$$

and for spherical micelles, it is given by

$$R_r = R_{r=0} \left(\frac{l_c + r}{l_c} \right) . \tag{27}$$

Aside from the constraints on the chain conformations discussed in Ref. 36, we have imposed the additional constraint due to the presence of the other chains, as described above. Thus, while generating the chains, a particular conformation of a chain is rejected when a bond goes beyond the conical section defined by the radius given in Eq. (26) [for rodlike micelles], and Eq. (27) [for spherical micelles]. This additional restriction generates more extended conformations of the PEO head chains, as compared to those corresponding to a single chain attached to a wall. As S decreases from 3 (for a sphere) to 2 (for a rod), the radius, R_r, of the confining conical section decreases [compare Eqs. (27) and (26)], which results in more

extended PEO chain conformations. In other words, the lower the curvature of the micellar-core surface, the more extended the chains are, since there is less available space for the chains to expand laterally.

In the determination of the bond-density distribution, the micelle head layer was divided into discrete "shells", such that the number of bonds, n_m, between the mth shell and the $m+1$th shell (see Fig. 1b) can be counted while each of the chain conformations is generated. The thickness of the shells determines the precision of the estimated l_{hl} value. We have chosen to set the thickness of each shell to be 0.5Å. The value of n_m is the average of 40,000 accepted conformations. The cumulative number of bonds, Σn_m, that is, the total number of bonds between the micellar-core surface and the mth shell, was then plotted as a function of the distance from the micellar core. The thickness, l_{hl}, was then estimated as the distance from the micellar-core surface where the limiting value of the total number of bonds $3j' = 3(j + \frac{2}{3}) = 3j + 2$, was approached, see Fig.2. As seen in Fig.2, the l_{hl} values determined numerically are not strong functions of l_c. However, we found that they do depend significantly on the shape factor, S. We also found that we can fit the estimated values of l_{hl} to a linear function of j, for j=4-10, given by

$$l_{hl} \simeq 5.1 + 1.825j \quad (\text{Å}) \tag{28}$$

for spherical micelles, and

$$l_{hl} \simeq 6.05 + 1.85j \quad (\text{Å}) \tag{29}$$

for cylindrical micelles.

B. Prediction of the Critical Micelle Concentration (CMC)

Application of the principle of multiple chemical equilibria between micelles of different sizes[38,39] makes possible the determination of the micelle size distribution, $\{X_n\}$, through the simultaneous solution of the distribution and mass

balance equations.[12,38,39,14,40] Specifically,

$$X_n = \frac{(X_1 e)^n}{e} e^{-\beta n g_{mic}(n)} , \tag{30}$$

and

$$X = \sum_n n X_n , \tag{31}$$

where X is the total surfactant mole fraction, X_1 is the monomer mole fraction, and X_n is the mole fraction of micelles having aggregation number, n. The first equation results from the conditions imposed by chemical equilibrium involving the micelles and the free monomers in solution, and the second constitutes the mass-balance relation. The CMC can be evaluated by plotting X_1 as a function of X, the estimated CMC being the concentration at which the plot exhibits a sharp break due to the onset of micellization[41].

An approximate way of calculating the CMC makes use of the following relation which is valid for micelles that exhibit extensive one-dimensional growth ($n >> 1$),

$$CMC \sim \exp\left(\frac{g_{mic}}{kT} - 1\right) . \tag{32}$$

Combining this with Eq. (1), which can be rewritten as $-k_s = d(ln\ CMC)/dm_s$, gives an approximate relation for the salt constant, k_s, namely,

$$k_s = -\frac{dg_{mic}}{dm_s} = -\left(\frac{dg_{s/hc}}{dm_s} + \frac{dg_\sigma}{dm_s} + \frac{dg_{s/hl}}{dm_s}\right) . \tag{33}$$

Note that the various free-energy contributions in Eq.(33) are in units of kT. Eq.(33) is a central result which indicates that we can predict the salt constant, k_s, in the context of our theoretical formulation. Indeed, values of $dg_{s/hc}/dm_s$, dg_σ/dm_s and $d_{s/hl}/\mathrm{dm_s}$ can be evaluated for each type of salt and surfactant considered. Values of $dg_{s/hc}/dm_s = dg_{s/w}/dm_s$ were calculated from Eq.(7) and are reported in Table III. It

can be seen from Eq. (8) that $dg_a/dm_s \simeq (d\sigma_a/dm_s)(g_a/\sigma_o)$. These values are reported in Table II and Table V. It can also be deduced from Eq.(17) that $dg_{s/hl}/dm_s = j\ \phi_{hl}\ dv/dm_s$. Note that these values of $dg_{s/hc}/dm_s$, dg_a/dm_s, and $dg_{s/hl}/dm_s$ are roughly constant over a broad range of salt concentrations. By breaking down the salt constant into its component parts, it is possible to determine the relative magnitude of each contribution to k_s.

III. MATERIALS AND EXPERIMENTAL METHODS

A. Materials and Sample Preparation

Homogeneous C_iE_j surfactants were obtained from Nikko Chemicals, Tokyo, and used without further purification. To ensure uniformity in the results, measurements were conducted using the same lot number for each surfactant: $C_{12}E_6$ (Lot 9011), $C_{12}E_8$ (Lot 9054), and $C_{10}E_6$ (Lot 1054). The high purity of the surfactants was confirmed by the absence of any detectable minimum in the measured surface tension versus surfactant concentration curves of aqueous solutions of each surfactant. Salts were of the analytical reagent grade from Mallinckrodt, and were further purified to remove any organics by ignition at 450°C overnight. Salt solutions were prepared by weight, using deionized water which was purified using a Milli-Q ion-exchange system. A known weight of surfactant was then added to each of the salt solutions. The prepared surfactant solutions were utilized within the same day. Since the occurrence of evaporation was possible at room temperature, which, in turn, could change the surfactant concentration of the samples, proper precautions against evaporation were taken. These included placing samples in stoppered flasks, and sealing the flasks while awaiting measurement.

Before use, all glassware were immersed in a 1N NaOH-ethanol bath for at least 8 hours, then in a 1N nitric acid bath for another 8 hours, followed by thorough rinsing with Milli-Q water. The glassware were then dried in an oven. The Wilhelmy platinum plate, to be used in surface tension measurements, was rinsed with distilled

water, then with acetone, and again with distilled water, and flamed until red hot before each surface tension measurement.

B. Measurement of the Critical Micelle Concentration

The critical micelle concentrations (CMC's) of surfactant solutions with and without added salts were measured using the surface tension method. It is well known that as the surfactant concentration, X, is increased, both the hydrophobicity of the surfactant tails and the high water-air interfacial free-energy, drive the adsorption of the surfactant molecules onto the surface. The increase in the surface pressure due to surfactant surface adsorption leads to a lowering of the surface tension, σ. Beyond a certain surfactant concentration, the CMC, it becomes more favorable, from a free-energy point of view, for the surfactant molecules added to the solution to form micelles, rather than continue to adsorb onto the surface. This is reflected in a negligible change in surface tension with increasing surfactant concentration beyond the CMC. The break in the σ versus X curve, therefore, approximates the concentration at which micellization first takes place. In order to determine this "break", the surface tensions of at least 12 surfactant solutions were measured and plotted as a function of the logarithm of the surfactant mole fraction, X. Linear regression was utilized to determine the best fit line on either side of the break in the curve, the intersection of these two lines being taken as the experimental CMC value (see Fig. 3). The accuracy of the experimental CMC is bounded by the surfactant concentrations of the experimental points immediately bounding the experimental CMC value, adjusted to account for errors from solution preparation.

Surface tension measurements were performed using the Wilhelmy plate tensiometer (Kruss K10T). All measurements were carried out in a thermostated device maintained at a constant temperature of 25°C. Each surfactant sample was equilibrated for 45-90 minutes, depending on the time needed to attain a constant surface tension value, maintained for at least 30 minutes, as monitored using a chart

recorder.

The concentrations (mole fractions) of the surfactant samples were varied within a two order of magnitude range (10^{-7}-10^{-5} for $C_{12}E_6$ and $C_{12}E_8$, and 10^{-6}-10^{-4} for $C_{10}E_6$).

The CMC's of $C_{12}E_6$ in water, and in 1, 2 and 3 molal solutions of NaCl, LiCl, KCl, KBr and KI were determined using the method outlined above. In addition, in order to validate the salt trends established from the $C_{12}E_6$ experiments, CMC determinations of $C_{12}E_8$ and $C_{10}E_6$ in water and in 1m and 2m solutions of KCl, KBr and KI were done. Note that in the latter experiments, only the anion effects were studied, since the initial CMC studies with $C_{12}E_6$ indicated that the variation of the anion had a more significant effect on the CMC as compared to that of the cation.

IV. RESULTS AND DISCUSSIONS

A. Experimental Results

1. Critical Micelle Concentration. The experimentally determined CMC's of $C_{12}E_6$, $C_{12}E_8$, and $C_{10}E_6$ in various salt solutions are shown in Figs. 4-7. The resulting uncertainty in the measured CMC is in the range 5-20%, determined using the method shown in Fig. 3. The range of uncertainty for each reading is not shown in Figs. 4-7 since the curves are in close proximity to each other). Note that this uncertainty can be reduced by making measurements at more surfactant concentrations. This would decrease the differences in surfactant concentrations between adjacent measurement points, and consequently, the difference in the concentrations of the measured points closest to the experimental value of the CMC as determined using the linear regression of the plots.

Figs. 4-7 indicate that for all three surfactants the CMC decreases as the salt concentration increases for all the salts examined. The order of decreasing the CMC is consistent with that found in previous work[6], namely, $Cl^- > Br^- > I^-$ for the anion (see Figs. 5-7), and $Na^+ > K^+ > Li^+$ for the cation (see Fig. 4). Furthermore, a comparison

of Figs. 5 and 7 shows that the CMC's of $C_{10}E_6$ in the aqueous salt solutions examined, $C_{10}E_6$ being less hydrophobic than $C_{12}E_6$ (shorter alkane chain, and therefore more soluble in water), is an order of magnitude higher than that for $C_{12}E_6$. Changing the length of the PEO head from an E_6 to an E_8 chain increases the free energy of transferring the head from the bulk salt solution to the micelle head layer, giving rise to a slightly higher CMC for $C_{12}E_8$ (see Fig. 6) as compared to $C_{12}E_6$ (see Fig. 5).

2. Salt Constant, k_s. In agreement with previous experimental work on salt effects on the CMC of nonionic surfactants[1-7], we have found that the logarithm of the measured CMC's varies linearly with salt concentration, according to Eq. (1). The salt constant, k_s, for $C_{12}E_6$ in aqueous salt solutions were determined from the linear regression of *ln CMC* versus m_s, and the results are shown in the second column of Table IV.

3. Surface Tension of Aqueous Surfactant Solutions. The surface tensions of the aqueous surfactant solutions primarily reflect the balance between the solubilities of the hydrophobic alkyl tails and the hydrophilic PEO heads. Increasing the salt concentration decreases the solubility of the surfactant molecules. This corresponds to a decreased surfactant adsorption at the surface, and, therefore, decreases the surface tension of the solution, as seen in Figs. 8-10, which plot the surface tension (at 25°C) of $C_{12}E_8$ as a function of KCl, KBr, and KI concentration. Furthermore, the salt effect on the surfactant solution surface tension varies according to the salting-out trend for the hydrocarbon tail, which is in the order KCl > KBr > KI. Recall that this order is related to the volume contraction effects discussed in Section IIAa, and shown in the third column of Table I. Thus, $\sigma_{KCl} < \sigma_{KBr} < \sigma_{KI}$.

It is interesting to note that there appears to be a slight increase in the surface tension of the surfactant solution at concentrations near the CMC upon the addition of KI, as compared to the that in pure water. We speculate that the increase in σ may be due to the possible specific interactions between the iodide ions and the

poly(ethylene oxide) heads[42]. This gives the PEO heads a pseudo-charge such that the concentration of surfactants adsorbed at the surface will decrease due to the added repulsive electrostatic interactions between the "effectively charged" PEO heads of the adsorbed surfactant molecules.

B. Theoretical Results

1. Parameter Estimation. In Section II, it was shown that in order to determine the free-energy contribution of transferring a surfactant tail from the bulk salt solution to bulk hydrocarbon, it is necessary to know the free-energy change corresponding to the transfer of the tail from the bulk salt solution to pure water, $g_{s/w}$. This can, in turn, be determined through the use of Eq.(7) once the parameters v_c, $\bar{V}_s^0$, β_o, and V_s are known. The first three parameters are easily determined, as mentioned earlier. However, liquid salt volumes at atmospheric conditions cannot be determined experimentally; thus the necessity for estimation. The estimation was done by using the theory embodied in Eq.(7), where an experimentally determined variation of $g_{s/hc}$ with salt concentration, C_s, (from solubility experiments), as well as inputs of v_c, $\bar{V}_s^0$, β_o, makes possible the determination of V_s. Considerable experimental data on the solubility of benzene in various salt solutions is available[43,13]. Accordingly, the results of these experiments were utilized to estimate V_s values of LiCl, NaCl, KCl, KBr, and NaI. In these calculations, v_c of benzene was estimated from density measurements reported in the CRC Handbook of Chemisty and Physics. These values, together with β_o from the CRC Handbook and $\bar{V}_s^o$ from Table I, were substituted into Eq.(7) in order to estimate V_s. No data for benzene solubility in KI solutions is available, however. Thus, an estimate for the V_s of KI was arrived at by using a relation that was found to be valid at high temperatures[44],

$$V_{KI} \approx V_{KCl} - V_{NaCl} + V_{NaI} \cdot \qquad (34)$$

The molar volume of KI predicted using Eq. (34) at 900°C, at which temperature

these salts are in the molten state, is accurate to within 2.4% of measured values[44]. A summary of V_s values deduced using the procedure outlined above are shown in the first column of Table I.

The second parameter value that needs to be determined is the enthalpy parameter, ν, appearing in Eq.(17). Based on dilution enthalpy measurements at 30°C[35], we have deduced a value of $\nu \approx 1$ kT/EO for PEO in pure water. There is no data available for dilution enthalpies for PEO in salt solutions. Note, however, that a comparison of the g_{mic} contributions shown in Table IV and to be discussed in Section IVB2, for $C_{12}E_6$, $C_{10}E_6$, and $C_{12}E_8$ in pure water, indicate that the dominant contribution to g_{mic} is $g_{s/hc}$, which is an order of magnitude larger than $g_{s/hl}$. Based on this, we have made the reasonable assumption that a change in g_{mic} due to salt effects on $g_{s/hl}$ will be very small as compared to the overall magnitude of g_{mic}.

2. Predicted Free Energy of Micellization, g_{mic}. One advantage of the theoretical framework presented here is that the magnitude of the salt effects on the different contributions to the micellization free energy, g_{mic}, can be identified, computed, and compared. This should be contrasted with previous work which has expressed all the salt effects in terms of changes in activity coefficients. The transfer free energies, $g_{s/w}$, for C_{11} (the tail for $C_{12}E_6$ and $C_{12}E_8$) and C_9 (the tail for $C_{10}E_6$) chains in 5 types of salts were calculated using Eq.(7) (See Section IIA and Table III). The g_σ values were calculated using Eq.(8) and Table II, while $g_{s/hl}$ was calculated using Eq.(24). The values of g_{pack} were calculated as for the salt-free case[12,30] using Eq.(10). These free-energy contributions were then incorporated into Eq.(2) to calculate the free-energy of micellization, g_{mic}, as reported for the various surfactants and salt conditions in Table V.

As seen in Table V, the dominant term in the micellization free energy is the transfer free-energy contribution, $g_{s/hc}$. It is not surprising, therefore, that the observed enhancement of micellization is in the order $Cl^- > Br^- > I^-$ for the anion, and $Na^+ > K^+ > Li^+$ for the cation, since this is the order of the salt effect on $g_{s/hc}$. The

dominance of the salt effect on the transfer free-energy contribution, $g_{s/hc}$, is also in agreement with earlier findings that the salt effects are virtually independent of the number of ethylene oxide segments in the PEO head[6]. Salt effects on the formation of nonionic surfactant micelles are primarily a consequence of the polarizing power of the ions, which is a function of the ion-charge density. Specifically smaller ions, such as Cl^- as compared to Br^- and I^-, cause a greater electrostriction of water, that is, a larger contraction in total volume upon mixing water and salt. This is shown in Table I, where the electrostriction of water, as reflected in the $(V_s\text{-}\bar{V}_s^o)$ values, is greatest for Cl^-, which causes the greatest increase in the internal pressure, and thereby "squeezes out" more effectively the hydrocarbon tail. The cation trend is not as clear, since the bare ion radius of Li^+ is much smaller than that of Na^+ and K^+, but it has the smallest $(V_s\text{-}\bar{V}_s^o)$ value. This anomalous behavior of Li^+ is also reflected in the lyotropic and the Hofmeister series. Li^+ is very strongly hydrated, such that water molecules in the inner hydration shell are very strongly bound. It is speculated that for the case of Li^+, therefore, the inner hydration shell becomes part of the "ion", such that it is the bare ion radius plus the inner hydration shell that determines the electrostriction of the rest of the "unbound" solvent molecules. The actual mechanism is far from being understood, however. In any case, the results indicate that the higher the charge density of the ion (which in this case is equivalent to a smaller hydrated radius), the lower is the solubility of the hydrocarbon tail in the aqueous solution, which would enhance micellization (decrease g_{mic}). These salt effects on the hydrophobic driving force are slightly balanced by the interfacial free-energy contribution to g_{mic}, whereby the more polarizing ions increase the interfacial free energy to a larger extent, and thereby inhibit micellization (increase g_{mic}). There is very little perceivable difference between the effects of the cations in the various chlorides, while the anion effect follows that for $g_{s/hc}$, namely, KCl > KBr > KI.

Trends in the values of g_{mic} can also be seen by varying the surfactant type. For example, shortening the tail, which is equivalent to making the surfactant less hydrophobic, decreases the free-energy advantage of forming micelles, as shown by

the lower g_{mic} values of $C_{12}E_6$ as compared to $C_{10}E_6$. Both $C_{12}E_6$ and $C_{10}E_6$ tend to form rodlike micelles in aqueous solutions, that is, $g_{mic,rod} < g_{mic,sph}$. On the other hand, it is interesting to note that $C_{12}E_8$ micelles tend to be spherical. A comparison of the values for $g_{mic,rod}$ and $g_{mic,sph}$ for $C_{12}E_8$ micelles in Table V shows that for $C_{12}E_8$ micelles, $g_{mic,rod} > g_{mic,sph}$. Ultimately, it is the balance of these free-energy contributions, therefore, that would determine the optimum shape of the micelle. The longer and more hydrophilic E_8 chain necessitates a higher transfer free energy, $g_{s/hl}$. Because $g_{s/hl}$ would be higher for C_iE_8 micelles as compared to micelles with shorter PEO heads, C_iE_8 micelles would tend to acquire a spherical shape since this minimizes $g_{s/hl}$, as seen in Table V. The formation of spherical micelles, however, would expose a larger area of the hydrocarbon core to the aqueous environment, thereby increasing the g_σ contribution, as seen in Table V.

3. Predicted Critical Micelle Concentrations. From the values of g_{mic} shown in Table V, the corresponding CMC's can be calculated as described in Section IIB, and compared with the experimentally deduced CMC's. These are shown in Figs. 4-7. Fig. 4 shows that the CMC of $C_{12}E_6$ in LiCl, NaCl and KCl solutions decreases upon increasing salt concentration, and that the agreement between theory and experiment is reasonable. The same trend, that is, decreasing CMC with salt concentration, is seen in Fig. 5, which shows the CMC variation as a function of the anion type, namely, KCl, KBr, KI. Although agreement is reasonable for CMC predictions in KCl and KBr solutions, there is a greater discrepancy between calculated and measured CMC's for $C_{12}E_6$ in KI solutions. This could be due to possible specific interactions between iodide and the PEO heads, which was not accounted for explicitly in our model, where the ions are treated as part of the *hypersolvent*. Fig. 5 also indicates that the variation of the CMC with the anion type is more significant than that with the cation type. Figs. 6 and 7 show the comparison of predicted and experimental CMC's of $C_{12}E_8$ and $C_{10}E_6$, respectively, in KCl and KBr solutions. Again, the predicted CMC's agree reasonably well with the experimentally deduced

CMC's.

4. Predicted Salt Coefficient, k_s. The theoretically predicted k_s values were calculated based on Eq.(33) in Section IIB, valid for micelles that exhibit extensive one-dimenstional growth (such as $C_{12}E_6$), using values of $dg_{s/hc}/dm_s$ and dg_{α}/dm_s reported in Table II and Table III. Table IV shows a comparison of these theoretically predicted k_s values with the experimental values, determined from a linear regression of the log CMC values. The predicted values compare well with the experimentally determined values, except for $C_{12}E_6$ in KI solutions, where the salt effects are overpredicted (predicted k_s values are larger than the measured values). As mentioned earlier (Section IVA2 and Ref.42), specific interactions between iodide ions and the polyethylene oxide heads are possible. This positive adsorption of iodides onto the PEO heads could effectively give an ionic character to the PEO heads, and thereby increase the value of $g_{s/hl}$ (it will be less advantageous to transfer the heads from the bulk salt solution to the micelle head layer in this case), due to an additional repulsive electrostatic contribution to the transfer free energy, $g_{s/hl}$. Thus, as the KI concentration is increased, so would the values of g_{mic}. By not accounting for any specific interactions between the PEO heads and the iodide ions, the CMC predictions are expected to be lower (leading to larger k_s values) as compared to the predictions when the specific interactions are accounted for. This is a reasonable explanation for the observed difference between the predicted and experimentally deduced k_s values for $C_{12}E_6$ in aqueous KI solutions seen in Table IV.

V. CONCLUDING REMARKS

The work presented in the chapter has shown that through an understanding of the effects of salts on the various free-energy contributions to the micellization process, and a quantitative treatment of these salt effects, the CMC of $C_{12}E_6$, $C_{12}E_8$, and $C_{10}E_6$ in aqueous salt solutions can be calculated using a suitable theoretical

framework. Without the use of any freely-adjustable parameters, the predicted CMC's are in reasonable agreement with measured values for all three surfactants in aqueous LiCl, NaCl, KCl, and KBr solutions. Our results indicate that the dominant salt effect is on the surfactant tails (in particular, the decreased solubility of the hydrocarbon tails in aqueous salt solutions, as reflected in the $g_{s/hc}$ values, as well as a significant, but smaller, effect on the interfacial free-energy contribution to g_{σ}, see Table V), and not on the hydrophilic PEO heads. Salt effects were likewise shown in the values of the surface tensions of the aqueous surfactant solutions, and the results were rationalized in terms of a decrease in the solubility of the hydrocarbon tails upon the addition of salts, thereby increasing the surface activity of the surfactants (lowering of the surface tension).

The theoretical framework developed in this chapter is unable to accurately predict CMC's of the surfactants studied in aqueous KI solutions. This is believed to be due to the possible specific interaction between I^- and the PEO heads. This specific interaction would give the PEO heads a *pseudo-ionic* character, and would thus add an electrostatic contribution, g_{elec}, to the micellization free energy. The theory, as developed, does not account for such specific ion effects. Indeed, the salts are only considered to be part of a *hypersolvent*, and their main role is assumed to be confined to inducing changes in the quality or character of the solvent. Apart from the lower predicted CMC's as compared to measured values, the measured surface tensions of the surfactant solutions at concentrations near the CMC were found to be slightly higher in the presence of KI as compared to that in pure water. The higher surface tensions correspond to a decreased adsorption of the surfactant molecules at the surface, which we speculate is due to the possible *pseudo-ionic* character of PEO in KI solutions which adds a repulsive electrostatic interaction between the PEO chains of surfactants adsorbed at the macroscopic solution-air surface.

In the process of calculating the free energies of micellization for $C_{12}E_6$, $C_{12}E_8$, and $C_{10}E_6$, it was determined that the optimum shape for $C_{12}E_6$ and $C_{10}E_6$ micelles

is a rod (they are predicted to exhibit one-dimensional growth), while $C_{12}E_8$ tends to form spherical micelles. In the next chapter, these predictions will be tested using light scattering techniques. Studies aimed at probing effects of solution conditions on the shape and size of the micelles will also be presented.

REFERENCES FOR CHAPTER 2

1. Becher, P. *J. Coll. Sci.* **1962**, 17, 325.

2. Hsiao, L.; Dunning, H. N.; Lorenz, P. B. *J. Phys. Chem.* **1956**, 60, 657.

3. Schick, M. J. *J. Colloid Sci.* **1962**, 17, 801; Schick, M. J.; Atlas, S. M.; Eirich, F. R. *J. Phys. Chem.* **1962**, 66, 1326.

4. Schott, H.; Suk Kyu Han *J. Pharm. Sci.* **1976**, 65, 975.

5. Nishikido, N.; Matuura, R. *Bull. of the Chem. Soc. of Japan*, **1977**, 50, 1690.

6. Ray, A.; Nemethy, G. *J. Amer. Chem. Soc.* **1971**, 93, 6787.

7. Zourab, Sh. M.; Sabet, V. M.; Abo-El Dahab, H. *J. Disp. Science and Technology* **1991**, 12, 25.

8. Hofmeister determined that electrolytes had a range of effectiveness in salting out proteins. [Arch. Exptl. Pathol. Pharmakol., 1888, 24, 247].

9. Mukerjee, P. *J. Phys. Chem.* **1965**, 69, 4038.

10. Gordon, J. E. *J. Phys. Chem.* **1970**, 74, 3823.

11. Morrison, T. J.; Billett, F. *J. Chem. Soc.*, **1952**, 3819.

12. Puvvada, S.; Blankschtein, D. *J. Chem. Phys.* **1990**, 92, 3710. Blankschtein, D.; Puvvada, S. *MRS Symp. Proc.* **1990**, 177, 129.

13. McDevit, W. F.; Long, F. A. *J. Am. Chem. Soc.* **1952**, 74, 1773.

14. Blankschtein, D.; Thurston, G. M.; Benedek, G. B. *Phys. Rev. Lett.* **1985**, 54, 955. Blankschtein, D.; Thurston, G. M.; Benedek, G. B. *J. Chem. Phys.* **1986**, 85, 7268.

15. Puvvada, S. P.; Blankschtein, D. *J. Phys. Chem.* **1992**, *96*, 5579.

16. Briganti, G.; Puvvada, S.; Blankschtein, D. *J. Phys. Chem.* **1991**, *95*, 8989.

17. Huang, Y. X.; Thurston, G. M.; Benedek, G. B. *J. Chem. Phys.* **1990**, 92, 1956.

18. Carvalho, B. L.; Briganti, G.; Chen, S. H. *J. Phys. Chem.* **1989**, 93, 4282.

19. Carale, T. R.; Blankschtein, D. *J. Phys. Chem.* **1992**,

20. Nikas, Y. J.; Blankschtein, D. *Langmuir* **1992**, *8*, 2680.

21. Tanford, C. *The Hydrophobic Effect*; Wiley: New York, 1980.

22. Nagarajan, R.; Ruckenstein, E. *J. Coll. Interface Sci.*, **1977**, 60, 221; **1979**, 71, 580.

23. Abraham, M. H. *J. Chem. Soc. Faraday Trans. 1* **1984**, 80, 153.

24. *Handbook of Chemistry and Physics*; R. C. Weast, Ed.; CRC Press: Florida, 1988.

25. Millero, F. J. In *Water and Aqueous Solutions: Structure, Theromodynamics and Transport Processes*; R. A. Horne, Ed.; Wiley Interscience: New York, 1972; p. 519.

26. δ is estimated to be 2.25Å for C_{12} and 1.88Å for C_{10} and assumed to be independent of the salt concentration.

27. Aveyard, R.; Saleem, S. M. *J. Chem. Soc. Faraday Trans. I* **1976**, 72, 1609.

28. Hiemenz, P. C. Principles of Colloid and Surface Chemistry, 2nd ed., p. 391, Marcel Dekker: New York (1986).

29. (a) Ben-Shaul, A.; Szleifer, I.; Gelbart, W. M. *J. Chem. Phys.* **1985**, 83, 3597. Szleifer, I.; Ben-Shaul, A.; Gelbart, W. M. *J. Chem. Phys.* **1985**, 83, 3612;
(b) Gruen, D. W. R. *J. Phys. Chem.* **1985**, *89*, 146, 153.

30. Naor, A.; Puvvada, S.; Blankschtein, D. *J. Phys. Chem.* **1992**, *96*, 7830.

31. Nagarajan, R.; Ruckenstein, E. *Langmuir* **1991**, *7*, 2934.

32. de Gennes, P. G. *Scaling Concepts in Polymer Physics*; Cornell University Press: Ithaca, NY, 1979.

33. Hurter, P. N.; Scheutjens, J. M. H. M.; Hatton, T. A. *Macromolecules* **1992**, *(in press)?*

34. See Refs. 12 and 14, where g_{mic} accounts for the free energy of forming a stationary micelle from monomers at given positions in solution, and the entropic contributions are explicitly accounted for in the full solution free-energy expression.

35. Maron, S. H.; Filisko, F. E. *J. Macromol. Sci.- Phys.* **1972**, *B6*, 79.

36. Sarmoria, C.; Blankschtein, D. *J. Phys. Chem.* **1992**, *96*, 1978.

37. Israelachvili, J. N.; Mitchell, D. J.; Ninham, B. W. *J. Chem. Soc., Faraday Trans. 2* **1976**, *72*, 1525.

38. Corkill, J. M.; Goodman, J. F.; Walker, T.; Wyer, J. *Proc. Royal Soc. London Ser. A* **1969**, *312*, 243.

39. Mukerjee, P. *J. Phys. Chem.* **1972**, *76*, 565.

40. For a more detailed description of the thermodynamic framework, refer to reference 15 [Blankschtein et al.].

41. Puvvada, S.; Blankschtein, D. *Proceedings of the 8th International Symposium on Surfactants in Solution*; Mittal, K. L., Shah, D. O., Eds.; Plenum: New York, in press.

42. Bailey, F. E.; Callard, R. W. *J. Appl. Polym. Sci.* **1959**, 1, 56;
Lundberg, R. D.; Bailey, F. E.; Callard, R. W. *J. Appl. Polym. Sci. A-1* **1966**, 4, 1563.

43. Saylor, J. H.; Whitten, A. I.; Claiborne, I.; Gross, P. M. *J. Am. Chem. Soc.* **1952**, 74, 1778.

44. The salt data used in the calculations were taken from *A Comprehensive Treatise on Inorganic and Theoretical Chemistry*, ed. by J. W. Mellor, Longmans, Green and Co., 1941, p.533;599.

Table I. Estimated values of liquid salt volumes.

SALT	V_s (ml/mol)	$\bar{V}_s^0$ (ml/mol)	V_s-$\bar{V}_s^0$ (ml/mol)
LiCl	20.74	16.99	3.75
NaCl	21.49	16.63	4.86
KCl	31.14	26.73	4.41
KBr	36.46	33.74	2.72
KI	47.30	45.14	2.16

Table II. Change in the dodecane-water interfacial tension with salt molality.

SALT	$d\sigma_i/dm_s$ (dyn/cm-molal)	dg_σ/dm_s (dyn/cm-molal)		
		$C_{12}E_6$	$C_{12}E_8$	$C_{10}E_6$
LiCl	1.56	0.092	0.103	0.091
NaCl	1.41	0.083	0.093	0.082
KCl	1.37	0.081	0.090	0.080
KBr	0.86	0.051	0.056	0.050
KI	-0.07	-0.004	-0.005	-0.004

Table III. Transfer free energies, $dg_{s/w}/dm_s$ (kT/molal salt) for C_9H_{19} and $C_{11}H_{23}$ Chains

SALT	C_9H_{19} V_i=162.24 ml/mol	$C_{11}H_{23}$ V_i=194.63 ml/mol
LiCl	-0.5596	-0.6714
NaCl	-0.7360	-0.8829
KCl	-0.6681	-0.8014
KBr	-0.4266	-0.5117
KI	-0.3493	-0.4190

Table IV. Salting-out coefficients, k_s.

	k (predicted) [from Eq.(33)	k (measured) [from Eq.(1)
$C_{12}E_6$ in LiCl Solutions	.58	.53
$C_{12}E_6$ in NaCl Solutions	.80	.81
$C_{12}E_6$ in KCl Solutions	.72	.69
$C_{12}E_6$ in KBr Solutions	.46	.48
$C_{12}E_6$ in KI Solutions	.42	.30

Table V. Contributions to the micellization free energy (in kT), at 25°C, from the various steps in the micellization process.

Solvent	g_{mic}	$g_{s/hc}$	g_{σ}	$g_{s/hl}$	g_{pack}
$C_{12}E_6$ in	optimum shape: rodlike micelles				
H_2O	-12.64	-18.46	2.99	1.48	1.35
1m LiCl	-13.22	-19.13	3.08	1.48	1.35
1m NaCl	-13.44	-19.34	3.08	1.48	1.35
1m KCl	-13.36	-19.26	3.07	1.48	1.35
1m KBr	-13.10	-18.97	3.04	1.48	1.35
1m KI	-13.06	-18.88	2.99	1.48	1.35
$C_{12}E_8$ in	optimum shape: spherical micelles				
H_2O	-12.01	-18.46	3.78	1.16	1.50
1m KCl	-12.72	-19.26	3.88	1.16	1.50
1m KBr	-12.46	-18.97	3.85	1.16	1.50
1m KI	-12.44	-18.88	3.78	1.16	1.50
$C_{12}E_8$ in	rodlike micelles				
H_2O	-11.93	-18.46	2.99	2.19	1.35
1m KCl	-12.66	-19.26	3.07	2.19	1.35
1m KBr	-12.40	-18.97	3.04	2.19	1.35
1m KI	-12.36	-18.88	2.99	2.19	1.35
$C_{10}E_6$ in	optimum shape: rodlike micelles				
H_2O	-9.82	-15.47	2.95	1.49	1.21
1m KCl	-10.41	-16.14	3.03	1.49	1.21
1m KBr	-10.20	-15.90	3.00	1.49	1.21
1m KI	-10.17	-15.82	2.95	1.49	1.21

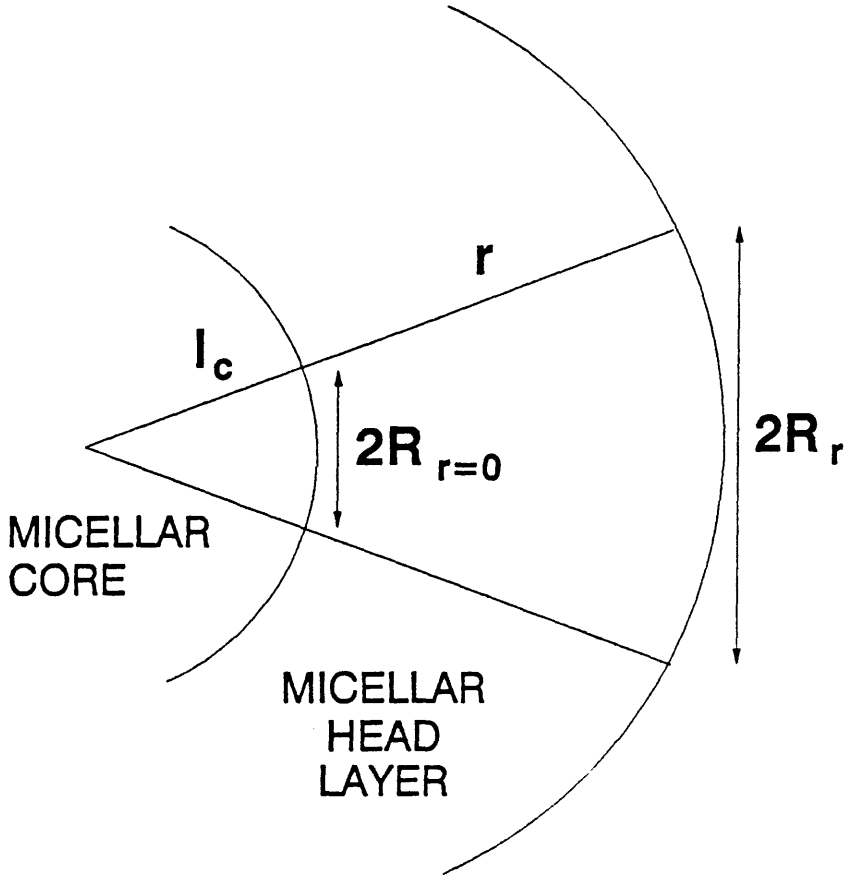

Figure 1. Confinement of a PEO head chain within a cone, where l_c is the micellar core-minor radius, and R_r is the radius of the cone at a distance r from the micellar-core surface.

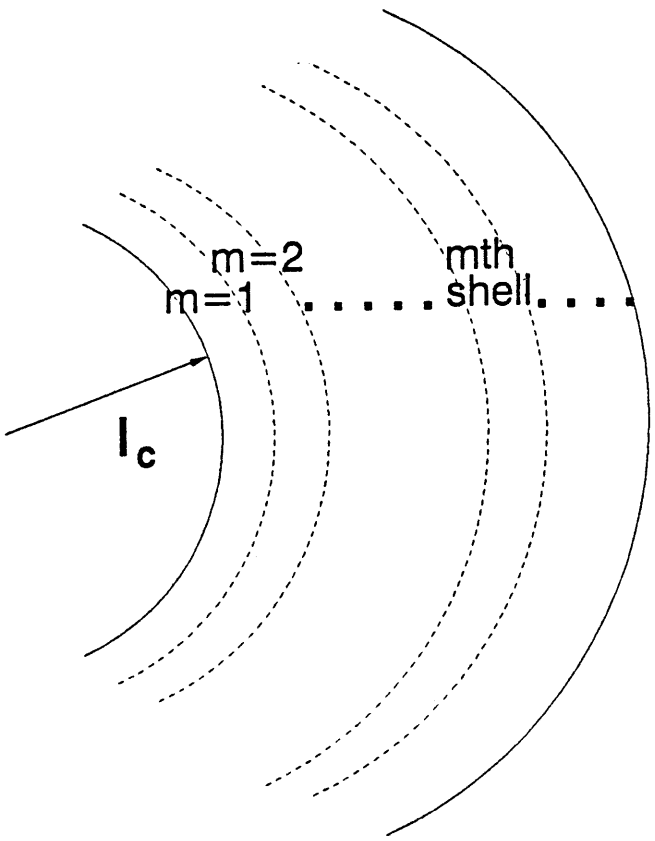

Figure 2. Division of the micelle head layer into concentric shells of 0.5Å thickness, where m is the shell number away from the micellar-core surface.

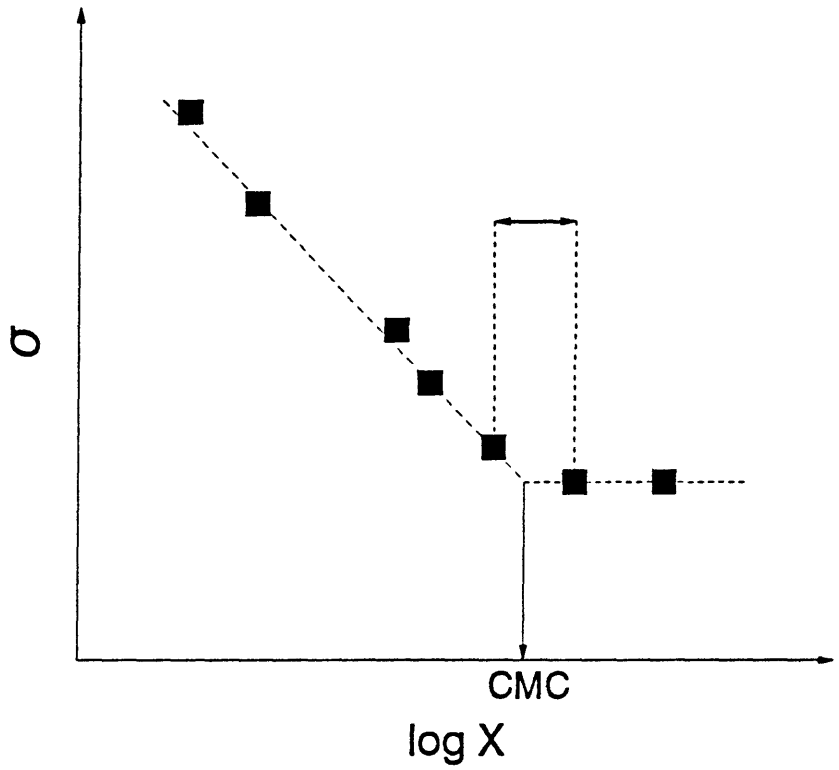

Figure 3. Schematic representation of the experimental determination of the CMC from a plot of the surface tension, σ, versus surfactant concentration, X. The arrow indicates the range of uncertainty of the measured CMC.

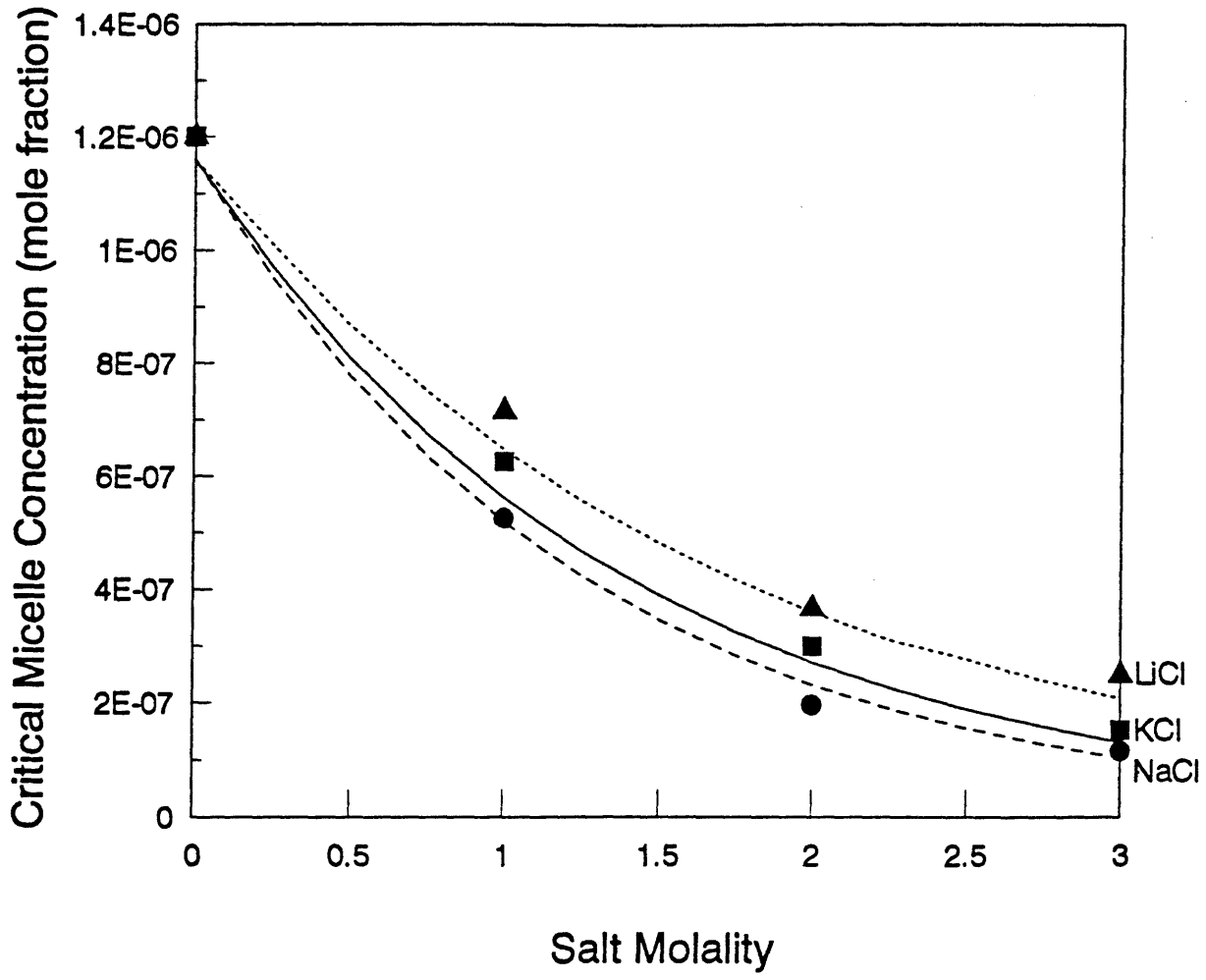

Figure 4. Comparison of calculated CMC's of $C_{12}E_6$ in aqueous solutions of LiCl (• • • •), NaCl (– – –) and KCl (———), with experimentally measured CMC's in LiCl (▲), NaCl (●) and KCl (■).

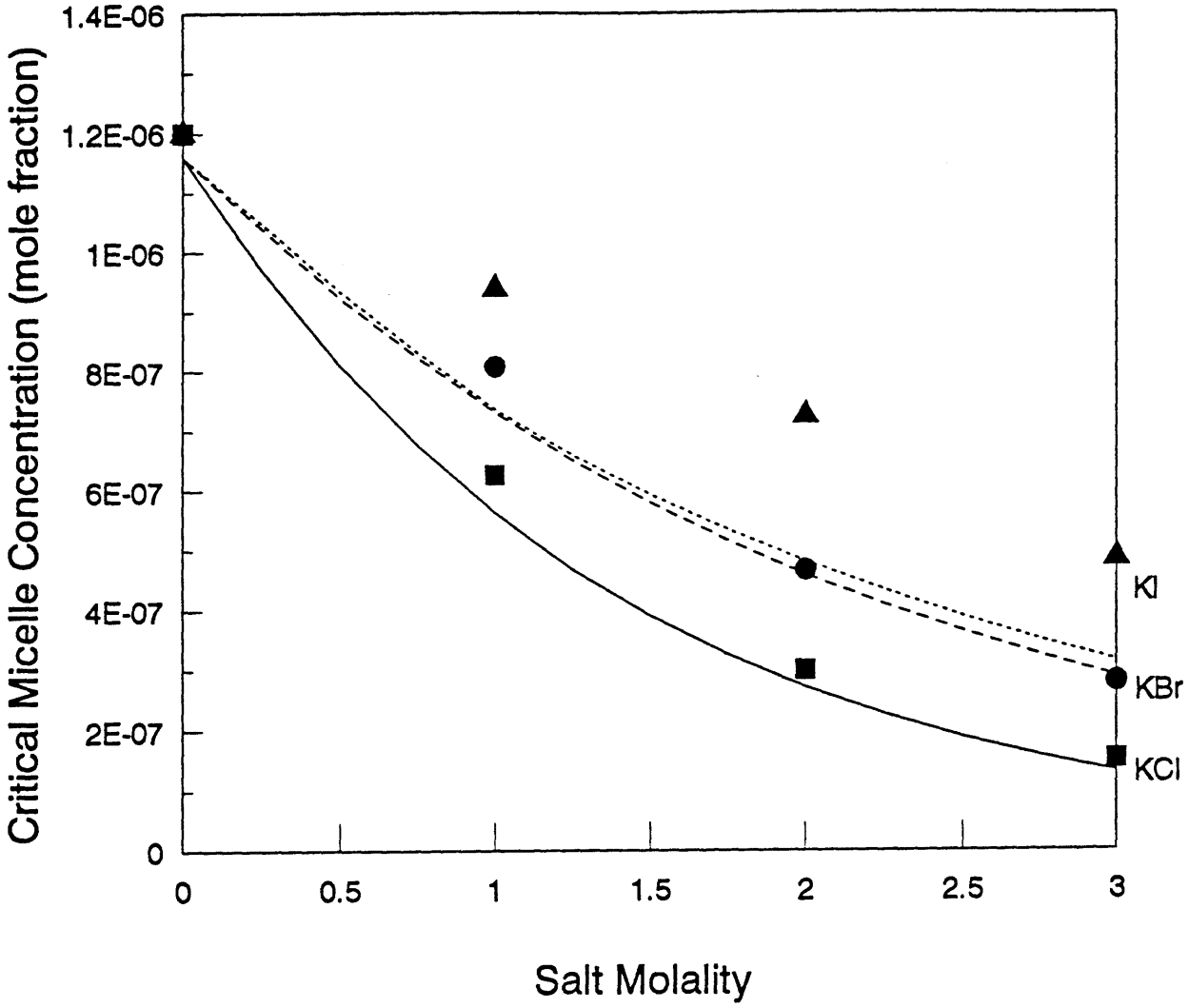

Figure 5. Comparison of calculated CMC's of $C_{12}E_6$ in aqueous solutions of KI (• • • •), KBr (– – –), and KCl (———), with experimentally measured CMC's in KI (▲), KBr (●) and KCl (■).

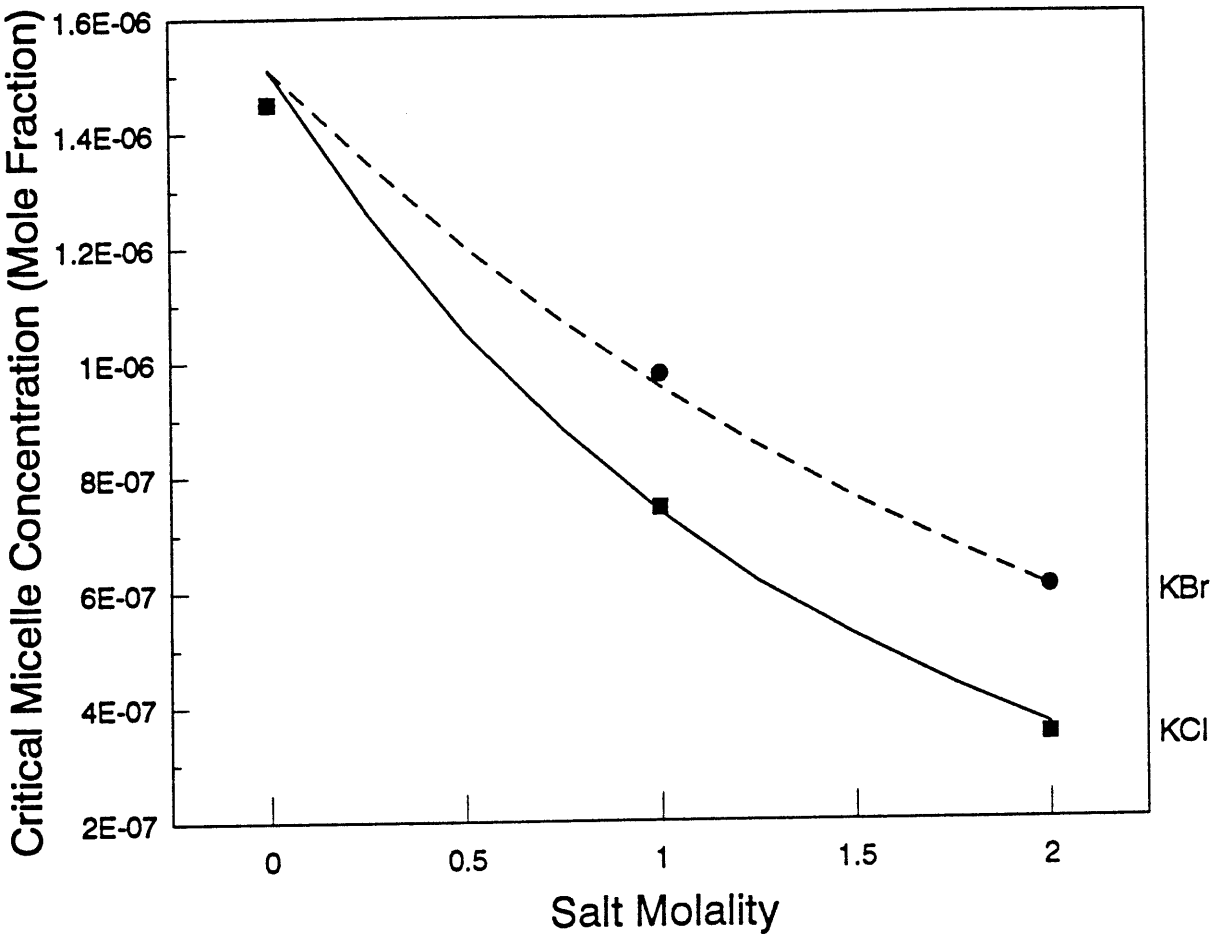

Figure 6. Comparison of calculated CMC's of $C_{12}E_8$ in aqueous solutions of KBr (——) and KCl (——), with experimentally measured CMC's in KBr (●) and KCl (■).

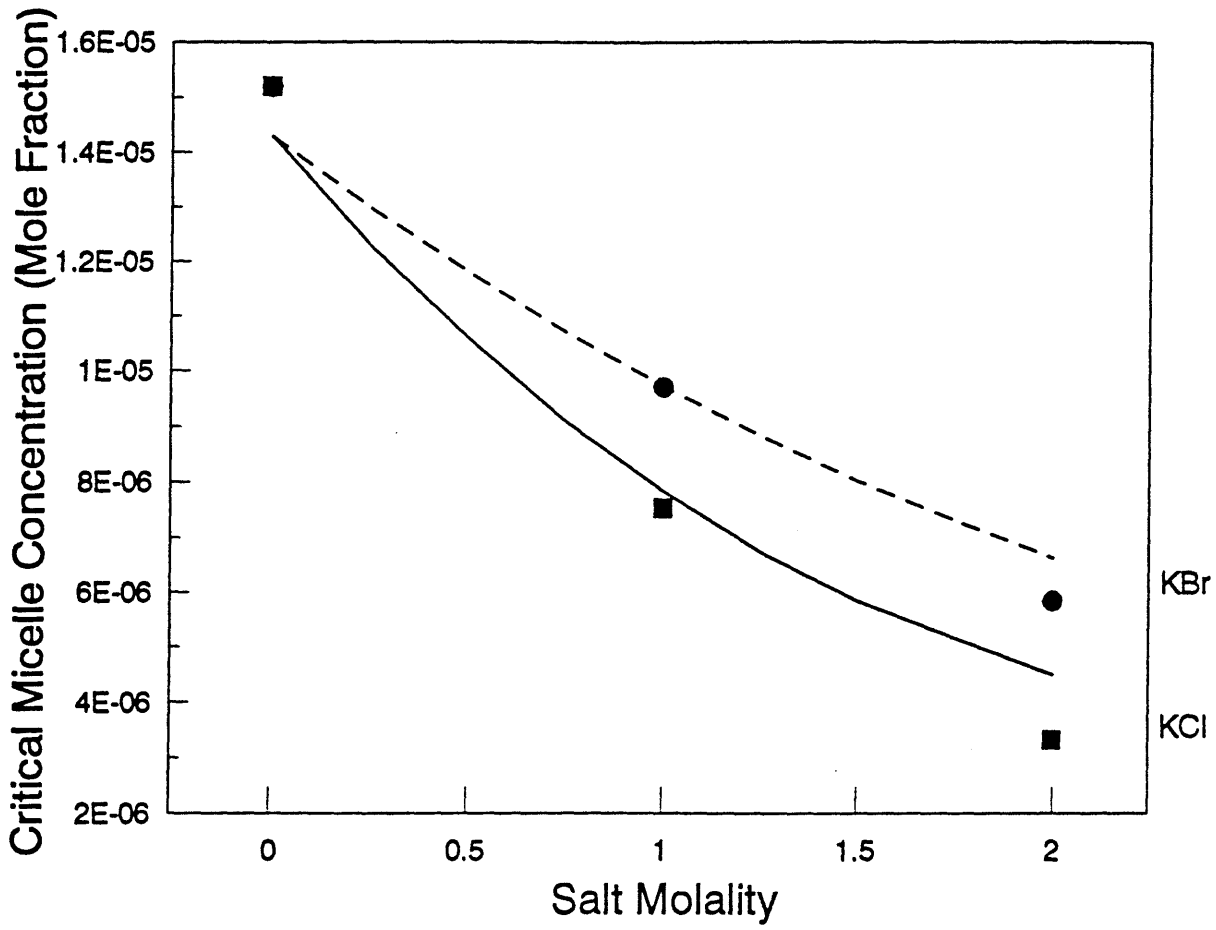

Figure 7. Comparison of calculated CMC's of $C_{10}E_6$ in aqueous solutions of KBr (——) and KCl (——), with experimentally measured CMC's in KBr (●) and KCl (■).

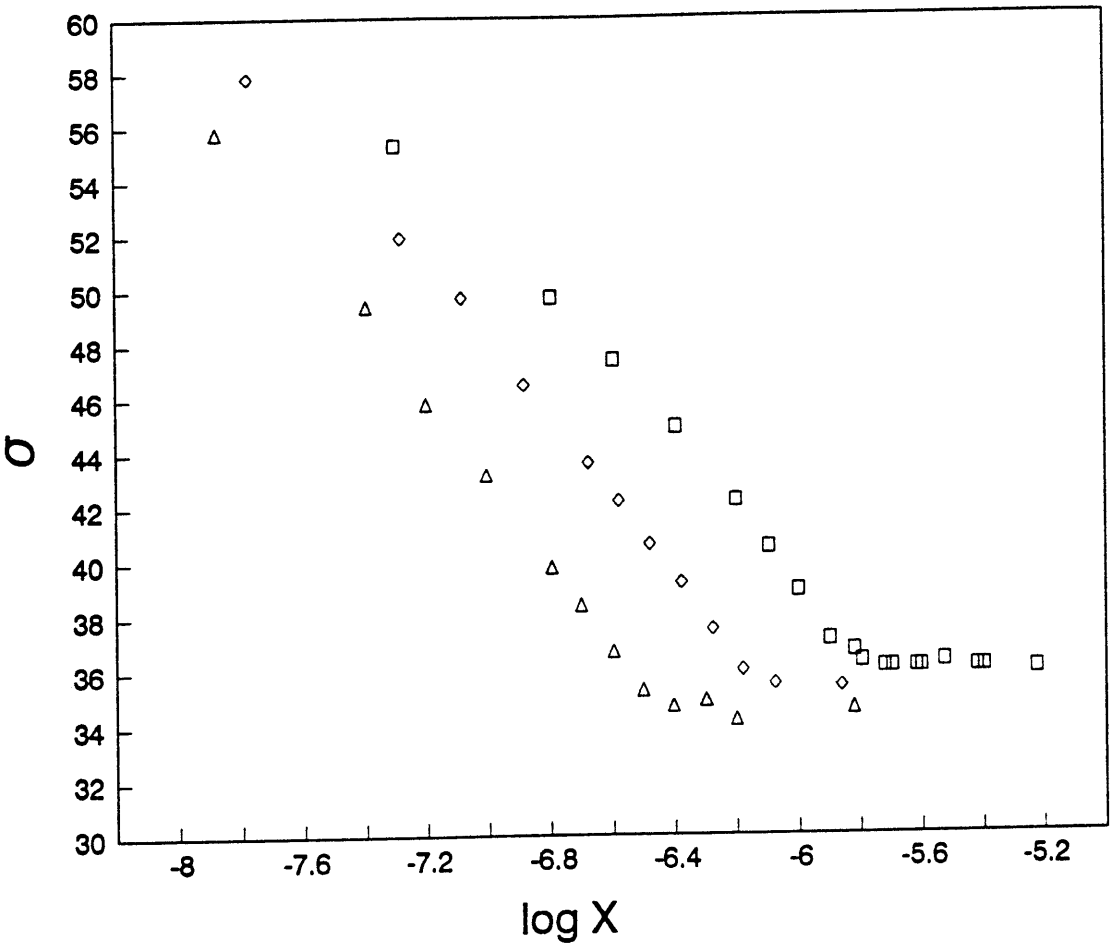

Figure 8. Measured surface tension as a function of surfactant concentration for $C_{12}E_8$ in pure water (□), 1m KCl (◇), and 2m KCl (△).

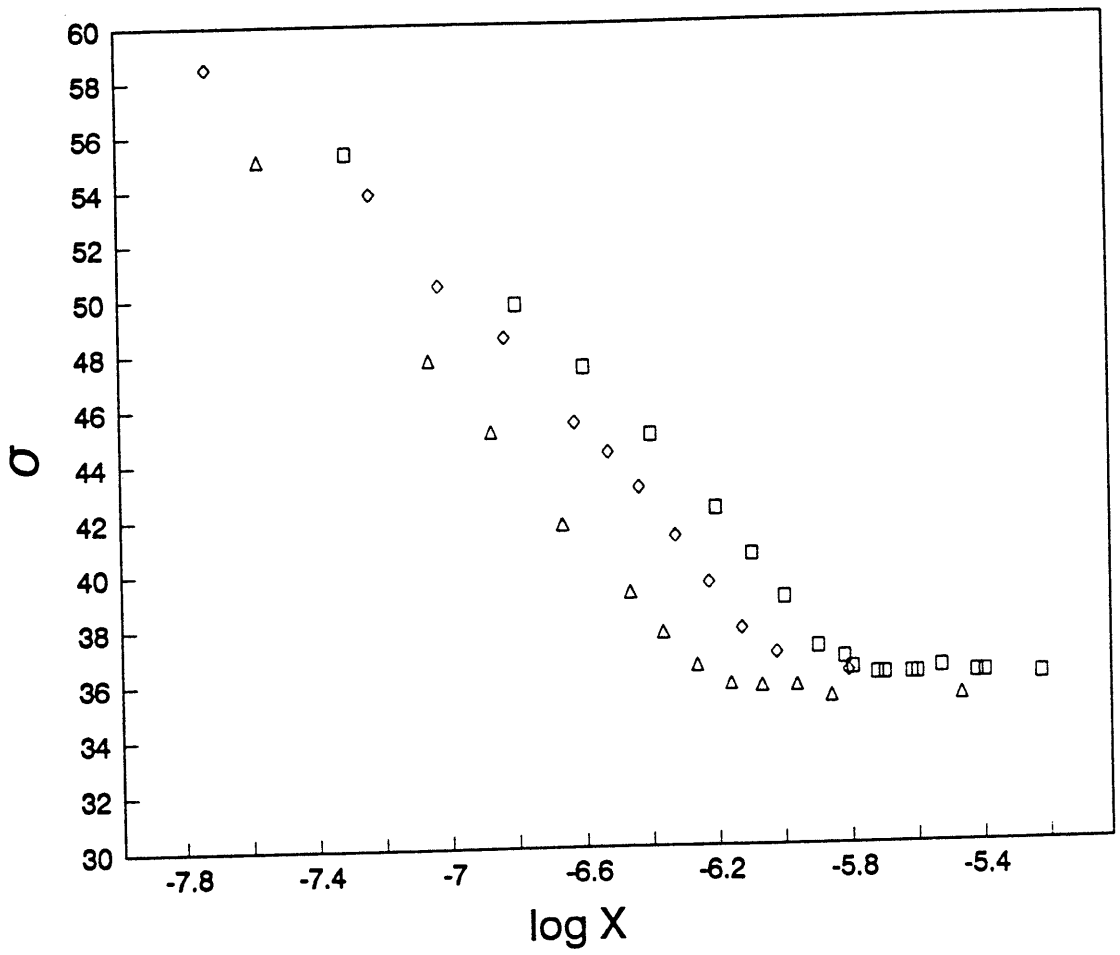

Figure 9. Measured surface tension as a function of surfactant concentration for $C_{12}E_8$ in pure water (□), 1m KBr (◇), and 2m KBr (△).

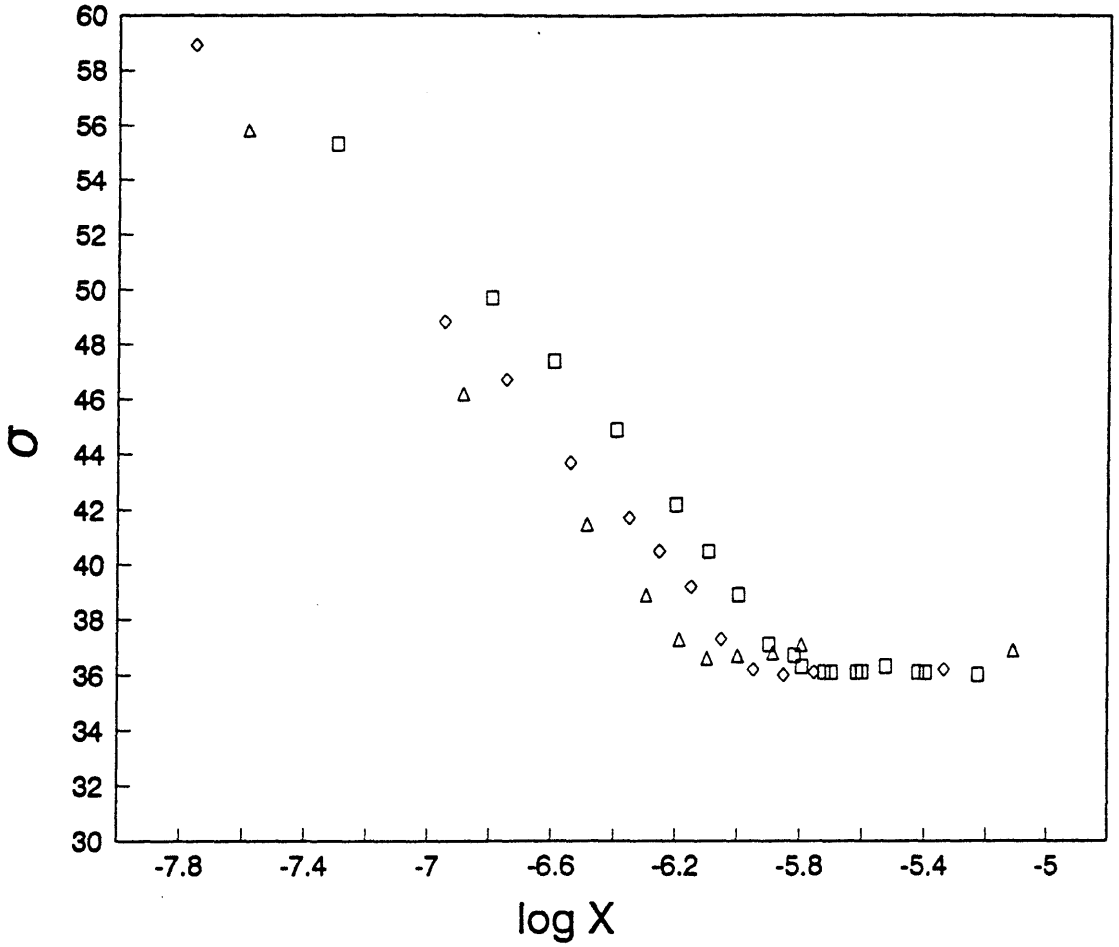

Figure 10. Measured surface tension as a function of surfactant concentration for $C_{12}E_8$ in pure water (□), 1m KI (◇), and 2m KI (△).

CHAPTER 3. LIGHT SCATTERING STUDIES OF MICELLAR SOLUTIONS

I. INTRODUCTION

Light scattering constitutes an important experimental technique which can be utilized to probe the shape, size, and size distribution of micellar aggregates, as well as the underlying structure of the micellar solution[1]. This technique does not perturb the thermodynamic equilibrium which exists in micellar solutions, and is therefore non-invasive. This experimental probe was utilized in the studies reported in this chapter in order to assess the effect of temperature and salts on the size distribution of C_iE_j micelles.

This chapter is organized as follows. Section II discusses light scattering theory, and describes both quasielastic light scattering (QLS) and static light scattering (SLS) intensity measurements. Section III describes the light scattering measurements conducted. Section IV presents the results, and a discussion of the results. Finally, Section V presents some concluding remarks.

II. LIGHT SCATTERING THEORY

Information regarding the structure of micelles can be derived from the light scattered by a micellar solution, through the use of various techniques, including quasielastic light scattering (QLS), and static light scattering (SLS) intensity measurements. In SLS, the intensity of light scattered by the micellar solution gives an indication of the size of the micellar aggregates present in the solution. The intensity of scattered light varies with the concentration of surfactants in the solution, as well as with scattering angle. The radius of gyration of the micelles, as well as the second virial coefficient, can be deduced from the variation of the scattered light intensity with scattering angle and surfactant concentration. In QLS, also referred to

as dynamic light scattering, the property of interest is the fluctuation of the intensity of scattered light about a mean value, which in micellar solutions results from the Brownian motion of the micellar aggregates. These fluctuations give an indication of the size of the micelles, as will be discussed in Section IIA below.

A. Quasielastic Light Scattering (QLS)

The intensity of scattered light, I, measured at a particular scattering angle, θ, with respect to the incident light having intensity, I_o, fluctuates about a mean intensity value because of the Brownian motion of the scattering particles. The time dependence of these intensity fluctuations can be described by the intensity autocorrelation function[2], $C(t)$. Note that $C(t)$ measures the correlation between the intensity of scattered light at any initial time, and the intensity after a finite time interval, Δt. In other words,

$$C(t) = \langle I(0)I(t)\rangle = \lim_{T\to\infty}\frac{1}{T}\int_0^T d\tau\ I(\tau)\ I(\tau+t)\ , \qquad (1)$$

where the initial time was taken as $t_0=0$, and $\Delta t=t$. In QLS, the total time during which a measurement is made, T, is divided up into discrete time intervals, $\Delta\tau$, which are small in relation to the time it takes for a fluctuation to relax back to its mean value. The intensity of scattered light is measured in each of these time intervals. $C(t)$ represents the average of the product of the intensities in these discrete time intervals as a function of the time between the intervals, t. Using discrete notation[3], therefore,

$$C(t) = \langle I(0)I(t)\rangle = \lim_{N\to\infty}\frac{1}{N}\sum_{j=1}^{N} I_j\ I_{j+m}\ , \qquad (2)$$

where $j=\tau/\Delta\tau$, $m=t/\Delta\tau$, and $N=T/\Delta\tau$ represents the total number of discrete time

intervals. At low values of t (or small m), the intensity measurements are highly correlated. For instance, at $t=0$,

$$C(0) = \langle I(0)I(0)\rangle = \langle I(0)^2\rangle = \langle I^2\rangle \geq \langle I(0)I(t)\rangle \ . \tag{3}$$

On the other hand, at large values of t, the correlation between the signals is lost, such that

$$C(t\rightarrow\infty) = \langle I(0)\rangle\langle I(t)\rangle = \langle I(0)\rangle^2 = \langle I\rangle^2 \ . \tag{4}$$

Between these two limits, the correlation function decays from $\langle I^2 \rangle$ to $\langle I \rangle^2$. In many applications, the decay occurs exponentially, that is,

$$C(t) = Ae^{-2\Gamma t} + B \ , \tag{5}$$

where A is a constant determined by the instrument design, B is the constant background term, and Γ is the "relaxation time" or correlation time. A comparison of Eqs. (4) and (5), in the limit $t\rightarrow\infty$, shows that $B = \langle I \rangle^2$. Using this value of B, in conjunction with Eqs. (3) and (5), in the limit $t\rightarrow 0$, gives $A = \langle I^2 \rangle - \langle I \rangle^2$ The decay of the correlation of the intensity fluctuations (recall that these are due to Brownian motion) depends on the diffusivity of the micelles, according to the equation

$$\Gamma = Dq^2 \ , \tag{6}$$

where D is the translational diffusion coefficient, and q is the scattering vector, given by

$$q = \frac{4\pi n}{\lambda}\sin\frac{\theta}{2} \ . \tag{7}$$

In Eq.(7), n is the index of refraction of the suspending fluid, λ is the wavelength of the laser light, and θ is the scattering angle, which for QLS is typically equal to 90°. The property of the scattering particles that is ultimately measured by QLS is, therefore, D, which is related to the particle shape and size. For the simplest case of spherical particles, the Stokes-Einstein relation yields[4]

$$D = \frac{kT}{6\pi\eta r_{sphere}}, \tag{8}$$

where k is the Boltzmann constant, T is the absolute temperature, η is the solvent viscosity, and r_{sphere} is the radius of the spherical particle. For a monodisperse system of nonspherical particles in the absence of interactions, the hydrodynamic radius, R_h, is defined as the radius of the sphere having the same diffusion coefficient as the arbitrarily shaped scattering particle. For polydisperse particles, the effective mean hydrodynamic radius, $\bar{R}_h$, is defined as

$$\bar{R}_h = \frac{kT}{6\pi\eta \langle D \rangle}, \tag{9}$$

where $\langle D \rangle$ is the z-average diffusion coefficient, the effective diffusion coefficient measured in QLS according to Eq.(6). In the presence of interactions, including excluded-volume interactions resulting from possible entanglements of micellar species, the length scale measured corresponds to a correlation length, that is,

$$\xi_h = \frac{kT}{6\pi\eta \langle D \rangle}. \tag{10}$$

Thus, in the semidilute regime of micellar solutions, as will be discussed in detail in Chapter 4, the relevant parameter is no longer the individual micelle hydrodynamic radius, $\bar{R}_h$, but instead the correlation length, ξ[5], which is a measure of the degree of entanglement, or the tightness of the micellar net. It should be noted that, as expressed in Eq.(10), QLS measures the collective-diffusion coefficient, in contrast to a self-diffusion coefficient, D_s, which describes the motion of a single micelle in solution[5].

Cumulants Analysis[6,7,5]. When there is a broad size distribution of particles, the measured autocorrelation function, $C(t)$, becomes a weighted average of contributions from the differently sized particles, namely,

$$\frac{C(t)}{C(0)} = \left(\sum_{i=1}^{\infty} G_i e^{-\Gamma_i t} \right)^2 , \tag{11}$$

where $\Gamma_i = D_i q^2$, with D_i being the diffusion coefficient of the ith species, and G_i is the fraction of the intensity scattered by the ith species. In the cumulants analysis method, the logarithm of the left-hand side of Eq.(11) is expanded in a power series in τ

$$\frac{1}{2} \ln\left(\frac{C(t)}{C(0)} \right) = \sum_{j=1}^{\infty} (-1)^j \frac{k_j}{j} t^j , \tag{12}$$

where the coefficients k_j are defined as the cumulants of G_i. The first cumulant, k_1, is related to the mean translational diffusion coefficient, $<D>$, using

$$<D> = \frac{k_1}{q^2} . \tag{13}$$

In turn, $<D>$ is related to the effective mean hydrodynamic radius, $\bar{R}_h$, according to Eq.(9).

B. Intensity Measurements

The total scattered light intensity, I_{total}, is due to two contributions, that is,

$$I_{total} = I_s + I_r , \tag{14}$$

where I_s is the contribution due to concentration fluctuations, and I_r is the contribution due to density fluctuations. In micellar solutions, I_r has been determined to represent well the contribution from the scattering attributed to the solvent (water)[8], and thus represents the background contribution. I_s depends on the scattering angle, θ, the solution refractive index increment, $(\partial n/\partial c)_{T,P}$, and the osmotic compressibility, $(\partial \pi/\partial c)^{-1}_{T,P}$, through the Ornstein-Zernike relation

$$I_s = \frac{AckT\left(\frac{\partial n}{\partial c}\right)^2_{T,P}}{(1+q^2\xi^2)\left(\frac{\partial \pi}{\partial c}\right)_{T,P}}, \qquad (15)$$

where, as explained earlier, q = $(4\pi n/\lambda)\sin(\theta/2)$ is the magnitude of the scattering vector, λ is the wavelength of the incident light, n is the index of refraction of the medium, A is an instrument constant, and ξ is the correlation length. In dilute solutions far from the critical point, the osmotic compressibility is related to the weight-average aggregation number, $<N_w>$, and the second virial coefficient, B, by the relation

$$<N_w>^{-1} = M\left(\frac{(\partial\pi/\partial c)_{T,P}}{kT} - 2Bc\right), \qquad (16)$$

where *M* is the molecular weight of the surfactant. For sufficiently dilute solutions, the term *2Bc* is negligibly small, leading to the approximate relation

$$I_s \sim \frac{Ac<N_w>\left(\frac{\partial n}{\partial c}\right)^2_{T,P}}{M(1+q^2\xi^2)}. \qquad (17)$$

At constant scattering angle, therefore, and at temperatures far below the critical temperature (where critical fluctuations are not significant), large increases in the intensity of scattered light could indicate an increase in $<N_w>$, reflecting micellar growth.

III. MATERIALS AND EXPERIMENTAL METHODS

A. Materials and Sample Preparation

Homogeneous C_iE_j surfactants were obtained from Nikko Chemicals, Tokyo,

and used without further purification. To ensure uniformity in the results, measurements were conducted using the same lot number for each surfactant: $C_{12}E_6$ (Lot 9011) and $C_{12}E_8$ (Lot 9054). The high purity of the surfactants was confirmed by the absence of any detectable minimum in the measured surface tension versus surfactant concentration curves of aqueous solutions of each surfactant. Salts were of the analytical reagent grade from Mallinckrodt, and were further purified to remove any organics by ignition at 450°C overnight. Salt solutions were prepared by weight, using deionized water which was purified using a Milli-Q ion-exchange system. Surfactant of a known weight was then added to each of the salt solutions. The prepared surfactant solutions were utilized within the same day.

Before use, all glassware were immersed in a 1N NaOH-ethanol bath for at least 8 hours, then in a 1N nitric acid bath for another 8 hours, followed by thorough rinsing with Milli-Q water. The glassware were then dried in an oven.

The scattering cells were first rinsed with a surfactant solution which was filtered through a 0.2 μm filter to remove dust, and then filled with the rest of the surfactant solution. The temperature was allowed to equilibrate for at least 30 minutes in the index matching fluid contained in the sample-cell assembly before measurements were made.

B. Light Scattering Measurements

Intensity and QLS measurements were performed at a scattering angle $\theta = 90°$, using a Brookhaven Model BI-200SM instrument. The light source is a Lexel 8 mW argon laser ($\lambda = 514$ nm). The signal analysis was performed using a BI-9000AT digital correlator. Intensity measurements were done on 1 weight percent solutions of $C_{12}E_6$ in pure water, 1m KCl, 1m KBr, and 1m KI. These measurements were performed as a function of temperature, in the range 15-50°C.

QLS measurements were performed on a 1 weight percent solution of $C_{12}E_8$ in pure water, 1m KCl, 1m KBr, and 1m KI at 25°C. Measurements for $C_{12}E_6$ and $C_{12}E_8$ in pure water were also done as a function of surfactant concentration, from

X≈0.0001 to X≈0.003, at 25°C and 35°C for $C_{12}E_6$, and at 35°C and 45°C for $C_{12}E_8$.

IV. RESULTS AND DISCUSSIONS

A. Quasielastic Light Scattering (QLS) Measurements. Fig. 1 shows plots of the average effective diameter (equal to twice the effective mean hydrodynamic radius, $\bar{R}_h$) of $C_{12}E_6$ micelles in water, at T=25°C and 35°C, as a function of surfactant concentration. Also shown are plots of the average effective diameter of $C_{12}E_8$ micelles in water, at T=35°C and 45°C, as a function of surfactant concentration. It is clear from the $C_{12}E_8$ plots that, at the two temperatures examined (T=35°C and 45°C), the tendency for one-dimensional growth is not strong for $C_{12}E_8$ micelles, which, as explained in Chapter 2, can be attributed to the large $g_{s/hl}$ value for $C_{12}E_8$ at these temperatures. In other words, even as the temperature is increased to 35°C and 45°C, the average effective diameter of the $C_{12}E_8$ micelles (≈60Å) is still approximately equal to twice the length of a $C_{12}E_8$ surfactant molecule (≈36Å), over the range of surfactant concentrations examined. The situation is radically different for $C_{12}E_6$ micelles. Indeed, as shown in Fig. 1, micellar growth is already induced at 25°C upon increasing $C_{12}E_6$ concentration, as reflected by an increase in the average effective diameter of the $C_{12}E_6$ micelles. The growth of the micelles with increasing surfactant concentration is consistent with predictions using thermodynamic theories of micellization and growth[7,9]. This phenomenon is magnified at 35°C, where there is more substantial growth. Temperature-induced micellar growth is a consequence of the lower transfer free energy of a PEO head, $g_{s/hl}$ as defined in Chapter 2, from the bulk aqueous solution to the micelle head layer. A lower value of $g_{s/hl}$ corresponds to less attractive interactions between the PEO heads and water, which is indeed observed when the solution temperature is increased[10]. It is noteworthy that beyond a certain $C_{12}E_6$ concentration (at X_{C12E6}≈0.001, see arrow in Fig. 1), the average effective diameter begins to decrease. This is because, at these solution conditions, QLS measures the average collective diffusion coefficient. Therefore,

when $C_{12}E_6$ micelles begin to entangle, as will be discussed in Chapter 4, the measured average effective diameter actually reflects the correlation length of the collective entangled net, and not the individual $C_{12}E_6$ micellar size. The growth and entanglement of elongated micelles will be discussed in detail in Chapter 4.

As discussed, one-dimensional growth of $C_{12}E_8$ micelles does not seem to be induced by an increase in temperature (raising it to 35°C and 45°C), nor by an increase in the surfactant concentration. To probe the effect of salts on micellar growth, the hydrodynamic radius of $C_{12}E_8$ micelles in pure water, 1m KCl, 1m KBr, and 1m KI was measured at 25°C, where the surfactant concentration was kept constant at 1 wt%. The effective mean hydrodynamic radius, $\bar{R}_h$, measured using QLS, and calculated using Eq.(9), where the viscosity of pure water at temperature, T was used for η, was found to be 29.7Å in pure water, 26.9Å in 1m KCl, 26.9Å in 1m KBr, and 22.9Å in 1m KI solutions. These findings suggest that at 25°C, the addition of salts to $C_{12}E_8$ aqueous solutions does not induce a significant change in $\bar{R}_h$. In addition, these findings indicate that $C_{12}E_8$ micelles remain roughly spherical in 1m salt solutions of KCl, KBr, and KI at 25°C. As alluded to briefly in Chapter 2, the $g_{s/hl}$ value for the longer E_8-PEO head chain is greater than that for an E_6-PEO head chain. Recall that $g_{s/hl} = \nu j \phi_{hl}$, where j is the number of EO units in the head, ϕ_{hl} is the average volume fraction of head chains in the micelle head layer, and ν is the enthalpy parameter defined in Chapter 2. The larger value of $g_{s/hl}$ for the longer E_8-PEO head chain inhibits micellar growth, since the decrease in the curvature of the micellar-core surface associated with micellar growth would cause an increase in ϕ_{hl}, and, therefore, would increase the magnitude of $g_{s/hl}$ even more.

B. Intensity Measurements

The intensity of scattered light from $C_{12}E_6$ micelles in pure water, as well as in aqueous salt (KCl, KBr, KI) solutions, was measured as a function of temperature, and the results are shown in Fig.2. All the curves indicate temperature-induced

micellar growth of $C_{12}E_6$ micelles, where the scattered light intensity increases rapidly for each solution beyond a certain temperature, T_{growth}. Note that $T_{growth} < 15°C$ for $C_{12}E_6$ in 1m KCl, $T_{growth} \approx 18°C$ in pure water and in 1m KBr, and $T_{growth} \approx 30°C$ in 1m KI (see arrows in Fig. 2). As indicated above, this marked change in intensity is an indicator of micellar growth since critical-fluctuation effects are expected to be small because, in all cases, growth occurs at temperatures well below the corresponding critical temperatures ($T_c - T_{growth} \approx 30°C$ in each case). Fig. 2 indicates that the addition of KBr increases only slightly the propensity of $C_{12}E_6$ micelles to grow, as shown by the fact that the measured intensities are only slightly higher than those in pure water. The addition of KCl, on the other hand, induces extensive $C_{12}E_6$ micellar growth, as reflected in the high intensity values even at low temperatures. Recall that the addition of KCl increases the micellar core-aqueous salt solution interfacial tension, σ_0, (see Table II in Chapter 2), and, therefore, would increase the interfacial free energy contribution, g_σ, to the micellization free energy. Recall that in Chapter 2, g_σ was given by

$$g_\sigma = \sigma_o \left(1 - \frac{(S-1)\delta}{l_c}\right)(a - a_o) , \qquad (18)$$

where σ_o is the interfacial tension between bulk hydrocarbon and the salt solution, δ is the Tolman distance, a measure of the interfacial thickness, a is the interfacial area per monomer [$= Sv_c/l_c$, where S is a shape factor (3 for spheres, 2 for cylinders and 1 for discs or bilayers), v_c is the volume of the hydrocarbon tail, and l_c is the micellar core-minor radius], and a_o is the screened interfacial area per monomer which corresponds to the bond between the hydrocarbon tail and the head. The increase in σ_0 upon the addition of KCl to the solution increases the tendency of the micelles to grow, since the lower curvature of the micellar-core surface, resulting from micellar growth, decreases the area of the micellar core, a-a_0, exposed to the aqueous salt environment. Equally interesting is the observation that KI seems to inhibit micellar growth, as compared to the pure water case. This is consistent with the picture presented earlier regarding the possible specific complexation between

I^- and the PEO heads, which effectively adds an electrostatic component to the head interactions. In other words, there could be an added electrostatic repulsion between the heads due to the *pseudocharge* assumed by the heads, which would not favor micellar growth. Accordingly, in the KI case, the transition to larger micelles occurs at higher temperatures. We speculate that the specific binding of I^- to the PEO heads is weakened by increasing temperature (decreased ion binding), which triggers a transition from spheroidal to rod-like micelles at the observed higher temperature, $T_{growth} \approx 30°C$.

V. CONCLUDING REMARKS TO CHAPTER 3

In summary, therefore, light scattering results have shown that $C_{12}E_6$ micelles grow with increasing both temperature and surfactant concentration. A possible transition to the entangled regime was indicated by the observed maximum in the measured average effective diameter of the $C_{12}E_6$ micelles as a function of surfactant concentration at T=35°C. The addition of KCl to the $C_{12}E_6$ solution substantially enhances micellar growth, while the addition of KI suppresses micellar growth. On the other hand, $C_{12}E_8$ micelles do not seem to exhibit growth upon increasing temperature and surfactant concentration, or by adding salts to the micellar solution.

The observed micellar growth of $C_{12}E_6$ micelles induced by increasing temperature and surfactant concentration, as well as by adding certain salts to the solution, presents interesting possibilities with regards to the underlying structure of the micellar solution. Chapter 4 deals with the possibility of generating micellar entanglements in the limit of extensive micellar growth, and examines changes in solution properties, specifically changes in solution viscosity, as a consequence of micellar entanglements.

REFERENCES FOR CHAPTER 3

1. For an introduction to light scattering in micellar solutions see Corti, M., "Proceedings of the International School of Physics Enrico Fermi-Physics of Amphiphiles: Micelles, Vesicles and Microemulsions", (ed. V. Degiorgio and M. Corti), North-Holland, The Netherlands (1985).

2. Clark, N. A.; Lunacek, J. H.; Benedek, G. B. *Am. J. Phys.* **1970**, *38*, 575.

3. Berne, B. J.; Pecora, R. *Dynamic Light Scattering*, John Wiley and Sons, Inc.: New York, 1976; p. 13.

4. Einstein, A. Investigation on the Theory of the Brownian Movement, Dover Publications: New York, 1956, p.58.

5. Candau, S. J. "Light Scattering" *in* Surfactant Solutions, New Methods of Investigation

6. Brown, J. C.; Pusey, P. N.; Dietz, R. *J. Chem. Phys.* **1975**, *62*, 1136.

7. Missel, P. J.; Mazer, N. A.; Benedek, G. B.; Young, C. Y.; Carey, M. C. *J. Phys. Chem.* **1980**, *84*, 1044.

8. Corti, M., Minero, C. and Degiorgio, V., J. Phys. Chem, 88, 309 (1984).

9. Puvvada, S.; Blankschtein, D. *J. Chem. Phys.* **1990**, 92, 3710.

10. Bjorling, M.; Karlstrom, G.; Linse, P. *J. Phys. Chem.* **1991**, *95*, 6706.

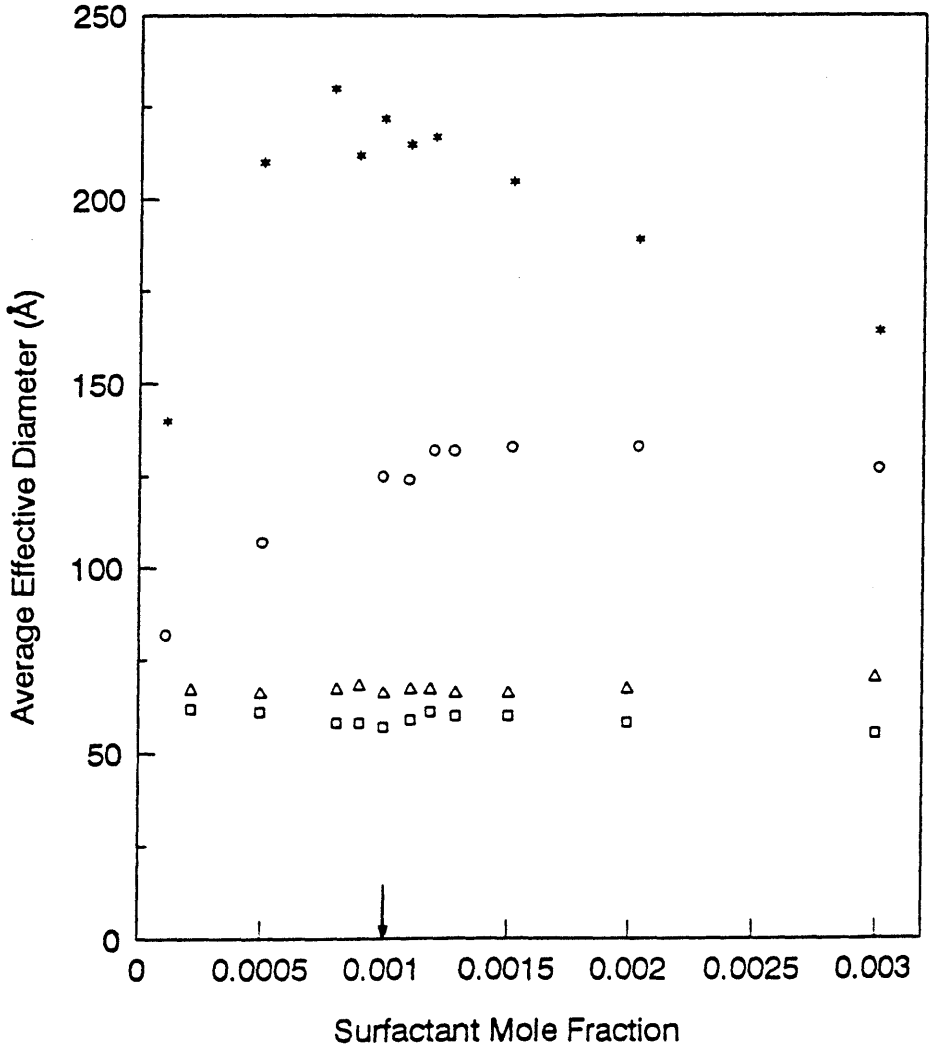

Figure 1. Average effective micelle diameter (in Å) as a function of surfactant mole fraction for $C_{12}E_8$ at T=35°C (□) and T=45°C (△), and for $C_{12}E_6$ at T=25°C (○) and T=35°C (*). The arrow indicates the onset of entanglements of $C_{12}E_6$ micelles at T=35°C.

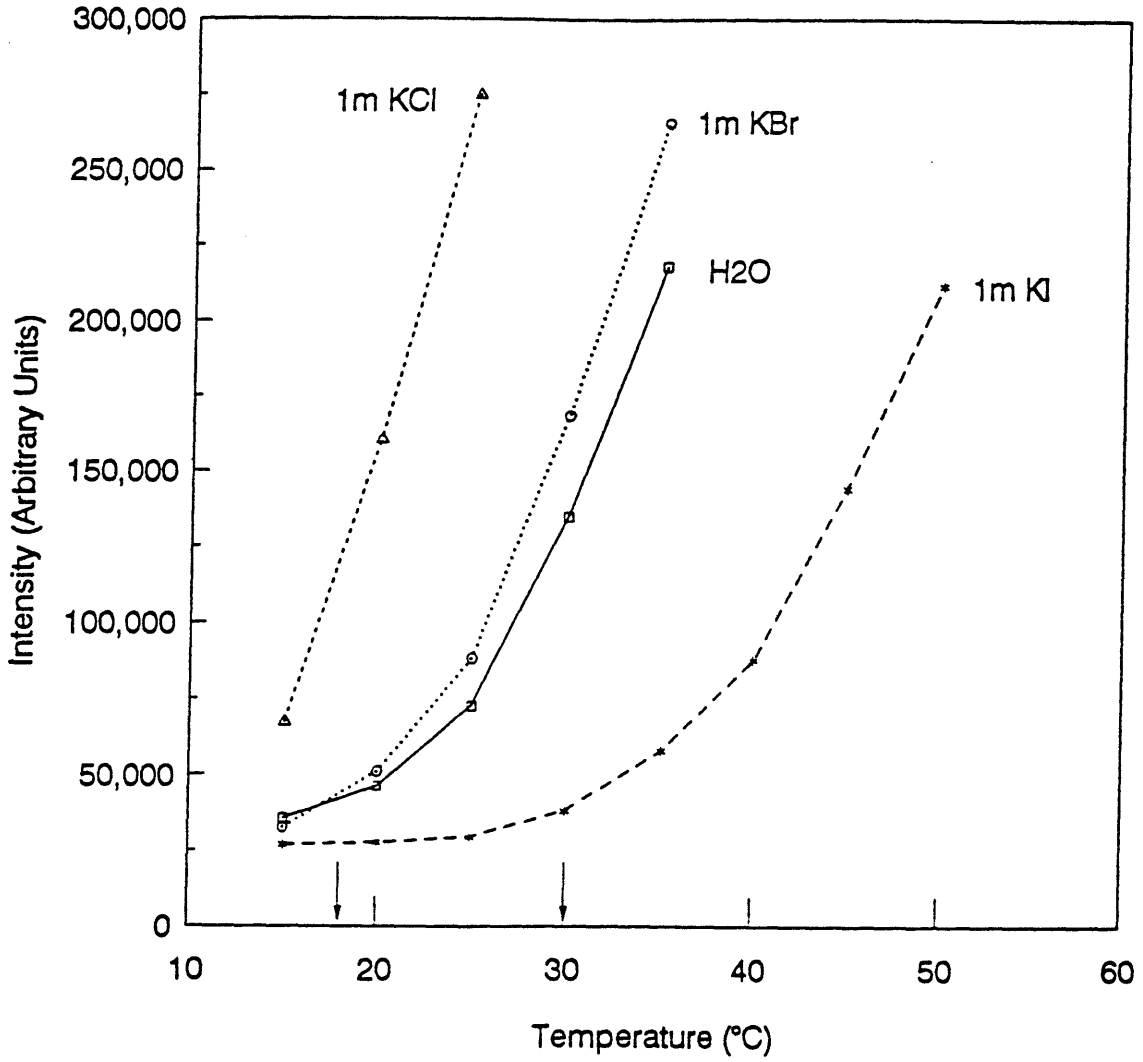

Figure 2. Intensity of scattered light as a funtion of temperature for $C_{12}E_6$ in water (□), 1m KCl (▵), 1m KBr (○) and 1m KI (*). The various lines are drawn to guide the eye.

CHAPTER 4. THEORETICAL AND EXPERIMENTAL DETERMINATIONS OF THE CROSSOVER FROM DILUTE TO SEMIDILUTE REGIMES OF MICELLAR SOLUTIONS

I. INTRODUCTION

A delicate balance of intermolecular forces, including van der Waals, electrostatic, steric, and hydrophobic, exists between surfactant molecules within a self-assembling micellar aggregate[1-5]. By modifying the molecular architecture of the surfactant, and/or by varying solution conditions, the balance of intermolecular forces may favor micellar growth into one-dimensional (rod-like) or two-dimensional (sheet-like) assemblies[3-5]. In the case of one-dimensional growth, beyond a certain length scale, known as the persistence length, the rod-like micelles become flexible and resemble polymers in solution[6]. Indeed, there is ample experimental evidence supporting the existence of long, flexible polymer-like micelles[6]. This phenomenon appears to be a general one, since it has been observed in solutions containing ionic[7-10], nonionic[11,12], as well as zwitterionic[13] surfactants.

If the tendency for one-dimensional growth is sufficiently strong, almost unlimited uniaxial micellar growth may occur[3-5,14-16]. In that case, the rod-like micelles may become sufficiently long so as to entangle with one another and form a transient network of overlapping micelles. Such a behavior would be analogous to that encountered in semidilute polymer solutions which consist of an entangled network of polymers[17]. Indeed, there is now increasing experimental evidence for the existence of such entangled micellar phases in many different surfactant solutions[6-13].

In view of the general occurrence of entangled micellar phases, it is of considerable interest to quantitatively assess whether entanglements occur in a particular micellar system, as well as to predict the conditions at which they occur. This is particularly important since the occurrence of entanglements may have an

impact on the theoretical description of the phase behavior, including phase separation, of the micellar system, and hence on the ability to predict surfactant solution properties. The analogy with polymer solutions suggests that the onset of entanglements can be described by the crossover surfactant concentration, X^*, marking the transition, or crossover, of the micellar solution from the dilute to the semidilute solution regimes[17,6]. In the dilute regime the micellar solution consists of rod-like micelles which are singly dispersed in the solvent, each characterized by its radius of gyration, whereas in the semidilute regime it consists of a transient network of entangled rod-like micelles, characterized by an average network size which is independent of micelle molecular weight[17,6].

To compute X^*, in this chapter formalisms developed for polymer solutions will be extended by explicitly incorporating the unique self-assembling nature of micelles. Indeed, in contrast to polymers, the shape and size of micellar aggregates are not necessarily fixed, and significant morphological changes can be induced by varying surfactant concentration, temperature, and other solution conditions[3-5]. Furthermore, micelles are dynamic entities which are continuously and reversibly exchanging monomers with one another, a process that can generate an entire distribution of micellar sizes. The resulting distribution and any equilibrium property derived from it can respond in a reversible manner to changes in solution conditions[3-5,14-16]. These salient features of micellar aggregates, as well as their intrinsic flexibility in the case of sufficient one-dimensional growth, are incorporated in the theoretical formulation to compute the crossover surfactant concentration, X^*, presented in Section II. It is noteworthy that the few previous attempts to compute X^* of micellar solutions did not include polydispersity effects or the self-assembling character of micelles[18-20].

Although the theory presented in this chapter can, in principle, be applied to any type of surfactant solution, it will be utilized to predict the crossover concentration of the nonionic surfactant n-dodecyl hexaethylene oxide ($C_{12}E_6$) in aqueous solution. The $C_{12}E_6$-H_2O system was selected because, as shown below, there is considerable evidence suggesting that $C_{12}E_6$ micelles exhibit one-dimensional

growth[21], and, of central importance to the present work, because a physically reasonable working model describing the behavior of this micellar system is available. Specifically, the predictions of a wide spectrum of micellar solution properties were found to compare very favorably with available experimental data[5,16,22]. Of most relevance to the present work is the availability[5,22] of a reliable theoretically predicted micellar size distribution, an essential input for the computation of X^* (see Sec. II).

As emphasized above, sufficient one-dimensional micellar growth is required for the occurrence of entangled micellar phases. In this respect, recent quasielastic light scattering (QLS), static light scattering (SLS), pulsed-field gradient NMR, and sedimentation experiments[23-25], as well as temperature-jump kinetic experiments[26] performed in the $C_{12}E_6$-H_2O system, at temperatures below the lower consolute (critical) temperature, T_c, suggest that the micelles present in solution are rod-like and grow considerably both with increasing surfactant concentration and temperature. Furthermore, there is also some evidence for increased micelle flexibility with increasing temperature[25]. This last observation is also consistent with an earlier small-angle neutron scattering (SANS) study[27] which suggested the existence of flexible rod-like micelles. On the other hand, other SANS measurements[28,29] and NMR experiments[30] have been interpreted as indicating the presence of small spheroidal micelles which do not exhibit growth. The latter interpretations have emphasized the role of critical fluctuations and intermicellar interactions, which should become very important in the vicinity of T_c, in determining the observed experimental behavior[31]. To shed some light on this controversy, transient fluorescence experiments, which are supposed to be sensitive only to individual micellar properties, were recently performed[32]. Although this latter study has unambiguously demonstrated micellar growth in the temperature range, T_c-35°C$<T<T_c$-7°C, attention has been drawn[33] to the fact that this experimental technique yields aggregation numbers which are weighed toward the low end of the distribution of aggregation numbers. In other words, sizes of large micelles cannot be measured by this technique[33]. More recently, highly precise SLS and QLS measurements[34] have clearly demonstrated that rod-

like micellar growth does occur, as well as pointed out that critical-fluctuation effects become important in the temperature range $T>T_c$-4°C.

In view of the experimental observations presented above, one can conclude that there is considerable evidence supporting the existence of rod-like, possibly flexible, micelles in the $C_{12}E_6$-H_2O system which grow with increasing temperature and surfactant concentration[21]. It is also noteworthy that this conclusion is consistent with our recent quantitative theoretical prediction[5] of the occurrence of a "sphere-to-rod" shape transition with increasing temperature and surfactant concentration in this system. It should be kept in mind, however, that because of the existence of a lower consolute (critical) point, the role of intermicellar interactions and critical fluctuations becomes increasingly important as one approaches T_c. In this chapter, the existence and growth of rod-like, flexible $C_{12}E_6$ micelles will be adopted as a working hypothesis for the computation of the crossover surfactant concentration, X^*, presented in Secs. II and V, as well as for the viscosity analysis presented in Secs. III and V.

Furthermore, this chapter also presents an attempt to experimentally estimate the $C_{12}E_6$ crossover concentration, X^*, based on a comparison of the predicted dilute-solution viscosities, calculated in the context of a generalized Doi-Edwards theory[35,20] applied to flexible, polydisperse rod-like micelles, with measured viscosities in the $C_{12}E_6$-H_2O system as a function of surfactant concentration and temperature (see Secs. III, IV and V). It should be noted that, with few exceptions[36,37], interpretations[38-40] of viscosity measurements in micellar systems have utilized the concept of an intrinsic viscosity, $\eta_{in}=\lim_{x\to 0}(\eta-\eta_s)/\eta_s X$, where η and η_s are the viscosities of the solution and the solvent, respectively, and X is the solute concentration. Strictly speaking, this concept is only valid for solute species which maintain their integrity as the solute concentration is varied. For macromolecules whose molecular sizes are fixed on synthesis, taking the dilute-solution limit, $X\to 0$, eliminates interparticle interactions and therefore isolates the contribution of each macromolecule to the solution viscosity. Consequently, this concept can be used to

extract properties of individual macromolecules such as their size, shape and hydration state. In contrast, in the case of self-assembling species, such as micellar aggregates, changing concentration can significantly affect micelle shape and size, particularly under conditions where micellar growth is known to occur. In that case, the physical significance of taking the dilute-solution limit, $X \to 0$, is lost, and no meaningful conclusions regarding individual micellar properties at finite concentrations can be drawn. Similar complications have recently been shown to occur in the interpretation of osmotic pressure measurements of micellar solutions to obtain average micelle aggregation numbers[41].

The remainder of this chapter is organized as follows. Sec. II describes the general theoretical approach to predict the crossover surfactant concentration, as well as its application to the $C_{12}E_6$-H_2O system. Sec. III presents a theoretical description of the specific viscosity in the limit of dilute solutions. Sec. IV describes the viscosity measurements conducted. Sec. V describes the experimental and theoretical results. Finally, Sec. VI presents a summary and discussion of the results.

II. THEORETICAL APPROACH TO PREDICT THE CROSSOVER SURFACTANT CONCENTRATION

A. General Considerations

As emphasized in Sec. I, the analogy with polymer solutions will be exploited in order to predict the crossover surfactant concentration of micellar solutions. Recall that in monodisperse polymer solutions, the crossover concentration, X^*, is the concentration which signals the transition, or crossover, from the dilute to the semidilute solution regimes[17]. In other words, X^* is defined as the polymer concentration at which the various polymer coils begin to overlap[17]. Thus, at X^*, the following condition is satisfied

$$Nv \simeq V_T \,, \tag{1}$$

where N is the number of polymer coils, v is the volume occupied by each coil, and V_T is the total volume of the solution.

Note that the actual transition from the dilute to the semidilute regimes is not a sharp one. It begins at the concentration where the polymer coils "touch", but at this point each coil still maintains its identity. As the concentration is increased, the coils begin to overlap and entangle; however, the coils, although overlapping, are not yet in the semidilute regime. Further increase in polymer concentration will eventually induce the system to reach the point at which the coils are completely entangled and look very much like a polymer network. Under these conditions, a coil segment cannot distinguish whether another segment is part of the same coil or belongs to a different one. This signals the entrance into the semidilute regime[17]. Therefore, the condition given in Eq. (1) is associated with a lower limit of a relatively broad transition region, that is, it reflects the concentration at which the polymer coils first "touch".

The volume occupied by a polymer coil, v, has been bracketed by[42]

$$\langle R_g^2 \rangle^{3/2} \leq v \leq \frac{4\pi}{3} \langle R_g^2 \rangle^{3/2} \,, \tag{2}$$

where $\langle R_g^2 \rangle$ is the mean square polymer-coil radius of gyration, the mean-square distance of the coil segments from the center of gravity[43]. The higher bound in Eq. (2) will be used in our calculations.

In applying these concepts to a polymer-like micelle of aggregation number n, it follows from Eq. (2) that the volume it occupies is given by

$$v_n = \frac{4\pi}{3} \langle R_g^2 \rangle_n^{3/2} \,, \tag{3}$$

where $\langle R_g^2 \rangle_n$ is the mean square radius of gyration of an n-type micelle, hereafter

referred to as an n-mer.

As described in Sec. I, in the case of one-dimensional growth, micelles are expected to become flexible when their length exceeds the persistence length, ξ. The origin of ξ can be attributed to the finite diameter of the micelle, and, in the case of nonionic surfactants treated in this paper, also to the steric interactions between the hydrophilic surfactant moieties at the micelle core-water interface[44]. Note that although micelle flexibility should vary with the structure of the surfactant molecule, and possibly also with solution conditions which may affect the delicate balance of intramicellar forces, it is not expected to depend significantly on intermicellar interactions, specially for nonionic surfactants where these interactions are of a shorter range. To model flexible, rod-like micelles, the worm-like chain model of Kratky and Porod[45] will be adopted. Specifically, this model will be used to evaluate $<R_g^2>_n$ of an n-mer. In this model, a worm-like structure is described as a continuously curving chain, wherein the direction of curvature at any point is random. The mean square radius of gyration, $<R_g^2>$, is given by[46,47]

$$<R_g^2> = \frac{L\xi}{3} - \xi^2 + \frac{2\xi^3}{L} - \frac{2\xi^4}{L^2}[1-\exp(-\frac{L}{\xi})] , \qquad (4)$$

where ξ is the chain persistence length, and L is the chain contour length. Note that ξ increases with increasing stiffness, but is (on the basis of the model) independent of L. It follows from Eq. (4) that in the limit of very short (rigid) chains, that is, for $\xi \gg L$, one obtains

$$<R_g^2> \simeq \frac{L^2}{12} , \qquad (5)$$

which is the well-known result for a rigid rod, while in the limit of very long (semiflexible) chains, that is, for $\xi \ll L$, one obtains

$$\langle R_g^2 \rangle \simeq \frac{L\xi}{3} \ . \qquad (6)$$

Recalling[43] that for a freely-jointed (fully flexible) chain, the "persistence length" is equal to half the chain bond length, a, that is, $\xi = a/2$, Eq. (6) reduces to $\langle R_g^2 \rangle \simeq La/6$, which is the well-known result for a Gaussian coil. It follows then, that Eq. (4) provides a reasonable description of the entire shape evolution from a rigid rod to a flexible worm to a Gaussian coil as the flexibility parameter, L/ξ, increases. This is particularly important when dealing with micellar aggregates which can change their shape, size and size distribution, and possibly also their flexibility, as the temperature, surfactant concentration, or other solution conditions are varied.

Adopting Eq. (4) to describe a worm-like micelle of aggregation number n, the mean square radius of gyration, $\langle R_g^2 \rangle_n$, is given by

$$\langle R_g^2 \rangle_n = \frac{L_n\xi}{3} - \xi^2 + \frac{2\xi^3}{L_n} - \frac{2\xi^4}{L_n^2}\left[1 - \exp\left(-\frac{L_n}{\xi}\right)\right] , \qquad (7)$$

where L_n is the contour length of the n-mer, and, as explained earlier, ξ is independent of L_n.

Eq. (1) can be conveniently generalized to the case of a polydisperse system of micelles at the crossover point. Specifically, one requires that the total volume occupied by the micelles be equal to the solution volume, V_T , that is,

$$\sum_n N_n v_n = V_T = N_s V_s + N_w V_w \ , \qquad (8)$$

where N_n is the number of n-mers, v_n is the volume occupied by an n-mer, N_s and N_w are the total number of surfactant and water molecules, respectively, and V_s and V_w are the molecular volumes of a surfactant and a water molecule, respectively. Note that in defining V_T it was assumed that, at the dilute surfactant concentrations of interest, partial molecular volumes can be replaced by molecular volumes. Using

mole fraction units, with $X=N_s/(N_s+N_w)$, the total surfactant mole fraction, and $X_n=N_n/(N_s+N_w)$, the mole fraction of n-mers, at the crossover surfactant concentration, X^*, Eq. (8) can be rewritten as

$$\sum_n X_n^* v_n = X^* V_s + (1-X^*) V_w , \tag{9}$$

where X^*_n denotes the n-mer mole fraction at X^*.

As discussed in Sec. I, a salient characteristic of self-assembling structures like micelles is the dependence of the size distribution, $\{N_n\}$, or equivalently, $\{X_n\}$, on solution conditions, notably surfactant concentration and temperature. Accordingly, the left-hand side of Eq. (9), that is, $\Sigma_n X^*_n v_n$, is an explicit function of surfactant concentration, X, temperature, T, as well as other variable solution conditions. This adds an interesting new dimension to the computation of X^* in self-assembling micellar solutions which is not present in typical macromolecular systems such as polymer solutions, where the size distribution is fixed upon synthesis due to the chemical, rather than physical, nature of the intra-macromolecular bonds.

Returning to the computation of the volume of an n-mer, v_n, in view of Eqs. (3) and (7), it is apparent that v_n is a function of the contour length of the n-mer, L_n, which in turn is a function of the aggregation number, n. To establish a relation between L_n and n, it is useful to utilize a simple geometric model of a micelle that exhibits one-dimensional growth. The spherocylindrical micelle model[48], depicted schematically in Fig. 1, provides a convenient representation of such a micelle. Using this model micelle, in the context of geometric packing constraints, it is possible to relate L_n to n as follows

$$L_n = \frac{n v_c}{\pi l_c^2} + \frac{2 l_c}{3} + 2 l_{hg} , \tag{10}$$

where v_c and l_c are the volume and effective length (equivalent to the micelle-core minor radius) of the surfactant hydrophobic moiety, respectively, and l_{hg} is the

effective length of the surfactant hydrophilic moiety. Numerical values of these molecular parameters for $C_{12}E_6$ are given in Table 1.

B. Application to the $C_{12}E_6$-H_2O System

The application of the formalism developed in Sec. IIA requires the availability of a reliable theoretical expression for the micellar size distribution, $\{X_n\}$, which can then be used in Eq. (9) to compute the surfactant crossover concentration curve, $X^*(T)$. In this respect, a recently developed molecular-thermodynamic approach to predict micellar solution properties[5] will be used. The new approach consists of blending a molecular model of micellization[5], which captures the delicate balance of intermolecular forces operating at the micellar level, with a thermodynamic framework for micellar solutions[16], which captures the salient features of the solution at the macroscopic level. The theoretical formulation has been successfully utilized to predict micellar properties of aqueous solutions of nonionic surfactants, belonging to the alkyl polyethylene oxide (C_iE_j) and glucoside families, as a function of surfactant molecular architecture, surfactant concentration, temperature, and concentration of solution modifiers such as urea[5,22].

In the context of the molecular-thermodynamic approach, the distribution of micellar sizes is given by[5]

$$X_n = \frac{(X_1 e)^n}{e} \exp[-\beta n g_{mic}] , \qquad (11)$$

where $g_{mic}(n,l_c,sh)$ is the free energy of micellization, X_1 is the monomer mole fraction, and $\beta = 1/kT$, where T is the absolute temperature and k is the Boltzmann factor. Note that $g_{mic}(n,l_c,sh)$ represents the free-energy change when a surfactant molecule is transferred from bulk solvent (H_2O in the present case) to a micelle characterized by an aggregation number, n, core-minor radius, l_c, and shape, sh, present in the same solvent[5].

The expression for X_n in Eq. (11) assumes either the absence of intermicellar interactions[1-4], or a mean-field type description[16] where the average interaction between two micelles is proportional to the number of monomer-monomer pairs. In addition, Eq. (11) was found[15a] to be valid for the case of excluded-volume interactions between long, rod-like micelles, suggesting that its range of applicability may in fact be quite broad. Moreover, the mean-field treatment of intermicellar interactions has also been successfully utilized[5,16,22] to describe the phase behavior, including phase separation, of aqueous solutions of C_iE_j nonionic surfactants, including $C_{12}E_6$, and of the zwitterionic surfactant C_8-lecithin, in the presence of added electrolytes[49] and urea[50] over a wide range of surfactant concentrations and temperatures which covers the range of $X^*(T)$ values calculated in this paper. This lends credence to the use of Eq. (11) for the determination of the crossover surfactant concentration versus temperature curve, $X^*(T)$, in the $C_{12}E_6$-H_2O system (see also the discussion in Sec. VI).

The free energy of micellization, g_{mic}, in Eq. (11) is calculated using the molecular model of micellization[5,22]. Specifically, this model was adopted to predict the variation of g_{mic} with temperature for the $C_{12}E_6$-H_2O system, see Table 2. Note that in addition to Eq. (11), the surfactant mass-balance equation

$$X = X_1 + \sum_n nX_n \,, \tag{12}$$

must also be satisfied. A simultaneous solution of Eqs. (11) and (12), utilizing the values of g_{mic} given in Table 2, enables us to predict $X_n(X,T)$. These values of $X_n(X,T)$ can then be utilized in Eq. (9) to compute $X^*(T)$.

III. THEORETICAL PREDICTION OF VISCOSITY IN THE DILUTE-SOLUTION LIMIT

In the dilute-solution limit, the contributions of macromolecules to the

solution viscosity can, to a first approximation, be assumed to be additive[43]. Accordingly, for a micellar solution containing a distribution, $\{X_n\}$, of micellar species, the specific viscosity, η_{sp}, can be written as[43]

$$\eta_{sp} = \sum_n \eta_{sp,n} , \tag{13}$$

where $\eta_{sp} = \eta/\eta_s - 1$ is the relative increase in viscosity due to the presence of the micellar species, η_s being the viscosity of the solvent plus monomers present in solution, which, because of the very low value of X_1, is roughly equal to the solvent viscosity, and $\eta_{sp,n}$ is the relative increase in the viscosity of the solution upon the addition of micelles of aggregation number n. In order to estimate $\eta_{sp,n}$ in the case of the rod-like micelles present in the $C_{12}E_6$-H_2O system, the Doi-Edwards theory[35,51], originally formulated to compute the viscosity of solutions containing monodisperse, rigid, rod-like macromolecules, was generalized and used for the case of polydisperse, flexible, rod-like micelles.

In the original theory[35], an expression for the dilute solution specific viscosity of monodisperse, rigid, rod-like macromolecules of length L, was derived by relating the solution viscosity[46,51] to the rotatory diffusivity calculated using the Riseman-Kirkwood theory[52]. The resulting expression for the specific viscosity in the dilute limit is given by

$$\eta_{sp} \sim cL^3 , \tag{14}$$

where c is the number density of rod-like macromolecules.

To incorporate flexibility into the original Doi-Edwards theory, a formulation[53,20] was adopted which introduces an effective rod length,

$$L^* = (\xi L)^{1/2} , \tag{15}$$

to bridge the rod-like behavior between the rigid-rod limit, $\xi > L$, and the random-coil limit, $\xi < L$. Utilizing Eqs. (14) and (15) for flexible, rod-like micelles of aggregation number n, contour length L_n, number density c_n, and persistence length ξ, in Eq. (13)

yields the following expression for the dilute limit of the specific viscosity of the micellar solution

$$\eta_{sp} = \sum_{n} c_n (L_n \xi)^{3/2} \quad . \tag{16}$$

Noting that c_n, the number density of n-type micelles, can be expressed as $X_n /(XV_s + (1-X)V_w)$, where, as stated earlier, V_s and V_w are the molecular volumes of a surfactant and a water molecule, respectively, Eq. (16) can be rewritten as

$$\eta_{sp} = \frac{\sum_{n} X_n (L_n \xi)^{3/2}}{XV_s + (1-X)V_w} \quad . \tag{17}$$

Expressions for X_n [see Eq. (11), with g_{mic} given in Table 2], and L_n [see Eq. (10)] will be derived, following the procedures described in Sec. II, in order to predict the variation of η_{sp} with surfactant concentration and temperature for the $C_{12}E_6$-H_2O system. Values of V_s and V_w are given in Table 1. There is no agreement between reported experimental data for the ξ values in the $C_{12}E_6$-H_2O system[27,54]. Accordingly, several values of ξ will be adopted to determine the best fit of Eq. (17) to the experimentally measured curves in the very low surfactant concentration limit (for details, see Sec. V).

IV. VISCOSITY MEASUREMENTS

As stated in Sec. I, $C_{12}E_6$ micelles display a "sphere-to-rod" shape transition as the temperature is increased beyond approximately 18°C[5]. In addition, the lower consolute (critical) temperature, T_c , is approximately 51°C[22,55]. These two temperatures define a convenient temperature window within which the viscosity measurements can be conducted.

A. Materials and Sample Preparation

Homogeneous $C_{12}E_6$ was obtained from Nikko Chemicals, Tokyo (Lot No. 9011) and used without further purification. The high purity of the surfactant was confirmed by the absence of any detectable minimum in the measured surface tension versus surfactant concentration curves, as well as by comparing the measured value of $T_c \approx 51.14°C$ for the $C_{12}E_6$-H_2O system with values reported in the literature for highly purified samples[55]. Surfactant solutions were prepared using deionized water which was further purified using a Milli-Q ion-exchange system. These solutions were utilized within the same day. Proper precautions against evaporation were taken, since significant evaporation could change the surfactant concentration of the samples during viscosity measurements. Consequently, samples were first placed in sealed test tubes in a water bath while their temperature was brought to the required experimental temperature, such that the equilibration time after transferring the solutions to the viscometer was reduced considerably.

B. Data Collection and Analysis

The kinematic viscosities, η, of fresh surfactant solutions of various concentrations in the range $10^{-6} \leq X \leq 10^{-2}$ and at two temperatures, 35°C and 45°C, were measured using Cannon-Ubbelohde capillary viscometers immersed in a water bath having a temperature stability of ±0.01°C. The time it takes for a definite amount of sample to go through the capillary was measured to the nearest 0.1 second, and was then converted to kinematic viscosity values using constants from calibration procedures (using viscosity standards)[56]. To avoid the need for kinetic-energy corrections[56], flow times were kept to between 200 and 1000 seconds, by varying the diameters of the capillaries of the viscometers used. The viscosity of a sample was measured at least 3 times. More readings were made when the scatter exceeded ±0.4 second.

The absence of a shear-rate dependence of the viscosities at T=35°C up to

a surfactant mole fraction $X=0.005$ was verified by measurements using a Rheometrics Fluids Spectrometer (RFS2), employing a Couette geometry. On the other hand, the most concentrated sample tested at T=45°C that did not exhibit shear-thinning had a mole fraction $X=0.003$. In view of this, only viscosity data corresponding to samples which exhibited Newtonian behavior are reported in this paper. Studies are currently being conducted to probe the surfactant concentration range where non-Newtonian behavior was detected.

In order to obtain an experimental estimate of the crossover surfactant concentration, X^*, the measured viscosities will be compared with those predicted theoretically in Sec. III assuming dilute-solution behavior. Specifically, X^* will be estimated as that surfactant concentration at which an experimental curve first deviates from the theoretical dilute-solution prediction. This is based on the definition of dilute solution as a state in which the contributions of the various solution components to the solution properties are additive, thus reflecting the absence of interactions between these components. Since the crossover surfactant concentration, X^*, is intimately related to the existence of excluded-volume repulsive interactions, the dilute-solution approximation is expected to break down as X^* is approached. For complete details of the experimental X^* estimation, see Sec. V.

V. EXPERIMENTAL AND THEORETICAL RESULTS

A. Experimental Viscosity Behavior

Fig. 2 presents the measured viscosities, η, converted to centipoise (cP) units[56], as a function of $C_{12}E_6$ mole fraction, X, at T=35°C (squares) and T=45°C (circles). Several interesting observations can be made about the viscosity behavior. At fixed temperature, there is a pronounced increase in viscosity with surfactant concentration (for example, at T=35°C and $X=0.001$, $\Delta\eta/\Delta X \sim 1000$, while at $X=0.004$, $\Delta\eta/\Delta X \sim 3000$). I believe that this behavior reflects both micellar growth with

increasing surfactant concentration, as well as the formation of a transient network of entangled micelles which first forms at $X>X^*$.

Although viscosity measurements at more than two temperatures are probably needed in order to make definitive statements, in view of the results presented in Fig. 2, it is tempting to suggest that the variation of viscosity with temperature depends on the range of surfactant concentrations studied. Specifically, the η versus X curves at 35°C and 45°C intersect at X_a≈0.0005 (see the inset), thus generating two concentration domains, each characterized by a different temperature dependence of the viscosity. In the first domain, $X<X_a$, the viscosity exhibits the conventional behavior, that is, it decreases with increasing temperature. This follows from the fact that at very low surfactant concentrations micellar growth is not significant, and therefore the solution-viscosity behavior reflects primarily the decrease in solvent viscosity with temperature. In the second domain, $X>X_a$, the temperature dependence is reversed, that is, the solution at 45°C exhibits a higher viscosity than at 35°C. This behavior is consistent with previous studies in C_iE_j-H_2O systems which reported[31,34,57] an increase in solution viscosity with increasing temperature. This temperature behavior appears to be indicative of micellar growth with increasing temperature, which results in a higher resistance to flow, and compensates for the decrease in solvent viscosity at the higher temperatures. However, as emphasized in Sec. I, it is important to recognize that both intermicellar interactions and critical-fluctuation effects may affect the viscosity results, specially in the vicinity of T_c. In this respect, it is noteworthy that the viscosity is expected to exhibit a rather weak divergence as $T\rightarrow T_c$[58]. Since $T_c\approx$51°C in the $C_{12}E_6$-H_2O system, it appears reasonable to assume that the observed increase in viscosity with temperature in the range 35°C≤T≤45°C is only weakly affected by critical fluctuations. On the other hand, one cannot rule out the possibility that intermicellar interactions, for example, of the attractive van der Waals type, may also contribute to the observed viscosity values.

B. Experimental Determination of Persistence Length

The viscosity data at 35°C, taken from Fig. 2, are replotted as specific viscosity, η_{sp}, versus $C_{12}E_6$ mole fraction, X, in Fig. 3. Calculated η_{sp}'s in the dilute limit for various ξ values, utilizing the theoretical formulation described in Sec. III, were superimposed on the measured η_{sp} versus X data in the low concentration limit ($X<0.001$) in order to determine the persistence length, ξ, which best fits the data. Three representative cases are shown in Fig. 3, where it is clear that the theoretical prediction for $\xi=70$Å (full line) yields the best fit. Fig. 4 shows that a fit of comparable quality is obtained in the dilute limit ($X<0.0005$) using $\xi=60$Å (full line) for the η_{sp} versus X data at 45°C. Note that the values $\xi=70$Å and $\xi=60$Å are smaller than previously reported values for $C_{12}E_6$ and other C_iE_j nonionic surfactants. In Sec. VI I speculate about the possible origin of these low values.

C. Experimental Estimation of Crossover Surfactant Concentration

Attention will now be shifted to the experimental estimation of the $C_{12}E_6$ crossover concentration, X^*. Using the value $\xi=70$Å deduced above, the calculated η_{sp} versus X curve as well as the experimental data at 35°C (taken from Fig. 3) are replotted in Fig. 5 to highlight the deviation of the predicted dilute-limit η_{sp} versus X curve (full line) from the experimental data (squares). As explained in Sec. IV, the surfactant mole fraction at which the deviation first occurs constitutes a reasonable estimate of the crossover surfactant concentration, X^*. As indicated by the broken arrow in Fig. 5, $X^*\simeq0.00121$. A similar consideration at 45°C, using $\xi=60$Å, yields an experimentally estimated value of $X^*\simeq0.00052$ (broken arrow in Figure 4).

An independent estimation of X^* at 45°C was obtained using available[24] QLS data for the $C_{12}E_6$-H_2O system. As in polymer solutions[59], the collective-diffusion coefficient first decreases upon increasing X, goes through a minimum that corresponds to X^*, and then increases with X[33,6]. Accordingly, by identifying the

location of the minimum in the reported[24] collective-diffusion coefficient versus $C_{12}E_6$ concentration curve, a value of X^*~0.0004 was deduced. Note that a very precise identification of the minimum was not possible due to the rather pronounced flatness of the curve near the minimum[24]. Note also that while in polymer solutions the primary interactions responsible for the occurrence of the observed minimum are of the repulsive excluded-volume type, in the $C_{12}E_6$-H_2O system, which exhibits phase separation, attractive interactions become important as one approaches T_c. Under such conditions, the identification of X^* with the minimum of the collective-diffusion coefficient versus $C_{12}E_6$ concentration curve may be more ambiguous.

D. Theoretical Prediction of Crossover Surfactant Concentration

Equation (9) indicates that knowledge of ν_n and $X_n(X,T)$ is needed to predict the variation of X^* with temperature for the $C_{12}E_6$-H_2O system. Using the values of ν_c, l_c, and l_{hg} given in Table 1 in Eq. (10) yields the required L_n values, which can then be used in Eqs. (7) and (3) to compute ν_n. In addition, values of ξ in the temperature range of interest, 20-60°C, are needed to calculate $X^*(T)$. In this respect, the viscosity interpretations presented above suggest that ξ is temperature dependent. Specifically, ξ was found to decrease with increasing temperature, taking on values of $\xi = 70$Å at 35°C and $\xi = 60$Å at 45°C. Note that the observed $\xi(T)$ variation is consistent with the expected decrease in steric interactions between the hydrophilic ethylene oxide moieties with increasing temperature, an effect which is primarily responsible for the observed one-dimensional micellar growth in aqueous solutions of C_iE_j nonionic surfactants[5]. Since experimental values of ξ are only available at 35°C and 45°C, and there being no definite agreement between various reported experimentally deduced values of ξ for the $C_{12}E_6$-H_2O system[27,54], representative constant values of ξ, in the range $50\text{Å} \leq \xi \leq 250\text{Å}$, were selected, in order to illustrate the variation of X^* with temperature over the entire range 20-60°C. In the actual calculations, an iterative procedure was utilized to simultaneously solve Eqs. (9), (11)

and (12), utilizing the g_{mic} values given in Table 2, the molecular parameters given in Table 1, and representative constant ξ values, until the calculated X^* value was equal to the surfactant concentration, X, initially assumed in the mass-balance relation [Eq. (12)]. The predicted variations of X^* versus temperature for three representative persistence lengths, $\xi = 50$Å (solid line), $\xi = 150$Å (dotted line), and $\xi = 250$Å (dashed line), are presented in Fig. 6. The experimentally measured[22] coexistence curve delineating the boundary between the one-phase and two-phase regions of the phase diagram is also shown in Fig. 6 . It is interesting to note that the predicted X^* versus temperature curves intersect the coexistence curve in the vicinity of the lower consolute (critical) point, that is, the minimum of this curve. To further emphasize this interesting feature, in Fig. 7 I have replotted the X^*(T) curve, corresponding to $\xi = 50$Å, in the vicinity of the critical point ($X_c \sim 0.00086$, $T_c \sim 51.14$°C). As can be seen from Figs. 6 and 7, the two-phase envelope, as well as the one-phase region beneath it, are divided into two regions by the X^*(T) curve. For $X < X^*$(T), the micellar solution is in the dilute regime. On the other hand, for $X > X^*$(T), the micellar solution is in the semidilute regime.

Fig. 6 also illustrates the fact that the X^*(T) values are higher at lower temperatures. This is to be expected[5,16] since micellar growth is very limited under these conditions, and consequently the volume occupied by each micelle decreases considerably. This, in turn, will increase the X^*(T) values. Furthermore, at constant temperature, as micelle flexibility decreases (larger ξ values), each micelle occupies a larger volume, leading to lower X^*(T) values.

X^* at 35°C (with $\xi = 70$Å) and 45°C (with $\xi = 60$Å) were also calculated. The results, $X^* \sim 0.00148$ at 35°C (full arrow in Fig. 5), and $X^* \sim 0.00098$ at 45°C (full arrow in Fig. 4), compare well with those deduced from our viscosity measurements, namely $X^* \sim 0.00121$ at 35°C, and $X^* \sim 0.00052$ at 45°C.

E. Effect of Micelle Size Polydispersity on Predicted Crossover Surfactant Concentration and Viscosity

The role of micelle-size polydispersity in the calculation of the crossover surfactant concentration curve, $X^*(T)$, was examined by comparing the results obtained utilizing the full micellar size distribution, $\{X_n\}$, with those derived assuming that the micelles are monodisperse having an aggregation number corresponding to $<n>_n$, the number-average micelle aggregation number. Note that for given values of X and T, the value of $<n>_n$ was calculated[5,16] using the full micellar size distribution, that is, $<n>_n=(\Sigma_n nX_n)/(\Sigma_n X_n)$. This $<n>_n$ value was then used in Eqs. (10), (7) and (3) to compute ν_n, for $n=<n>_n$. Furthermore, in this case the summation on the left-hand side of Eq. (9) simply becomes $X_n\nu_n$, with $n=<n>_n$, and $X_n=X/<n>_n$. In practice, various values of X were initially assumed until a value which matched the X^* value calculated from Eq. (9) was found. The resulting X^* versus T curve, for $n=<n>_n$ and $\xi=50$Å, is shown by the dotted line in Fig. 8. As can be seen, the X^* values in this case are larger than those obtained when the full distribution is accounted for (full line in Fig. 8). This is primarily because the large contribution of the micelles having higher aggregation numbers to the total volume occupied by the micelles is underestimated when taking the number average; thus, more micelles are needed to fill up the solution volume, V_T. On the other hand, when monodispersity with $n=<n>_w$ is assumed, where $<n>_w=(\Sigma_n n^2X_n)/(\Sigma_n nX_n)$ is the weight-average micelle aggregation number, and the calculations just described are repeated, with $<n>_w$ instead of $<n>_n$, the predicted X^* values (dashed line in Fig. 8) are very close to, although somewhat smaller than, those obtained when the full distribution is considered. This is due to the fact that taking the weight average, as opposed to taking the number average, allows for a larger contribution of the bigger micelles to the total volume occupied by the micelles; thus, less micelles are needed to fill up the solution volume, V_T.

The need to consider the full micellar size distribution, $\{X_n\}$, to predict the

specific viscosity in the dilute limit (see Sec. III) was also examined. Figure 9 shows the predicted specific viscosities versus X at 35°C and for $\xi = 70$Å, assuming that the micelles are monodisperse with (*i*) aggregation number $n = \langle n \rangle_w$ (dashed line), and (*ii*) aggregation number $n = \langle n \rangle_n$ (dotted line). It is clear from Fig. 9 that the curve corresponding to $\langle n \rangle_w$ gives a reasonable approximation to the predictions using the more extensive calculations involving the entire micellar size distribution (full line). This observation is in line with the well-known expectation that the "viscosity-average" aggregation number, $\langle n \rangle_\eta$, which can be deduced from viscosity measurements, is closer to $\langle n \rangle_w$ rather than to $\langle n \rangle_n$. The better agreement between the η_{sp} values predicted using $\langle n \rangle_w$ rather than $\langle n \rangle_n$ likewise follows from the fact that the weight-average procedure reflects more realistically the contributions of the larger micelles to the viscosity, which in turn, are underestimated when using the number-average procedure. It is noteworthy that a similar conclusion was reached[36] in the case of rigid rod-like micelles, approximated as ellipsoidal bodies. Considering that the aggregation numbers of the micelles in those studies[36] were not very large ($n < 1300$), the rigid-rod approximation appears to be a reasonable one. However, when the micelles exhibit significant growth, as is the case in the present study, micelle flexibility becomes more important. The agreement between the predicted viscosity of a polydisperse distribution of flexible micelles and that of a monodisperse system of flexible micelles having $n = \langle n \rangle_w$, can thus be seen as an extension of the conclusion reached in Ref. 36.

VI. SUMMARY AND DISCUSSION

Self-assembling fluids, such as micellar solutions, are of considerable theoretical and practical interest. For this reason, micellar solutions continue to be the subject of extensive investigation. A central objective of our recent research efforts in the area of isotropic micellar solutions has been to develop a theoretical framework capable of predicting micellization characteristics, phase behavior, and phase separation of these complex fluids by utilizing available information about the

surfactant molecular architecture and solution conditions[5,16,22,41,49]. It is therefore of great importance, for the purpose of modelling more accurately the phase behavior of these systems, to determine (*i*) the physical characteristics of the micellar aggregates, including their shape, size distribution and intrinsic flexibility, and (*ii*) the underlying structure of the isotropic micellar solution, that is, whether micelles are singly dispersed in the solvent or are entangled within a network structure. It has been the purpose of the study presented in this chapter to shed light on aspect (*ii*), by presenting a theoretical framework aimed at predicting the crossover surfactant concentration, X^*, which marks the onset of micellar entanglements and associated profound change in the underlying structure of the isotropic micellar solution. The theoretical formulation incorporates the essential unique features of micellar systems, principally self-assembling behavior, micelle polydispersity and flexibility.

This general theoretical framework was then applied to the $C_{12}E_6$-H_2O system. The theoretical predictions suggest that entanglements do occur in this system as the temperature or the surfactant concentration is increased, which is due primarily to the one-dimensional micellar growth induced by these changes in solution conditions. Hence, Fig. 6 shows that the $X^*(T)$ curve bisects the phase diagram into dilute (for $X \ll X^*$) and semidilute (for $X \gg X^*$) regimes. More specifically, in the very dilute regime ($X \ll X^*$) the micelles can be viewed as singly dispersed worm-like structures, each characterized by its radius of gyration, which can possibly be represented as effective rods, as was done in our viscosity calculations. In this concentration range the relevant interacting species are the "independent" micelles, and a mean-field type description of intermicellar interactions, where the average interaction between two micelles is modelled[16] as being proportional to the number of monomer-monomer pairs, appears reasonable since no long-range interactions exist (as is the case for nonionic surfactants). On the other hand, in the fully-entangled regime ($X \gg X^*$), the micelles are predicted to lose their "independence" in favor of a transient network of entangled micelles, where the relevant interacting species are now micelle segments of length comparable to ξ_{net}, the average network size, which is

independent of micelle molecular weight. Interestingly, a mean-field treatment of intermicellar interactions appears appropriate in this case as well, since, the solution being fully entangled, each micelle segment experiences a similar environment. Thus, for both $X<X^*$ and $X>X^*$, the expression for the micellar size distribution given in Eq. (12), primarily valid in the context of a mean-field description of intermicellar interactions, can be used. Whether Eq. (12) remains valid in the broad crossover region connecting the dilute and semidilute regimes remains to be definitively resolved. However, the accuracy of our recent predictions[5,16,22] in the $C_{12}E_6$-H_2O system, coupled with the validity of Eq. (12) in the two limits considered above, suggests that Eq. (12) captures the essential physical factors also in the broad crossover region. Further support for this contention are indications, based on viscosity and relaxation-time experiments, that micellar entanglements do not prevent micellar growth[60].

An interesting result of our calculations is the close proximity of the X^* values predicted utilizing either the full micellar size distribution or the assumption of monodisperse micelles with an aggregation number $n=<n>_w$, the weight-average micelle aggregation number (see Fig. 8). It is noteworthy that a description in terms of monodisperse micelles has been used in previous X^* determinations *a priori*. Our calculations indicate that such an assumption indeed has a substantial basis, a result that can assist considerably in simplifying the calculations of X^* in future studies.

The theoretical predictions of X^* compare favorably with the experimental estimations deduced from an interpretation of our viscosity measurements. Also presented is a comparison of the predicted X^* value at 45°C with that deduced using available QLS data. Because of the lack of precision in the determination of the minimum of the reported collective-diffusion coefficient versus surfactant concentration curve, as well as the possible effect of attractive intermicellar interactions, additional studies utilizing a combination of viscosity, SLS, QLS and SANS measurements are essential to shed more light on the occurrence of entanglements in the $C_{12}E_6$-H_2O system, as well as in other C_iE_j-H_2O solutions which

are known to exhibit one-dimensional micellar growth. In this respect, the $C_{12}E_5$-H_2O system, which exhibits significant micellar growth[61], appears to be an excellent candidate.

As with the findings regarding X^*, viscosity predictions based on the full micellar size distribution are also closely approximated by those assuming a monodisperse population of micelles with $n = <n>_w$ (see Fig. 9). This result should be of considerable practical utility for the interpretation of viscosity data of self-assembling micellar fluids of the type considered in this paper.

The concept of the crossover concentration in polydisperse systems in general, and in polydisperse micellar systems in particular, is by no means evident and requires further clarification and study. It can be argued that the smaller micelles may be able to diffuse through the network of entangled micelles (of higher aggregation numbers) without affecting this network, particularly if the effective length of the micelle is less than ξ_{net}. Their contribution to entanglements, and therefore to X^*, is not clear-cut. In fact, the contribution of these same lower-aggregation number micelles to the total volume of the micelle domains is very small. Thus, numerically at least, these smaller micelles should have very little impact on X^*. This expectation is corraborated in Table 3. In Table 3, the minimum aggregation number cut-off, n_{cutoff}, refers to the smallest aggregation number considered to have a non-negligible contribution to the total volume occupied by the micelles used in the X^* calculations. In other words, micelles with $n < n_{cutoff}$ are considered to have negligible contributions to entanglements since they are free to diffuse, perhaps unhindered, through the entangled network. The value of n_{cutoff} is estimated by the aggregation number of a micelle whose contour length is equal to ξ_{net} at X^*. In addition, at X^*, ξ_{net} is of the order of the average micelle radius of gyration computed using $n = <n>_w$. It is clear from Table 3 that ignoring the contribution of micelles with $n < n_{cutoff}$ to the entanglements has negligible effect on the value of X^*.

Finally, a discussion on the persistence-length values, $\xi = 70$Å (at 35°C) and $\xi = 60$Å (at 45°C), deduced from our viscosity measurements is in order. The lack of

agreement between reported experimentally deduced ξ values for the $C_{12}E_6$-H_2O system encouraged us to attempt an estimation of ξ using our viscosity measurements. Although the deduced ξ values are consistent with (*i*) the finite diameter of a $C_{12}E_6$ micelle, and (*ii*) the decrease in steric interactions between the hydrophilic ethylene oxide moieties with increasing temperature, they are smaller than previously reported persistence-length values for $C_{12}E_6$ as well as other C_iE_j surfactants. This indicates the need for (*i*) alternate estimations of ξ using a combination of other experimental techniques, including SLS, QLS and SANS measurements, which have proven to be very useful in the case of ionic surfactants[6], and (*ii*) the development of a fundamental theoretical description of ξ at the molecular level. In addition, one can speculate about possible factors which may tend to yield a smaller effective value of ξ. Strictly speaking, the worm-like chain model of Kratky and Porod [see Eq. (4)] does not incorporate explicitly the competition between repulsive excluded-volume interactions (tending to expand the chain) and attractive interactions (tending to contract the chain). At θ-solvent conditions, that is, when $T=\theta$, where θ is the *theta* temperature, these two opposing interactions exactly balance each other resulting in an unperturbed Gaussian chain[43]. As emphasized in the discussion following Eq. (6), the Kratky-Porod model reduced to the Gaussian-chain model in the limit of a fully-flexible chain. In other words, Eq. (4) or its generalized version Eq. (7), describe the unperturbed conformations of a worm-like chain. For $T<\theta$ (good solvent), the chain is more expanded than a Gaussian chain, while for $T>\theta$ (poor solvent) it is less expanded than a Gaussian chain. For $C_{12}E_6$ in water, the *theta* temperature has been estimated to be approximately 20°C, as reflected in the change of the second-virial coefficient from being repulsive to being attractive[24]. Since the temperatures at which the viscosity measurements were conducted (35°C and 45°C) are both larger than $\theta \approx 20$°C, this implies that the solvent is poor, and consequently, that the micelles should be in a less expanded state. Note that the existence of stronger attractive interactions (decreasing solvent quality) with increasing temperature is also consistent with the

presence of a lower consolute (critical) temperature at T_c~51°C. In other words, in order to effectively yield the required less expanded micelle conformations in this temperature range, an effective smaller value of ξ is derived when fitting the viscosity data. Clearly, further experimental and theoretical examination of this important issue is in order.

Overall, I believe that the theoretical framework presented in this chapter for the determination of the crossover from dilute to semidilute solution regimes of micellar solutions will enhance our ability to identify and characterize the underlying structure of isotropic micellar solutions. This is particularly important for the development of theoretical descriptions of the phase behavior of these complex fluid systems. We were pleased that light scattering studies have already been conducted as a result of this work[62]. It is hoped that the study presented in this chapter will stimulate further experimental and theoretical work to help clarify some of the challenging issues put forward.

REFERENCES FOR CHAPTER 4

1. Tanford, C. *The Hydrophobic Effect*; Wiley: New York, 1980.

2. Israelachvili, J. N. *Intermolecular and Surface Forces*; Academic: New York, 1985.

3. Israelachvili, J. N.; Mitchell, D. J.; Ninham, B. W. *J. Chem. Soc. Faraday Trans. 2*, **1976**, *72*, 1525.

4. Nagarajan, R.; Ruckenstein, E. *J. Colloid Interface Sci.* **1977**, *60*, 221; **1979**, *71*, 580.

5. Puvvada, S.; Blankschtein, D. *J. Chem. Phys.* **1990**, *92*, 3710;
   Blankschtein, D.; Puvvada, S. *MRS Symposium Proceedings* **1990**, *177*, 129;
   Puvvada, S.; Blankschtein, D. In *Surfactants in Solution*; Mittal, K. L.; Shah, D. O., Eds.; Plenum: New York (in press); and references cited therein.

6. For a recent comprehensive review on experimental and theoretical aspects of one-dimensional flexible (worm-like) surfactant micelles, see: Cates, M. E.; Candau, S. J. *J. Phys.: Condens. Matter* **1990**, *2*, 6869; and references cited therein.

7. Porte, G.; Appell, J.; Poggi, Y. *J. Phys. Chem.* **1980**, *84*, 3105;
   Appell, J.; Porte, G. *J. Colloid and Interface Sci.* **1981**, *81*, 85;
   Porte, G.; Appell, J. *J. Phys. Chem.* **1981**, *85*, 2511;
   Appell, J.; Porte, G.; Poggi, Y. *J. Colloid and Interface Sci.* **1982**, *87*, 492;
   Appell, J.; Porte, G. *Europhys. Lett.* **1990**, *12*, 185.

8. Candau, S. J.; Hirsch, E.; Zana, R. *J. Physique* **1984**, *45*, 1263;
   Candau, S. J.; Hirsch, E.; Zana, R. *J. Colloid and Interface Sci.* **1985**, *105*, 521;
   Candau, S. J.; Hirsch, E.; Zana, R.; Delsanti, M. *Langmuir* **1989**, *5*, 1225.

9. Hoffmann, H.; Rehage, H.; Platz, G.; Schorr, W.; Thurn, H.; Ulbricht, W. *Colloid Polym. Sci.* **1982**, *260*, 1042;
   Hoffmann, H.; Platz, G.; Rehage, H.; Schorr, W. *Advan. Colloid Int. Sci.* **1982**, *17*, 275;
   Hoffmann, H.; Ebert, G. *Angew. Chem. Int. Ed. Engl.* **1988**, *27*, 902.

10. Imae, T.; Ikeda, S. *J. Phys. Chem.* **1986**, *90*, 5216;
    Imae, T.; Ikeda, S. *Coll. Polym. Sci.* **1987**, *265*, 1090.

11. Imae, T.; Ikeda, S. *Coll. Polym. Sci.* **1984**, 262, 497; **1985**, *263*, 756;
    Imae, T. *J. Phys. Chem.* **1988**, *92*, 5721;
    Imae, T. *Langmuir* **1989**, *5*, 205.

12. Kato, T.; Anzai, S.; Seimiya, T. *J. Phys. Chem.* **1987**, *91*, 4655; **1990**, *94*, 7255.

13. Schurtenberger, P.; Scartazzini, R.; Magid, L. J.; Leser, M. E.; Luisi, P. L. *J. Phys. Chem.* **1990**, *94*, 3695;
Schurtenberger, P.; Magid, L. J.; Penfold, J.; Heenan, R. *Langmuir* **1990**, *6*, 1800.

14. Mukerjee, P. *J. Phys. Chem.* **1972**, *76*, 565.

15. (a) Ben-Shaul, A.; Gelbart, W. M. *J. Phys. Chem.*, **1982**, *86*, 316;
(b) Gelbart, W. M.; Ben-Shaul, A.; McMullen, W. E.; Masters, A. *J. Phys. Chem.* **1984**, *88*, 861.

16. Blankschtein, D.; Thurston, G. M.; Benedek, G. B. *Phys. Rev. Lett.* **1986**, *54*, 955;
Blankschtein, D.; Thurston, G. M.; Benedek, G. B. *J. Chem. Phys.* **1986**, *85*, 7268.

17. de Gennes, P. G. *Scaling Concepts in Polymer Physics*; Cornell University Press: Ithaca, New York, 1979.

18. Imae, T. *Coll. Polym. Sci.* **1989**, *267*, 707.

19. Imae, T. *J. Phys. Chem.* **1989**, *93*, 6720.

20. Zhou, A.; Chu, B. *J. Colloid Interface Sci.* **1989**, *133*, 348.

21. For a critical discussion of micellar growth with temperature in aqueous solutions of C_iE_j surfactants, with particular emphasis on $C_{12}E_6$ and $C_{12}E_5$, see: Lindman, B.; Wennerstrom, H. *J. Phys. Chem.* **1991**, *95*, 6053.

22. Briganti, G.; Puvvada, S.; Blankschtein, D. *J. Phys. Chem.* (in press).

23. Brown, W.; Johnsen, R.; Stilbs, P.; Lindman, B. *J. Phys. Chem.*, **1983**, *87*, 4548.

24. Brown, W.; Rymden, R. *J. Phys. Chem.*, **1987**, *91*, 3565.

25. Kato, T.; Seimiya, T. *J. Phys. Chem.* **1986**, *90*, 3159.

26. Strey, R.; Pakusch, A. In *Surfactants in Solution*; Mittal, K. L.; Bothorel, P., Eds.; Plenum: New York, **1977**; Vol. 4, p. 465.

27. Ravey, J. C. *J. Colloid Interface Sci.* **1983**, *24*, 289.

28. Triolo, R.; Magid, L. J.; Johnson, J. S.; and Child, H. R. *J. Phys. Chem.* **1982**, *86*, 3689.

29. Zulauf, M.; Weckstrom, K.; Hayter, J. B.; Degiorgio, V.; Corti, M. *J. Phys. Chem.* **1985**, *89*, 3411.

30. Staples, E. J.; Tiddy, G. J. T. *J. Chem. Soc. Faraday Trans. 1* **1978**, *74*, 2530.

31. Degiorgio, V. In *Proceedings of the International School of Physics Enrico Fermi - Physics of Amphiphiles: Micelles, Vesicles and Microemulsions*; Degiorgio, V.; Corti, M., Eds.; North-Holland Physics Publishing: Amsterdam, 1985; p. 303.

32. Zana, R.; Weill, C. *J. Phys. (Paris) Lett.* **1985**, *46*, L-953.

33. Makhloufi, R.; Hirsch, E.; Candau, S. J.; Binana-Limbele, W.; Zana, R. *J. Phys. Chem.* **1989**, *93*, 8095.

34. Wilcoxon, J. P.; Kaler, E. W. *J. Chem. Phys.* **1987**, *86*, 4684.

35. Doi, M.; Edwards, S. F. *J. Chem. Soc., Faraday Trans. 2* **1978**, *74*, 560; **1978**, *74*, 918.

36. Nagarajan, R. *J. Colloid Interface Sci.* **1982**, *90*, 477;
Nagarajan, R.; Shah, K. M.; Hammond, S. *Colloids and Surfaces* **1982**, *4*, 147.

37. Kohler, H. H.; Strnad, J. *J. Phys. Chem.*, **1990**, *94*, 7628.

38. Scheraga, H. A.; Mandelkern, L. *J. Am. Chem. Soc.* **1953**, *75*, 179;
Kushner, L. M.; Hubbard, W. D.; Parker, R. A. *J. of Research of the NBS* **1957**, *59*, 113;
Ekwall, P.; Mandell, L.; Solyom, P. *J. Colloid Interface Sci.* **1971**, *35*, 519;
Guveli, D. E.; Kayes, J. B.; Davis, S. S. *J. Colloid Interface Sci.* **1979**, *72*, 130.

39. Imae, T.; Sasaki, M.; Ikeda, S. *J. Colloid Interface Sci.* **1989**, *127*, 511.

40. Stigter, D. *J. Phys. Chem.* **1966**, *70*, 1323.

41. Puvvada, S.; Blankschtein, D. *J. Phys. Chem.* **1989**, *93*, 7753.

42. Cotton, J. P.; Nierlich, M.; Boue, F.; Daoud, M.; Farnoux, B.; Jannink, G.; Duplessix, R.; Picot, C. *J. Chem. Phys.* **1976**, *65*, 1101.

43. Flory, P. J. *Principles of Polymer Chemistry*; Cornell Univ. Press: Ithaca, New York; 1953.

44. Appell, J.; Porte, G. *J. Colloid Interface Sci.* **1982**, *87*, 492.

45. Kratky, O.; Porod, G. *Recl. Trav. Chim. Pays-Bas* **1949**, *68*, 1106.

46. Yamakawa, H. *Modern Theory of Polymer Solutions*; Harper and Row: New York, 1971.

47. Cantor, C. R.; Schimmel, P. R. *Biophysical Chemistry*; W. H. Freeman and Co.: New York, 1980.

48. Missel, P. J.; Mazer, N. A.; Benedek, G. B.; Young, C. Y.; Carey, M. C. *J. Phys. Chem.* **1980**, *84*, 1044.

49. Huang, Y. X.; Thurston, G. M.; Blankschtein, D.; Benedek, G. B. *J. Chem. Phys.* **1990**, *92*, 1956.

50. Carvalho, B. L.; Briganti, G.; Chen, S. H. *J. Phys. Chem.* **1989**, *93*, 4282.

51. Bird, R. B.; Hassager, O.; Armstrong, R. C.; Curtiss, C. F. *Dynamics of Polymeric Liquids*; John Wiley & Sons: New York, 1977.

52. Riseman, J.; Kirkwood, J. G. *J. Chem. Phys.* **1950**, *18*, 512.

53. Ying, Q.; Chu, B. *Macromolecules* **1987**, *20*, 362.

54. Magid, L. J.; Triolo, R.; Caponetti, E.; Johnson, J. S., Jr. In *Surfactants in Solution*; Mittal, K. L.; Bothorel, P., Eds.; Plenum: New York, 1986; Vol. 4; p. 155.

55. Schubert, K. V.; Strey, R.; Kahlweit, M. *J. Colloid Interface Sci.* **1991**, *141*, 21.

56. ASTM Method D445-88.

57. Elworthy, P. H.; McDonald, C. *Kolloid Z. Z. Polym.* **1964**, *195*, 16.

58. For a review on critical viscosity measurements, see: Sengers, J. V. *Int. J. Thermophys.* **1985**, *6*, 203; and references cited therein.

59. Munch, J. P.; Hild, G.; Candau, S. *Macromolecules* **1983**, *16*, 71.

60. Candau, S. J.; Hirsch, E.; Zana, R.; Adam, M. *J. Colloid Interface Sci.* **1988**, *122*, 430.

61. Brown, W.; Pu, Z.; Rymden, R. *J. Phys. Chem.* **1988**, *92*, 6086.

62. Kole, T. M.; Fisch, M. R. *J. Phys. Chem.* (submitted for publication).

Table 1. Molecular parameters for the $C_{12}E_6$-H_2O system (from refs. 1, 5 and 16).

l_c	13Å
l_{hg}	12.4Å
v_c	323.3Å^3
V_s	750Å^3
V_w	30Å^3

Table 2. Free energy of micellization, g_{mic} (n) = A/n + B, as a function of temperature.

Temperature (°C)	A (kT)	B (kT)
20	16.89	-12.58
25	19.19	-12.64
30	21.02	-12.69
35	22.73	-12.73
40	24.26	-12.77
45	25.48	-12.80
50	26.46	-12.82
55	27.23	-12.84
60	27.85	-12.86

Table 3. The effect of neglecting the contribution of micelles having low aggregation numbers to the calculation of the crossover surfactant concentration

Temperature (°C)	n_{cutoff}	X^* (Mole Fraction Units)	
		Full Micellar Size Distribution, $\{X_n\}$	$\{X_n\}$, with $n > n_{cutoff}$
293	130	$9.166*10^{-3}$	$9.178*10^{-3}$
298	238	$4.973*10^{-3}$	$4.977*10^{-3}$
303	366	$3.232*10^{-3}$	$3.233*10^{-3}$
308	537	$2.209*10^{-3}$	$2.210*10^{-3}$
313	748	$1.592*10^{-3}$	$1.592*10^{-3}$
318	969	$1.233*10^{-3}$	$1.233*10^{-3}$
323	1188	$1.008*10^{-3}$	$1.008*10^{-3}$
328	1397	$8.592*10^{-4}$	$8.592*10^{-4}$

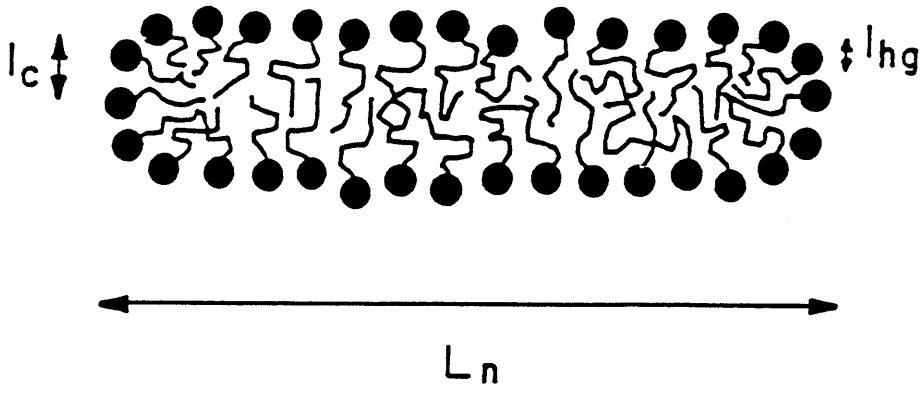

Figure 1. Pictorial representation of a spherocylindrical micelle.

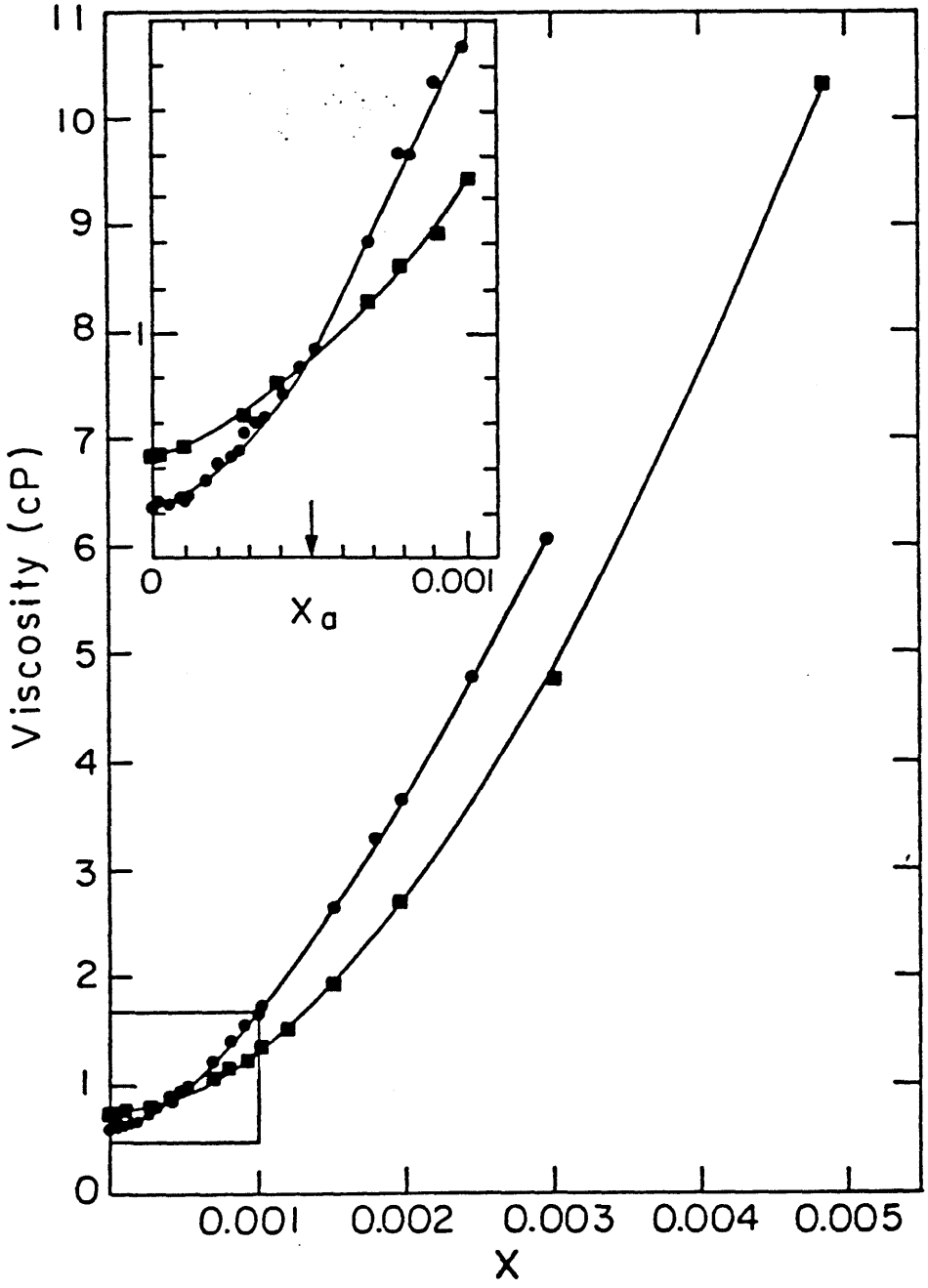

Figure 2. Measured micellar solution viscosity, η, in cP, as a function of $C_{12}E_6$ mole fraction, X, at T=35°C (■), and T=45°C (●). Note that, as shown in the inset, the η vs. X curves at 35°C and 45°C intersect at $X_a \approx 0.0005$. The various lines are drawn to guide the eye.

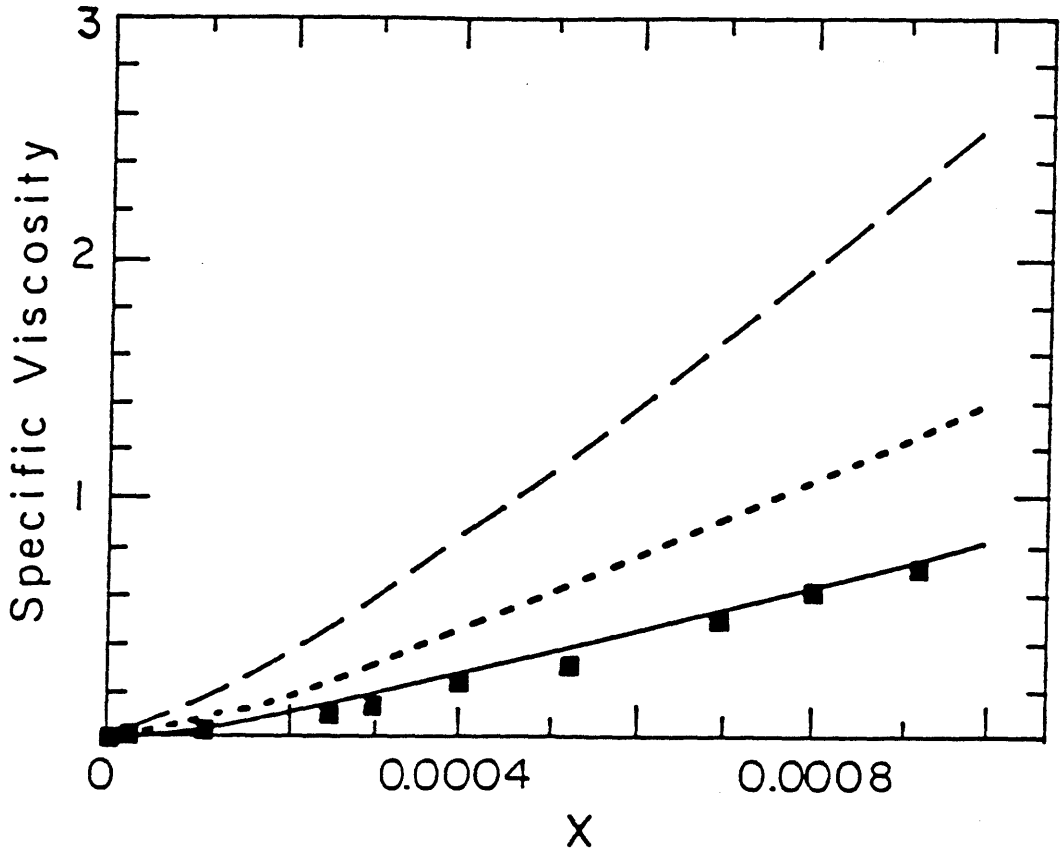

Figure 3. Comparison of the measured specific viscosity as a function of $C_{12}E_6$ mole fraction, X, in the dilute limit at 35°C (■, data extracted from Fig. 2) with predicted dilute solution specific viscosities for three representative persistence lengths: $\xi = 70$Å (——), $\xi = 100$Å (• • • •), $\xi = 150$Å (– – –).

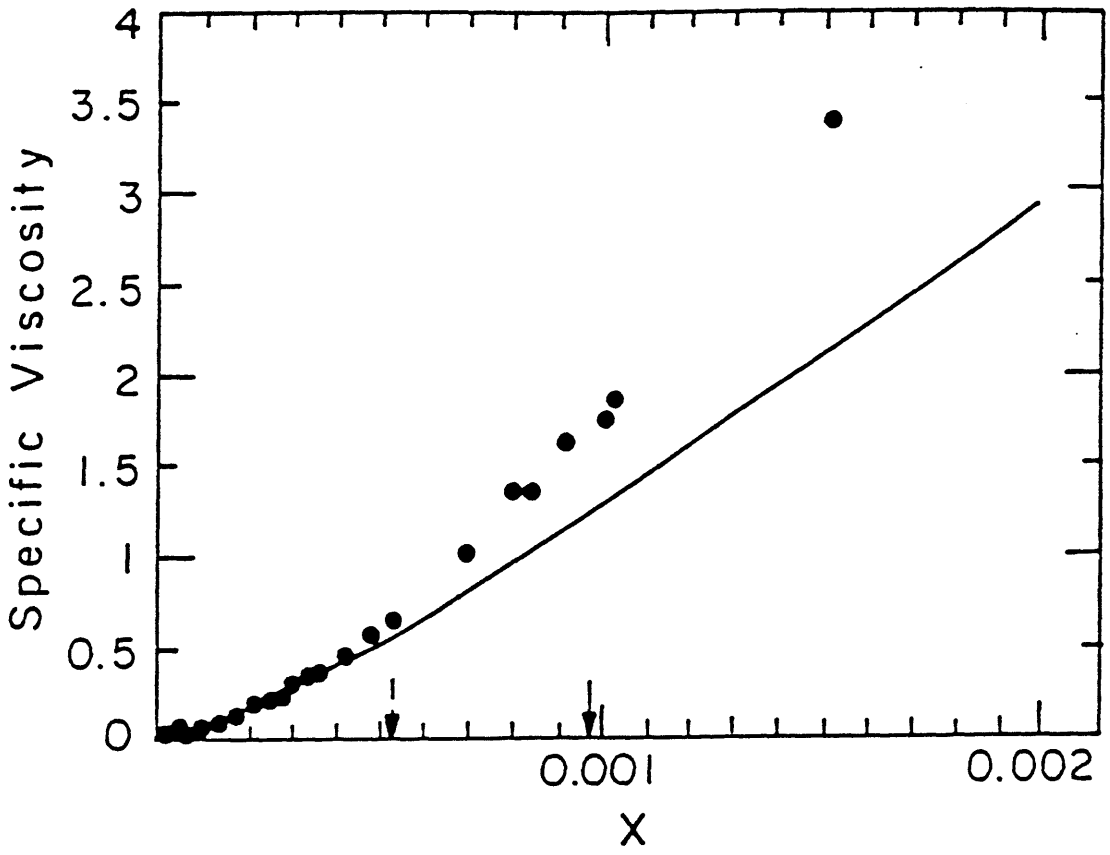

Figure 4. Comparison of the measured specific viscosity as a function of $C_{12}E_6$ mole fraction, X, at 45°C (● , data extracted from Fig. 2) with predicted dilute solution specific viscosity for $\xi = 60$Å. The $C_{12}E_6$ mole fraction, $X^* \sim 0.00052$, at which the two deviate is indicated by the broken arrow. The full arrow corresponds to the predicted value of $X^* \sim 0.00098$.

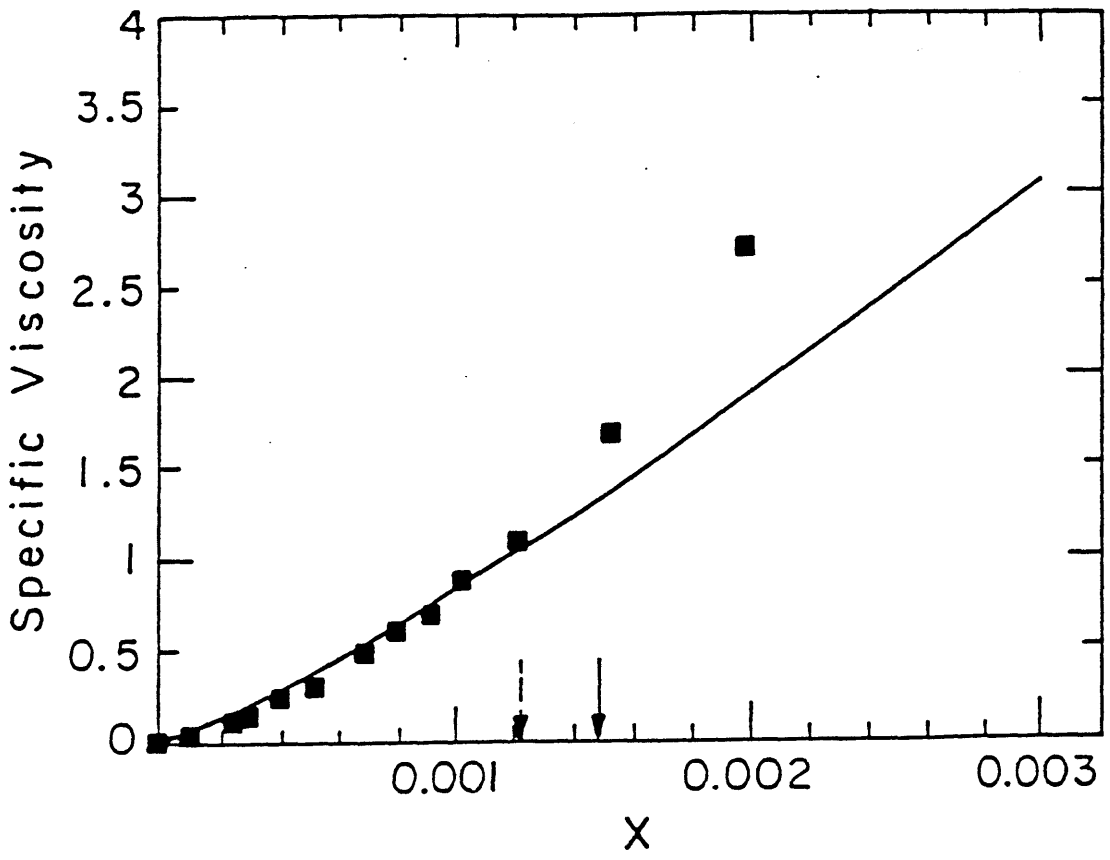

Figure 5. Comparison of the measured specific viscosity as a function of $C_{12}E_6$ mole fraction, X, at 35°C (■, data extracted from Fig. 2) with the predicted dilute solution specific viscosity for $\xi = 70$Å. The $C_{12}E_6$ mole fraction, $X^* \sim 0.00121$, at which the two deviate is indicated by the broken arrow. The full arrow corresponds to the predicted value of $X^* \sim 0.00148$.

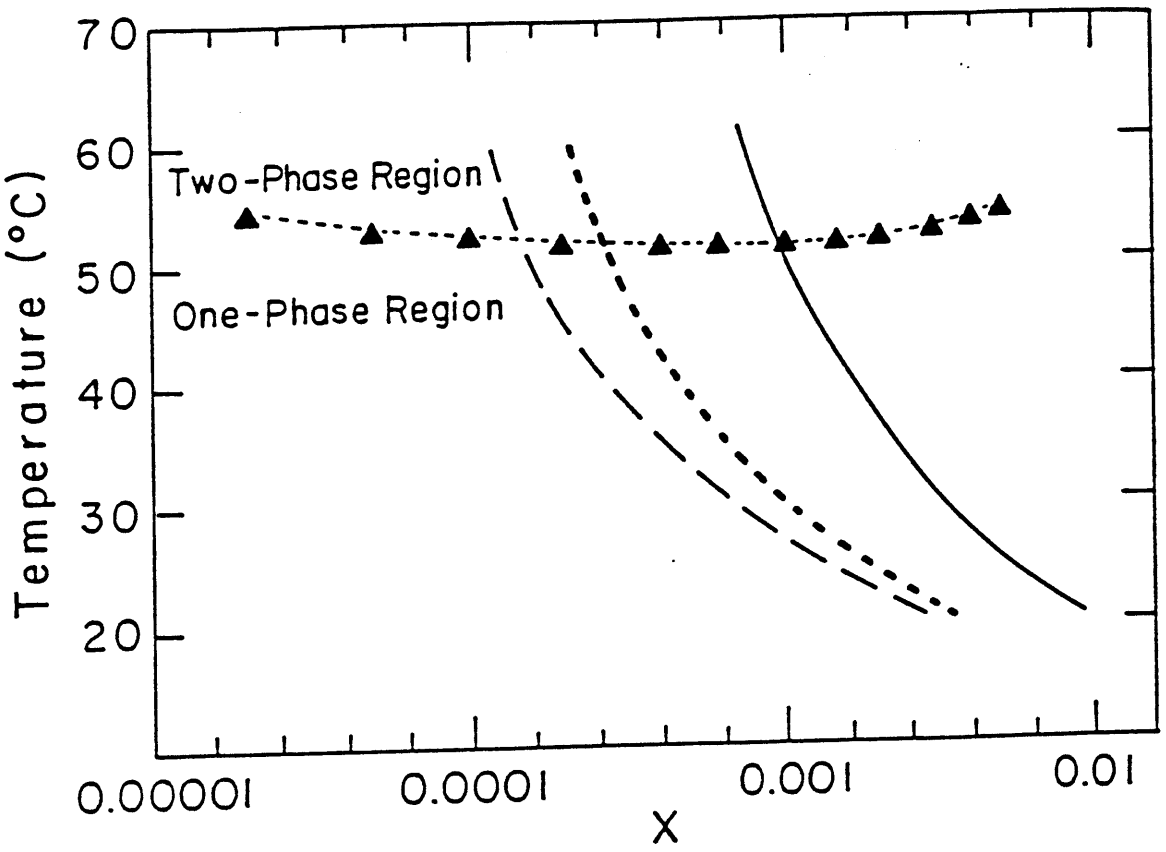

Figure 6. Predicted $C_{12}E_6$ crossover concentration, X^*, as a function of temperature for three representative persistence lengths: $\xi = 50$Å (——), $\xi = 150$Å (• • • •), and $\xi = 250$Å (– – –). Also shown is the experimental coexistence curve for the $C_{12}E_6$-H_2O system (▲ , where the dotted line is drawn to guide the eye).

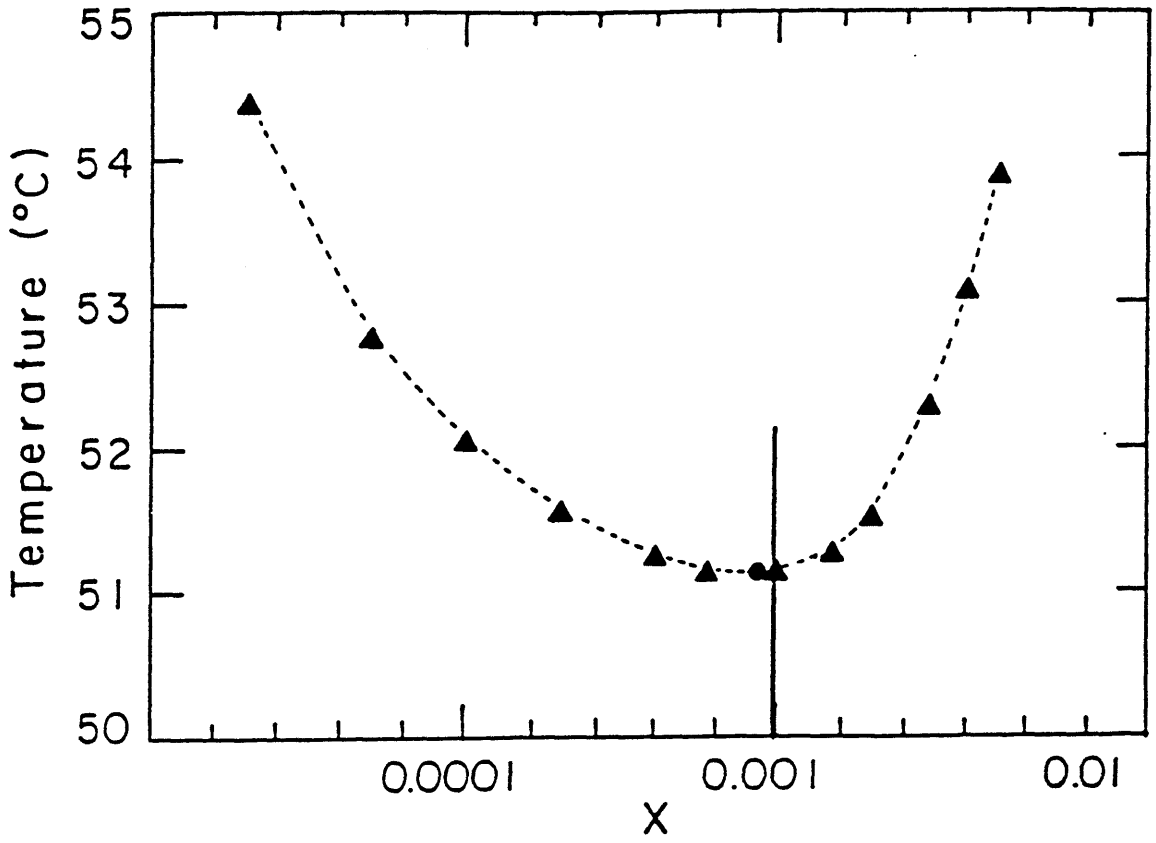

Figure 7. Expanded version of Figure 6, for $\xi = 50$Å, to emphasize the intersection of the crossover concentration curve, $X^*(T)$, with the coexistence curve in the vicinity of the critical point, $X_c = 0.00086$, $T_c = 51.14$°C (●).

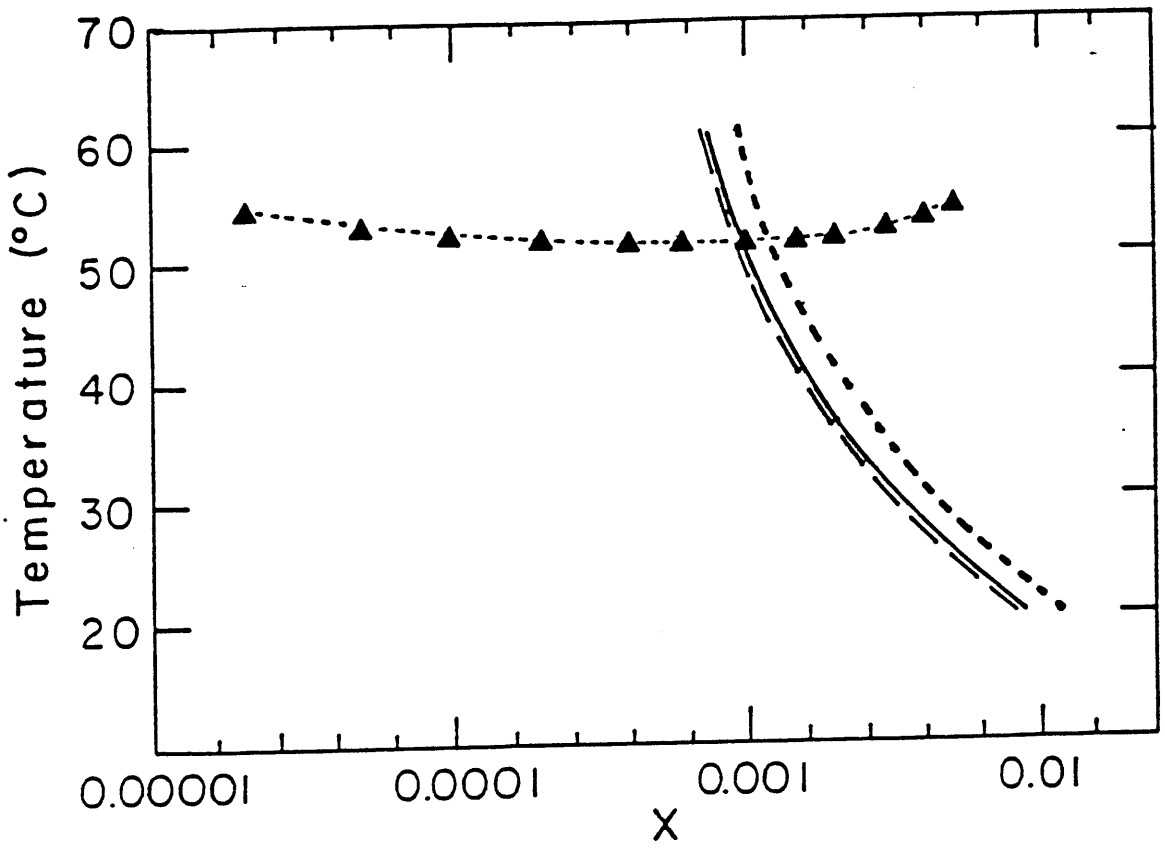

Figure 8. Predicted $C_{12}E_6$ crossover concentration, X^*, as a function of temperature for $\xi = 50$Å: a polydisperse distribution of micelles (——), monodisperse micelles with $n = \langle n \rangle_w$ (– – –), and monodisperse micelles with $n = \langle n \rangle_n$ (• • • •).

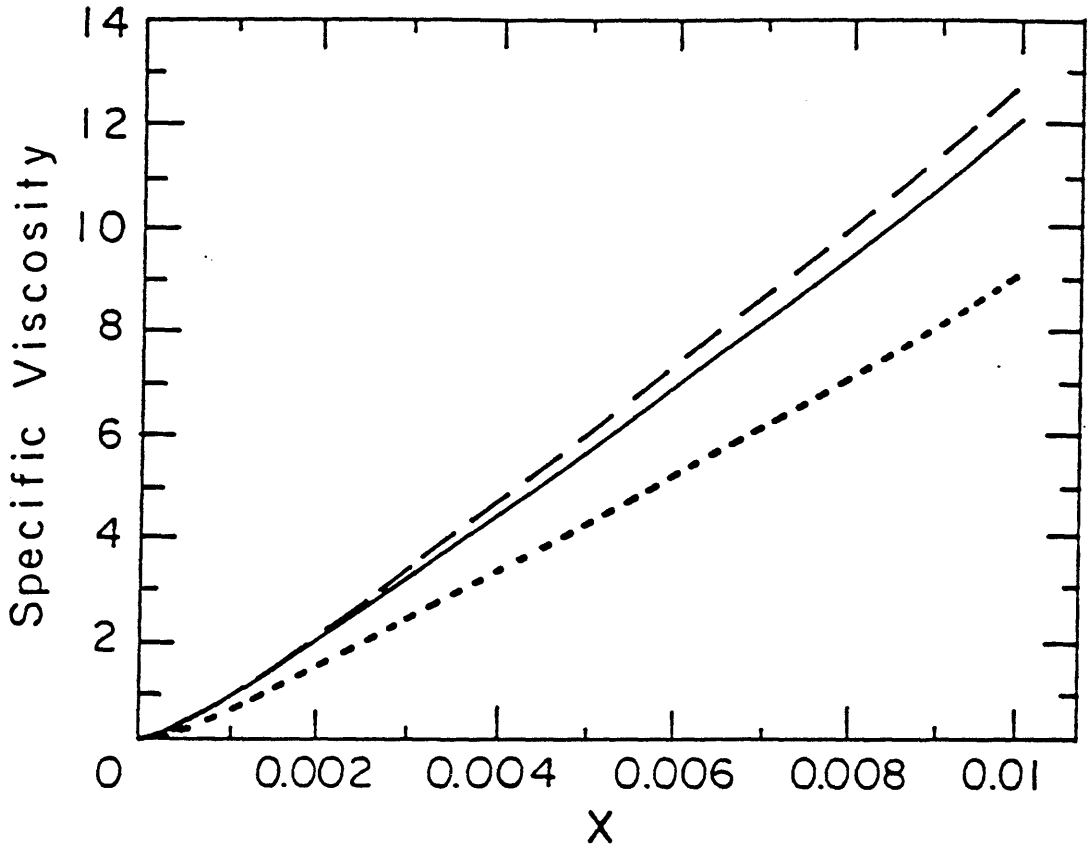

Figure 9. Comparison of predicted specific viscosities as a function of $C_{12}E_6$ mole fraction for: a polydisperse micellar size distribution (——), monodisperse micelles with $n = \langle n \rangle_w$ (– – –), and monodisperse micelles with $n = \langle n \rangle_n$ (• • • •) at 35°C, and for $\xi = 70$Å.

CHAPTER 5. SALT EFFECTS ON INTERMICELLAR INTERACTIONS

I. INTRODUCTION

In the previous chapters, we focused primarily on salt- and temperature-induced effects on intramicellar interactions, which can bring about changes in the morphology of the micelles present in solution, as well as in micellar solution properties, such as, the CMC, the crossover surfactant concentration, and the solution viscosity. In this chapter, attention will be focused on intermicellar interactions, which, as explained in Chapter 1, depend on both the morphology of the micelles as well as on solution conditions.

Aqueous micellar solutions of C_iE_j nonionic surfactants, such as $C_{10}E_6$, $C_{12}E_6$, and $C_{12}E_8$, the surfactants examined in this thesis, can exhibit phase separation into two coexisting liquid phases upon increasing the solution temperature[1,2,3]. This is in contrast to solutions of other surfactants, for example, the zwitterionic surfactant C_8-lecithin, which can exhibit phase separation upon cooling. A study of the phase separation behavior of surfactant solutions could shed light on (*i*) the types of interactions that occur between micellar aggregates, and (*ii*) the modes by which these interactions are affected by changes in solution conditions, particularly salt type and concentration, as well as temperature. For example, phase separation upon increasing temperature is an indicator of the temperature dependence of the interactions between the micelles present in solution[4]. Similarly, the effect of salts on phase-separation behavior is a sensitive indicator of the mode by which salts modulate the strength of interactions between the various micellar species present in solution.

Salts have indeed been observed to have significant effects on the phase separation of micellar solutions. Experimental studies[5,6,7] have shown that certain salts, such as iodides, can reduce the tendency for phase separation. This effect of the salts has been termed "salting-in". On the other hand, certain salts can enhance phase

separation, an effect called "salting-out". Salts of the latter type include the chlorides and the bromides examined in this thesis.

Previous experimental studies have focused on correlating salt effects on phase separation to other salt properties. For example, a correlation was found[8] between the lyotropic numbers of certain ions and cloud-point changes in surfactant solutions, induced by a specified concentration of these ions (at constant surfactant concentration). Recall that lyotropic numbers[9] were introduced to describe various salt trends, including the change in the surface tension of water and the change in the solubility of gases and nonpolar molecules[10], as a function of salt type. The lyotropic series is similar to the Hofmeister series, which is derived from studies on the salting-out of proteins[11]. Attempts have also been made[12,13] to separate the effects of the anions and the cations on the phase separation of aqueous solutions of alkylphenoxy poly(ethylene oxide), C_iPhE_j, surfactants.

At the theoretical level, studies of phase separation in aqueous solutions of C_iE_j and C_iPhE_j surfactants were carried out in the past in the context of the Flory-Huggins theory of polymer solutions[5,6,14], with micellar aggregates modelled as polymer molecules having an unchanging identity. In this thesis, an attempt was made to develop a theoretical framework that incorporates explicitly the self-assembling nature of micelles, as reflected in the chemical equilibrium existing between the various micellar species, as well as in the resulting distribution of micellar sizes. In addition, the interactions between micelles were resolved into their component parts. Specifically, the contributions of the micelle head layers, reflecting the interpenetration of the hydrophilic PEO head chains, and the micellar cores, reflecting van der Waals forces, to the intermicellar interactions were characterized and quantified at a molecular level.

Clouding phenomena have commonly been used to identify the position of the coexistence curve[15,16], which delineates the boundary between the one-phase and two-phase regions of the temperature versus surfactant concentration phase diagram. The cloud point is defined as the temperature at which a surfactant solution of given surfactant concentration becomes turbid[17], signalling the separation of the solution

into two coexisting phases. It has been shown that for single-surfactant aqueous solutions, the cloud-point curve and the coexistence curve are identical within experimental error[18]. On the experimental side of this thesis, therefore, cloud-point curves of the surfactants $C_{12}E_6$, $C_{12}E_8$, and $C_{10}E_6$ in various aqueous salt solutions were measured and analyzed to shed light on the magnitude of the relevant interactions that occur between micelles. From a theoretical mean-field interpretation of the experimentally measured coexistence curves, an attempt was made to rationalize the effects of salts and temperature at a molecular level, as well as to formulate a theoretical framework capable of predicting the phase separation of C_iE_j surfactant solutions in the presence of salts.

The rest of this chapter is organized as follows. Section II describes the cloud-point measurements that were conducted. Section III presents (1) the theory for phase separation of micellar solutions utilizing a mean-field description of the free energy of intermicellar interactions, and (2) the development of a statistical-thermodynamic description, as well as the implementation of concepts and methodologies from colloid and interface science, to calculate the interactions between micelles of various shapes (spheres and rods). Specifically, calculations of the van der Waals interactions between micellar cores, as well as of the interactions resulting from the interpenetration of the PEO head chains present in the hydrophilic layers of two approaching micelles, will be presented. Section IV discusses the experimental cloud-point measurements presented in Section II. Section V rationalizes these experimental results in light of the theoretical developments presented in Section III. Finally, Section VI presents a summary of the main results, as well as some concluding remarks.

II. MATERIALS AND EXPERIMENTAL METHODS

A. Materials and Sample Preparation

Homogeneous C_iE_j nonionic surfactants were obtained from Nikko Chemicals,

Tokyo, and used without further purification. To ensure uniformity in the results, measurements were conducted using the same lot number for each surfactant: $C_{12}E_6$ (Lot 9011), $C_{12}E_8$ (Lot 9054), and $C_{10}E_6$ (Lot 1054). These surfactants were chosen because they are available in a highly purified form, and the temperature range over which phase separation occurs can be easily measured (higher than 0°C, and sufficiently lower than 100°C since oxidation of poly(ethylene oxide) surfactants can occur at high temperatures[19]). The high purity of the surfactants was confirmed by the absence of any detectable minimum in the measured surface tension versus surfactant concentration curves of aqueous solutions of each surfactant. Salts were of the analytical reagent grade from Mallinckrodt, and were further purified to remove any organics by ignition at 450°C overnight. Salt solutions were prepared by weight, using deionized water which was purified using a Milli-Q ion-exchange system. Surfactant of known weight was then added to each of the previously weighed salt solutions contained in pre-washed test tubes (each containing a magnetic stirring bar), which were then covered with teflon tape and sealed tight with a screw cover. The cloud points of the prepared surfactant solutions were measured within the same day.

Before use, all glassware were immersed in a 1N NaOH-ethanol bath for at least 8 hours, then in a 1N nitric acid bath for another 8 hours, followed by thorough rinsing with Milli-Q water. The glassware were then dried in an oven.

B. Cloud-Point Curve Measurements

The sealed test tubes containing the surfactant solutions were immersed in a transparent thermoregulated device. Temperature was controlled to within ±0.01°C by connecting the device to an external water-bath circulator. The samples were heated slowly, and mixed using a magnetic stirrer to ensure temperature uniformity within the solution. At the first sign of turbidity, stirring was stopped to prevent non-equilibrium effects, and heating rates were reduced to approximately 0.01°C per minute. The cloud-point temperature, T_{cp}, was taken to be the arithmetic average of

the temperature, T_{cloud}, at which a marker behind the sample tube was rendered unreadable, and the temperature, T_{clear}, at which the two-phase solution became clear again upon cooling. The procedure was repeated whenever the difference between T_{cloud} and T_{clear} was greater than 0.04°C.

The concentrations of the surfactant samples were varied within a two-order of magnitude range (mole fractions between 10^{-4} and 10^{-2}). The cloud-point curves of $C_{12}E_6$ in water, and in 1, 2, and 3 molal solutions of LiCl, NaCl, KCl, KBr, and KI were determined using the method outlined above. The measurements for $C_{12}E_6$ indicated a stronger anion effect as compared to the cation effect. Accordingly, experiments were conducted in order to probe the effect of anion variations on the cloud-point temperatures of $C_{12}E_8$ and $C_{10}E_6$ in water and in 1m and 2m solutions of KCl, KBr, and KI.

III. THEORY

A. Mean-Field Interaction Free-Energy Model

Initial efforts to model intermicellar interactions, and thus rationalize and quantify the phase separation behavior of the systems studied, utilized a mean-field approximation to describe the interactions in the system[20]. Specifically, the free energy of intermicellar interactions was modelled as a quadratic expression in surfactant concentration, that is,

$$G_{interactions} = -\frac{1}{2} C N_s \phi_s , \qquad (1)$$

where C is the interaction parameter, N_s is the number of surfactant molecules in the system, and ϕ_s is the volume fraction of surfactant. The interaction parameter, C, reflects, at a mean-field level of description, the strength of the interactions between micellar aggregates, and, therefore, could be a function of solution conditions such as salt type and concentration, as well as temperature. In the absence of salts, C was

found to vary linearly with temperature[20]. Therefore, as a first approximation, C was assumed to vary linearly with temperature even in the presence of salts.

The system of interest is a multicomponent solution composed of (1) C_iE_j nonionic surfactant molecules (of a single type) which exist as monomers or aggregates of size n (n-mers), (2) a single, fully-dissociated salt type, and (3) water. The various surfactant species (monomers and n-mers) are related to one another by the requirement of chemical equilibrium[21], while the concentration of the ions in solution (the cations and the anions arising from the dissociation of the salt) are constrained by the electroneutrality requirement. Accordingly, the solution effectively becomes a ternary system (surfactant, salt, and water) having two independent concentrations: the monomer concentration, and the salt concentration. It is noteworthy that phase separation experiments on aqueous solutions of octylphenyl poly(ethylene oxide) surfactants having 7-8 EO units/surfactant indicated[5] that after phase separation the salt distribution coefficient (the ratio of the salt concentration in the dilute phase to that in the concentrated phase) is very close to unity. Accordingly, the simplifying assumption that the salt species can be considered part of the solvent was made. In other words, the water molecules and the ions present in solution were considered collectively as a *hypersolvent*. The system is thus effectively reduced to a binary solution of nonionic surfactant and *hypersolvent*.

The coexistence curve can be generated theoretically by determining the surfactant concentrations of the two coexisting phases at each salt condition (salt type and salt concentration, m_s), temperature, T, and pressure, P, typically equal to 1 atmosphere. The coexisting surfactant concentrations, Y and Z, can be determined by imposing the phase equilibrium conditions, which require that the chemical potentials of the solution species be equal in the two coexisting phases. Specifically,

$$\begin{aligned} \mu_w^I(T,P,Y) &= \mu_w^{II}(T,P,Z) \ , \\ \mu_n^I(T,P,Y) &= \mu_n^{II}(T,P,Z) \ , \end{aligned} \qquad (2)$$

where I and II refer to the coexisting phases, w refers to the *hypersolvent*, and n

refers to a micelle having aggregation number, n. At a fixed pressure, the simultaneous solution of these two equations yields the surfactant concentrations of the two coexisting phases, Y and Z, as a function of temperature and salt type and concentration (through the parameter C, see below), and hence the entire coexistence curve for each salt type and concentration. In the context of the mean-field theory of micellar solution behavior[20], the chemical potential of a water molecule can be expressed as

$$\mu_w = \mu_w^o + kT\left[\ln(1-X) + X - \sum_m X_m\right] + \frac{1}{2}\frac{C(T,P,m_s)\phi_s^2}{\gamma}, \qquad (3)$$

while the chemical potential of a micelle having aggregation number, n, is given by

$$\mu_n = \mu_n^o + kT\left[\ln X_n + 1 + n\left(X - 1 - \sum_m X_m\right)\right] + \frac{1}{2}nC(T,P,m_s)[(1-\phi_s)^2 - 1] . \qquad (4)$$

In Eqs. (3) and (4), μ_w^0 and μ_n^0 are the standard-state chemical potentials of water and n-mers, respectively, X is the total surfactant mole fraction, X_n is the mole fraction of n-mers, ϕ_s is the total surfactant volume fraction, $\gamma = \Omega_s/\Omega_w$, where Ω_s and Ω_w are the molecular volumes of surfactant and water, respectively, k is the Boltzmann constant, and T is the absolute temperature. The micellar size distribution, $\{X_n\}$, is given by[16]

$$X_n = \frac{(X_1 e)^n}{e} e^{-\beta n g_{mic}(n)}, \qquad (5)$$

where the values of g_{mic} are determined using the formalism presented in Chapter 2. Using the appropriate g_{mic} values in Eq.(5), one can calculate the various moments of the micellar size distribution, including the zeroth moment, ΣX_m, appearing in Eqs. (3) and (4). Thus, the chemical potentials, and, consequently, the calculated coexistence curve, are only a function of the interactions between the micelles, embodied in the mean-field interaction parameter $C(T,m_s)$. Note, that the variation of C with m_s depends also on the salt type.

We first determined the values of $C(T,m_s)$, through the use of the equilibrium conditions given in Eq.(2) in conjunction with Eqs.(3) and (4), needed to generate theoretical coexistence curves which yield the best fit to the experimentally measured coexistence curves. These fitted values of $C(T,m_s)$ were then analyzed to shed light on the effects of salt type and concentration on the relative strengths of intermicellar interactions.

B. Molecular Modelling of Intermicellar Interactions

In the previous chapters, various micellar morphologies were examined. For example, in Chapters 2 and 3, it was determined that $C_{12}E_8$ micelles in aqueous solutions tend to remain spheroidal over a range of temperatures, surfactant concentrations, and salt conditions, while $C_{12}E_6$ and $C_{10}E_6$ micelles in aqueous solutions have a tendency to grow in one dimension. For those $C_{12}E_6$ micelles which exhibit significant one-dimensional growth in aqueous solutions, these aggregates can be described reasonably well as wormlike micellar structures. Recall that wormlike micelles exhibit significant one-dimensional growth, and are characterized by a finite degree of flexibility due to the liquid-like nature of the hydrocarbon core. Consequently, for the C_iE_j surfactants considered in this thesis, when modelling the interactions between C_iE_j micelles in aqueous salt solutions, two main micellar morphologies were examined: spherical micelles, and wormlike micelles.

The wormlike micelles were modelled as a succession of micellar segments (rods) of length equal to the persistence length, ξ. Recall that the persistence length is the distance beyond which a micelle is considered flexible. Breaking down a wormlike micelle into a succession of rods of length ξ, is analogous to the polymer concept of representing a polymer chain by an equivalent freely-jointed chain, where in the present case the effective freely-jointed chain segment is equal to the persistence length. Therefore, in this equivalent freely-jointed chain representation, the orientation of monomers beyond a given persistence length would be independent of the orientation of monomers contained within that persistence length. In an

analogous manner, the orientation of a micelle "segment" (a rod having length = ξ) can be assumed to be independent of the orientations of the two segments to which it is physically connected to. Note that the present way to model wormlike micelles is somewhat different from that presented in Chapter 4, where the entire wormlike micelle was represented as an effective rigid rod whose length decreases with increasing flexibility, as measured by ξ. That description was reasonable, since the desired prediction was that of the crossover surfactant concentration, X^*, at which the micellar domains just begin to overlap, and, therefore, the micelles remain singly dispersed in close proximity to each other. On the other hand, in evaluating intermicellar interactions, greater attention must be given to modelling the precise morphology, including the flexibility, of the micelles. For example, in Chapter 4, it was found that in the two-phase region, dilute solutions typically coexist with semidilute solutions. Accordingly, the possibility of modelling the interactions both in the dilute regime, where the micelles are singly dispersed, and in the semidilute regime, where the micelles are fully entangled, should be considered. Breaking a wormlike micelle into a number of rod segments of length, ξ, would enable the calculations to be done regardless of whether the solution is in the dilute or in the semidilute solution regimes.

In general, the free energy of interactions can be represented as a sum of pairwise interactions between micellar aggregates, either spherical micelles or micelle rod segments of length ξ in the case of wormlike micelles. Note that in the case of wormlike micelles, we have made the approximation that the micelle rod segments of length, ξ, are not only independently oriented, but are also disconnected. It is noteworthy that this approximation will yield an upper bound for the predicted strengths of intermicellar interactions, since it allows two adjacent segments to interact freely, whereas, in actual fact, the distance of closest approach between two segments is limited due to connectivity constaints.

The resulting interaction free-energy expression takes the following form[22]

$$G_{interactions} = \frac{1}{2}\int\int_{V} u_{12}(\vec{r}_{12})\,\rho_{12}^{(2)}(\vec{r}_1,\vec{r}_2)\,d\vec{r}_1\,d\vec{r}_2 \ , \qquad (6)$$

where $u_{12}(\vec{r}_{12})$ describes the interaction potential between two aggregates (recall that for a wormlike micelle, an aggregate refers to a rod segment of length, ξ), and $\rho_{12}^{(2)}(\vec{r}_1,\vec{r}_2)d\vec{r}_1 d\vec{r}_2$ is the probability that one aggregate is in the volume element $d\vec{r}_1$ at $\vec{r}_1$ while the second aggregate is in the volume element $d\vec{r}_2$ at $\vec{r}_2$. The probability density, $\rho_{12}^{(2)}(\vec{r}_1,\vec{r}_2)$, in Eq.(6) can be broken down into independent density distributions using a correlation-function representation. Specifically,

$$\rho_{12}^{(2)}(\vec{r}_1,\vec{r}_2) = \rho_1(\vec{r}_1)\,\rho_2(\vec{r}_2)\,g_{12}(\vec{r}_1,\vec{r}_2) \ , \qquad (7)$$

where $\rho_1(\vec{r}_1)$ is the density distribution of the first aggregate, $\rho_2(\vec{r}_2)$ is the denstiy distribution of the second aggregate, and g_{12} is the correlation function. Note that in the system of interest, the spheres (or the rod segments of length, ξ) are identical (1=2), since there is a single surfactant type in solution which forms micelles of the same diameter (and the same persistence length for micelles that exhibit one-dimensional growth). It will also be assumed that (*i*) an aggregate has an equal probability of being anywhere in the solution volume, that is, $\rho_1(\vec{r}_1)=\rho_1$ and $\rho_2(\vec{r}_2)=\rho_2=\rho_1$, independent of position, and (*ii*) the aggregates are totally uncorrelated, that is, the position of one aggregate is independent of the position of another, that is, $g_{12}=1$. In that case, Eq.(7) yields $\rho_{12}^{(2)}(\vec{r}_1,\vec{r}_2)=\rho_1^2$. Utilizing the result, $\rho_{12}^{(2)}=\rho_1^2$, coupled with the coordinate transformation, $(\vec{r}_1,\vec{r}_2)\rightarrow(\vec{r}_1,\vec{r}_{12})$, where $\vec{r}_{12}$ is the distance between the centers (for spheres) or symmetry axes (for rods) of the two interacting aggregates, in Eq.(6) yields

$$G_{interactions} = \frac{1}{2}\rho_1^2\int\int_{V} u(\vec{r}_{12})\,d\vec{r}_1\,d\vec{r}_{12} \ , \qquad (8)$$

where $\rho_1=N_1/V$ is the number density of aggregates, that is, the number of aggregates, N_1 (either the number of spherical micelles, or the number of micelle rod segments of length, ξ) in a solution having volume, V. Integrating with respect to $\vec{r}_1$,

and noting that $\int_v d\vec{r}_1 = V$, and $V\rho_1 = N_1$, Eq.(8) yields

$$G_{interactions} = \frac{1}{2} N_1 \rho_1 \int_V u(\vec{r}_{12}) d\vec{r}_{12} \ . \tag{9}$$

As mentioned in the preceding section, in the mean-field theory of micellar solutions, the free energy of interactions is described by Eq.(1). Values of the mean-field interaction parameter, C, in Eq.(1) were deduced from experimentally measured cloud-point curves. In order to relate the two free-energy expressions given in Eqs. (1) and (9), as well as relate the experimental cloud-point curves to the free energy of interactions given in Eq.(9), a relation between the number of aggregates, N_1, and the number of surfactant molecules in solution, N_s, needs to be established. This relation between N_s and N_1 can be found using a mass-balance relation involving the hydrocarbon tails. Specifically, for spherical micelles, one obtains

$$N_s v_c = N_1 \frac{4}{3} \pi l_c^3 \quad \Rightarrow \quad N_s = \frac{4}{3} \frac{\pi l_c^3 N_1}{v_c} \ , \tag{10}$$

while for wormlike micelles (micellar rod segments of length, ξ), one obtains

$$N_s v_c = N_1 \pi l_c^2 \xi \quad \Rightarrow \quad N_s = \frac{\pi l_c^2 \xi N_1}{v_c} \ , \tag{11}$$

where l_c is the micellar core-minor radius, and v_c is the volume of the hydrocarbon tail.

A determination of the contribution of the relevant intermicellar interactions to the free energy of interactions, Eq.(9), was done for spherical and wormlike micelles. The specific interactions that were considered include: (1) van der Waals attractive interactions between the hydrocarbon cores of two micellar aggregates, and (2) possible PEO head layer interactions, which could range from being purely repulsive, as in good-solvent conditions where the PEO head chains in the micellar

hydrophilic layers behave as short polymer brushes, to being attractive due to the interpenetration of PEO head chains under poor-solvent conditions, which can be achieved by increasing the concentration of certain salts like chlorides, or increasing the temperature of the solution. This approach is similar to the characterization of the interactions between "water-in-oil" microemulsion droplets in terms of an attractive contribution and a repulsive entropic contribution due to the interpenetration of the penetrable aliphatic layers of two approaching microemulsion droplets. Values of the second virial coefficient calculated from the resulting interaction potentials compared favorably with those measured using light scattering[23]. Note that in this thesis, we have actually developed a molecular description of these interactions and have utilized it to calculate the attractions due to the interpenetration of the micelle head layers under poor-solvent conditions. It should also be noted that, for completeness, the possible contribution of the micelle head layers to the van der Waals attractions was also determined (see Section VB). Next, we consider separately intermicellar interactions in the case of spherical and wormlike micelles.

1. Spherical Micelles

For spherical micelles, integration of Eq.(9) using spherical coordinates (r,θ,φ) results in the following simplified form of the free energy of interactions,

$$G_{interactions} = \frac{1}{2} N_1 \rho_1 \int_0^{2\pi} \int_0^{\pi} \int_{\delta}^{\infty} u(r) r^2 dr \sin\theta \, d\theta \, d\varphi = 2\pi N_1 \rho_1 \int_{\delta}^{\infty} u(r) r^2 dr \ . \qquad (12)$$

Note that the lower radial limit of integration, δ, in Eq. (12) was determined by the distance of closest approach between the hydrocarbon cores of two aggregates, which, in turn, depends on the degree of interpenetration of the head layers of the two aggregates. Recall that in the mean-field theory, $G_{interactions}$ is given by Eq.(1). Using the fact that $\phi_s = \Omega_s N_s / V$, where Ω_s is the volume of a surfactant molecule, together

with the expression for N_s given in Eq. (10), in Eq.(1) yields

$$G_{interactions} = -\frac{1}{2}CN_s\phi_s = -\frac{1}{2}\frac{C\Omega_s N_s^2}{V} = -\frac{1}{2}C\Omega_s N_1\rho_1\left(\frac{4}{3}\pi\frac{l_c^3}{v_c}\right)^2 . \quad (13)$$

Equating Eqs.(13) and (12) in the following relation between the mean-field interaction parameter, C, and the interaction potential, $u(r)$,

$$C = -\frac{9v_c^2\int_\delta^\infty u(r)r^2dr}{4\pi\Omega_s l_c^6} , \quad (14)$$

and

$$\frac{\gamma C}{k} = -\frac{9v_c^2\int_\delta^\infty u(r)r^2dr}{4\pi\Omega_w l_c^6 k} , \quad (15)$$

where, as explained earlier, $\gamma = \Omega_s/\Omega_w$, is the ratio of the volume of a surfactant molecule, Ω_s, to that of a water molecule, Ω_w, k is the Boltzmann constant, and r is the distance between the centers of the spherical micelles (see Fig.1).

2. Wormlike Micelles

For wormlike micelles, which are broken down into independent rod segments of length, ξ, integration of Eq.(9) using cylindrical coordinates (r,θ,z) results in the following equation

$$\frac{G_{interactions}}{Unit\,Length} = \frac{1}{2}N_1\rho_1\int_0^\pi\int_\delta^\infty u(\vec{r})\,r\,dr\,d\theta = \frac{\pi}{2}N_1\rho_1\int_\delta^\infty u(r)\,r\,dr , \quad (16)$$

where the last equality is a result of the simplifying assumption that the interaction potential between two rods, $u(\vec{r})$, is independent of θ. Two simple cases were

examined: the interaction between crossed rods (see Fig.2), and the interaction between parallel rods (see Fig.3). Note that the crossed- and parallel-rod configurations represent a lower and an upper bound, respectively, for the strengths of intermicellar interactions between wormlike micelles. A more rigorous treatment, which entails an averaging of the interactions over all possible values of θ, should yield an average interaction whose magnitude is in between those corresponding to the crossed-rod and parallel-rod configurations. Similar to the treatment of the interactions between spherical micelles, the interaction parameter, $\gamma C/k$, in the case of wormlike micelles, can be related to the interaction potential, $u(r)$, through the use of Eqs.(1), (11), and (16). Specifically, one obtains

$$C = -\frac{v_c^2 \int_{\delta}^{\infty} u(r) r\, dr}{\pi \Omega_s l_c^4 \xi}, \tag{17}$$

and

$$\frac{\gamma C}{k} = -\frac{v_c^2 \int_{\delta}^{\infty} u(r) r\, dr}{\pi \Omega_w l_c^4 \xi k}. \tag{18}$$

3. Van der Waals Interaction Potentials

Van der Waals attractive interactions[24,25] originate from electromagnetic fluctuations. There are basically two contributions to van der Waals forces in polar solvents such as water. The first contribution arises from interactions between permanent dipolar molecules which occur at essentially zero frequency, and which are temperature dependent. The second contribution, which involves molecular polarization and is temperature independent, is referred to as the dispersion force. Note that the spontaneous and transient electric polarization in a molecule can arise

due to the motion of electrons, molecular distortion, or molecular orientation. This polarization will, in turn, induce spontaneous fluctuations in the surrounding medium. Therefore, even if the time average of the dipole moment (for nonpolar molecules) is zero, the instantaneous attractive force between the two molecules can still give rise to a finite time average.

In order to simplify the treatment of van der Waals forces, the complexities of polarizabilities, which reflect the charge fluctuations in the material, are lumped together into a parameter called the Hamaker constant, A[26]. Within this approach, the van der Waals interactions between bodies of different shapes are expressed as a product of the Hamaker constant and powers of the characteristic dimensions of the different interacting bodies. The zero frequency contribution to the Hamaker constant, which is the dominant contribution for water-hydrocarbon systems[24,25], can be estimated by

$$A_0 \sim \frac{3}{4}kT\left(\frac{\epsilon_1 - \epsilon_2}{\epsilon_1 + \epsilon_2}\right)^2, \qquad (19)$$

where ϵ_1 and ϵ_2 are the static dielectric constants of the interacting phases (hydrocarbon cores) and the medium (aqueous solution), respectively. Eq.(19) indicates that the Hamaker constant, and, therefore, the van der Waals attraction between hydrocarbon phases separated by water, increases with temperature. Note that, in principle, the static dielectric constants, ϵ_1 and ϵ_2, can also be temperature dependent. However, an estimate of the Hamaker constant, A_0, at various temperatures using Eq.(19) (see Table I), indicates that the overall temperature dependence of A_0 is weak over the limited temperature range of interest, where increasing the temperature from 20°C to 75°C increases the value of A_0 (in ergs), and, therefore, of the attraction between the cores, by less than 20%.

Typically, calculated values of the Hamaker constant, A, are found to decrease with increasing salt concentration[27]. A plot of this decay of the Hamaker constant is shown in Fig.4. The decay of the Hamaker constant indicates a weakening of the

van der Waals attractions between hydrocarbon phases upon the addition of salts to an aqueous solution. The presence of the ions, with their polarizing fields, breaks down the successive spontaneous polarization of solvent molecules which gives rise to the attractive dispersion interactions.

In the following discussions, van der Waals interactions between (1) spheres, and (2) micelle rod segments of length, ξ, will be discussed and applied to the analysis of intermicellar interactions.

Spheres. The contribution of the van der Waals interactions between micellar cores to $G_{interactions}$, and, therefore, to the mean-field interaction parameter, $\gamma C/k$, can be determined by substituting the relevant interaction potential, $u(r)$, in Eq.(15). The well-known van der Waals potential for spheres[28] was used. Specifically,

$$u_{sphere}^{vdW}(r) = -\frac{A}{6}\left(\frac{2a^2}{r^2-4a^2}+\frac{2a^2}{r^2}+\ln\frac{r^2-4a^2}{r^2}\right), \qquad (20)$$

where A is the Hamaker constant (where we have utilized measured Hamaker constants for hydrocarbon phases interacting across water), a ($=l_c$) is the sphere radius, and r is the distance between the centers of the spheres (see Fig.1).

Eq.(20) indicates that at very small separation distances, $r \approx 2a$,

$$u_{sphere}^{vdW}(r) = -\frac{A}{6}\left(\frac{a}{2(r-2a)}\right). \qquad (21)$$

On the other hand, in the limit of very large separation distances, r>>a, Eq.(20) reduces to

$$u_{sphere}^{vdW}(r) = -\frac{16A}{9}\left(\frac{a}{r}\right)^6. \qquad (22)$$

As can be seen from Eq.(21), the interaction potential decays very slowly (inversely proportional to the distance between the surfaces of the spheres, $r-2a$) in the vicinity of the spherical particle. Verwey and Overbeek explained this slow decay in the

following way: "This slow decay is understandable by the fact that for r/a≈2, only small parts of the spheres are very close together. A small change of the distance between the spheres has a substantial effect only on the elements surrounding the points of closest approach, whereas, for the bulk of the material involved in the interaction the relative change of the distances, and the consequent change in attractive energy, are small."[29] On the other hand, at large separations between the two spheres, the decay of the attraction is much faster. At these distances, Eq. (22) indicates that the decay is proportional to the inverse sixth power of the distance, which is the decay observed for van der Waals forces between two molecules. These observations are summarized in Fig.5, which shows a plot of the van der Waals potential given in Eq. (20) as a function of the normalized distance, r/a, indicating the rapid decay of the van der Waals potential to zero for $(r/a)>2$.

Crossed Rods. The van der Waals potential between two crossed rods (*cr*) is given by[30]

$$u_{cr}^{vdW}(r) = -\frac{A}{3}\left(\frac{1-\frac{1}{2}d^2}{1-d^2}E(d)-K(d)\right), \tag{23}$$

where E(d) and K(d) are complete elliptic integrals, d = $2a/r$ is the modulus, a ($=l_c$) is the crossectional radius of the rod, r is the distance between the rod axes (see Fig.2), and A is the Hamaker constant. In the limit of large separation distances between the rods, an expansion of Eq.(23) in powers of a/r ($<<1$) yields[30]

$$u_{cr}^{vdW}(r) = -\frac{\pi}{2}A\frac{a^4}{r^4}\left(1+5(\frac{a}{r})^2+21.875(\frac{a}{r})^4+91.7448(\frac{a}{r})^6+...\right), \tag{24}$$

while in the limit of small separation distances, ($r\approx 2a$), Eq.(23) yields[30],

$$u_{cr}^{vdW}(r) = -\frac{A}{6}\frac{a}{r-2a}. \tag{25}$$

Note that the large separation distance limit in the case of crossed rods does not

decay as fast as in the case of spheres [compare Eqs. (24) and (22)]. On the other hand, the small separation distance limit is twice as large as that for spheres [compare Eqs. (25) and (21)]. The last result simply reflects the fact that one of the radii of curvature of a rod is infinite, while a sphere has two finite and equal radii of curvature.

Parallel Rods. For parallel rods (*pr*), the van der Waals interaction potential is given by[30]

$$u_{pr}^{vdW}(r) = -\frac{3}{72}\pi a^4 \xi A\left(\frac{d^2}{dr^2}+\frac{1}{r}\frac{d}{dr}\right)U_3 , \tag{26}$$

where

$$U_3 = \frac{16r}{\pi^2 a^4}d^4\left(\int_0^{\pi/2}\frac{\cos^2\phi\, d\phi}{\sqrt{1-d^2\sin^2\phi}}\right)^2 , \tag{27}$$

with

$$d^2 = \left(1-\sqrt{1-\frac{4a^2}{r^2}}\right)^{\frac{1}{2}} . \tag{28}$$

At large separations ($r>>a$), this yields

$$u_{pr}^{vdW}(r) = -\frac{3}{8}\pi\frac{a^4}{r^5}\xi A\left(1+6.25(\frac{a}{r})^2+31.90(\frac{a}{r})^4+150.7(\frac{a}{r})^6+...\right) , \tag{29}$$

while for $r\to 2a$, the van der Waals attraction becomes infinitely large, such that

$$u_{pr}^{vdW}(r) = -\frac{A}{24}\frac{\xi}{a}\left(\frac{a}{r-2a}\right)^{3/2} . \tag{30}$$

As expected, the van der Waals interaction potential in the parallel-rod case is proportional to the length of the parallel rods, ξ [see Eqs. (29) and (30)]. This should be contrasted with the crossed-rod case which is independent of ξ [see Eqs.

(24) and (25)], because only those portions of the interacting rods closest to each other contribute significantly to the van der Waals potential.

In all the calculations presented later (see Section VB), experimental values of the Hamaker constant, A, and the full van der Waals potentials, given in Eqs.(20), (23) and (26) for spheres, crossed rods, and parallel rods, respectively, were used. For the potential for parallel rods [Eq. (26)], U_3 was determined numerically as a function of a/r using Eq.(27), and expressed in terms of a power series in a/r. From this resulting expression, the potential, $u_{pc}^{vdW}(r)$, was then determined using Eq. (26).

4. Interactions Between Micelle Head Layers

As mentioned earlier, the interactions between micelle head layers could range from being purely repulsive to adding an attractive contribution to the intermicellar interactions due to the interpenetration of PEO head chains under poor-solvent conditions. Below, we consider each possibility separately.

Steric Stabilization Forces. For PEO chains under good-solvent conditions, the strong attractive interactions between the PEO head chains and the water molecules result in the chains behaving as short polymer brushes tending to maximize contact with the solvent. This can be linked to the *hydration* of the PEO heads, which can give rise to a repulsive interaction between the C_iE_j micelles[31,32]. Furthermore, the hydrophilic PEO head chains, which are attached at one end to the surface of the hydrocarbon core of each C_iE_j micelle, also prevent the close approach of these micellar cores, thus very effectively reducing the magnitude of the attractive van der Waals contributions between the micellar cores described in Section IIIB3.

The *hydration* of the PEO head chains[31], or the attractive dipolar interactions between the PEO head chains and water[32], is believed to be weakened as the temperature is increased[33], or upon the addition of certain salts such as chlorides to the aqueous solution. This could lead to a poor-solvent condition for the PEO

chains, such that the chains would prefer to be in contact with themselves much more than with the aqueous medium. This is consistent with the experimental observations that aqueous solutions of poly(ethylene oxide) phase separate upon increasing temperature[34]. The effects of salts on PEO head-solvent interactions have also been studied experimentally[35,36]. Salts, such as KCl and KBr, have been shown to promote the phase separation of aqueous PEO solutions, as reflected by the lowering of the temperature at which phase separation is observed upon the addition of these salts.[36] The addition of KI, on the other hand, first increased and then decreased the cloud-point curves[36].

An examination of the coexistence (cloud-point) curves of PEO-H_2O[37] and C_iE_j-H_2O[3] solutions revealed similarities in the shapes of the two sets of coexistence curves. This seems to suggest that the interactions responsible for phase separation are strongly a PEO head phenomenon. It is also interesting to note that although the shapes of the coexistence curves in both the PEO and the C_iE_j case are similar, the location of the critical points are different. To see this more clearly, we would like to compare the T_c value of a C_iE_j aqueous solution with the T_c value of an "equivalent" PEO aqueous solution, where the PEO chain has *j* ethylene oxide untis. For example, T_c of a $C_{12}E_{12}$-H_2O solution is reported[39] to be 98°C, while T_c of a PEO (having 49 EO units)-H_2O solution is higher than 170°C. It is noteworthy that shorter PEO chains in aqueous solution exhibit having even higher T_c values[34], primarily because of the larger configurational entropy of mixing corresponding to the shorter chains. These findings suggest that the grafting of the PEO chains to the micellar-core surface of C_iE_j micelles may play a significant role in modulating the interactions between micelles, as compared to those existing between "equivalent" PEO polymer chains in solution. Note that the configurational entropy of mixing of PEO chains and water is greatly reduced in the micellar head layers, as compared to the case of free PEO chains in water, because the grafted PEO chains in the micelle head layer behave effectively as "one PEO chain" having an infinitely large molecular weight. This, in turn, would tend to reduce the T_c values (as can be seen by using a simple Flory-Huggins description of polymer solutions[38]. Note that there

could also be a contribution to the attractions leading to lower T_c values for C_iE_j solutions, as compared to PEO solutions, due to the van der Waals attractions between the micellar-hydrocarbon cores described earlier.

Attractive Interactions Between Micelle Head Layers. The change in the *quality* of the solvent, which leads to less attractive interactions between the PEO chains and the aqueous solvent, can lead to an *effective* attractive interaction between the micelle head layers of two approaching C_iE_j micelles. An analysis of the various phases and phase-transition boundaries (including the lamellar and hexagonal phases) of the C_iE_j homologous series of nonionic surfactants[39] suggests that interactions between PEO heads of adjacent micelles (dipole-dipole) may provide an additional attractive force. In addition, the direct measurement of forces between $C_{12}E_5$ layers adsorbed on mica surfaces has been conducted as a function of temperature.[40] Crossed-cylindrical molecularly smooth mica surfaces[41] were first rendered hydrophobic by electrostatic binding of cationic surfactants (dimethyl dioctadecyl ammonium bromide) onto the negatively charged mica surfaces. $C_{12}E_5$ surfactant molecules were then adsorbed onto this hydrophobic surfaces, such that the PEO heads extended towards the bulk aqueous solution between the cylindrical surfaces. As the separation distance between the surfaces was decreased, the force between the $C_{12}E_5$-covered mica surfaces was observed to change from being repulsive to being attractive and then back to being highly repulsive. The depth of the attractive minimum was observed to increase as the temperature was increased (see Fig.6).

The weakening of the repulsion, as well as the appearance of an attractive minimum in the $C_{12}E_5$ force measurements with increasing temperature, suggest the possibility that the overlap of micelle PEO head layers under poor-solvent conditions may lead to an attractive contribution to the interactions between C_iE_j micelles. Note that the overlap of micelle PEO head layers is enthalpically advantageous under poor-solvent conditions since it brings about an increase of PEO head-head contacts. Associated with this phenomenon, however, is a decrease in the mixing entropy due to the increase in the concentration of PEO chains upon overlap of two PEO micelle

head layers. We have carried out an analysis of these competing enthalpic and entropic contributions to the interactions between micelle head layers in the context of a modified Flory-Huggins theory of polymer solutions, which constitutes a reasonable description when the solution polymer concentration is high, which is the case in the micelle head layers under consideration.

In the micelle head layer, the configurational entropy of the centers of mass of the PEO polymer chains is vanishingly small, as was mentioned earlier, since the PEO chains are grafted at one end to the micellar-core surface[42]. The PEO head chains, therefore, behave as if they were an effective single polymer chain having a very large (infinite) molecular weight. Accordingly, the well-known[38] Flory-Huggins configurational entropy expression for grafted PEO chains and solvent in the micelle head layer (*hl*) reduces to

$$s_{hl}(\phi) = -k\frac{V_{hl}}{\Omega_w}[(1-\phi)\ln(1-\phi)] , \qquad (31)$$

where V_{hl} is the volume of the micelle head layer, Ω_w is the volume of a water molecule, and ϕ is the volume fraction of PEO heads in the micelle head layer. The enthalpy of mixing PEO heads and water in the micelle head layer can be expressed as

$$h_{hl}(\phi) = kT\frac{V_{hl}}{\Omega_w}[\chi\phi(1-\phi)] , \qquad (32)$$

where χ is the Flory-Huggins chi parameter. The free energy of the micelle head layer, $G_{hl}=h_{hl}-Ts_{hl}$, can be obtained by combining Eqs. (31) and (32). Specifically, one obtains

$$G_{hl}(\phi) = kT\frac{V_{hl}}{\Omega_w}[(1-\phi)\ln(1-\phi)+\chi\phi(1-\phi)] . \qquad (33)$$

Upon overlap of micelle head layers belonging to two approaching micelles, the environment surrounding each of the PEO head chains changes, primarily because of a change in the concentration of the PEO heads, ϕ, in the overlap region.

There is thus a corresponding change in the free energy associated with the overlap region in the micelle head layer. For a small overlap volume, δV_{ov}, where *ov* indicates the overlap region, the corresponding change in the free energy, $\delta(\Delta G_{hl}^{ov})$, resulting from the mixing of a portion of one micelle head layer (having volume fraction, ϕ_1) with an equal portion of micelle head layer from a second micelle (having volume fraction, ϕ_2), such that the resulting overlap region has a concentration of PEO heads, $\phi_f = (\phi_1 + \phi_2)$, is given by

$$\begin{aligned}\delta(\Delta G_{hl}^{ov}) = \frac{kT\delta V_{ov}}{\Omega_w}[&(1-\phi_f)\ln(1-\phi_f) + \chi\phi_f(1-\phi_f) \\ &- (1-\phi_1)\ln(1-\phi_1) - \chi\phi_1(1-\phi_1) \\ &- (1-\phi_2)\ln(1-\phi_2) - \chi\phi_2(1-\phi_2)] \ .\end{aligned} \tag{34}$$

Note that in Eq.(34), ϕ_f and δV_{ov} are explicit functions of *r*, and therefore, $\Delta G_{hl}^{ov}(r)$ is also a function of *r*. Accordingly, the total change in the free energy, $\Delta G_{hl}^{ov}(r)$, upon overlap of two micelle head layers can be determined by integrating over the total volume of overlap. Note that the free-energy change, $\Delta G_{hl}^{ov}(r)$, can also be viewed as a potential of mean force associated with the reversible work that needs to be done to bring two micelle head layers from infinite separation to a separation distance, *r*. The resulting potential, $u^{ov}(r)$, can be expressed as

$$u^{ov}(r) \sim \Delta G_{hl}^{ov}(r) = \int_{V_{ov}} \delta(\Delta G_{hl}^{ov}(r,R)) \ . \tag{35}$$

Using Eq.(34) for $\Delta G_{hl}^{ov}(r)$ in Eq.(35) yields

$$\begin{aligned}u^{ov}(r) \sim \frac{kT}{\Omega_w}\int_{V_{ov}}[&(1-\phi_f)\ln(1-\phi_f) + \chi\phi_f(1-\phi_f) \\ &- (1-\phi_1)\ln(1-\phi_1) - \chi\phi_1(1-\phi_1) \\ &- (1-\phi_2)\ln(1-\phi_2) - \chi\phi_2(1-\phi_2)]\ \delta V_{ov}(r,R) \ .\end{aligned} \tag{36}$$

Accordingly, the determination of $u^{ov}(r)$ using Eq.(36) requires the determination of (*i*) the volume fraction of PEO heads in the overlap region before

(ϕ_1 and ϕ_2) and after (ϕ_f) overlap, and (*ii*) the differential volume of overlap, δV_{ov}. Note that ϕ_f and δV_{ov} vary with the distance from the micellar-core surface, R, and the distance between the micellar centers or axes, r. It is thus necessary to estimate the volume fraction profile of head chains, $\phi(R)$, a distance R away from the micellar-core surface. Specifically, $\phi(R)$ is estimated as the volume of a PEO head chain contained between distances R and $R+\delta R$ from the micellar-core surface, divided by the volume of the micelle head layer per surfactant molecule, $\delta v_{hl}(R)$, within a distance R and $R+\delta R$ from the micellar-core surface. The volume of PEO between R and $R+\delta R$ is estimated using the average number of EO units of a single PEO head chain between R and $R+\delta R$, denoted by $\delta n_{EO}(R)$, multiplied by the volume of an EO unit, V_{eo}, where $V_{EO}=63.5$ (Å^3) is the dry volume of a monomer of polyethylene oxide[43]. Therefore,

$$\phi(R) \sim \frac{V_{EO}\delta n_{EO}(R)}{\delta v_{hl}(R)} . \qquad (37)$$

Note that $\delta n_{EO}(R)$ was estimated in a manner analogous to the method employed in Chapter 2, where a Monte-Carlo RIS approach was utilized to generate PEO chain conformations. In this way, the bond distribution in the micelle head layer was determined. The micelle head layer was divided into discrete "shells", each 0.5Å in thickness (see Fig.7). The number of bonds contained within each shell was counted for each generated chain, and the average of 40,000 accepted conformations was determined and taken as the value of $\delta n_{bonds}(R)$ [$=3\delta n_{EO}(R)$], the number of bonds of a single PEO head chain contained within shell m a distance $R=0.5m$Å from the micellar-core surface. On the other hand, as described earlier, $\delta v_{hl}(R)$ is equal to the volume of the micelle head layer between R and $R+\delta R$ divided by the number of surfactant molecules within the micellar aggregate, and is given by

$$\delta v_{hl}^{sph}(R) = \frac{4\pi(R+l_c)^2\delta R}{\frac{4}{3}\pi l_c^3/v_c} = \frac{3v_c(R+l_c)^2\delta R}{l_c^3} , \qquad (38)$$

for spherical micelles, and

$$\delta v_{hl}^{rod}(R) = \frac{2\pi L(R+l_c)\delta R}{\pi l_c^2 L/v_{hc}} = \frac{2v_{hc}(R+l_c)\delta R}{l_c^2}, \qquad (39)$$

for rodlike micelles, where L is the length of the micelle. Using Eqs. (37), (38), and (39), the volume fraction of PEO in the micelle head layer can be written in the following compact form for both spherical and rodlike morphologies

$$\phi(R) \sim \frac{\frac{V_{EO}\frac{\delta n_{bonds}(R)}{3}}{Sv_c(R+l_c)^{S-1}\delta R}}{l_c^S}, \qquad (40)$$

where S is a shape factor ($S=2$ for rods, and $S=3$ for spheres), and $\delta n_{bonds}(R)$ is determined as discussed above (for further details see Appendix A).

As seen in Eq.(40), $\phi(R)$ varies only in one dimension (distance R from the micellar-core surface). The change in $\phi(R)$ when the micelle head layer of a C_iE_j micelle overlaps with that of another C_iE_j micelle will depend on the shape of the micellar-core surface at which one end of each of the PEO head chains is grafted. In addition, in the case of rodlike micelles, the change in $\phi(R)$ will also depend on the relative orientation of one micellar rod with respect to another. In the simplest case of symmetric volume fraction profiles, which constitutes an exact description for planar grafting surfaces, and a simplifying approximation for curved surfaces, and allowing the micelle head layers to interpenetrate freely, the volume fraction profiles before and after overlap behave as shown in Fig.8, where $\phi_f(R) \approx \phi_1(R) + \phi_2(r-2l_c-R)$ [for a descriptions of r, R, and l_c, see Fig.9]. To determine $\phi_f(R)$, the volume fraction after overlap, we made the simplifying assumption that there is no distortion of the volume fraction profiles upon overlap. This is equivalent to saying that the presence of the PEO heads from one micelle does not affect the distribution of the EO segments of the heads in the other micelle head layer, and that the profiles are

simply additive. Note that in the cases of interest, that is, where the overlap results in an attraction, the overlap is not very large so that the possible distortion of the profiles are not huge. Using the numerically generated profiles ϕ_1, ϕ_2, and ϕ_f, together with the value of δV_{ov}, in Eq.(36) permits a determination of $u(r)^{ov}$ as a function of R, r, and χ.

The differential overlap volume, δV_{ov}, depends explicitly on the shape of the micelle. As an illustration, we consider the parallel-rod morphology, described in detail in Fig.9. Using geometrical considerations, the overlap volume, δV_{ov}, the cross-section of which is shown by the dark strip in Fig.9, for parallel rods of length, ξ, is given by

$$\delta V_{ov}(R) = 2\sqrt{(l_c+l_h)^2-(r-l_c-R)^2}\,\xi\,\delta R \ . \qquad (41)$$

IV. EXPERIMENTAL RESULTS

The results of the cloud-point curve measurements are shown in Figs.10-20 for the C_iE_j surfactants considered in this thesis under various salt conditions. As shown in Figs.10-12, the addition of LiCl, NaCl, and KCl to $C_{12}E_6$-H_2O solutions promotes phase separation, as reflected by the decrease of the cloud-point temperatures with increasing salt concentration. Among these chloride salts, NaCl causes the largest decrease in the cloud-point temperatures, followed by KCl, and LiCl. A similar analysis of the anion effect reveals that KCl causes the biggest decrease of the cloud-point temperatures, followed by KBr, with a much weaker effect of KBr as compared to that of KCl (compare Figs. 12 and 13). The addition of KI, on the other hand, suppresses phase separation, thus increasing cloud-point temperatures (see Fig.14). The same anion trend is established for $C_{10}E_6$ (compare Figs.15-17) and $C_{12}E_8$ (compare Figs.18-20), that is, KCl reduces cloud-point temperatures much more than KBr, while KI increases cloud-point temperatures. The order of the effect of the ions on the cloud-point temperature variations is analogous to the order of the effect of

the ions on the CMC, discussed in Chapter 2. The more polarizing chlorides, for example, induce the biggest change in micellar solution properties, both CMC's and cloud-point temperatures, which can be related to the fact that the more "polarizing" ions change the solvent *quality* more significantly. This change in solvent *quality* was quantified at the level of the CMC through changes in the solubility of the tails, and changes in the free energy of dilution of the PEO heads (see Chapter 2). In considering phase-separation behavior, on the other hand, the solvent *quality* was quantified through changes in the Flory-χ parameter, as discussed in Section IIIB.4.

The effects of varying the lengths of the C_iE_j head (E_j) and tail (C_i) is also reflected in the cloud-point curves. Increasing the number of ethylene oxide units (j) in the heads (going from $C_{12}E_6$ to $C_{12}E_8$) decreases the tendency to phase separate, that is, these solutions phase separate at higher temperatures (compare Figs.12-14 and Figs.15-17). On the other hand, increasing the hydrophobicity of the tails, by increasing i, (for example, going from $C_{10}E_6$ to $C_{12}E_6$) increases the tendency to phase separate, that is, these solutions phase separate at lower temperatures (compare Figs.12-14 and Figs.18-20).

The critical temperature, T_c, and the critical concentration, X_c, which correspond to the lowest point in each of the measured cloud-point curves, for $C_{12}E_6$ in aqueous salt solutions are shown in Table II. It is noteworthy that the reported X_c values shown in Table II are approximately constant for $C_{12}E_6$ in chloride and bromide aqueous solutions. For both of these salts, a simple displacement of the curves along the temperature axis is observed. The X_c's corresponding to the cloud-point curves of $C_{12}E_6$ in KI solutions, on the other hand, appear to increase as the KI concentration is increased. As discussed in the molecular-thermodynamic theory of micellar solution phase behavior[16], X_c is a sensitive function of the size distribution of the micelles, such that the longer the micelles, the smaller the values of X_c. These experimental results indicate that the size distributions of the micelles are roughly constant at the critical temperature for surfactants in aqueous KCl and KBr solutions, while the distribution shifts to smaller sizes in KI solutions. Again, this observation

is consistent with the suppression of micellar growth upon increasing KI concentrations which was indicated by the light scattering results discussed in Chapter 3. We had conjectured in Chapters 2 and 3 that the suppression of micellar growth in KI solutions is due to the possible complexation of I^- with the PEO head chains, coupled with the observed positive adsorption of KI onto hydrocarbon-aqueous solution interfaces[44]. Note that it was also observed[44] that the presence of hydroxy (-OH) groups at the $C_{12}H_{23}OH$-H_2O interface greatly increased the adsorption of KI onto that interface, which leads us to believe that even in the absence of specific interactions between I^- and PEO, the presence of the PEO heads induces an increase in the concentration of I^- in the vicinity of the micellar-core surface. The net result of these possible mechanisms is the generation of a *pseudo-charge* in the micelle head layer, which adds a repulsive electrostatic contribution to the intermicellar interactions, and therefore increases the phase separation temperature of C_iE_j solutions upon addition of KI. It is interesting to note that the addition of KI to aqueous PEO solutions first increases, and then decreases the cloud-point temperatures of the PEO aqueous solution[45]. This observation suggests that there is a subtle difference between the mechanism by which KI affects the phase behavior of aqueous PEO polymer solutions, as compared to that of aqueous C_iE_j solutions. One difference is the absence of a hydrocarbon-aqueous solution interface in the former case, on which KI was shown to be positively adsorbed. It is also plausible that the length of the PEO chains could also be a factor, such that the accessibility of the EO units to specific interactions with I^- is increased when the PEO chains are shorter. It is therefore probable that there is a bigger net increase in the concentration of I^- in the vicinity of the PEO chains present in the C_iE_j micelle head layer, as compared to that in aqueous solutions of free PEO polymer chains.

V. THEORETICAL RESULTS

A. Mean-Field Interaction Free-Energy Model

As described in Section IIIA, the magnitude of the intermicellar interactions can be deduced from the measured cloud-point curves in the context of the mean-field approach to model the intermicellar interaction free energy, Eq.(1). The determination of the value of the normalized intermicellar interaction parameter, γC, as a function of salt type and concentration, as well as temperature, was performed by calculating the coexisting surfactant concentrations, Y and Z [see Eqs. (2), (3), and (4)] that would best reproduce the experimentally measured cloud-point curves. Recall that γ is the ratio of the volume of a surfactant molecule to that of a water molecule. The fitting procedure which was employed for the cloud-point curves is illustrated in Fig.21, where the experimental cloud-point curve of $C_{12}E_6$ in 1m NaCl is shown and compared with the calculated curve using $(\gamma C)_c = 1.09\ kT$, and $(d(\gamma C/k)/dT)_c = 16$ (recall that linearity of C versus temperature was assumed). Plots of the values of C as a function of temperature for $C_{12}E_6$-H_2O solutions under varying salt conditions are shown in Fig.22. Fig.22 shows that the addition of KCl significantly increases the value of C, while the increase in the value of C upon the addition of KBr is not as significant as that induced by the addition of KCl. Furthermore, KI decreases the value of C, which, as discussed in Section IV, is conjectured to be caused by the specific complexation between I^- and the PEO micelle head layer, adding a repulsive electrostatic contribution to the intermicellar interactions, and thereby making these interactions less attractive (lower C values).

Another interesting observation can be made using this method of analyzing the cloud-point curves. A summary of the fitting parameters, $(\gamma C/kT)_c$, used to reproduce the experimentally measured cloud-point curves of $C_{12}E_6$ in various salt solutions are presented in Table II. Inspection of Table II reveals that $(\gamma C)_c$ for all the surfactant solutions studied is approximately constant at a value $(\gamma C)_c \approx 1\ kT$.

This is true regardless of the marked changes in the critical temperatures, T_c, induced by the various salts. These results indicate that the magnitude of the attractive intermicellar interactions, on a per surfactant molecule basis, required to induce phase separation is approximately of the same order as the thermal energy of a C_iE_j molecule.

B. Van der Waals Interactions

For spherical micelles, the van der Waals contribution to γC was calculated using Eqs.(15) and (20), where various values of δ, the distance of closest approach between two micelles were used, ranging from $(2l_c+2l_{hl})$, corresponding to no interpenetration of micelle head layers, to $(2l_c+l_{hl})$, corresponding to the full interpenetration of micelle head layers but with no distortion of the volume-fraction profiles of each of the interacting micelle head layers. Recall that l_c is the micellar core-minor radius, and l_{hl} is the average thickness of the micelle head layer, estimated using the Monte-Carlo RIS approach as discussed in Chapter 2. It can be seen from the results summarized in Table III that the attractive van der Waals contribution for spherical micelles decreases slightly with increasing head chain length, consistent with the greater stabilization brought about by longer head chains, which act to increase the distance between the micellar-core regions. However, in all cases, the attractive van der Waals contribution to the intermicellar interactions is small, of the order of 0.01 kT, even in the case where there is substantial interpenetration of PEO chains.

Similarly, for interacting crossed-rodlike aggregates, the use of Eqs.(18) and (23) gives the van der Waals contribution to $(\gamma C/kT)_c$. The results are summarized in Table IV. As in the case of spherical micelles, although the attraction of the cores increases with decreasing combined thickness of the interacting micelle head layers, the magnitude of the attraction is still too small, of the order of 0.01 kT. For parallel rods, on the other hand, one expects that the van der Waals attractive contribution

should be bigger, since this geometry dictates that greater portions of the micelles are closer to other micelles, as compared to the other two geometries considered (spherical and crossed-rodlike micelles). This is indeed the case, as shown in Table V, where the van der Waals attractions between parallel rods calculated using Eqs.(18) and (26) for rodlike micelles of $C_{12}E_4$, $C_{12}E_6$, and $C_{12}E_8$ are tabulated. The van der Waals attractions between parallel rods are indeed an order of magnitude larger than those between crossed-rodlike micelles. Note that the actual interaction between micellar segments would correspond approximately to that between these two extremes (crossed and parallel rods). In either case, the van der Waals attractions are too small to be able to explain the observed phase separation (recall that $(\gamma C/kT)_c \approx 1$ is needed). It is noteworthy that this result is also consistent with the magnitude of the calculated van der Waals interactions between sterically stabilized dispersions, where for a particle radius which is roughly equal to the stabilizing layer thickness, the magnitude of the attraction was estimated to be 0.05kT[46]. Note that in Ref.46, only a crude estimation was done using the limiting form of the van der Waals potential valid at very small separation distances. The actual attraction would thus be even less than 0.05 kT, consistent with our calculations using the full expression for the van der Waals potential.

Although the method of calculating the van der Waals interactions between micelles is analogous to calculations done on colloidal particles stabilized by grafted polymers, where only the van der Waals contribution resulting from the colloidal particles are considered[47], for the sake of completeness, we have also considered the possible contribution of the PEO hydrophilic head layer to the van der Waals attraction between micelles. In so doing, the micelle head layer was represented as a PEO solution which could interact with another micelle head layer through van der Waals forces. The closest distance of approach between these two "phases" was assumed to be the order of the diameter of a water molecule (≈3Å)[48]. The Hamaker constant was estimated using Eq.(19), where ϵ_1 was taken to be the static dielectric constant of the equivalent PEO solution. These dielectric constants are available experimentally as a function of PEO concentration[49], where the PEO

concentration in the micelle head layer was calculated as described as in Chapter 2. The results of the calculations indicate that even an assumed van der Waals interaction between the micelle head layers, modelled as *frozen* PEO solutions, is insufficient to account for the needed attractions between the micelles, the contribution per surfactant molecule being of the order of 0.1 kT.

In addition to the failure of the van der Waals potential to account for the magnitude of the attractions necessary to induce the observed phase separation, the addition of salts should further decrease this contribution, since salts effectively break down the instantaneous dipolar interactions that make up the van der Waals attraction, as explained in Section IIIB3, resulting in lower Hamaker constant values when salts are added to aqueous solutions. This is contrary to the experimentally observed effects of chlorides and bromides on phase separation, where the addition of these salts promote phase separation, which corresponds to an increased attractive intermicellar interaction. (Note that the specific mechanisms involved when KI is added to aqueous solutions renders the use of the *hypersolvent* approach questionable. Accordingly, the KI case will not be discussed any further under this *hypersolvent* approach.) Since van der Waals attractions are incapable of inducing the observed phase separation, there is a need to identify other molecular mechanisms that can be used to rationalize the magnitude of the attractions needed to drive the observed phase separation, and the salt effects on these attractions. Accordingly, we decided to focus on the interactions between the micelle head layers, with the hope of identifying additional attractions over certain ranges of solution conditions.

C. Interpenetration of Micelle PEO Head Chain Layers

The volume fraction profile of PEO chains in the micelle head layer, $\phi_{hl}(R)$, where R is the distance from the micellar-core surface, can be determined using the Monte-Carlo RIS approach discussed in Chapter 2 (see also Appendix A). The resulting volume fraction profiles, $\phi_{hl}(R)$, for rodlike micelle head layers of $C_{12}E_4$,

$C_{12}E_6$, and $C_{12}E_8$, with $l_c = 15.41$Å, are shown in Fig.23. Although the longer chains (for example, E_8) extend farther into the aqueous environment, as seen in Fig.23, the segments of the longer chains likewise have a greater probability of folding back towards the micellar-core surface, resulting in a higher concentration of PEO segments at a given distanc, R, and, therefore, in a higher $\phi_{hl}(R)$ value, as compared to those for the shorter chains (E_4 and E_6). Upon overlap, the volume fraction profiles within the micelle head layer change, as shown in Fig.8. Depending on the degree of overlap, which determines the magnitude of the change in the volume fraction profiles, the free energy associated with the micelle head layer, as modelled using a modified Flory-Huggins approximation, could either increase (due to the entropic disadvantage associated with increasing the PEO volume fraction), or decrease (due to the enthalpic advantage under poor-solvent conditions, measured by the Flory-Huggins chi parameter, χ, where higher values of χ correspond to poorer solvent conditions). The relative magnitudes of the enthalpic, $h_{hl}(\phi_f)-[h_{hl}(\phi_1)+h_{hl}(\phi_2)]$, and entropic, $-T\{s_{hl}(\phi_f)-[s_{hl}(\phi_1)+s_{hl}(\phi_2)]\}$, contributions to $\delta(\Delta G_{hl}^{ov}(R))$ [given in Eq.(34)] are illustrated in Fig.24 for parallel $C_{12}E_6$ rodlike micelles separated by a distance $r = 60$Å. As shown in Fig.24, changing the χ parameter from $\chi = 0.8$ to $\chi = 1.0$ (that is, making the solvent poorer) increases the depth of the enthalpic contribution to the potential, while the entropic contribution, which is only a function of the PEO concentrations, remains the same for the two cases. Therefore, the resulting $\delta(\Delta G(R))$ value is slightly deeper when $\chi = 1$.

The potential functions resulting from the integration of Eq.(35) are shown in Fig.25 for parallel rodlike $C_{12}E_4$, $C_{12}E_6$, and $C_{12}E_8$ micelles as a function of distance between the axes or centers of the micelles, r, for $\chi = 0.8$. Fig.25 shows that there is a slight minimum in the potential function for all the surfactants examined, and that a steep rise in the potential occurs farther from the micellar-core surface for the longer PEO chains. This indicates that the probability of allowing the interpenetration of micelle head layers is higher for the shorter PEO chains. This phenomenon is magnified for higher χ values, as shown in Fig.26, where $\chi = 1$. A

comparison of Figs.25 and 26 shows that an increase in χ (poorer-solvent quality), which can be induced either by adding salts such as chlorides[50] to the aqueous solution, or by increasing temperature[51], increases the depth of the attractive minimum in the potential function, and the potential barrier is pushed closer to the micellar-core surface. In fact, for $C_{12}E_4$, the potential is attractive throughout the overlap region ($r = 2l_c+l_{hl}$ to $r = 2l_c+2l_{hl}$) when $\chi=1$. These results are consistent with the experimental observation that T_c increases in the order $T_{c,C12E4}<T_{c,C12E5}<T_{c,C12E6}<T_{c,C12E8}$. Another interesting observation is the similarity between the potential functions calculated using the theory developed in this chapter and the measured force curves between $C_{12}E_5$ layers adsorbed on mica[33]. Fig.6 shows that in the surface-force measurements, the depth of the attractive well increases, and the steep repulsive wall moves closer to the surface as temperature is increased. This temperature effect parallels the effect of χ seen in Figs.25 and 26, and redrawn for aqueous $C_{12}E_6$ solutions for various χ values in Fig.27. Fig.27 shows that for $\chi=0.6$, the potential is repulsive at all values of r, while for $\chi=0.8$, a slight minimum in the potential function appears. The minimum becomes deeper, and the steep repulsive wall is pushed closer to the micellar-core surface as χ is increased further to a value of 1. Finally, at $\chi=1.2$, the potential is attractive throughout the overlap region ($r=2l_c+l_{hl}$ to $r=2l_c+2l_{hl}$). The theory for the interpenetration-induced attractions between PEO head layers presented in this chapter is thus qualitatively consistent with the experimentally observed temperature and salt effects on phase separation, as well as with the experimental results of surface-force measurements.

VI. SUMMARY AND CONCLUSIONS

In this chapter, we presented the experimentally determined cloud-point curves of aqueous salt solutions of $C_{10}E_6$, $C_{12}E_6$, and $C_{12}E_8$ as a function of salt type and concentration. The measured cloud-point curves indicate significant salt effects on intermicellar interactions. LiCl, NaCl, KCl, and KBr were seen to increase the attractions between micelles, and thereby promote phase separation, while the

addition of KI was observed to decrease the attractions between micelles, and thus to suppress phase separation. The effect of KI on intermicellar interactions is consistent with the conjecture that we presented in Chapters 2 and 3, whereby the specific attractive interactions between I^- and the PEO micelle head layer adds a repulsive electrostatic contribution to intermicellar interactions, thus forcing phase separation to occur at higher temperatures, where we believe the specific I^--PEO interactions are weakened due to thermal effects. This is also consistent with the effect of KI on intramicellar interactions, which, in turn, affects the onset of micellization, as characterized by the CMC (see Chapter 2), as well as the micellar size distribution, as reflected by the intensity of scattered light (see Chapter 3).

The origin of the intermicellar attractions necessary to induce the observed phase separation was traced to the interpenetration of the PEO micelle head layers of two approaching micelles under poor-solvent conditions, although there is also a very small (but insufficient) contribution due to the van der Waals attractions between the micellar cores. The interpenetration of PEO micelle head layers is free energetically more advantageous in the presence of salts such as chlorides, as well as upon increasing temperature, both of which increase the Flory-χ parameter. This corresponds to a decrease in the solvent *quality*, such that PEO chains prefer to be in contact with other PEO chains, rather than with the solvent.

In summary, the theory for the new attractive intermicellar interactions resulting from the interpenetration of PEO chains can qualitatively account for both the temperature and the salt effects (through the χ parameter) on the phase separation of aqueous salt solutions of C_iE_j micelles. This theory is also consistent with the observed similarity between the shapes of the cloud-point curves of PEO-H_2O and C_iE_j-H_2O solutions, as well as with the effects of salt type and concentration on these cloud-point curves. Furthermore, it was noted that the grafting of the PEO heads on the micellar-core surface effectively reduces the translational entropy of the PEO chains, such that the attractions necessary to overcome the entropic disadvantage associated with phase separation is smaller for micellar solutions as compared to polymer solutions. This explains the observed decrease in the cloud-

point temperatures of C_iE_j aqueous surfactant solutions as compared to those of PEO aqueous solutions. Finally, the theory can also account for the observed effect of increasing the length of the E_j head, leading to an increase in the T_c values.

APPENDIX A

As described in Section III, the bond density distribution, n_m versus m, where m is the number of shells of thickness δR (taken to be 0.5Å) from the micellar-core surface, (see Fig.7), can be determined using a Monte-Carlo RIS approach. This procedure was applied to three poly(ethylene oxide) head chains, E_4, E_6, and E_8. The resulting n_m versus m profile is very rough because of the discretization of space during the simulation runs. Accordingly, in order to represent the numerically generated distribution by an equivalent smooth curve, $\delta n_{bonds}(R)$, the following procedure was used. The cumulative number of bonds, $\underline{\Sigma} n_m$, was plotted as a function of the distance from the micellar core, R. The plot of $\underline{\Sigma} n_m$ versus R can be approximated very well by a third-degree polynomial, as shown in Fig.28. Specifically,

$$\sum_m n_m \sim AR^3 + BR^2 + CR + D \ . \tag{A1}$$

The derivative of Σn_m with respect to R gives the number of bonds between R and $R + \delta R$, that is,

$$\frac{\delta (\sum_m n_m)}{\delta R} \sim \frac{\delta n_{bonds}}{\delta R} \sim 3AR^2 + 2BR + C \ , \tag{A2}$$

or

$$\delta n_{bonds} \sim (3AR^2 + 2BR + C)\delta R \ . \tag{A3}$$

The volume fraction of PEO in the micelle head layer thus becomes [see Eq.(40)]

$$\phi(R) \sim \frac{\frac{V_{EO}}{3}\delta n_{bonds}(R)}{\frac{S v_c (R + l_c)^{S-1} \delta R}{l_c^S}} \sim \frac{\frac{V_{EO}}{3}(3AR^2 + 2BR + C)\delta R}{\frac{S v_c (R + l_c)^{S-1} \delta R}{l_c^S}} \ , \tag{A4}$$

or

$$\phi(R) \sim \frac{\frac{V_{EO}}{3}(3AR^2+2BR+C)l_c^S}{Sv_c(R+l_c)^{S-1}}, \qquad \text{(A5)}$$

where S is a shape factor ($S=2$ for rods, and $S=3$ for spheres). For each PEO head chain bond density distribution, therefore, the coefficients A, B, and C were determined, and Eq.(A5) was used to determine the volume fraction profiles in the micelle head layers composed of E_4, E_6, and E_8 chains. These volume fraction profiles are functions of the curvature of the surface, as shown for $C_{12}E_6$ micelles in Fig.29.

REFERENCES FOR CHAPTER 5

1. For a comprehensive review of micellar solution phase behavior, see (a) Surfactants in Solution, edited by K. L. Mittal and B. Lindman, Plenum Press, New York (1984); and (b) Proceedings of the International School of Physics Enrico Fermi-Physics of Amphiphiles: Micelles, Vesicles and Microemulsions, edited by V. Degiorgio and M. Corti, North-Holland Physics Publishing, The Netherlands (1985).

2. Lang, J. C.; Morgan, R. D. *J. Chem. Phys.* **1980**, *73*, 5849.

3. Clunie, J. S.; Corkill, J. M.; Goodman, J. F.; Symons, P. C.; Tate, J. R. *Trans. Faraday Soc.* **1967**, *63*, 2839.

4. Blankschtein, D.; Thurston, G. M.; Benedek, G. B. *J. Chem. Phys.* **1986**, *85*, 7268.

5. Doren, A.; Goldfarb, J. *J. Colloid Interface Sci.* **1970**, *32*, 67.

6. Weckstrom, K.; Zulauf, M. *J. Chem. Soc., Faraday Trans. I* **1985**, *81*, 2947.

7. (a) Imae, Sasaki, Abe and Ikeda, Langmuir, **4**, 414 (1988);
   (b) Schott, H., J. Colloid and Interface Science, **43**, 150 (1973).

8. Schott, H. Colloids and Surfaces, **11**, 51 (1984).

9. Buchner, E. H., Rec. Trav. Chim., **53**, 288 (1934); Kolloid Z., **75**, 1 (1936).

10. McBain, J. W., Colloid Science, D. C. Heath and Co., Boston (1950).

11. Hofmeister determined that electrolytes had a range of effectiveness in salting out proteins. [Arch. Exptl. Pathol. Pharmakol., 1888, 24, 247].

12. Schott, H., Royce, A. E., and Suk Kyu Han, J. Colloid and Interface Science, **98**, 196 (1984).

13. Holtzscherer, C. and Candau, F., J. Colloid and Interface Science, **125**, 97 (1988).

14. Kjellander, R. *J. Chem. Soc., Faraday Trans. 2* **1982**, *78*, 2025.

15. Huang, Y. X.; Thurston, G. M.; Blankschtein, D.; Benedek, G. B. *J. Chem. Phys.* **1990**, *92*, 1956.

16. Puvvada, S.; Blankschtein, D. *J. Chem. Phys.* **1990**, *92*, 3710.

17. Shinoda, K., Nakagawa, T., Tamamushi, B. and Isemura, T., Colloidal Surfactants, Academic Press, New York (1963).

18. Fujita, H. *Polymer Solutions*, Elsevier: Amsterdam, 1990; p. 287.

19. Schick, M. J., Nonionic Surfactants, (ed. M. J. Schick), Dekker, New York (1966).

20. Blankschtein, D.; Thurston, G. M.; Benedek, G. B. *J. Chem. Phys.* **1986**, *85*, 7268.

21. Corkill, J. M.; Goodman, J. F.; Walker, T.; Wyer, J. *Proc. Royal Soc. A* **1969**, *312*, 243.

22. Hansen, J. P.; McDonald, I. R. Theory of Simple Liquids, Academic Press: New York (1976).

23. Lemaire, B.; Bothorel, P.; Roux, D. *J. Phys. Chem.* **1983**, *87*, 1023;
Brunetti, S.; Roux, D.; Bellocq, A. M.; Fourche, G.; Bothorel, P. *J. Phys. Chem.* **1983**, *87*, 1028.

24. Mahanty, J. and Ninham, B. W., Dispersion Forces, Academic Press, London (1976).

25. Israelachvili, J. N. Intermolecular and Surface Forces, Academic Press, London (1985).

26. Hamaker, H. C., Physica, **4**, 1058 (1937).

27. Parsegian, V. A., in Physical Chemistry: Enriching Topics is Colloid and Surface Science, van Olphen, H. and Mysels, K. J., eds., Theorex, 1975, pp. 27-72.

28. Verwey, E. J.; Overbeek, J. Th. G. Theory of the Stability of Lyophobic Colloids, Elsevier: Amsterdam, 1948.

29. Mahanty, J. and Ninham, B. W., Dispersion Forces, Academic Press, London (1976).

30. Spaarnay, M. J. *Recueil* **1959**, *78*, 680.

31. Graham, N. B.; Zulfiqar, N. E.; Nwachuku, N. E.; Rashid, A. *Polymer*, **1989**, *30*, 528.

32. Bjorling, M.; Karlstrom, G.; Linse, P. *J. Phys. Chem.* **1991**, *95*, 6706.

33. Napper, D. H. Polymeric Stabilization of Colloidal Dispersions, p. 143, Academic Press: London (1983). It is likely that increasing temperature disrupts specific interactions between water and PEO (H-bonds), thereby decreasing the solvency of water for PEO. The evidence for this is far from conclusive, however.

34. Kjellander, R.; Florin, E. *J. Chem. Soc., Faraday Trans. 1* **1981**, *77*, 2053.

35. (a) Boucher, E. A. and Hines, P. M., J. Polymer Science, **14**, 2241 (1976);
(b) Boucher, E. A. and Hines, P. M., J. Polymer Science, Polymer Physics Ed., **16**, 501 (1978).

36. Florin, E., Kjellander, R., and Eriksson, J. C., J. Chem. Soc., Faraday Trans. 1, **80**, 2889 (1984).

37. Saeki, S.; Kuwahara, N.; Nakata, M.; Kaneko, M. *Polymer*, **1976**, *17*, 685.

38. Flory, P. J. Principles of Polymer Chemistry, Cornell University Press: Ithaca, 1953.

39. Mitchell, D. J.; Tiddy, G. J. T.; Waring, L.; Bostock, T.; McDonald, M. P. *J. Chem. Soc., Faraday Trans. 1* **1983**, *79*, 975.

40. Claesson, P. M., Kjellander, R., Stenius, P. and Christenson, H. K., J. Chem. Soc., Faraday Trans. 1, **82**, 2735 (1986).

41. The technique was developed by Israelachvili, J. N. (in J. Chem. Soc. Faraday Trans. 1, **74**, 975, (1978) with G. E. Adams; and in J. Colloid Interface Science, **44**, 259 (1973).)

42. Napper, D. H. Polymeric Stabilization of Colloidal Dispersions, p. 218, Academic Press: London (1983).

43. Sarmoria, C.; Blankschtein, D. *J. Phys. Chem.* **1992**, *96*, 1978.

44. Aveyard, R.; Saleem, S. M.; Heselden, R. *J. Chem. Soc., Faraday Trans. 1* **1977**, *73*, 84.

45. Florin, E.; Kjellander, R.; Eriksson, J. C. *J. Chem. Soc., Faraday Trans. 1* **1984**, *80*, 2889.

46. Napper, D. H. Polymeric Stabilization of Colloidal Dispersions, p. 125, Academic Press: London (1983).

47. Napper, D. H. Polymeric Stabilization of Colloidal Dispersions, p. 125, Academic Press: London (1983).

48. Jeon, S. I.; Lee, J. H.; Andrade, J. D.; de Gennes, P. G. *J. Colloid Interface Sci.* **1991**, *142*, 149.

49. Zaslavsky, B. Y.; Miheeva, L. M.; Rodnikova, M. N.; Spivak, G. V.; Harkin, V. S.; Mahmudov, A. U. *J. Chem. Soc., Faraday Trans. 1* **1989**, *85*, 2857.

50. Boucher, E. A.; Hines, P. M. *J. Polym. Sci.* **1978**, *16*, 501.
Ataman, M.; Boucher, E. A. *J. Polym. Sci.* **1982**, *20*, 1585.

51. Gregory, P.; Huglin, M. B. *Makromol. Chem.* **1986**, *187*, 1745.

Table I. Zero-frequency Hamaker constant, A_0, as a function of temperature, where ϵ_{H2O} and ϵ_{C12H26} are the static dielectric constants of water and dodecane, respectively.

Temperature (°C)	ϵ_{H2O}	ϵ_{C12H26}	A_0 (kT)	A_0 x 10^{14} (erg)
20	80.362	2.015	0.713	2.7
25	78.540	2.009	0.713	2.8
30	76.765	2.003	0.712	2.8
35	75.035	1.997	0.711	2.9
40	73.348	1.991	0.710	2.9
45	71.704	1.985	0.710	2.9
50	70.099	1.979	0.709	3.0
55	68.533	1.973	0.708	3.0
60	67.003	1.967	0.707	3.1
65	65.509	1.961	0.706	3.1
70	64.049	1.955	0.706	3.1
75	62.620	1.949	0.705	3.2

Table II. Value of the mean-field interaction parameter, $(\gamma C/kT)_c$, at the critical point (T_c, X_c) for $C_{12}E_6$ in various aqueous salt solutions.

Solvent	T_c (°C)	X_c ($x10^{-3}$)	$(\gamma C/kT)_c$
no salt	51.14	.633	1.08
1m NaCl	39.29	.680	1.09
2m NaCl	30.27	.687	1.09
3m NaCl	23.39	.626	1.08
1m LiCl	43.61	.667	1.08
2m LiCl	39.24	.651	1.08
3m LiCl	36.61	.593	1.08
1m KCl	39.84	.666	1.08
2m KCl	32.09	.627	1.08
3m KCl	26.09	.540	1.06
1m KBr	47.15	.640	1.08
2m KBr	43.38	.658	1.08
3m KBr	41.24	.638	1.08
1m KI	59.75	.976	1.13
2m KI	63.11	1.14	1.15
3m KI	64.75	1.39	1.18

Table III. Contribution of attractive van der Waals interactions between spherical hydrocarbon cores to the mean-field interaction parameter, $(\gamma C/kT)_c$, for $C_{12}E_4$, $C_{12}E_6$, and $C_{12}E_8$.

	$C_{12}E_4$	$C_{12}E_6$	$C_{12}E_8$
$2l_c+1.9l_{hl}$	.009	.007	.005
$2l_c+1.8l_{hl}$	.010	.008	.005
$2l_c+1.7l_{hl}$	.010	.009	.006
$2l_c+1.6l_{hl}$	.011	.009	.007
$2l_c+1.5l_{hl}$	.013	.011	.007
$2l_c+1.4l_{hl}$	.014	.012	.008
$2l_c+1.3l_{hl}$	.016	.013	.010
$2l_c+1.2l_{hl}$	.018	.015	.011
$2l_c+1.1l_{hl}$	.020	.017	.012
$2l_c+l_{hl}$	.023	.019	.014

Table IV. Contribution of attractive van der Waals interactions between the hydrocarbon cores of crossed-rodlike micelles to the mean-field interaction parameter, $(\gamma C/kT)_c$, for $C_{12}E_4$, $C_{12}E_6$, and $C_{12}E_8$.

	$C_{12}E_4$	$C_{12}E_6$	$C_{12}E_8$
$2l_c+1.9l_{hl}$	.0024	.0021	.0017
$2l_c+1.8l_{hl}$	.0026	.0023	.0018
$2l_c+1.7l_{hl}$	.0028	.0024	.0019
$2l_c+1.6l_{hl}$	.0029	.0026	.0021
$2l_c+1.5l_{hl}$	.0031	.0028	.0022
$2l_c+1.4l_{hl}$	.0034	.0030	.0023
$2l_c+1.3l_{hl}$	.0036	.0032	.0026
$2l_c+1.2l_{hl}$	.0038	.0036	.0028
$2l_c+1.1l_{hl}$	.0043	.0038	.0031
$2l_c+l_{hl}$	.0046	.0041	.0034

Table V. Contribution of attractive van der Waals interactions between the hydrocarbon cores of parallel-rodlike micelles to the mean-field interaction parameter, $(\gamma C/kT)_c$, for $C_{12}E_4$, $C_{12}E_6$, and $C_{12}E_8$.

	$C_{12}E_4$	$C_{12}E_6$	$C_{12}E_8$
$2l_c+1.9l_{hl}$	.026	.023	.020
$2l_c+1.8l_{hl}$	.027	.024	.021
$2l_c+1.7l_{hl}$	.028	.026	.022
$2l_c+1.6l_{hl}$	.030	.027	.023
$2l_c+1.5l_{hl}$	.031	.028	.024
$2l_c+1.4l_{hl}$	.033	.030	.025
$2l_c+1.3l_{hl}$	.035	.032	.027
$2l_c+1.2l_{hl}$	.037	.034	.029
$2l_c+1.1l_{hl}$	.039	.036	.031
$2l_c+l_{hl}$	.042	.038	.033

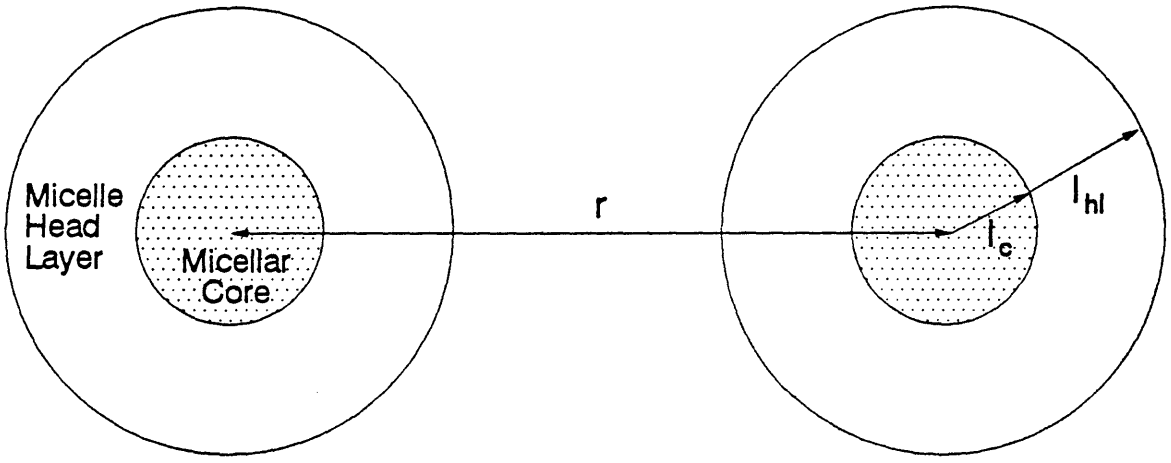

Figure 1. Interacting spherical micelles separated by a distance, r between their centers, where l_c is the micellar core-minor radius, and l_{hl} is the thickness of the micelle head layer.

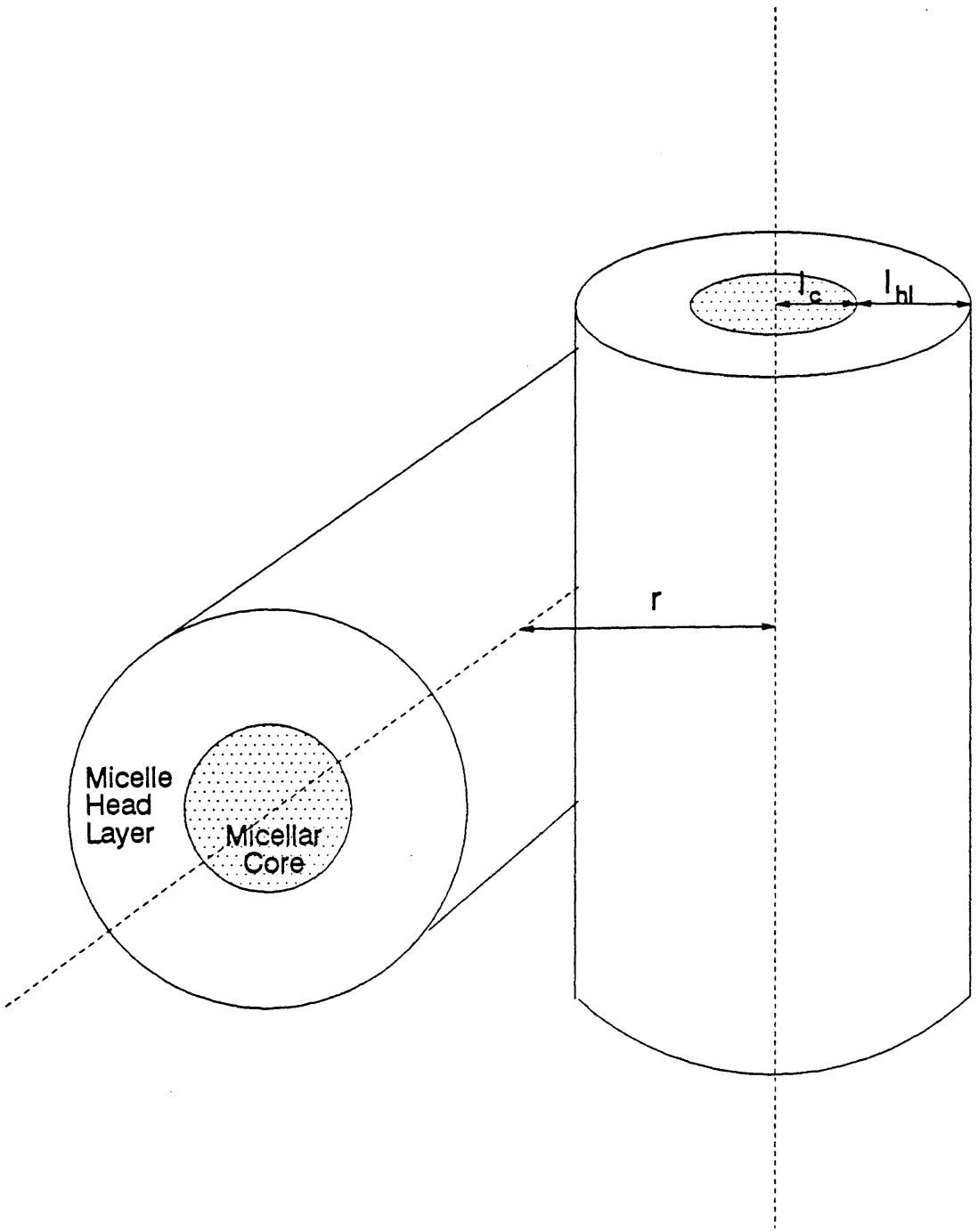

Figure 2. Interacting crossed rodlike micelles separated by a distance, r between their axes, where $l_c(=a)$ is the micellar core-minor radius, and l_{hl} is the thickness of the micelle head layer.

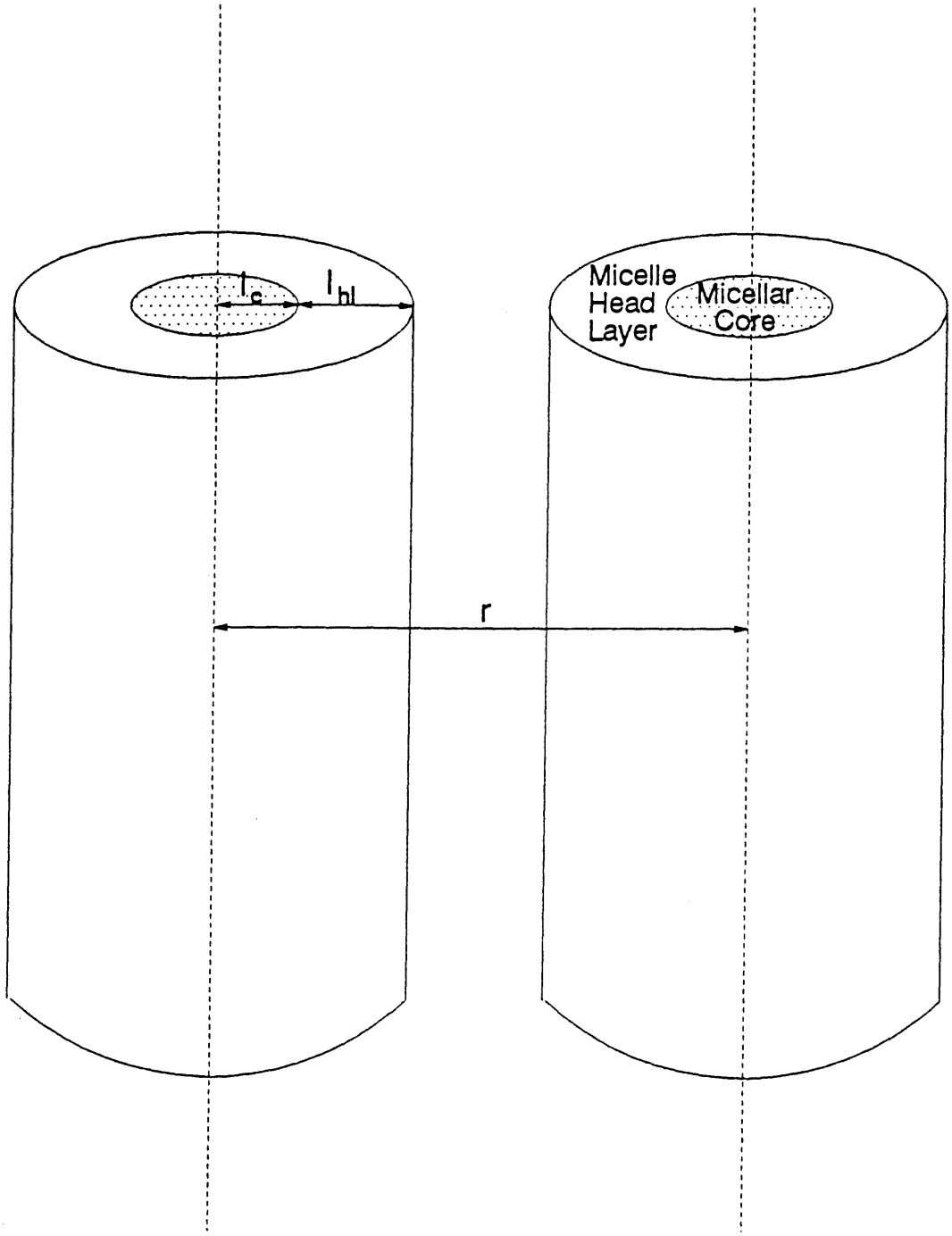

Figure 3. Interacting parallel rodlike micelles separated by a distance, r between their axes, where $l_c(=a)$ is the micellar core-minor radius, and l_{hl} is the thickness of the micelle head layer.

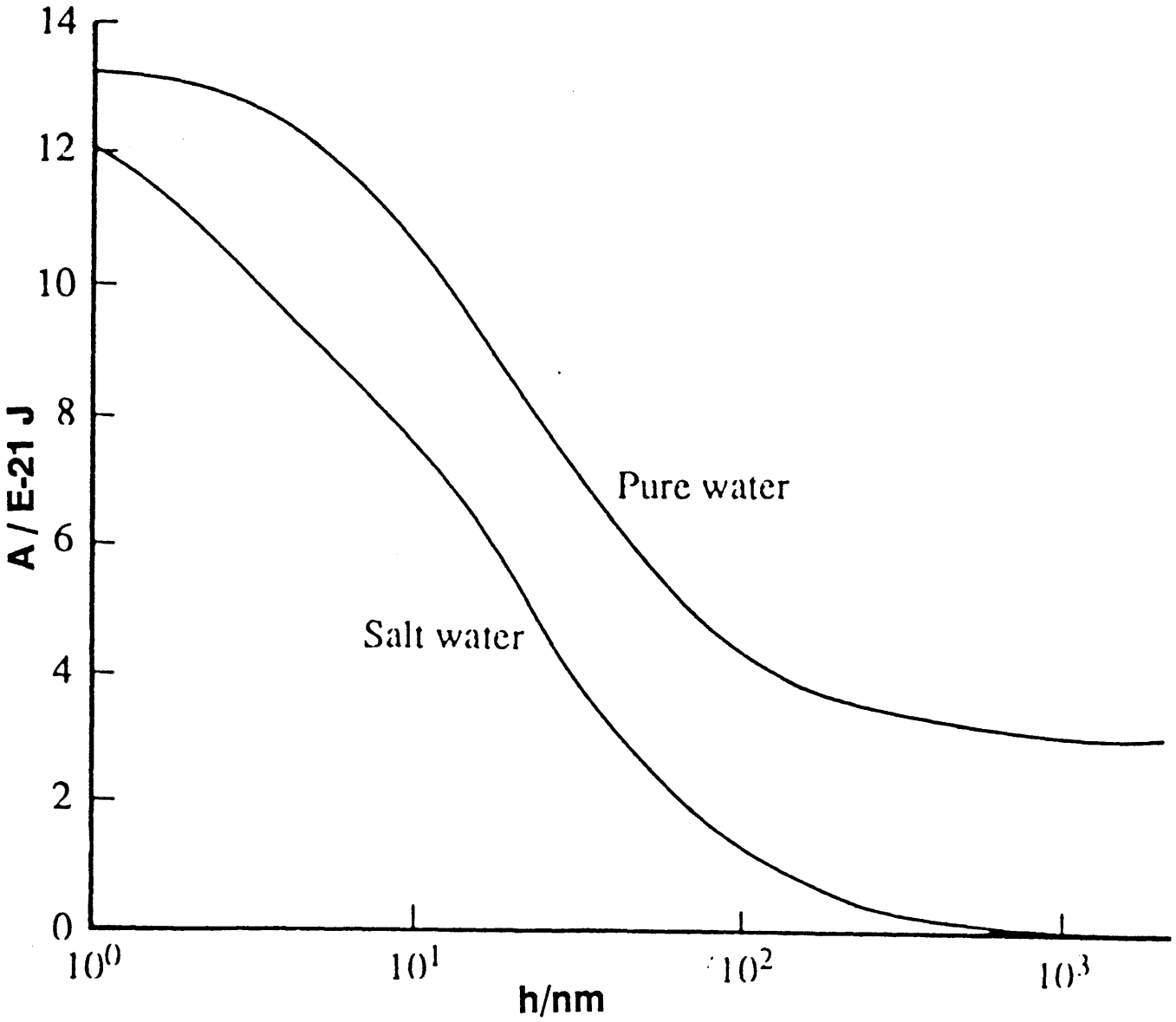

Figure 4. Calculated Hamaker constant, A, for PST spheres across pure and salt water [from Ref.27].

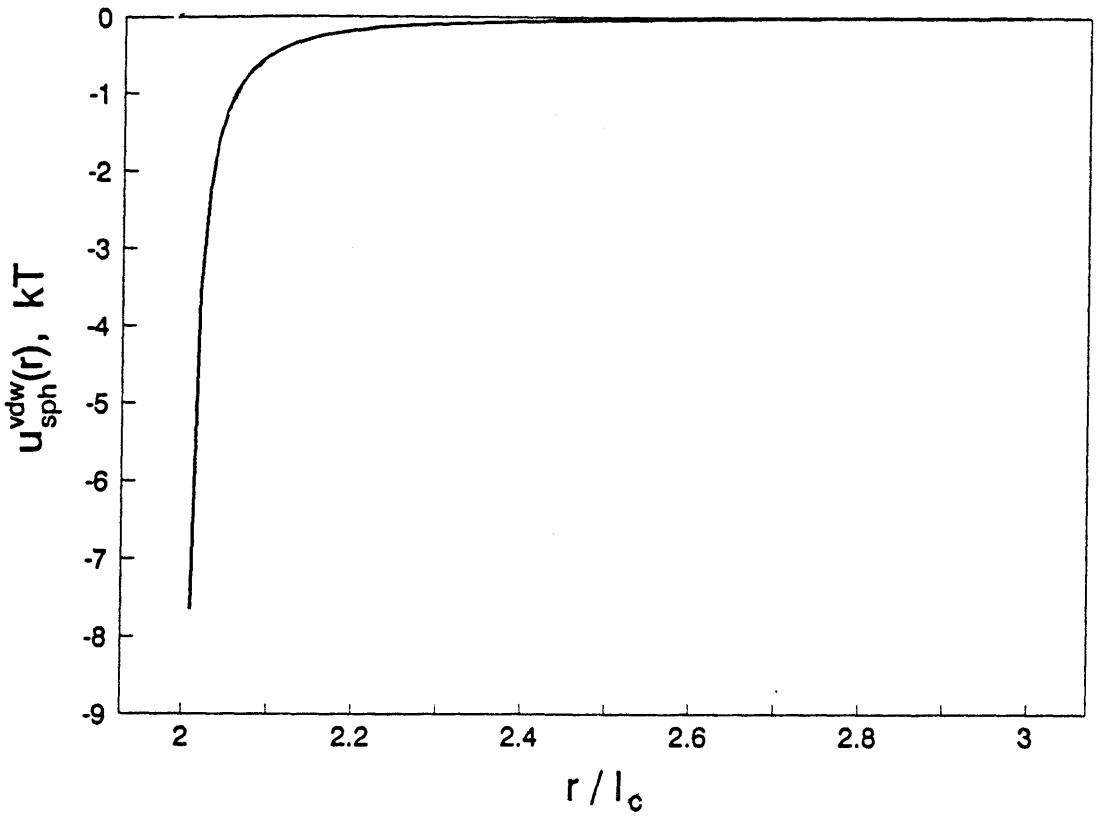

Figure 5. Van der Waals potential, $u^{vdw}_{sph}(r)$, in kT, given in Eq. 20, as a function of the normalized distance between two spherical micellar cores, r/a, where r is the center-to-center distance between them, and $a=l_c$ is the micellar-core radius.

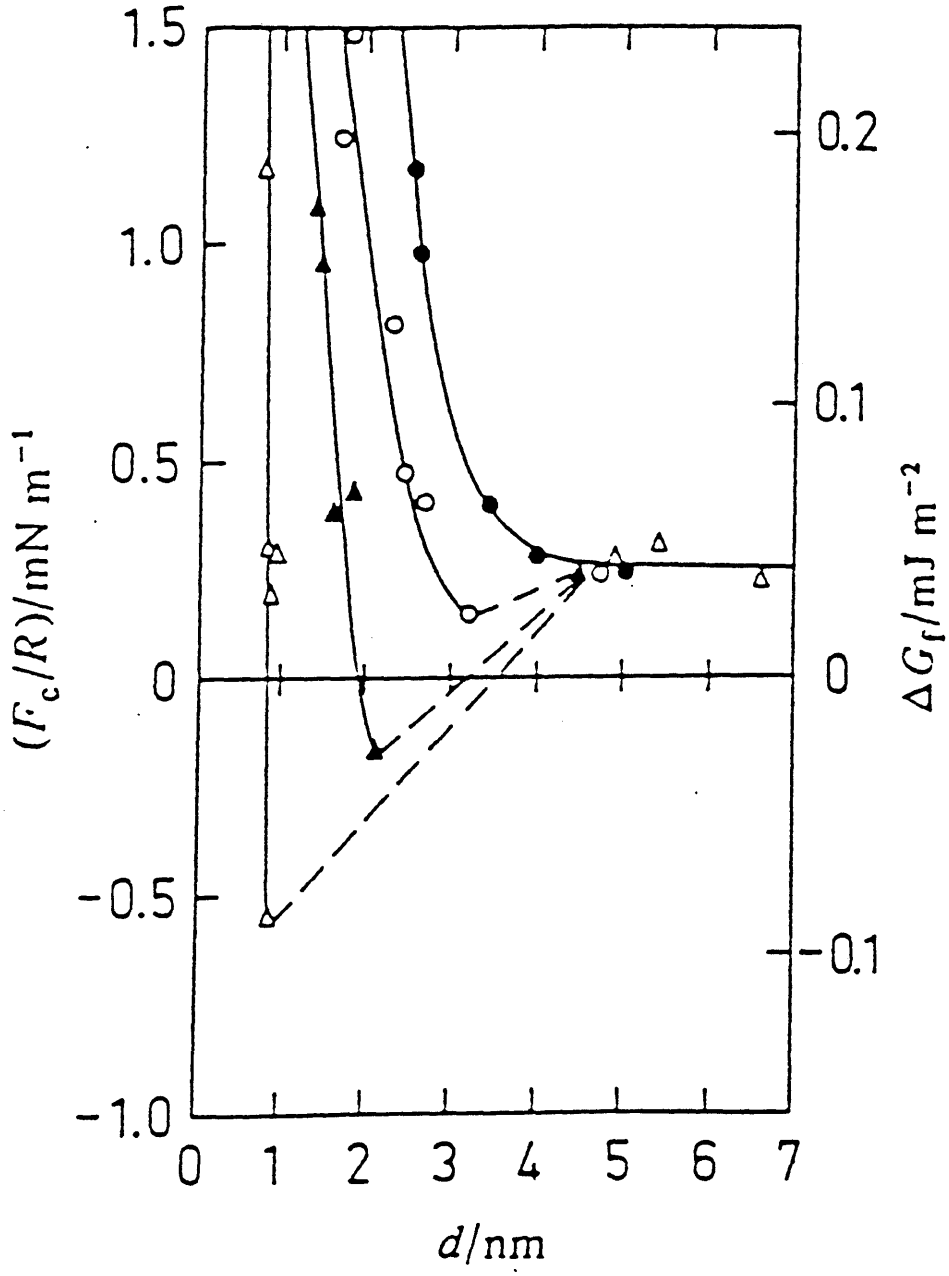

Figure 6. Measured force between $C_{12}E_5$-coated mica surfaces as a function of the distance between the surfaces for T = 15°C (●), 20°C (○), 30°C (▲), and 37°C (△) [from Ref.39].

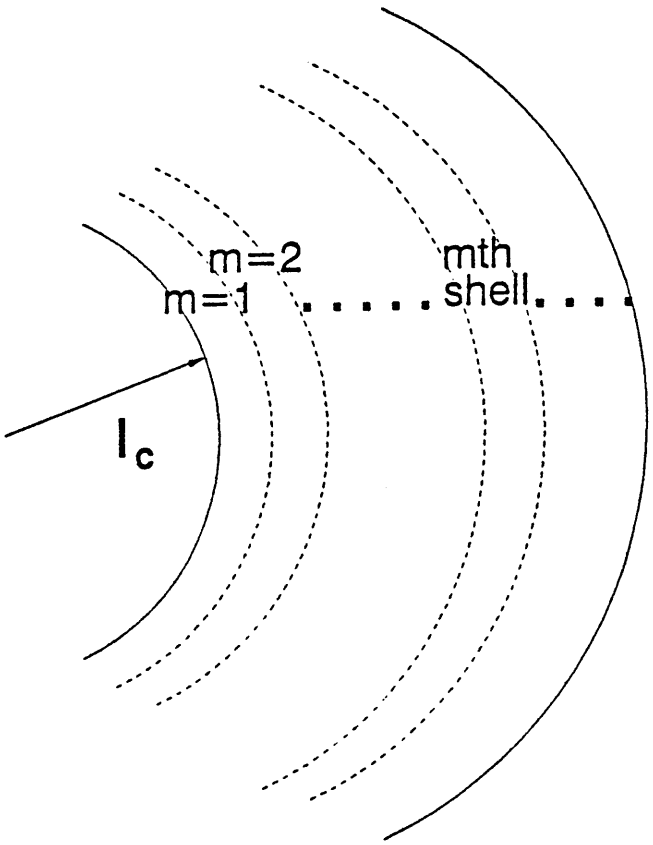

Figure 7. Division of the micelle head layer into concentric shells having 0.5Å thickness, where m is the shell number away from the micellar core surface.

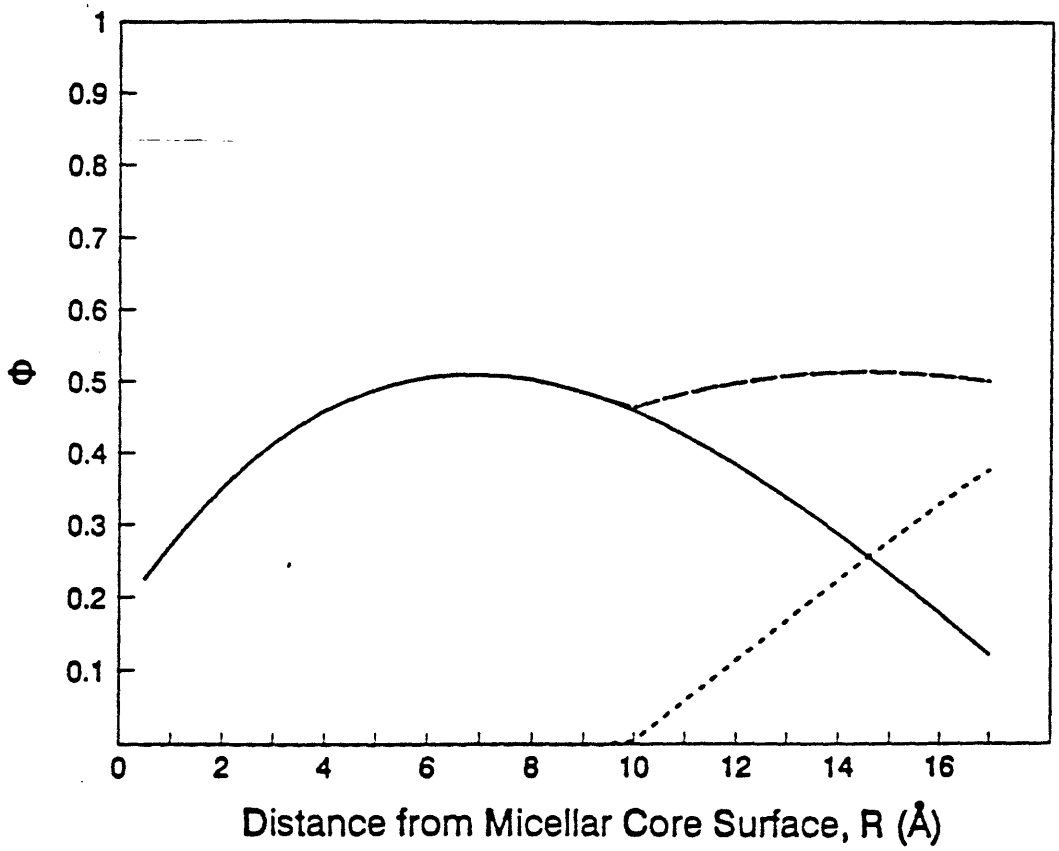

Figure 8. Volume fraction of PEO in the micelle head layer as a function of the distance from the micellar-core surface for: one micelle head layer before overlap, $\phi_1(R)$, (——), a second micelle head layer before overlap, $\phi_2(r\text{-}2l_c\text{-}R)$, (• • • •), and after the overlap of the two micelle head layers, $\phi_f(R)$, (– – –), where the distance between the micelle core surfaces, $r = 50$Å and $l_c = 15.41$Å.

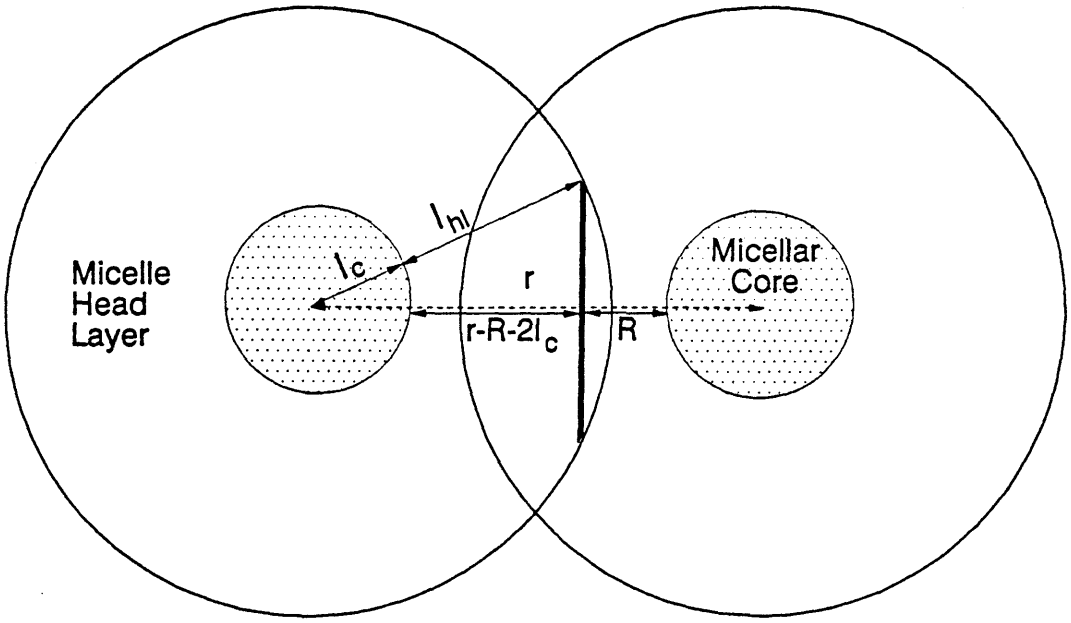

Figure 9. Cross-section of two interpenetrating parallel rodlike micelles, where the differential overlap volume, $\delta V_{ov}(r,R)$, depicted by the dark strip, is a function of the distance between the micelles, r, the distance from the micelle core surface, R, the micellar core-minor radius, l_c, the thickness of the micelle head layer, l_{hl}, and the persistence length, ξ.

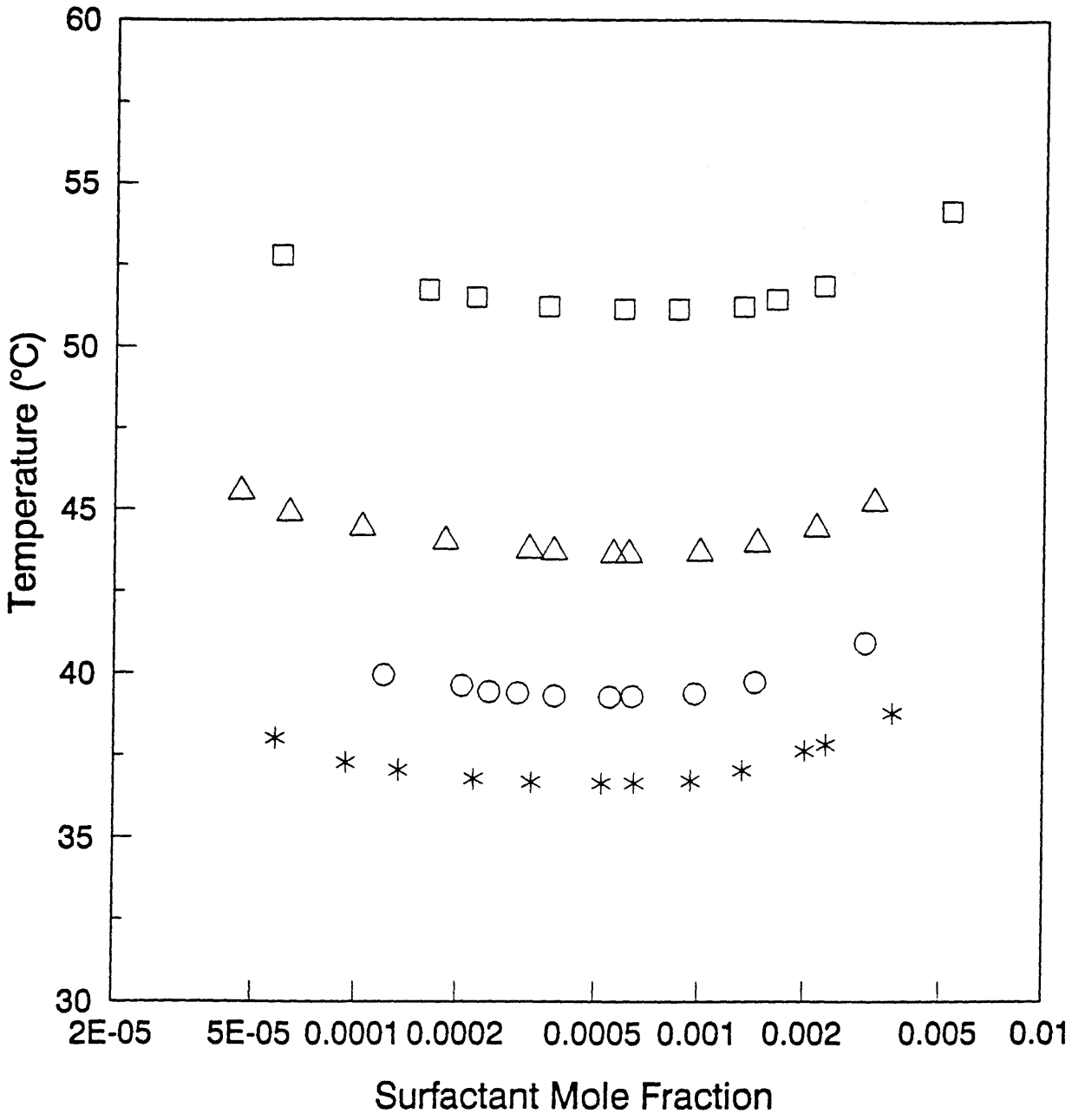

Figure 10. Measured cloud-point temperatures as a function of surfactant mole fraction for $C_{12}E_6$ in H_2O (□), 1m LiCl (△), 2m LiCl (○), and 3m LiCl (*).

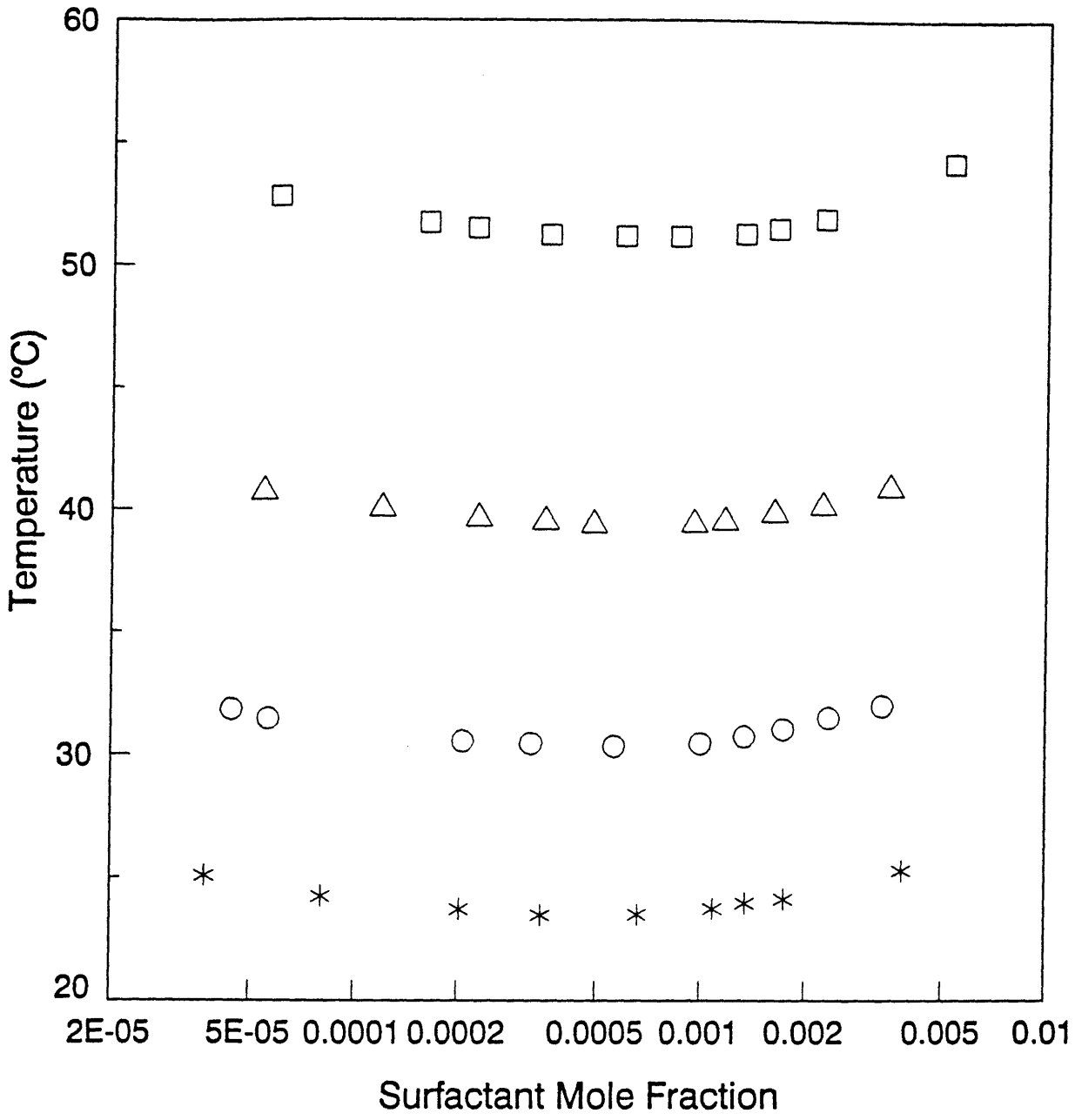

Figure 11. Measured cloud-point temperatures as a function of surfactant mole fraction for $C_{12}E_6$ in H_2O (□), 1m NaCl (△), 2m NaCl (○), and 3m NaCl (*).

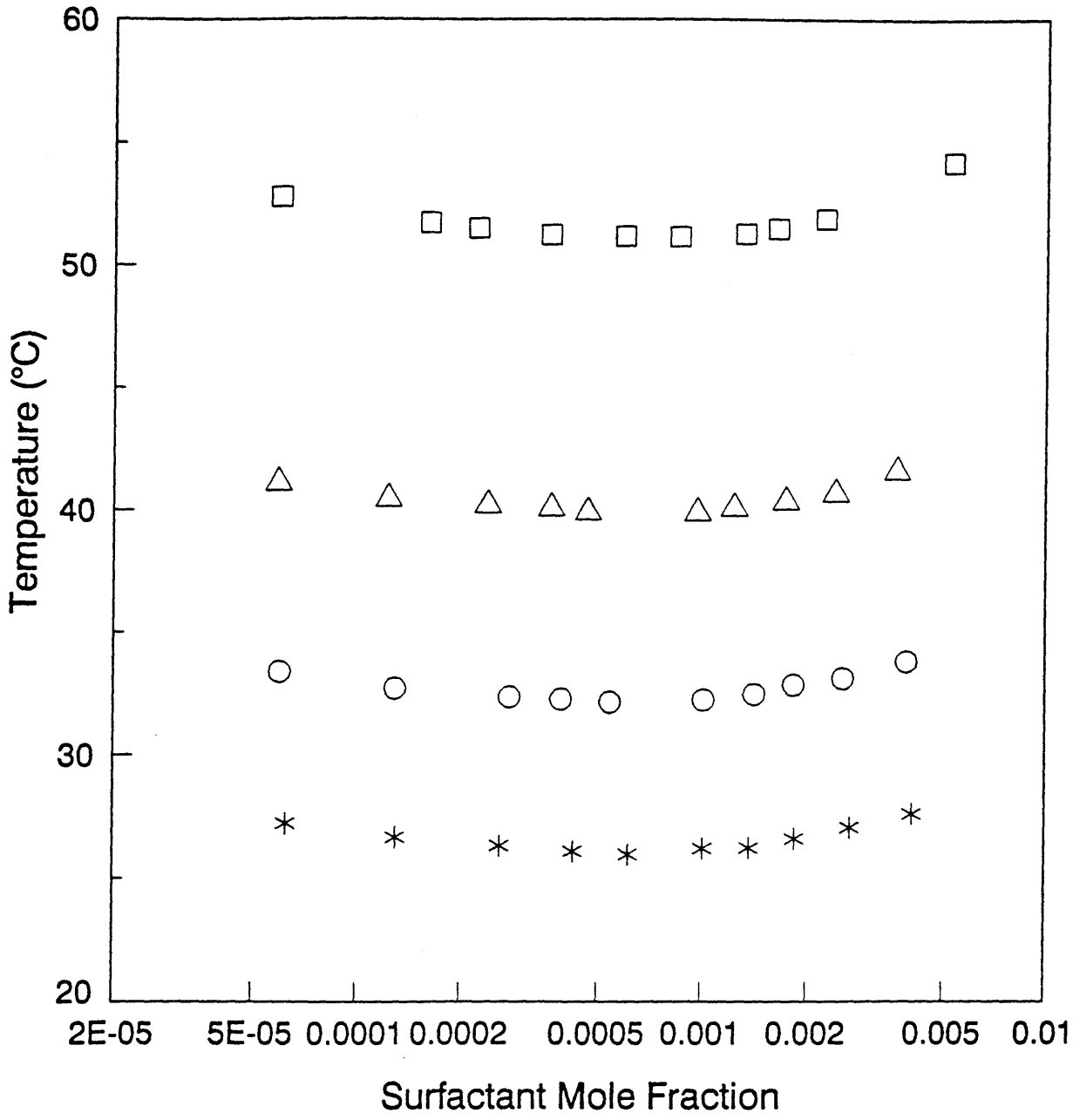

Figure 12. Measured cloud-point temperatures as a function of surfactant mole fraction for $C_{12}E_6$ in H_2O (□), 1m KCl (△), 2m KCl (○), and 3m KCl (*).

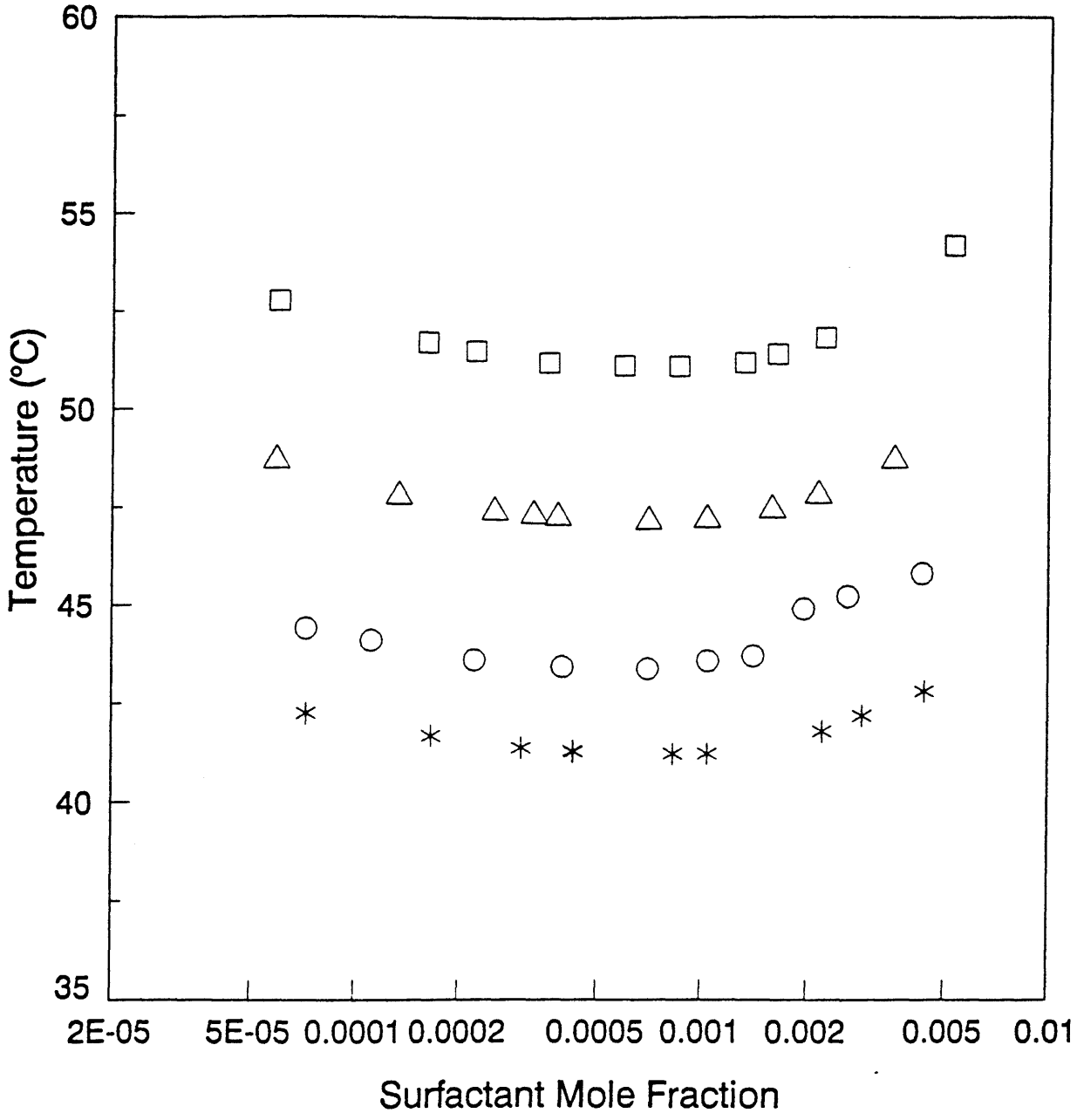

Figure 13. Measured cloud-point temperatures as a function of surfactant mole fraction for $C_{12}E_6$ in H_2O (□), 1m KBr (△), 2m KBr (○), and 3m KBr (*).

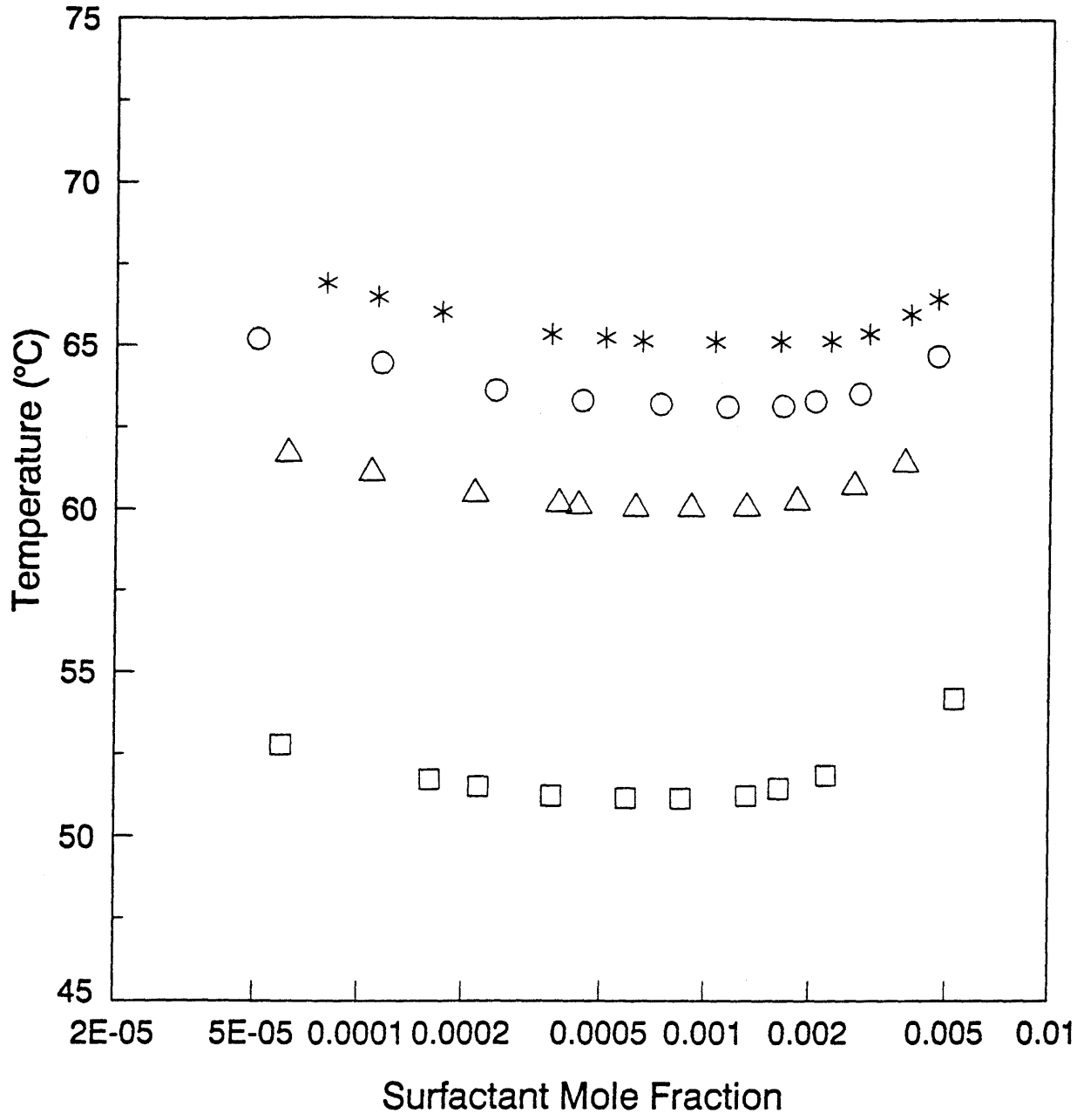

Figure 14. Measured cloud-point temperatures as a function of surfactant mole fraction for $C_{12}E_6$ in H_2O (□), 1m KI (△), 2m KI (○), and 3m KI (*).

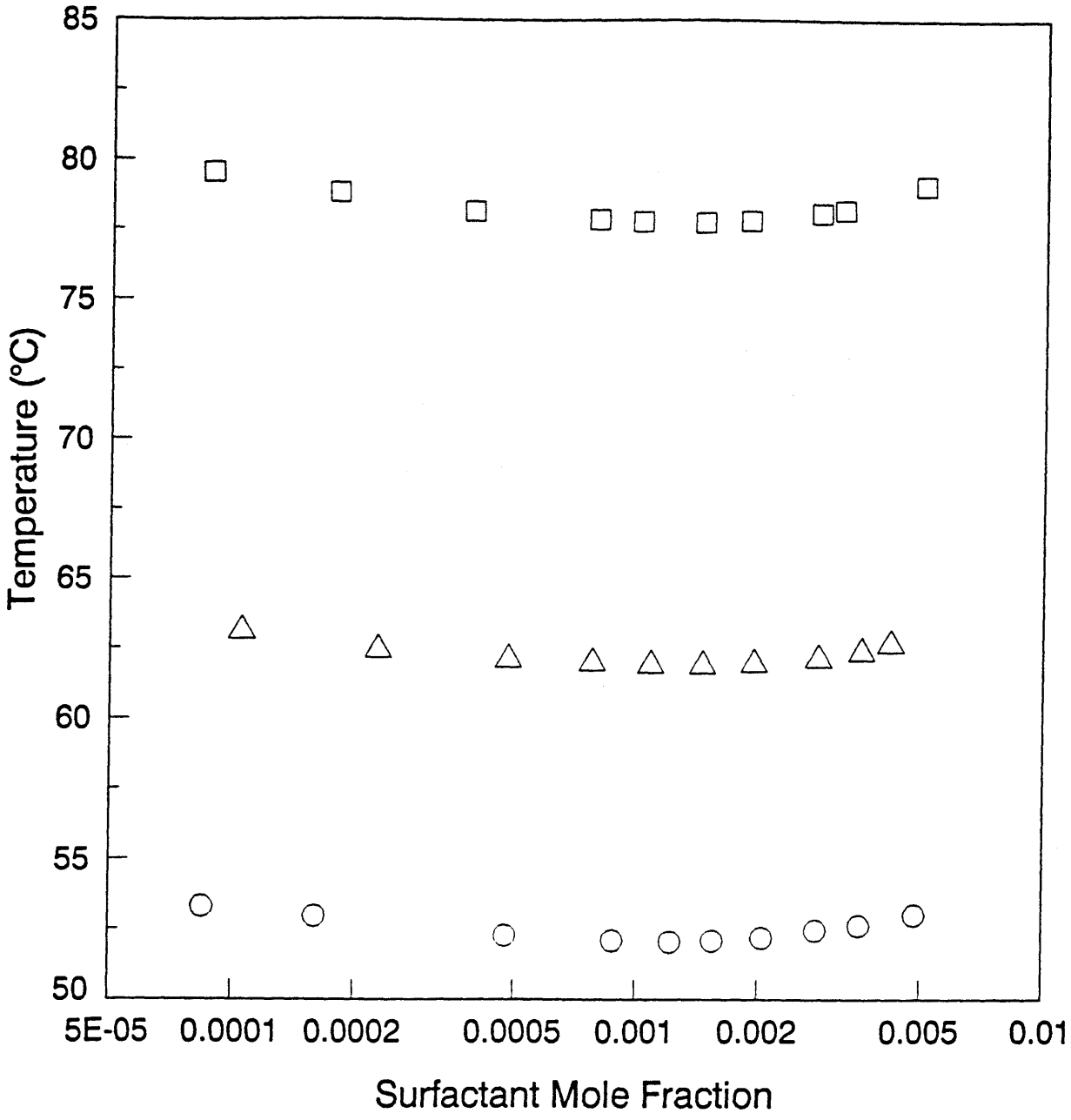

Figure 15. Measured cloud-point temperatures as a function of surfactant mole fraction for $C_{12}E_8$ in H_2O (□), 1m KCl (△), and 2m KCl (○).

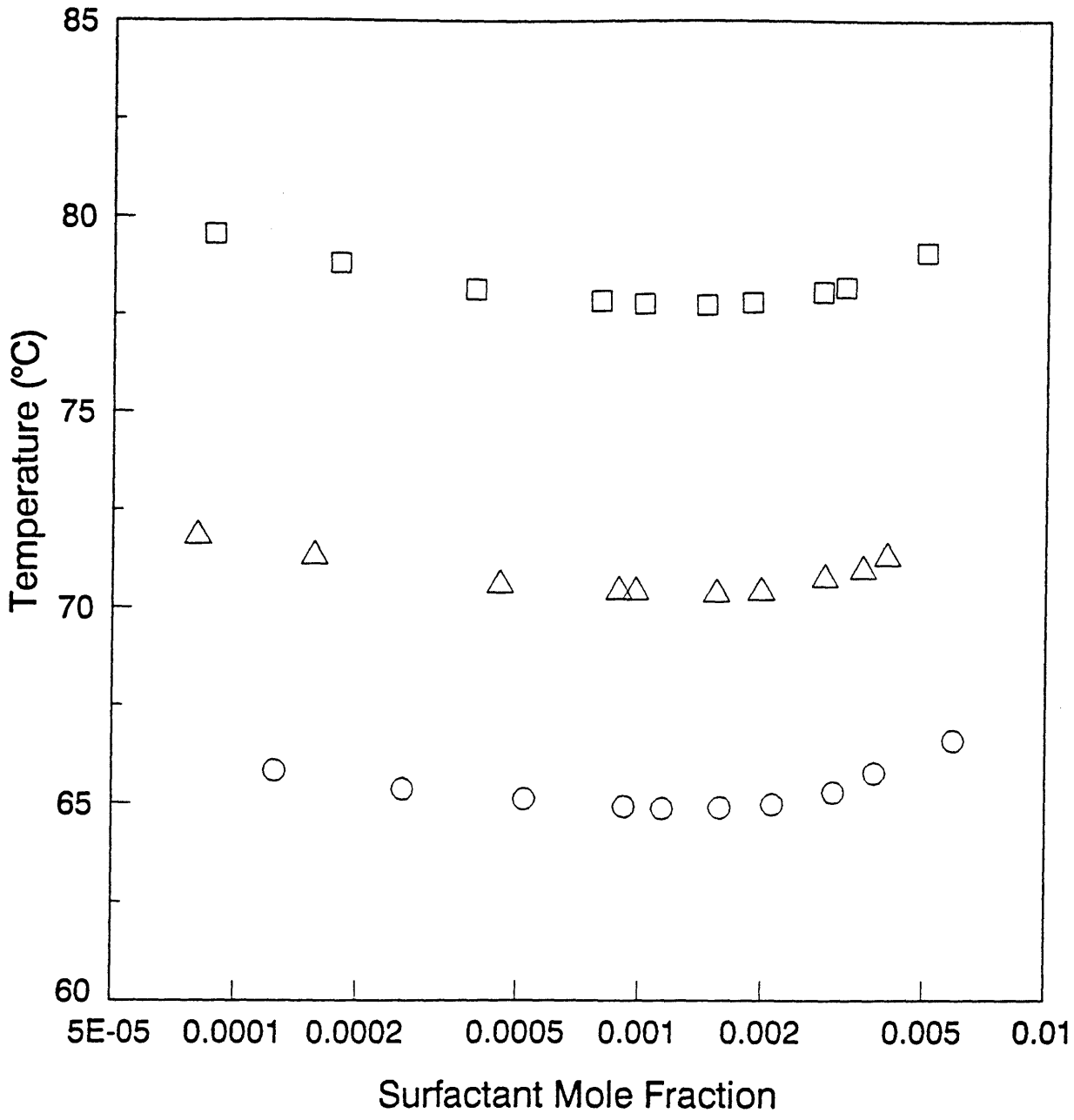

Figure 16. Measured cloud-point temperatures as a function of surfactant mole fraction for $C_{12}E_8$ in H_2O (□), 1m KBr (△), and 2m KBr (○).

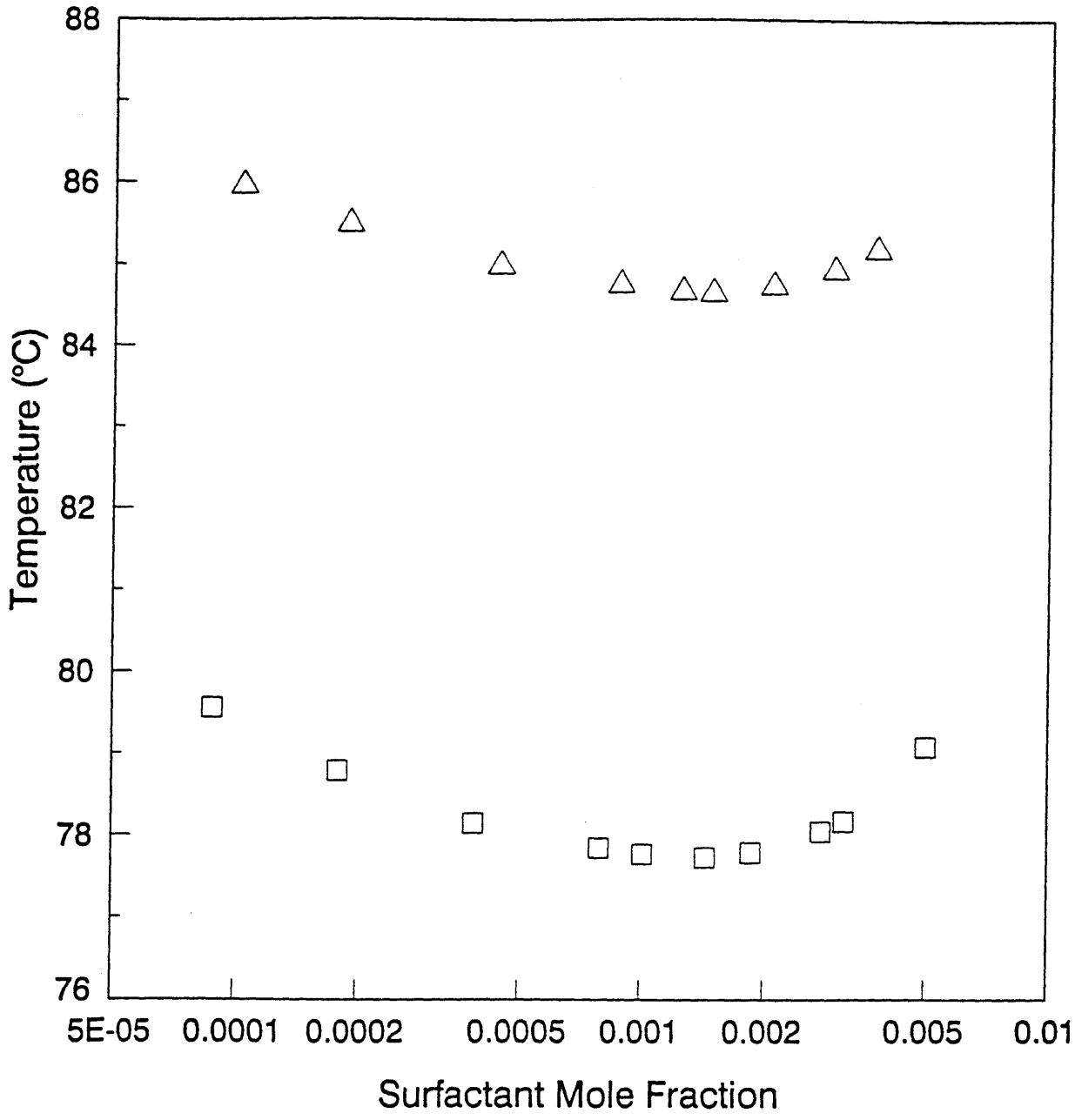

Figure 17. Measured cloud-point temperatures as a function of surfactant mole fraction for $C_{12}E_8$ in H_2O (□) and 1m KI (△). Note that the 2m KI solutions were oxidized upon the addition of $C_{12}E_8$.

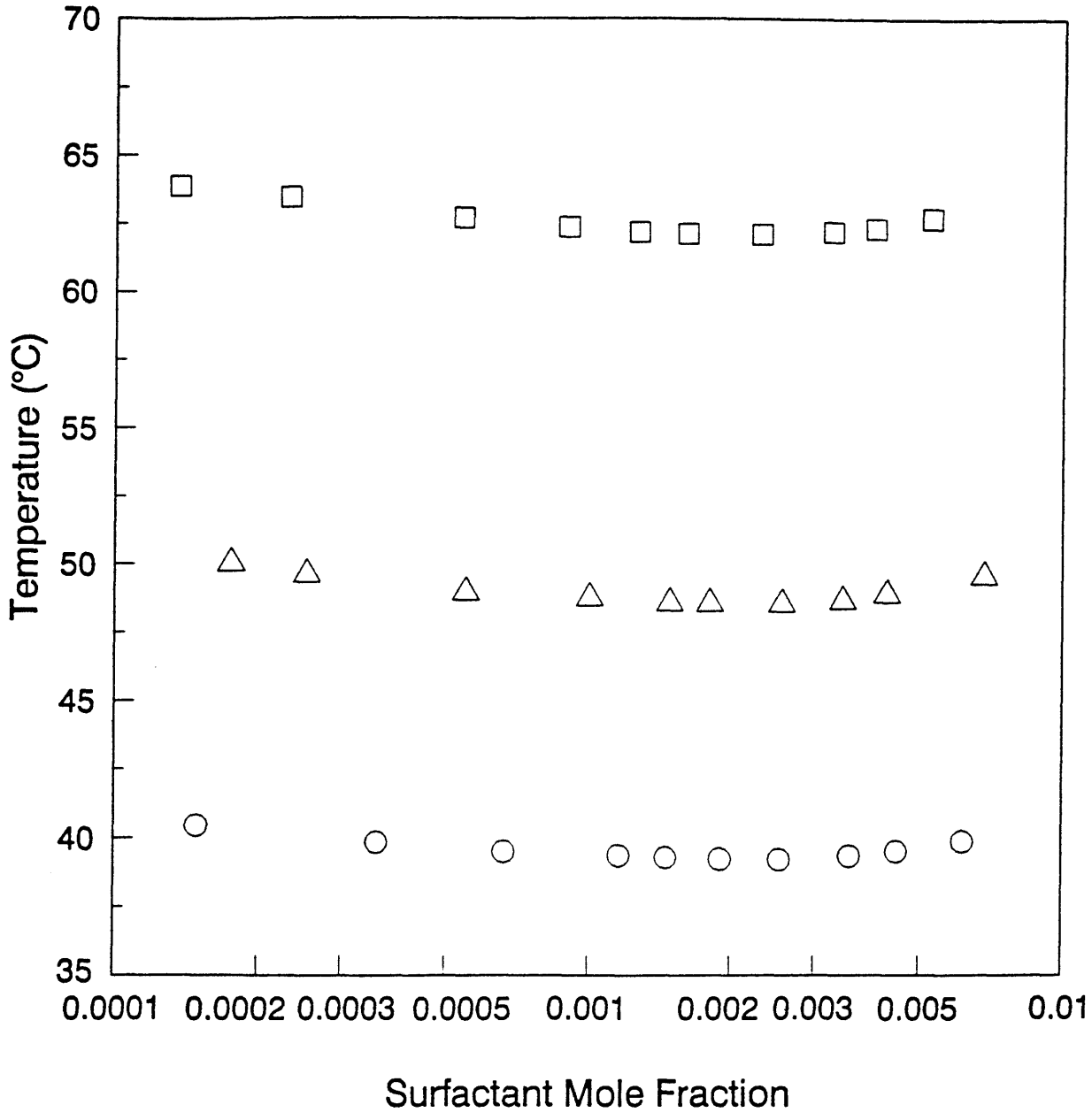

Figure 18. Measured cloud-point temperatures as a function of surfactant mole fraction for $C_{10}E_6$ in H_2O (□), 1m KCl (△), and 2m KCl (○).

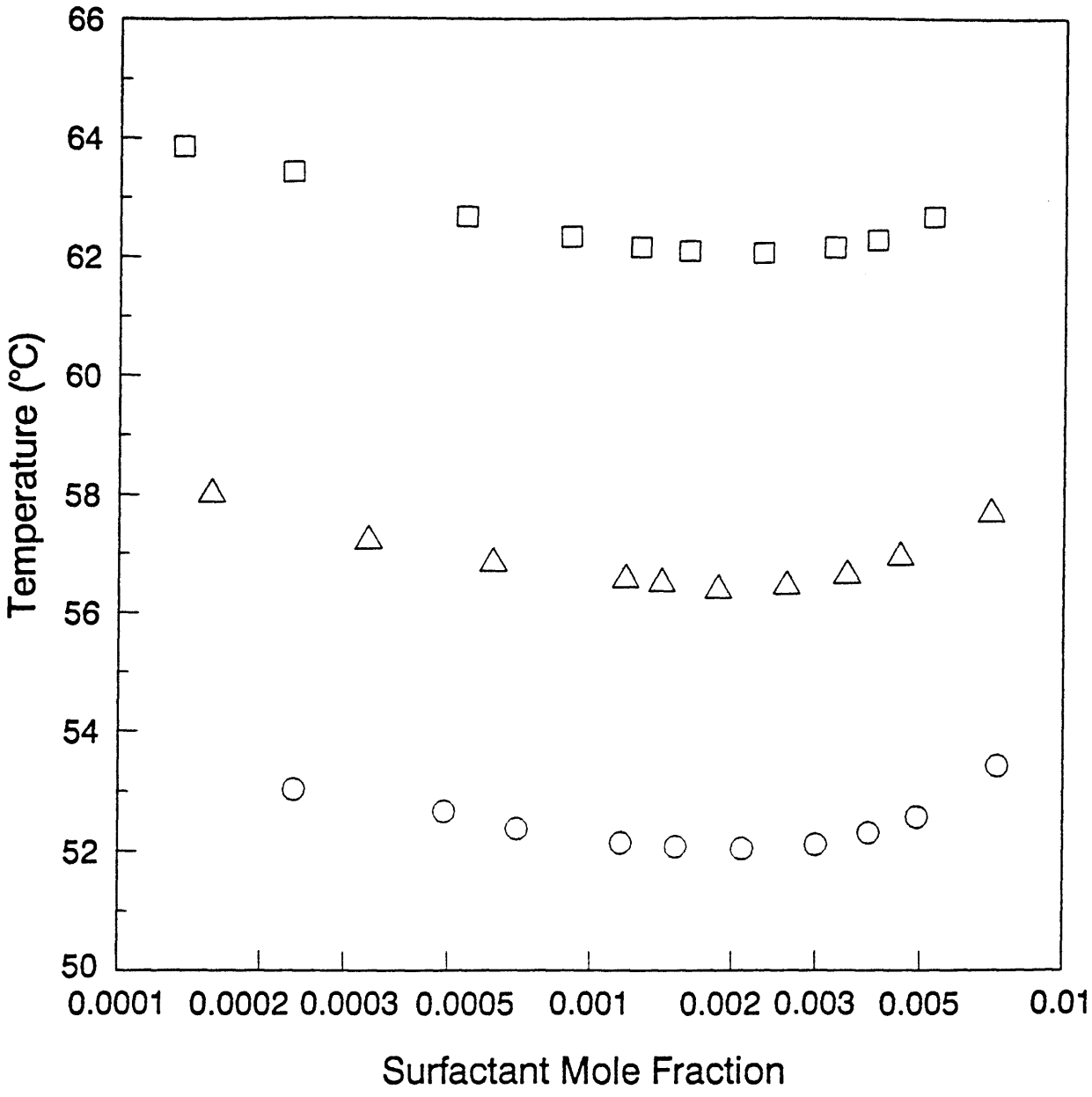

Figure 19. Measured cloud-point temperatures as a function of surfactant mole fraction for $C_{10}E_6$ in H_2O (□), 1m KBr (△), and 2m KBr (○).

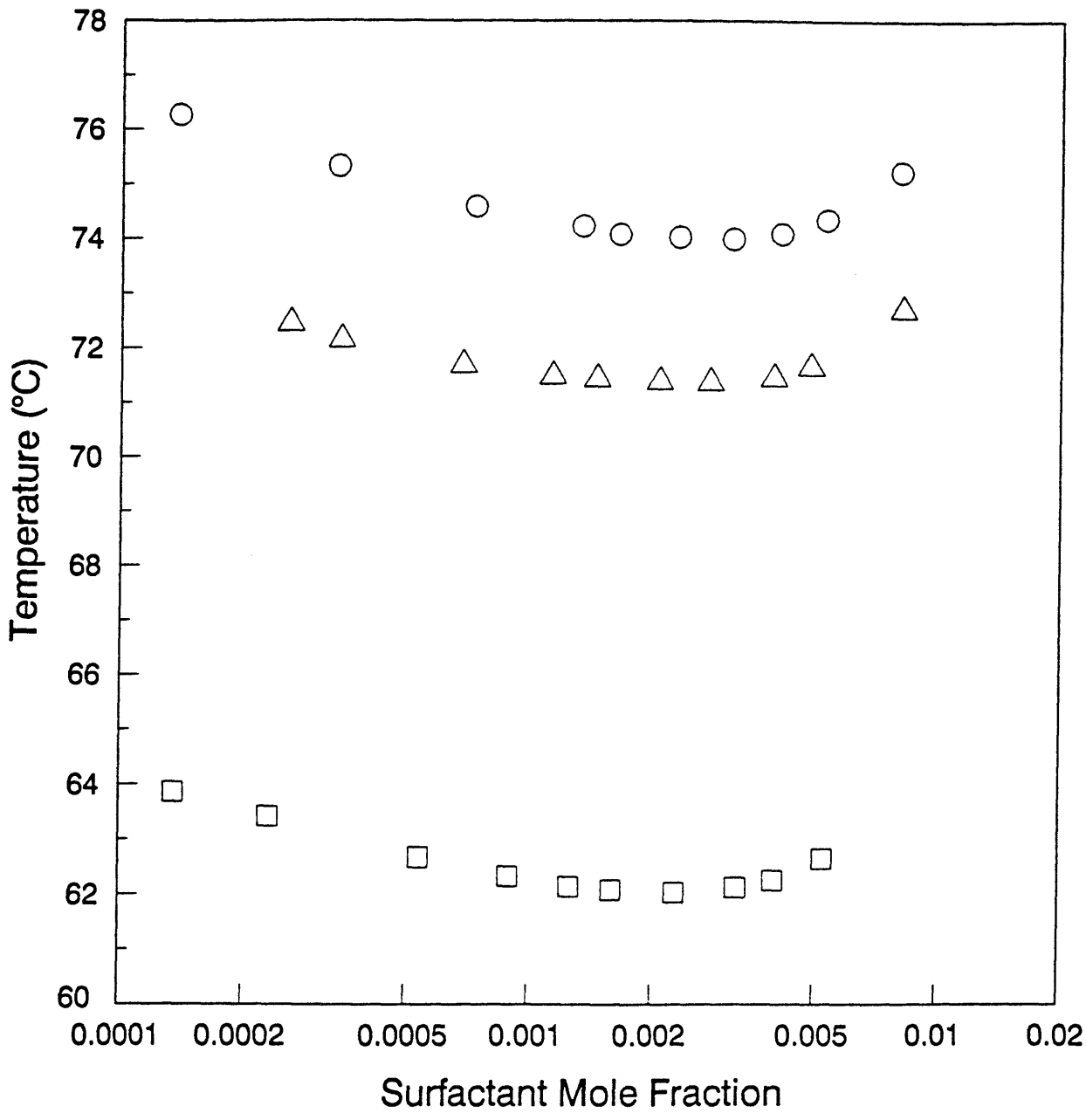

Figure 20. Measured cloud-point temperatures as a function of surfactant mole fraction for $C_{10}E_6$ in H_2O (□), 1m KI (△), and 2m KI (○).

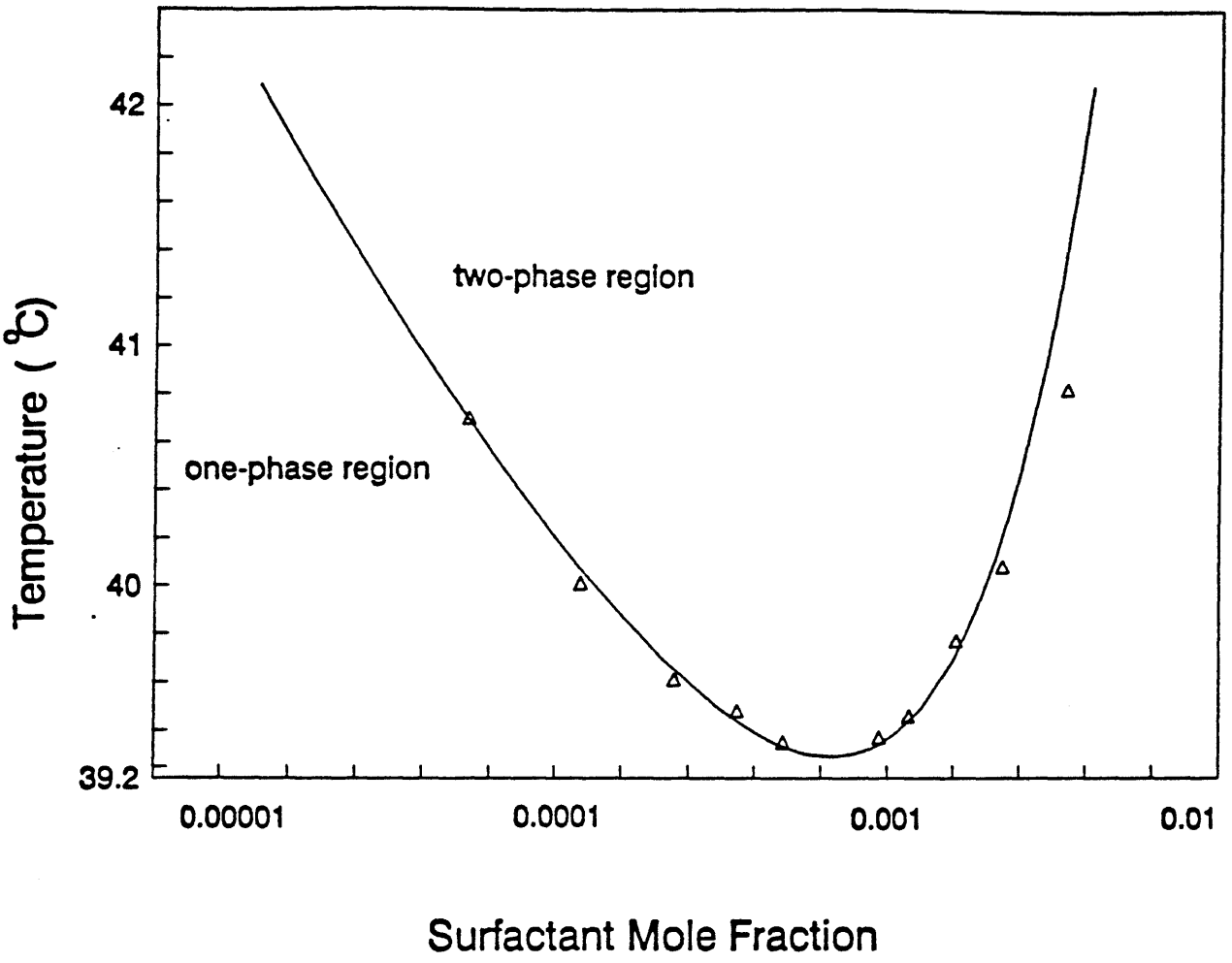

Figure 21. Cloud-point temperatures as a function of surfactant mole fraction for $C_{12}E_6$ in 1m NaCl (△). The solid line is the predicted coexistence curve, using $(\gamma C/kT)_c = 1.09$ and $d(\gamma C/k)_c/dT = 16$.

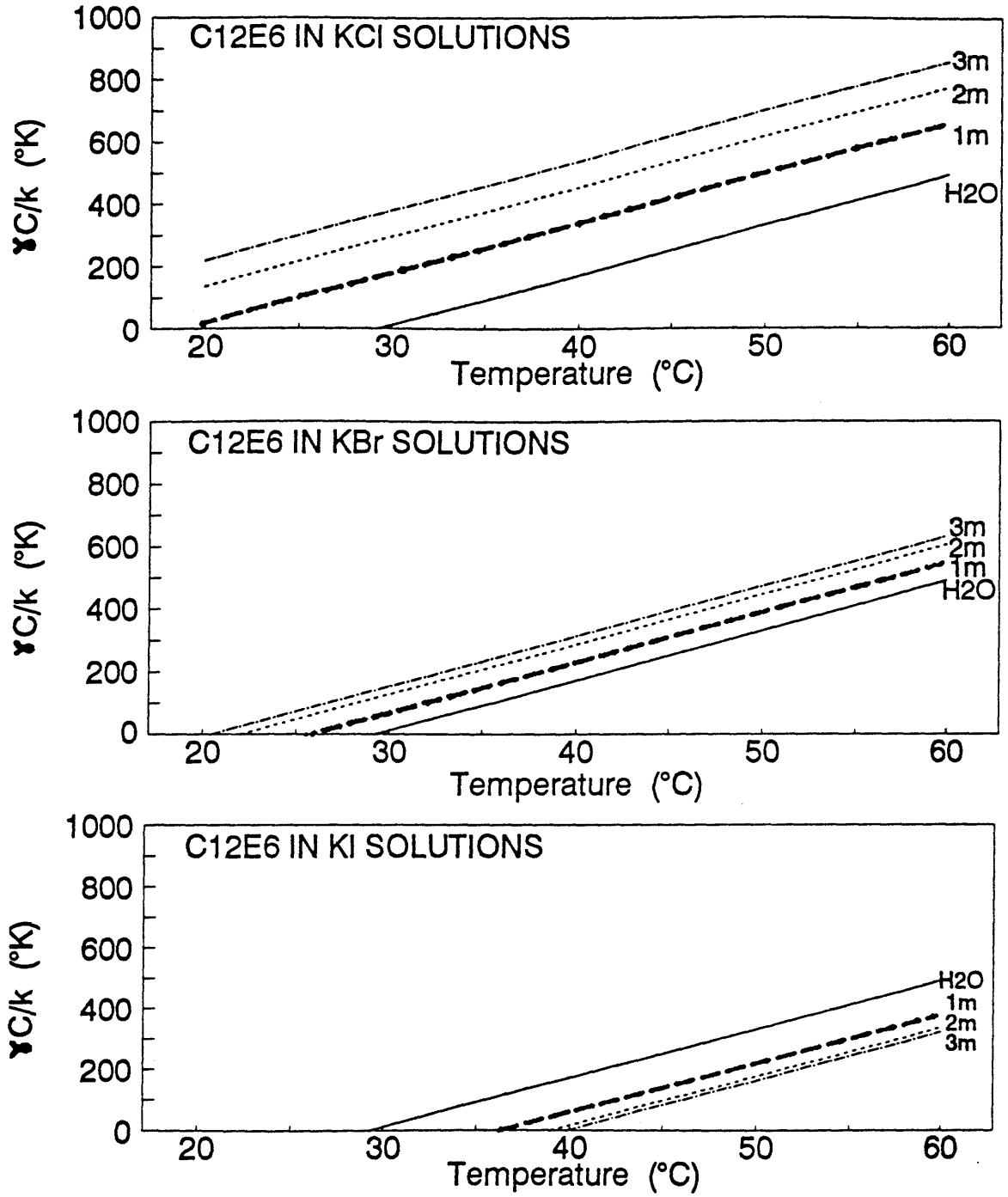

Figure 22. Normalized mean-field interaction parameter, $\gamma C/k$, determined from the experimentally measured cloud-point curves, as a function of temperature, for $C_{12}E_6$ in pure water (——), and in (a) KCl, (b) KBr, and (c) KI solutions, at 1 molal (– – –), 2 molal (• • • •), and 3 molal (– • – •) salt concentrations.

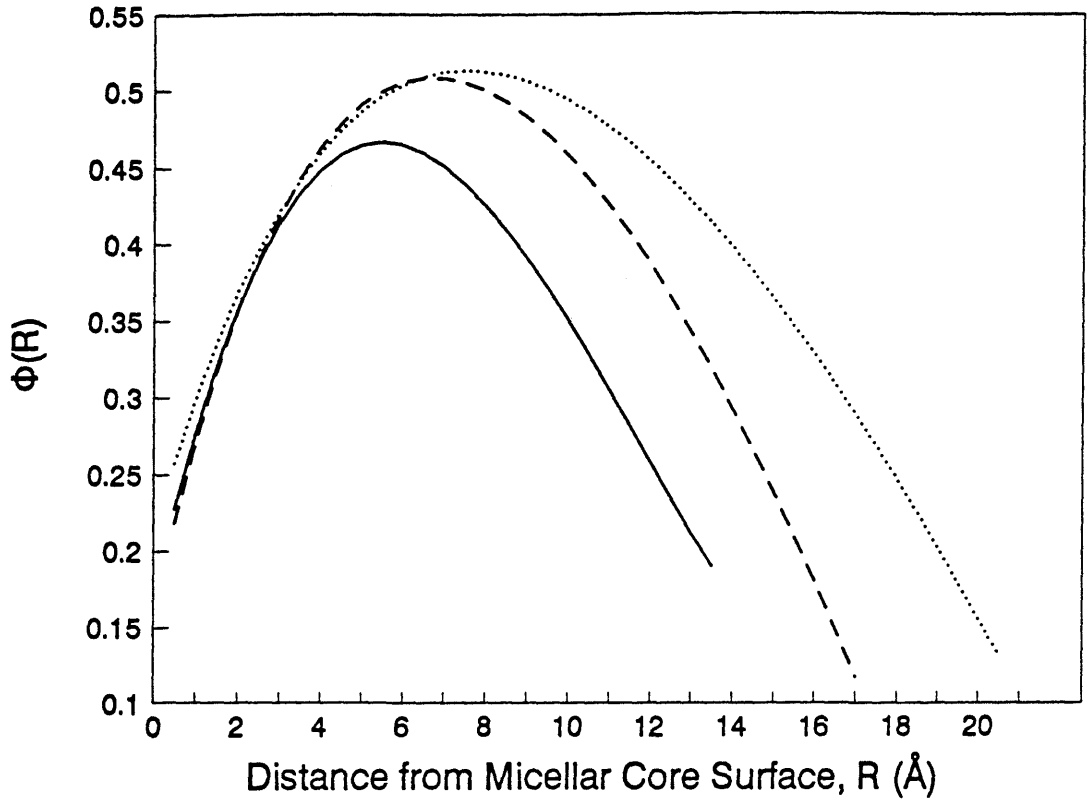

Figure 23. Volume fraction of PEO in the micelle head layer, ϕ_{hl}, as a function of the distance from the micellar-core surface, R, for: $C_{12}E_4$, (——), $C_{12}E_6$ (– – –), and $C_{12}E_8$ (• • • •), for $l_c = 15.41$Å.

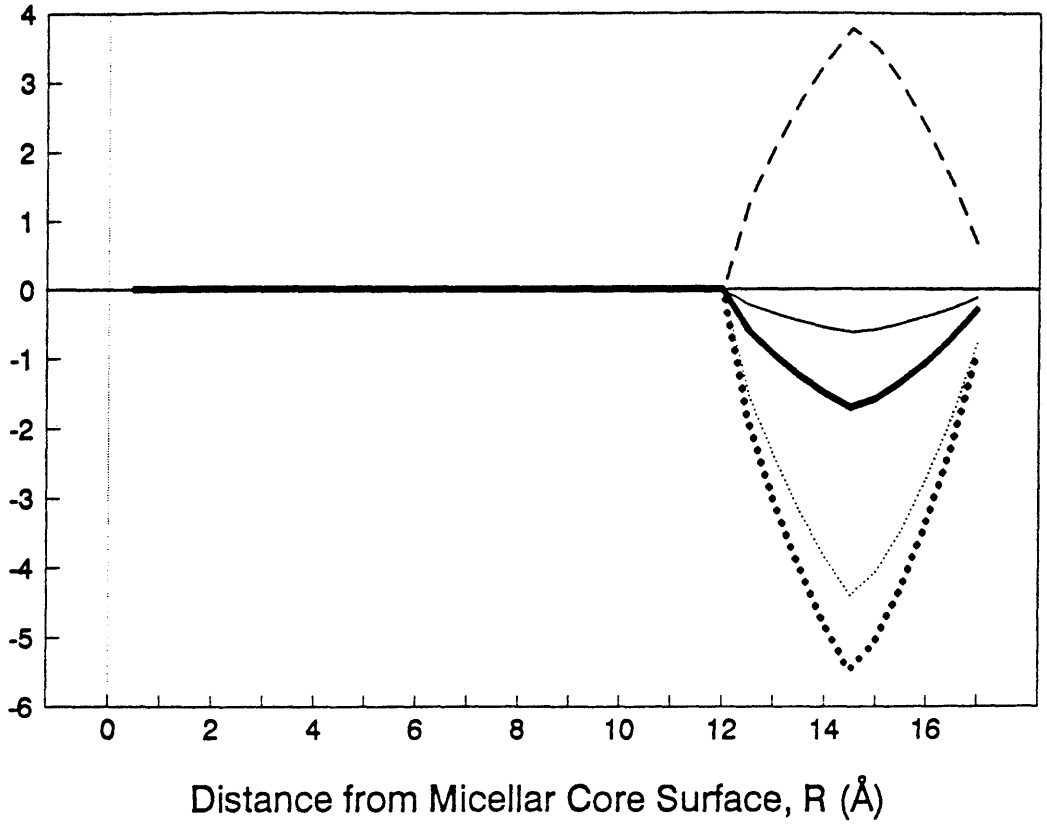

Figure 24. Change in the enthalpy, Δh_{hl} (• • • •, Eq.29), entropy, $-T\Delta s_{hl}$ (– – –, Eq.28), and free energy, $\Delta G_{hl} = \Delta h_{hl} - T\Delta s_{hl}$, (———, Eq. 30), as a function of distance from the micellar core surface, R, for parallel $C_{12}E_6$ rodlike micelles separated by a distance $r = 60$Å. Thin lines correspond to $\chi = 0.8$; thick lines correspond to $\chi = 1$.

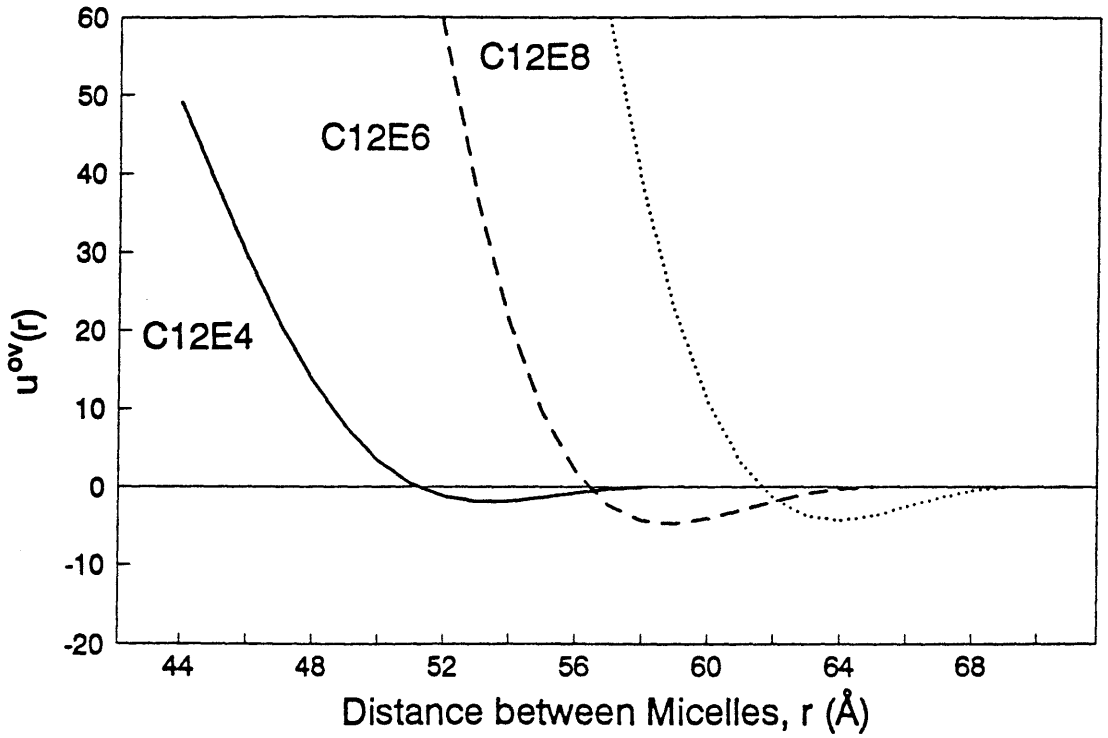

Figure 25. Interaction potential resulting from the overlap of micelle head layers, $u^{ov}(r)$, as a function of the distance between the axes of the parallel rodlike micelles, for: $C_{12}E_4$, (——), $C_{12}E_6$ (– – –), and $C_{12}E_8$ (• • • •), for $\chi = 0.8$.

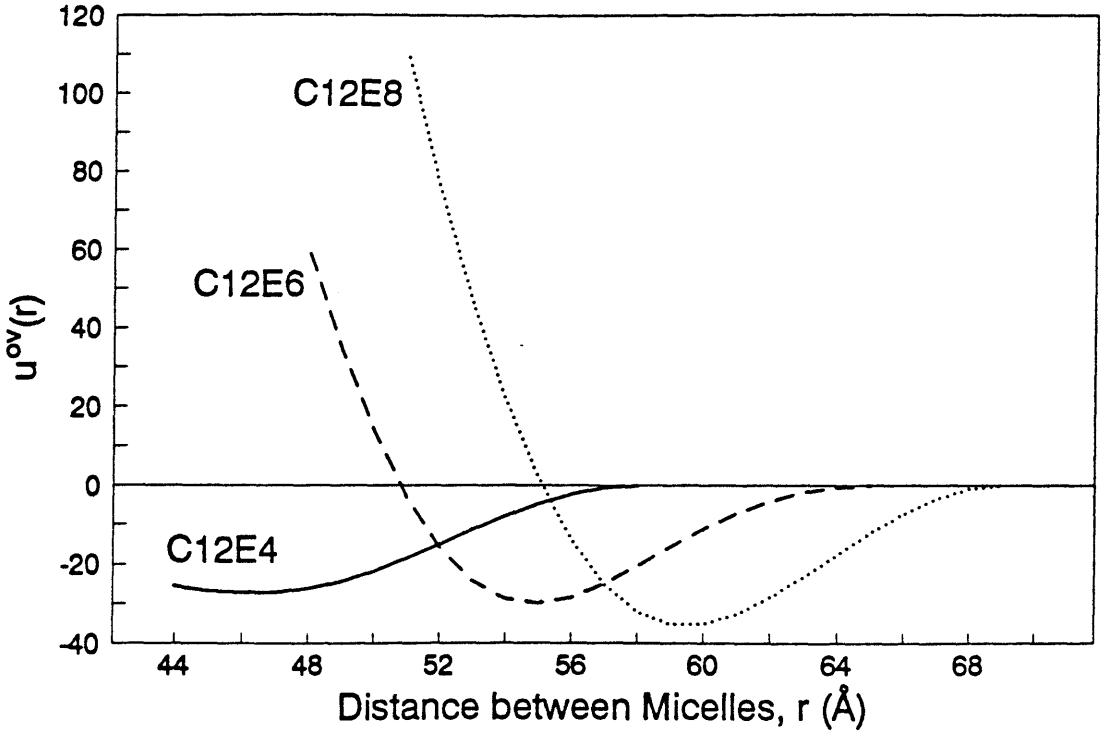

Figure 26. Interaction potential resulting from the overlap of micelle head layers, $u^{ov}(r)$, as a function of the distance between the axes of the parallel rodlike micelles, for: $C_{12}E_4$, (——), $C_{12}E_6$ (– – –), and $C_{12}E_8$ (• • • •), for $\chi = 1$.

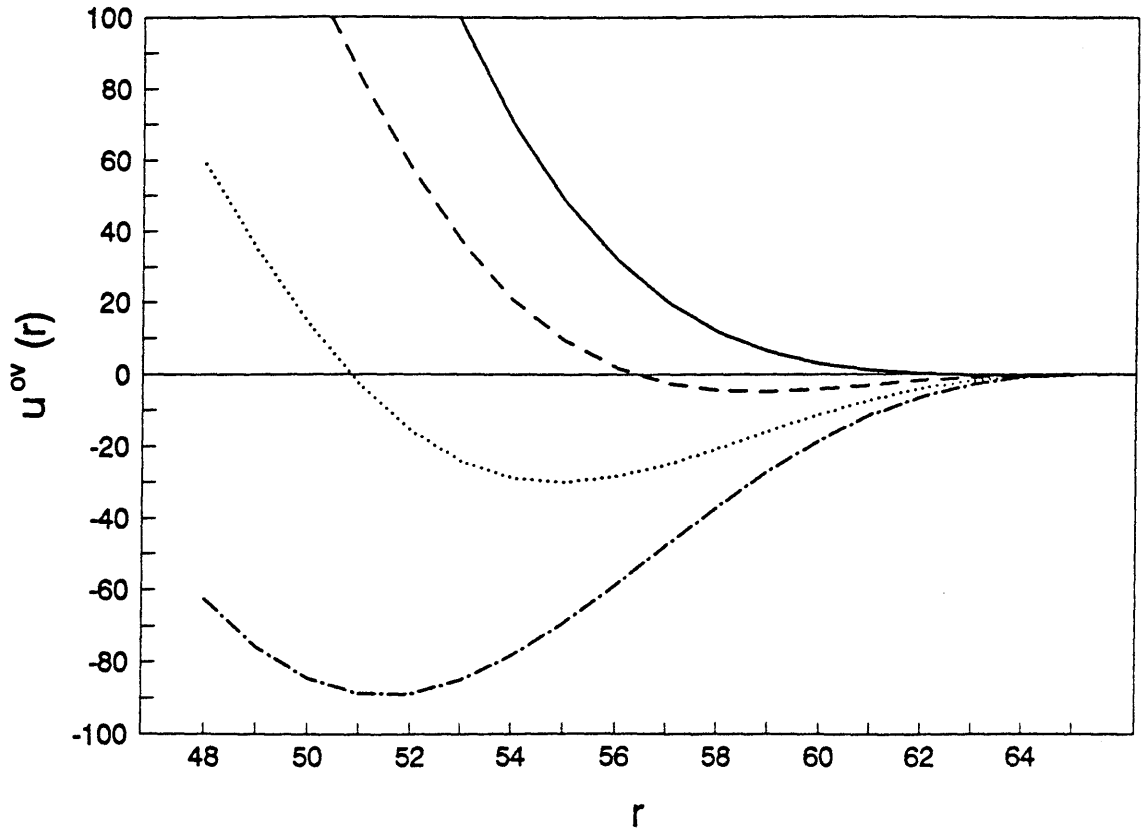

Figure 27. Interaction potential resulting from the overlap of micelle head layers, $u^{ov}(r)$, as a function of the distance between the axes of the parallel $C_{12}E_6$ rodlike micelles, for: $\chi = 0.6$ (——), $\chi = 0.8$ (– – –), $\chi = 1.0$ (• • • •), and $\chi = 1.2$ (– • – •).

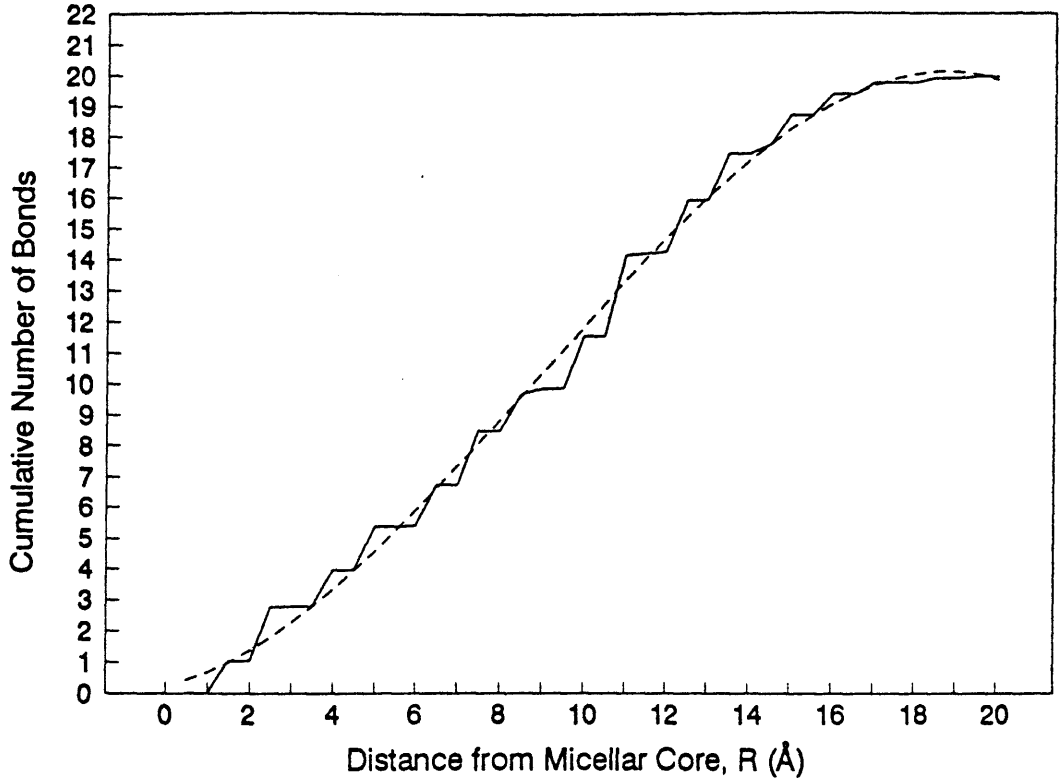

Figure 28. Cumulative number of bonds, Σn_m, between the micellar-core surface, $R=0$, and a finite distance from the micellar core, $R=0.5m$ Å, for an E_6 PEO head chain. The dashed curve corresponds to the best polynomial fit: $\Sigma n_m \approx AR^3+BR^2+CR+D$.

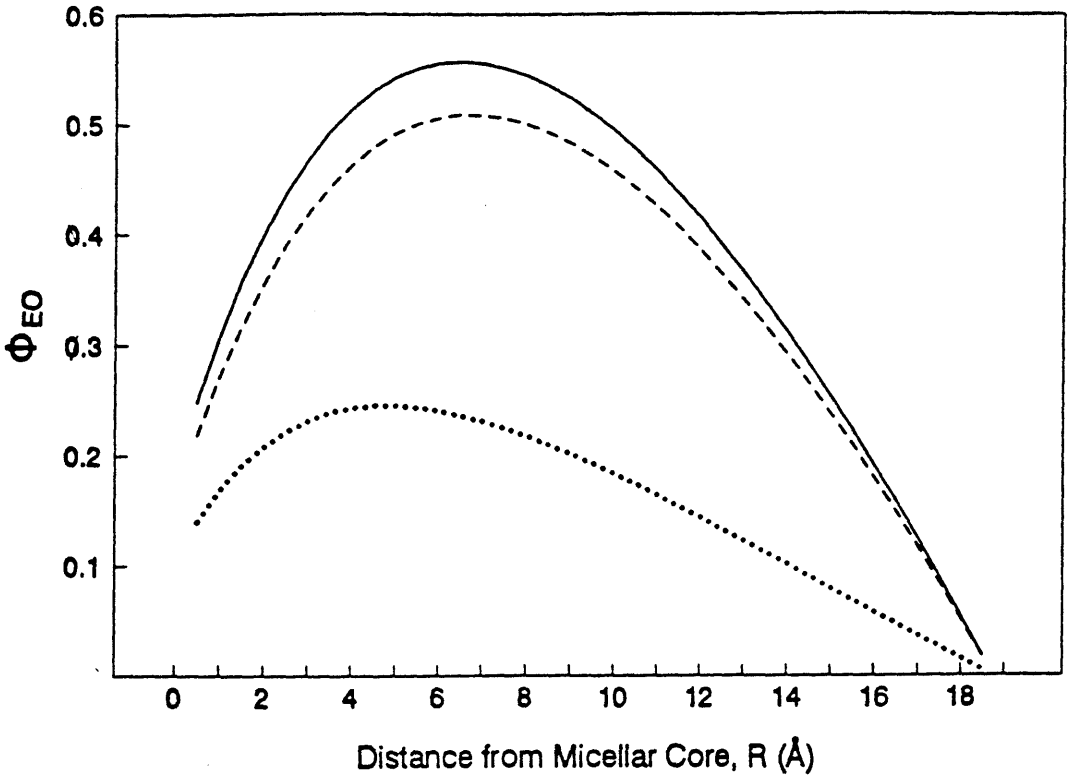

Figure 29. Volume fraction profiles, $\phi_{EO}(R)$, as a function of distance from the micellar core, R, for E_6 PEO head chains grafted to a spherical micelle core with $l_c = 15.4$Å (• • • •), cylindrical micelle core with $l_c = 15.4$Å (– – –), and $l_c = 13.5$Å (———).

CHAPTER 6. CONCLUSIONS AND FUTURE WORK

Nonionic surfactants can display a rich variety of micellar morphologies, as well as complex phase behavior in aqueous solutions. This results from a delicate balance of intramicellar and intermicellar interactions. In this thesis, we have investigated the modulation of these interactions by the addition of salts and the variation of temperature. Specifically, we have studied the behavior of three alkyl poly(ethylene oxide), C_iE_j, nonionic surfactants, $C_{10}E_6$, $C_{12}E_6$ and $C_{12}E_8$, in aqueous solutions of LiCl, NaCl, KCl, KBr, and KI.

All the salts studied (LiCl, NaCl, KCl, KBr, and KI) were found to decrease the CMC of $C_{12}E_6$, $C_{10}E_6$, and $C_{12}E_8$ in these aqueous salt solutions as compared to the pure water case. Light scattering results indicated that Cl^- and Br^- enhance one-dimensional micellar growth, while I^- suppresses one-dimensional micellar growth. We also found that Cl^- and Br^- decrease, while I^- increases, the cloud-point temperatures of the surfactant solutions examined in this thesis. For details see Chapter 2.

In this thesis, we have focused on developing a deeper fundamental understanding of salt effects on the various intramicellar (hydrophobic, interfacial, head transfer), as well as intermicellar (van der Waals, head chain interpenetration) interactions leading to the complex range of phenomena exhibited by aqueous salt solutions of C_iE_j surfactants. We developed a theoretical description of these interactions, using a variety of theoretical tools, in order to quantify the salt effects on these interactions. A detailed molecular-thermodynamic modelling of intramicellar interactions made possible the accurate prediction of the CMC (see Chapter 2), as well as of the growth and entanglement of C_iE_j micelles (see Chapters 3 and 4), as reflected in the micellar size distribution, and the crossover concentration, the surfactant concentration which marks the transition from the dilute micellar solution regime, where the micelles are singly dispersed, to the semidilute micellar solution regime, where the micelles are fully entangled. The micellar size distribution was

predicted based on the calculation of the free energy of micellization as a function of the aggregation number. The predicted micellar size distribution was a necessary input to our predicted dilute surfactant solution viscosities, which was calculated using the Doi-Edwards theory for rodlike macromolecules, modified to account for the self-assembling nature of the micellar aggregates, as well as for the polydisperse size distribution of the micelles (see Chapter 4). The predicted values of the CMC, the shape of the micelles, and the crossover surfactant concentration compared reasonably well with experimentally measured values.

The phase separation of the C_iE_j surfactant solutions upon increasing temperature indicates that the attractive intermicellar interactions increase with increasing temperature. Furthermore, the addition of salts was shown to modify the magnitude of these attractions, and to induce changes in the position of the cloud-point curves along the temperature axis. The magnitude of the attractive intermicellar interactions was derived from our measured cloud-point curves through the analysis of these curves using a mean-field approximation of the free energy of intermicellar interactions, formulated as a quadratic expression in surfactant concentration. The strength of the attractions was found to increase with temperature as well as with concentration of LiCl, NaCl, KCl, and KBr, while the addition of KI was shown to reduce the strength of the intermicellar attractions. Furthermore, it was found that the magnitude of the attractions at the critical temperature is about 1 kT, for all the surfactants and salt conditions examined (for details see Chapter 5).

The molecular modelling of the intermicellar interactions was guided by the finding that about 1 kT of attraction per surfactant molecule is required to explain the observed phase separation. The calculation of the van der Waals attraction between the micellar cores of spherical, crossed-rodlike, and parallel-rodlike micelles showed that van der Waals interactions are insufficient to account for the observed attractions. Furthermore, van der Waals interactions are not able to account for the effect of temperature and salts on intermicellar interactions. This led us to seek other sources of attractive intermicellar interactions, and motivated us to investigate the possible interpenetration of the micelle head layers. Specifically, the phase separation

of the micellar-solution was qualitatively explained by the theory formulated to model the interpenetration of the PEO head chains in the hydrophilic head layers of two approaching micelles. The strength of these attractions was captured through the use of a Flory χ-parameter, which reflects the quality of the solvent. Through this formalism, the effect of the addition of salts and the change in temperature on intermicellar interactions was rationalized. The predicted interaction potential between two micelles was found to be consistent with the observed decrease in the strength of attractive intermicellar interactions with increasing number of EO units in the heads, whereby surfactants with shorter PEO heads (for example, $C_{12}E_6$) phase separate at lower temperatures as compared to those with longer PEO heads (for example, $C_{12}E_8$). Furthermore, the predictions are also consistent with force measurements conducted between $C_{12}E_5$-coated mica surfaces, which showed an increase in the attractive forces with increasing temperature (for details see Chap.5).

The theoretial description and modelling of intermicellar interactions presented in this thesis, although qualitatively consistent with the experimental data, requires further development. In particular, additional theoretical work should be pursued to provide detailed quantitative predictions of the phase behavior of the systems considered in this thesis. The following theoretical developments are needed: (1) calculation of the PEO volume fraction profiles resulting from the interpenetration of the head chains of two approaching hydrophilic head layers when the volume fraction profiles of the two layers are not symmetric, which occurs for curved micellar-core surfaces, (2) incorporation of the distortion of the head chain volume fraction profiles upon overlap (recall that the theory presented in this thesis assumes that the volume fraction profiles are merely additive), (3) a molecular-level description of the Flory χ-parameter in order to capture more precisely the magnitude of the interactions between PEO chain segments as a function of salt type and concentration, as well as temperature, and (4) a molecular-level determination of the persistence length, ξ, which was utilized in the calculations of the crossover surfactant concentration, and the interaction free energy corresponding to wormlike micellar aggregates.

From an experimental point of view, the interpenetration of PEO head chains conjectured in this thesis presents interesting possibilities for additional experimental investigations.The most immediate one is the direct measurement of forces between C_iE_j-coated mica surfaces in aqueous salt solutions, using the surface-force apparatus. It would be very valuable to conduct experiments of this type as a function of (*i*) the number of ethylene oxide units in the PEO head chain, (*ii*) type and concentration of added salts, and (*iii*) temperature. Additional light scattering experiments should also be conducted to examine in more detail the effects of salts, temperature, and surfactant concentration on the micellar shape, size, and size distribution, through a combination of static light scattering, which measures the average radius of gyration of the micelles, and quasielastic light scattering, which measures the average micellar hydrodynamic radius. It would also be very useful to probe the effect of salts, temperature, and surfactant concentration on the second virial coefficient, as deduced from light scattering experiments, and compare these with the theoretical predictions of intermicellar interactions presented in this thesis.

We hope that the theoretical developments and experimental results presented in this thesis will provide a solid foundation as well as stimulate future work aimed at quantifying more precisely the phase behavior of micellar solutions, in general, and salt effects on micellar solution behavior, in particular.